

Department of

Earth and Environmental Sciences DISAT

PhD program in Chemical, Geological and Environmental Science  
Cycle XXXVI

Curriculum in Geological Sciences

# **Methodological approach to predict liquefaction effects on geo-structures: laboratory tests on real cases**

Surname: Romice

Name: Francesca

Registration number: 822683

Tutor: prof. Giovanni Battista Crosta

Supervisor: prof. Riccardo Castellanza

Company tutor: ing. Andrea Morotti

Coordinator: prof. Marco Giovanni Malusà

*To Simone and my family*



## ***Acknowledgements***

*This PhD project was financed by Matest which I want to thank for the great opportunity that they gave me with this research.*

*A special thanks to prof. Ing. Riccardo Castellanza who has always encouraged and support me on this path. His positive attitude has really help me in never give up. Great thank you also for prof. Giovanni Crosta who has listening and helping me whenever I needed.*

*In these years, I've found a friend, a mother, a colleague, a very special person who is prof. Nicoletta Fusi. Her help, her kindness, her support has been very precious for me. Any thanks will never be sufficiently comparable to everything she has given me in this period.*

*I'm a very lucky person and for this reason the list of people I had to thank might be very long! All the special people of the second floor would deserve an individual thanks, but I want to thank especially two people: Libero Sandrini and Nicola Bavaresco. You are definitely more than colleagues and if I'm here for sure it's also because of your help.*

*I want to thank my colleagues in Matest, Fabio Livraghi who has believed in me from the first day (he chose me for this project), Luca Pirozzolo who has prepared me to PhD (he's a PhD too!!), Agnese Di Salvo, the perfect mix between determination and sweetness. Thank you guys!!*

*Thanks to all my friends and my family to encouraged me also when I was not able to support myself, you will be always my safe place.*

*Finally, I want to thank my special love Simone, my first fan and my precious anchor. Thank you for your immense understanding over the years, I love you.*



## Index

Summary .....	1
Chapter 1 .....	3
1 Liquefaction phenomenon: a general overview.....	3
1.1 Introducing liquefaction .....	3
1.2 Liquefaction definition .....	5
1.3 Liquefaction classification .....	6
1.4 Mechanical behaviour of soil .....	9
1.4.1 Characteristic state .....	9
1.4.2 Critical state .....	11
1.5 Liquefaction susceptibility .....	13
1.5.1 Grain size distribution, water content and plasticity .....	14
1.5.2 Relative density .....	20
1.5.3 Initial static shear stress .....	20
1.5.4 Stress history .....	21
1.6 Liquefaction triggering.....	22
1.7 Liquefaction severity index .....	23
Chapter 2 .....	26
2 Methodological approach to liquefaction evaluation .....	26
2.1 Approaches to task .....	26
2.2 Experimental approach.....	28
2.3 Theoretical and numerical approach .....	29
Chapter 3 .....	30
3 In situ investigations to assess liquefaction effects .....	30
3.1 Introduction .....	30
3.2 CSR - Earthquake-induced cyclic stress ratio .....	30
3.3 CRR- Cyclic resistance ratio .....	32

3.3.1	Standard penetration test .....	39
3.3.2	Cone penetration test.....	43
3.3.3	Vs .....	46
3.4	Simplified procedure to obtain Factor of safety .....	47
Chapter 4	.....	49
4	Liquefaction susceptibility based on in-situ and norms: application on real case studies .....	49
4.1	Regulatory context .....	49
4.2	Case 1: Simulation of the dynamic behaviour of the Panaro embankments .....	51
4.2.1	Geological and seismic setting.....	51
4.2.2	Geognostic investigations .....	54
4.2.3	NTC18 analysis.....	56
4.3	Case 2: the evaluation of the foundation system of the engineering work called Ponte Canale Ancona .....	57
4.3.1	Geological and seismic setting.....	58
4.3.2	Geognostic investigations .....	61
4.3.3	NTC18 analysis.....	64
Chapter 5	.....	65
5	Laboratory tests to support advanced procedure for liquefaction effect on geostuctures .....	65
5.1	Introduction .....	65
5.2	Laboratory equipment .....	66
5.2.1	Cyclic triaxial test .....	67
5.2.2	Cyclic simple shear test.....	71
5.2.3	Resonant column test .....	74
5.2.4	Centrifuge test .....	75
Chapter 6	.....	79
6	Laboratory results on the two case studies .....	79
6.1	Research method .....	79

6.1.1	Geotechnical soil classification.....	79
6.1.2	Cyclic triaxial test .....	81
6.1.2.1	Equipment .....	82
6.1.2.2	Test procedure .....	85
6.1.3	Cyclic simple shear test.....	89
6.1.3.1	Test procedure .....	91
6.2	Results research .....	95
6.2.1	Case 1: Simulation of the dynamic behaviour of the Panaro embankments .....	95
6.2.2	Material .....	96
6.2.3	Cyclic triaxial test .....	102
6.2.3.1	Test program.....	102
6.2.3.2	Results .....	104
6.2.3.3	Discussion .....	123
6.2.4	Cyclic simple shear test.....	126
6.2.4.1	Test program.....	126
6.2.4.2	Results .....	128
6.2.4.3	Discussion .....	150
6.3	Case 2: Ponte canale Ancona .....	153
6.3.1	Materials.....	153
6.3.2	Cyclic triaxial test .....	155
6.3.2.1	Test program.....	155
6.3.2.2	Results .....	158
6.3.2.3	Discussion .....	178
Chapter 7.....		182
7 Constitutive model and numerical analysis: application on case studies 182		
7.1	Introduction .....	182
7.2	UBCSAND.....	183

7.3	Mohr-Coulomb .....	185
7.4	Numerical analysis .....	186
7.5	Case 1: Simulation of the dynamic behaviour of the Panaro embankments .....	187
7.5.1	Calibration of the parameters of the UBC SAND constitutive model.....	188
7.5.2	Numerical modelling.....	191
7.5.2.1	Dynamic input loads and seismic modelling.....	192
7.5.3	Results .....	195
7.5.4	Discussion .....	198
7.6	Case 2: the evaluation of the foundation system of the engineering work called Ponte Canale Ancona .....	200
7.6.1	Calibration of the parameters of the UBC SAND constitutive model.....	201
7.6.2	Numerical modelling.....	203
7.6.3	Results .....	207
7.6.4	Discussion .....	215
Chapter 8	.....	216
8	On-going developments for soil testing in static and dynamic conditions.....	216
8.1	Introduction .....	216
8.2	Automatic static triaxial equipment.....	217
8.3	Sample preparation and equipment requirements for cyclic tests	222
8.4	Cyclic automatic triaxial equipment.....	225
8.5	Discussion .....	228
Conclusion	.....	229
Bibliography	.....	232

## Summary

This thesis deals with the liquefaction and its effects on the mechanical behaviour of sand, in geotechnical structure. This phenomenon mostly occurs in saturated sand, emphasized in loose sand and at depth generally not exceeding 20 m.

Liquefaction is a phenomenon in which the strength and stiffness of a soil is reduced by earthquake shaking or other dynamic loading. Liquefaction happens when there is a loose of strength in saturated and cohesion-less soils because of increased pore water pressures and hence reduced effective stresses due to dynamic loading. Liquefaction has been responsible for tremendous amount of damage in historical earthquake around the world. Common examples of liquefaction-induced damages include tilting or overturning of buildings, flow failure of steeply sloping ground such as dams and lateral spreading of softly to moderately sloping ground.

The goal of this thesis is to study liquefaction and its effects from an engineering point of view. This means to propose of a complete methodological approach to cope with liquefaction phenomena interacting with geotechnical structures creating a mean to manage with its effects.

For getting this result, the work has been developed in an experimental, theoretical and numerical study; this path represents the typical and peculiar engineering approach for analysing a real phenomenon. In fact, it is necessary first to collect as more information as possible of the real problem by means of experimental tests carried out in situ and in the laboratory; secondly it is necessary to define a theoretical interpretative scheme for modelling the phenomenon. Thirdly, when the theoretical model has been corroborated by experimental evidences, to work numerical tools able to analyse boundary value problems for designing structures.

Due to in situ test, especially SPT and CPTU, susceptibility of soil will be provided and Factor of safety will be estimated, becoming the starting point for an advanced analysis through laboratory test. They will provide the evolution of the geo-mechanical behaviour under cyclic loading until liquefaction is reached, it means to evaluate liquefaction of soil under certain cyclic load corresponding to seismic conditions to analyse. In addition, laboratory tests allow to obtain curves to calibrate constitutive model, as UBCSAND, theoretically reproducing the behaviour of

liquefiable layer of soils valid for infinitesimal point, and not depending on state variables. Therefore, the input parameters of the liquefaction constitutive model should be calibrated to capture key aspects (liquefaction triggering and post-liquefaction deformation) of the cyclic test results. Then, numerical modelling returns reliable simulations allowing to properly identification of the critical portion of the structure to be secured. This procedure has been validated on two real cases.

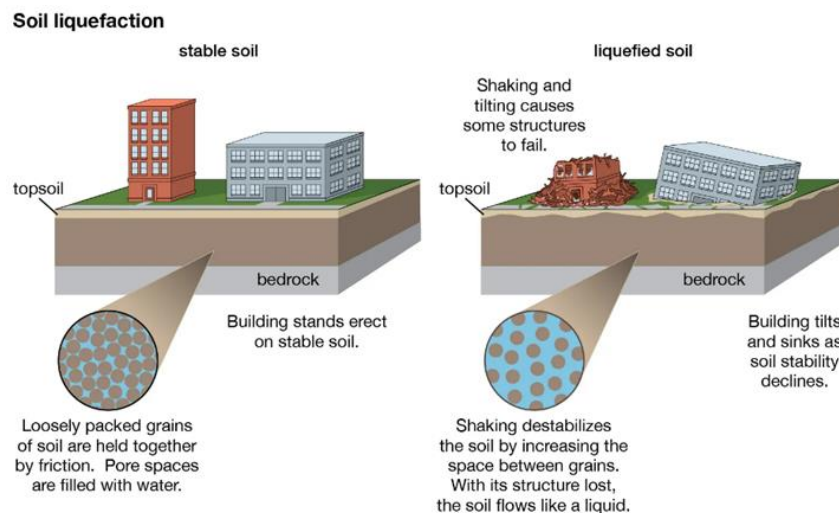
This research project was funded by Matest Spa, the leader in manufacture of material testing equipment for the construction industry. Matest has shown great interest in the development of new technologies in the field of dynamic (and static) triaxial machines, mostly linked with tests focused on liquefaction studies. This results in increasing the internal know-how and improving the machine's performance (in terms of hardware and software).

# Chapter 1

## 1 Liquefaction phenomenon: a general overview

### 1.1 Introducing liquefaction

It is universally known that saturated loose sand exhibits the phenomenon of liquefaction when it is subjected to cyclic loads occurring at relatively short intervals, not allowing for rapid dissipation of pore pressure. The phenomenon of liquefaction is identified with the near-total loss of strength of saturated sands and gravels of uniform grain size. The process of liquefaction transforms a soil element from a solid to a liquid state, resulting in episodes of instability in large soil masses, causing potentially extensive damage (Fig.1.1.). Fully understanding the mechanism of liquefaction remains one of the challenges of earthquake-related geotechnical engineering, as geomaterials do not exhibit identical reactions under similar seismic conditions.



**Figure 1.1 Schematic illustration of liquefaction: it occurs when loose soil, saturated with water is shaken by an earthquake, causing the soil to behave like a liquid.**

Identifying areas susceptible to liquefaction allows the effects to be predicted in geotechnical works with subsequent securing of these areas. Saturated incoherent soil in the absence of seismic stress is subject to lithostatic pressure, due to the weight of overlying sediments; during a seismic stress, cyclic shear stresses are induced in the soil due to the propagation of seismic waves to the surface, while the lithostatic pressure remains constant. The probability of a deposit reaching conditions for liquefaction also depends on the state of thickening, grain size composition, drainage conditions, seismic stress history, and the age of the deposit itself (more recent, Holocene age). The lower the degree of thickening of the material (high void index and low relative density), the greater the probability that, other things being equal, a deposit will reach the liquefaction state. From the liquefaction specification in (Jefferies & Been, 2015), it can be seen that the liquefaction can be induced by some reasons: the static loading; earthquake motion, vibration instruments, the vibration caused by wind, ice movement, etc. Some examples of liquefaction disaster occurred in last century will be shown in the below.

Liquefaction can induce destruction of land and structures according to four main modes: landslide or mudslides, lateral flow, soil oscillation and loss of bearing capacity. A typical example of this is the failure is Fort Peck Dam, which was damaged by a large slide occurring in its upstream shell near the end of construction in 1938 (Fig.1.2 a)

The Niigata earthquake in 1964 (Fig.1.2 b), which had a magnitude of 7.5 Mw, is certainly the event that focused world attention on the phenomenon of soil liquefaction. Since then, there have been some more examples of liquefaction induced by earthquakes listed here as San Fernando Valley (1971), Haicheng (1975), Tangshan (1976), Imperial Valley (1979), Armenia (1988), Loma Prieto (1989) and Turkey (1999).

San Fernando Valley event (Fig.1.2 c) shown no liquefaction effect during earthquake, but after minutes; it has been explained as a result of pore water pressures generated during the earthquake but no relation to any earthquake-related inertial forces

Most recently, during the earthquake in 2011 in Japan (Fig.1.2 d), soil liquefaction occurred and resulted in damages to many houses and buildings. Tamari (2018) showed that, in some areas, the sand boiling, a characteristic of liquefaction, occurred during the main shock first and expanded during the aftershocks; however, in some areas, there was no liquefaction during the main shock but the aftershocks.





**Fig 1.1 Example of liquefaction effect and damages: a) Fort Peck Dam - USA (1938); b) Niigata – Japan (1964); c) Lower San Fernando Dam - USA (1971); d) Japan earthquake 2011**

Since 1964, much work has been carried out to explain and understand soil liquefaction. Seed and Idriss could be considered as the pioneer of liquefaction analysis with their “simplified procedure” introduced in 1971 and update in over the years, to improve the evaluation of liquefaction risk in soil deposit in terms of Factor of Safety; it is identified as the ratio between the seismic demand (CSR, cyclic stress ratio) and the capacity of soil to resist liquefaction (CRR, cyclic resistance ratio).

## 1.2 Liquefaction definition

Casagrande (1936a) was able to indicate the unusual behaviour of fully saturated contractive sand under undrained conditions but were Terzaghi and Pack (1948) who referred to “spontaneous liquefaction” description of the sudden loss of strength of very loose sands that caused flow slides due to a slight disturbance. Mogami and Kubo (1953) also used the term liquefaction to describe a similar phenomenon observed during earthquakes, after Tokyo earthquakes in 1948.

Seed in 1975, used the term liquefaction “to describes a phenomenon in which a cohesionless soil loses strength during an earthquake and acquires a degree of mobility sufficient to permit movements ranging from several feet to several thousand feet”.

In 1978, Marcuson defined liquefaction as the transformation of a granular material from a solid to a liquefied state as a consequence of increased pore-water pressure and reduced effective stress. Increased pore-water pressure is induced by the tendency of soil to become compressed and densified when subjected to cyclic shear deformations (Robertson, 1997).

In 1985, the National Research Council’s Committee on Earthquake Engineering (NRCCE 1985) gave a broad definition which does not mention the increase in pore water pressure as a requirement for the liquefaction: “*All phenomenon giving rise to a loss of shearing resistance or the development of excessive strains as a result of transient or repeated disturbance of saturated cohesionless soils*”.

Jefferies (2016) stated that there are some definitions of liquefaction; however, none of them satisfy all requirements when applied in particular cases. This indicates that liquefaction definition still seems to be the subject of a continuing debate within the geotechnical profession.

### **1.3 Liquefaction classification**

Seed et al. (1976) introduced a classification of liquefaction as below:

- “Initial Liquefaction”: it occurs when water pore pressure is equal to confining pressure; even if it’s not related to the magnitude of the deformations that the soil might subsequently undergo, it defines a condition that is a useful basis for assessing various possible forms of subsequent soil behavior.

- "Initial Liquefaction with Limited Strain Potential" or "Cyclic Mobility”: cyclic stress applications cause limited strains to develop either because of the remaining resistance of the soil to deformation or because the soil dilates, the pore pressure drops and the soil stabilizes under the applied loads.

- “Liquefaction”: a soil will undergo continued deformation at a constant low residual stress or with no residual resistance, due to the build-up of high pore water pressures which reduce the effective confining pressure to a very low value.

In subsequent years, Robertson and Fear (1995), building on earlier work by Robertson (1994), proposed specific definitions of soil liquefaction which distinguished between Flow liquefaction from Cyclic softening. Cyclic softening was further divided into Cyclic liquefaction and Cyclic mobility. Robertson proposed a flow chart to distinguish different liquefaction according to these definitions (Fig.1.2).

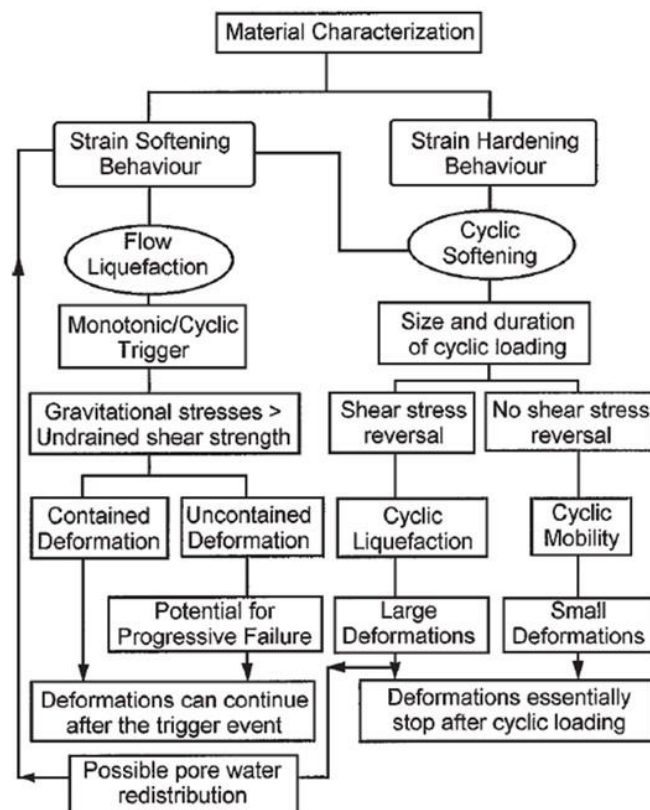


Fig 1.2 Suggested flow chart for evaluation of soil liquefaction (after Robertson and Wride, 1998)

### 1. Flow liquefaction

Even if flow liquefaction is not so common, it's possible to mention several examples of this phenomenon: Zealand flowslide (Koppejan et al., 1948), Fort Peck Dam (Casagrande, 1965), Aberfan flowslide (Bishop, 1973) and Stava tailings dam. Flow liquefaction occurs if the soil strain-softening and gravitational shear stresses are larger than the ultimate or minimum strength, causing collapse. The trigger could be either static or

dynamic, in undrained condition. The brittleness of the soil and the geometry of the ground could be important in understanding if fail or slide will occur. In general, sensitive clays, very loose deposits and silt deposits are more prone to expose flow liquefaction under undrained loading.

## 2. Cyclic softening

Cyclic softening (Fig.1.3) could be divided in two categories: cyclic mobility and cyclic liquefaction. It differs from flow liquefaction because it occurs in both strain-softening and strain-hardening condition, but as flow liquefaction in both static or dynamic stresses. Then, it occurs when shear stresses are lower than the ultimate shear strength, obtaining increasing deformation.



**Fig 1.3 Effects of liquefaction: a) Lateral spread; b) Sand boils**

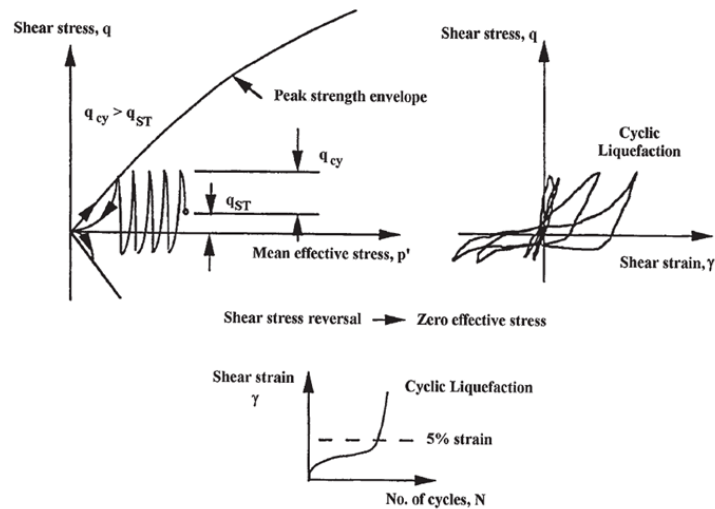
### ○ Cyclic mobility

This phenomenon occurs when shear stresses are different from zero and also effective stress didn't reach zero value, causing large deformation which accumulate in each cycle of shear stress.

### ○ Cyclic liquefaction

This phenomenon exists if both shear stress and effective stress lead to zero, under cyclic loading (Fig.1.4) causing large deformation. Generally, deformation will stop if cyclic loading stops. Cyclic liquefaction can occur

on dense sands if the magnitude of cyclic shear stress and number of cycles are large enough.



**Fig 1.4 Schematic of undrained cyclic behaviour of sand illustrating cyclic liquefaction (after Robertson 1994)**

In laboratory, the most accepted criterion for liquefaction in laboratory tests is that the sample is liquefied if one of the following conditions appears (Seed and Lee 1966; Ishihara 1993): pore water pressure increases to cell pressure leading to the loss of effective confining stress; axial strain in one cycle reaches 5%.

In this study, liquefaction is generally considered as the sudden loss of the soil shear resistance accompanied by the increase of the pore water pressure.

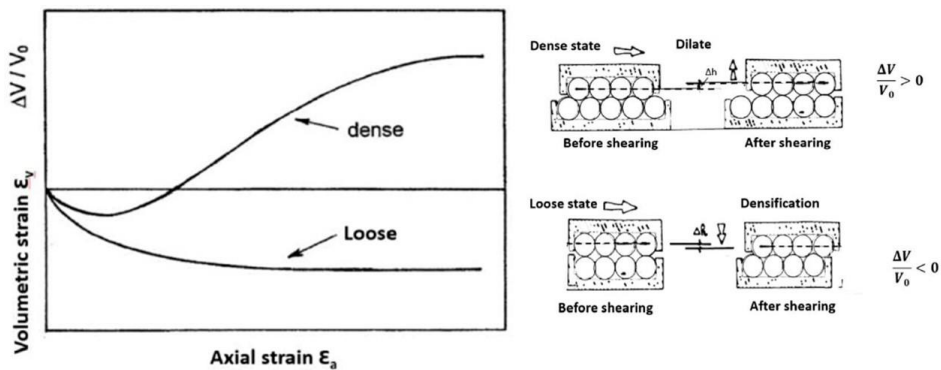
## 1.4 Mechanical behaviour of soil

### 1.4.1 Characteristic state

With the term “state” of a sand is defined the description of the physical conditions under which it exists. Void ratio (or density) and stress are the primary state variables for soils.

A soil subjected to shear loading could present two volumetric behaviour types, contractancy or dilatancy (Fig.1.5). Contractancy is a characteristic of soil relating to the decrease in volume when subjected to

shearing, because material tends to densified for slipping and rolling between grains due to the applied stress. Conversely, dilatancy is the state when the soil increases its volume due to shearing, as consequence of the mechanism of untangling and expansion of the granular stack.



**Fig 1.5 Dilatant and contractant volumetric behaviour of soils subjected to shear loading (Khai, 2020)**

In undrained conditions, on saturated sand, the volume of the sample remains constant. Thus, at the beginning of loading, an increase in pore water pressure is observed, then, for dense sands, the rate of generation of the pore water pressures decreases when the deviator stress increases and vanishes (zero) to become negative. These phases of positive and negative generations of pore water pressures correspond to the phases of contractancy and dilatancy of the material in drained shear. This stress level defines a threshold in the volumetric behavior of a granular soil called Characteristic State. It also called phase transformation.

The characteristic state separates two types of rheological behavior of the sand (Fig.1.6): contractancy in the sub-characteristic domain, limited in the plane (p, q) by two characteristics lines, and dilatancy in the upper characteristic domain up to the limit of rupture defined by the rupture limit lines.



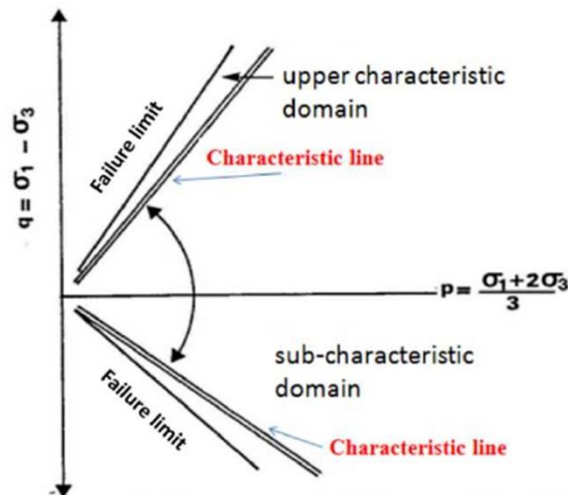


Fig 1.6 Characteristic criterion divides the contracting area of the material

In the case of loose sands, the characteristic lines are identical with the failure lines and the characteristic state merges with the critical state.

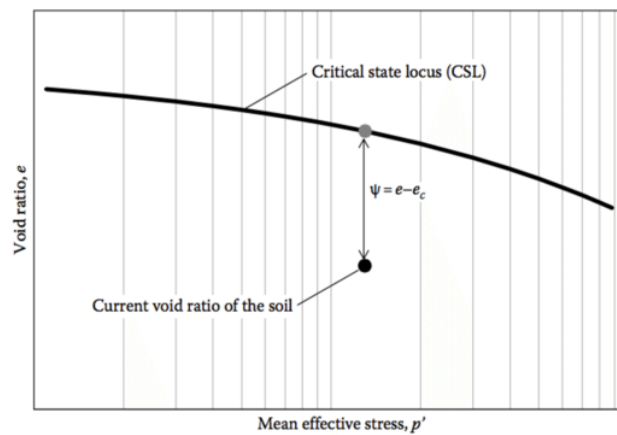
### 1.4.2 Critical state

Determination of the critical or steady state line of sand is important to several aspects of the engineering of sand fills or natural sand deposits. Critical state line and state parameters have been proven to be effective method to evaluate and predict the drained and undrained behaviors of sand. The behavior of the sand depends not only on density but also on the stress level applied to the specimen.

Following the state of art in Jefferies and Been (2016) the critical state was defined by Roscoe et al. (1958) and formalized by Poulus (1981) as: ‘the steady state of deformation for any mass of particles is that state in which the mass is continuously deforming at constant volume, constant normal effective stress, constant shear stress, and constant velocity. The steady state is obtained only after all particles have reached a statistically steady state condition and if all particles are completely broken, so that the shear stress needed to continue deformation and the velocity of deformation remains constant.’

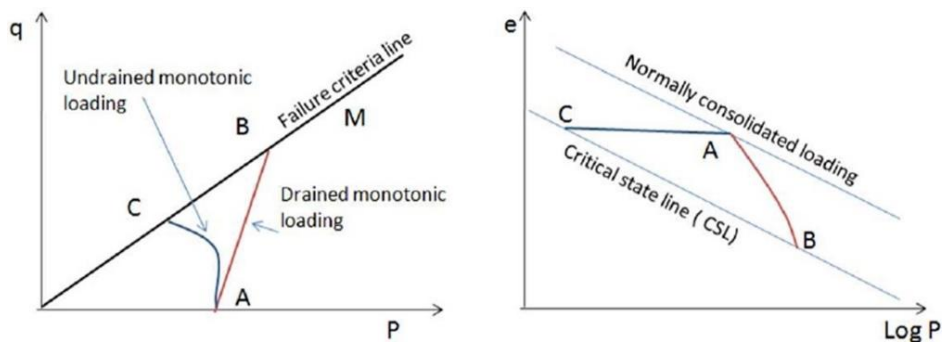
Been and Jefferies indicated that the critical state line is a unique structure. This measure of state is called state parameter and the definition is illustrated in Fig1.7. Thus, the state parameter  $\Psi$  is determined by the

void ratio ( $e$ ) and effective stress level ( $p'$ ) of sand relative to a critical state line. When the state of a sand is above the critical state line (CSL), corresponding to a positive  $\Psi$ , the sand tends to contract upon shearing, whereas state point is located below the CSL, corresponding to a negative  $\Psi$ , the tendency of sand is to dilate during shearing.



**Fig 1.7 Definition of state parameter  $\Psi$  (Jefferies & Been, 2015).**

The definition and roll of the critical state to the behavior soil in both drained condition (line AB) and undrained condition (line AC) can be seen in the Fig. 1.8 below.



**Fig 1.8 Critical state definition**



## 1.5 Liquefaction susceptibility

Soil liquefaction is a significant design issue for a wide range of structures. Liquefaction causes ground failures that comprise bearing capacity loss, lateral spreading, and flow, resulting in the settlement of structures. The risk of liquefaction of a soil deposit boosts if it is loose enough to contract under dynamic loading provided that sufficient drainage cannot occur resulting in induced pore water pressure is not likely to dissipate (Terzaghi, Peck & Mesri, 1996). The Niigata earthquake has attracted the attention of researchers in the field of soil liquefaction, helping in the definition of principle factors causing this phenomenon.

The risk of liquefaction, at a given site, is the result of the product of more factors, which can be divided in two macro-categories: "predisposing" factors and "triggering" factors.

Predisposing factors are generally related to the physical and mechanical characteristics of soils and define their susceptibility (vulnerability) to the phenomenon. These factors are listed below:

- Water content or degree of saturation;
- Density;
- Atterberg limits (liquid limit and plasticity index);
- Gradation (mean grain size and uniformity coefficient);
- Silt- and clay-size content (percent by weight finer than 0.074 mm);
- Aging and inner structure;
- Stress history (static overconsolidation, preshearing during prior earthquakes);
- Coefficient of lateral earth pressure at rest.

Triggering factors depend on the seismicity of the area in which the site falls ("hazard") and quantify the intensity of the seismic action needed to activate the phenomenon ("triggering").

Depending on the purpose of the study and the size of the area of investigation, the focus may be on only one of these aspects or an analysis of their combined effect. For example, in first-level seismic microzonation studies (medium and large scale) it may be sufficient to perimeter the areas of liquefaction susceptibility through various appropriate empirical criteria (e.g. the "Chinese criterion" introduced by Wang, 1979, the modified Chinese criterion proposed by Andrews and Martin, 2000, the Sherif and Ishibashi methods, 1978, or the method proposed by Bray et al., 2006) based on individual predisposing or triggering factors, while in the studies of greater depth (second and third level) or in the design phase (to the scale of the single artifact) Joint analysis of the triggers and predisposing factors for the estimation of the liquefaction risk is typically required. Considering that the phenomenon of liquefaction occurs only when the predisposing factors are all present and the intensity of the seismic action exceeds a certain threshold of activation, The risk of liquefaction is zero if even one of the two conditions is not met. For this reason, it is always advisable to check beforehand the presence of all the pre-liquefaction factors (usually through "empirical methods" based on standard and in situ test) and, only if the susceptibility conditions are all verified, proceed with the risk calculation through "engineering methods" that include the contribution of the seismic action to the site under consideration and require a deeper knowledge of the mechanical characteristics of the soil (through specific on-site and laboratory geotechnical tests).

### **1.5.1 Grain size distribution, water content and plasticity**

In the past years, it was supposed that only sand deposits are prone to liquefaction, because in finer grain excess of pore pressure was not considered to occur. More studies have confirmed that the reality is different, it means that also fine content could be taken in account for liquefaction potential risk.

Tsuchida (1970) developed a liquefaction criterion based on soil type, SPT N-value around the water table and maximum acceleration at the ground surface. The criterion is based on the field performance data obtained near the strong-motion accelerograph during the Niigata Earthquake of 1964, supplemented by the results of shaking table tests on saturated sand deposits as a guideline for extending those field performance data to the other intensity level of the earthquake motions. This criterion is summarized as follows:

1) Classify the soils by comparing the grain size accumulation curves with the ranges shown in Fig.1.9 as follows:

-Soils within the range (A): Very easily liquefiable soil.

-Soils within the range (B): Easily liquefiable soil but less liquefiable than the soils within the range (A).

-Consider that no liquefaction will take place for the soils that do not belong to either the ranges (A) or (B).

2) For soils falling in the ranges (A) or (B), obtain the critical N-value for liquefaction by Fig.1.10 in accordance with the maximum acceleration of the design earthquake;

3) Compare the SPT N-value at the site under consideration with the critical N-value obtained in the preceding step. The SPT N-value used for this comparison should be the one at the depth around the ground water table. If the SPT N-value is smaller than the critical N-value for liquefaction, consider that liquefaction will occur during the design earthquake. Exception is applied if the SPT N-value is greater than 16 but smaller than the critical N-value for liquefaction. In this exceptional case, the liquefaction that causes serious damage to the structures will not likely to occur though excess pore water pressure rises may be high.

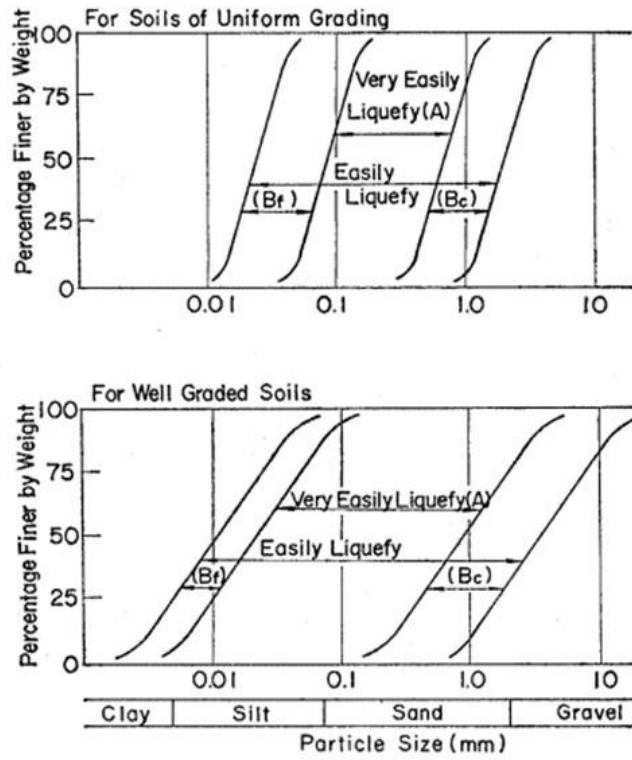


Fig 1.9 Range of grain-size curve for liquefaction soils

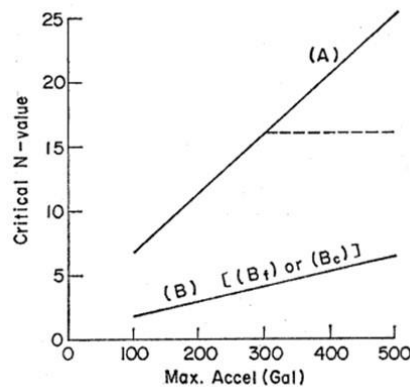


Fig 1.10 Critical N-value for liquefaction

By replacing the second factor with the SPT N-value corrected for the effective vertical stress and the third factor with the shear stress ratio, an extended form of the criterion is presented.

According to Fig.1.10, fine-grained soils (silts and finer) whose mean grain size (i.e., 50 percent of the sample weight is finer) is at least 0.02 millimeters are regarded as potentially vulnerable to liquefaction under some unspecified level of shaking. Ishihara, et al. (1980) claim that the Tsuchida (1970) chart is based only on the performance of soils of alluvial, diluvial, or volcanic origin, and the boundaries of "most liquefiable soils" are unconservative with regard to soils containing a high fraction of low plasticity clay-size particles such as are present in mine tailings. Tokimatsu and Yoshimi (1983) compiled field performance data from Japanese earthquakes that correlate observed ground behavior with gradation characteristics of local soils; soils containing up to 60 percent by weight silt-size particles and 12 percent clay-size particles (that is, particles smaller than 0.005 millimetres) exhibited moderate-to-extensive liquefaction (in terms of affected land area). Ishara (1985) affirmed that apart from sandy soil type, non-plastic silts fulfilling certain criteria can also liquefy under undrained conditions; plasticity characteristics, instead of grain size only, have an impact on the liquefaction potential of fine-grained soil. Furthermore, non-plastic cohesionless coarser silts particle shape of whom is bulky are prone to liquefaction (Ishihara, 1993), instead finer silts having platelike or platy shape is not in danger of liquefaction because they have enough cohesion to prevent it. With regards to clay, sensitive ones are prone to liquefaction.

After Niigata and Alaska earthquakes, the "Chinese criteria" have been developed to identify liquefaction potential (Seed & Idriss, 1982), based on liquid limit, fine content and water content. They affirmed that certain types of clayey materials may be vulnerable to severe strength loss as a result of earthquake shaking. These soils appear to have the following characteristics:

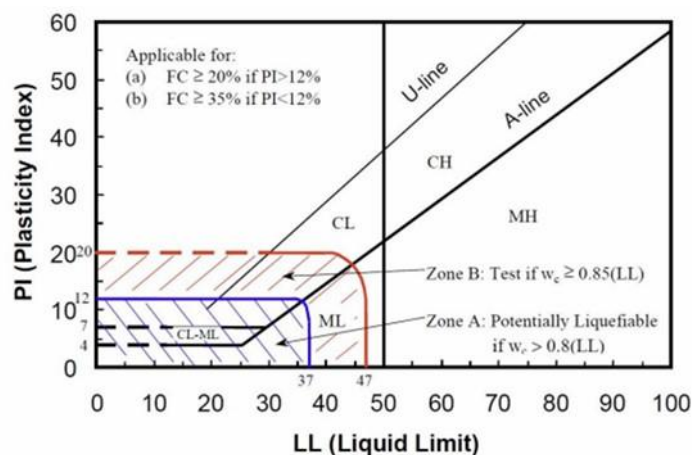
- Percent Finer than 0.005 mm: < 15%
- Liquid Limit (LL): < 35%
- Water content (wn %): > 0.9 x LL

Andrews & Martin (2000) propose modifications to the Chinese Criteria limits (Table1-1).

	Liquid limit (LL) < 32	Liquid limit (LL) ≥ 32
Clay Content < 10%	Susceptible	Further Studies Required (Considering non-plastic clay sized grains – such as mica)
Clay Content ≥ 10%	Further Studies Required (Considering non-plastic clay sized grains – such as mine and quarry tailings) Not Susceptible	Non susceptible

**Table 1-1 Modified Chinese Criteria proposed by Andrews & Martin (2000); Clay defined as grains finer than 0.002 mm**

Seed & Idriss proposed other criteria (Fig.1.11), in which the Plasticity Index (PI) is used in place of the percent clay fines used in the Chinese Criteria, while  $w_n$  (or  $w_c$ ) and LL are still part of the criteria. In the Seed et al. (2003) criteria, only Zone A soils are considered potentially susceptible to liquefaction triggering and can be evaluated using the simplified procedure (e.g., Youd et al. 2001). Soils falling in Zone B may be susceptible to liquefaction triggering, but in many cases cannot be evaluated using the simplified procedure, but rather need to be sampled and tested in the laboratory. Finally, Zone C soils (i.e., soils not plotting in Zones A or B in Figure 2) are generally not considered to be susceptible to liquefaction triggering, but may be sensitive.



**Fig 1.11 Liquefaction susceptibility criteria proposed by Seed et al. (2003).**

Bray and Sancio (2006) propose criteria for liquefaction susceptibility of fine-grained soils; their criteria are shown graphically in Fig.1.12. In this figure, three zones are identified: Susceptible, Moderately Susceptible, and Not Susceptible.

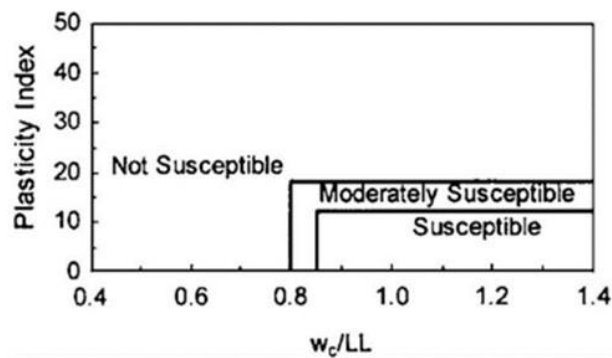


Fig 1.12 Liquefaction susceptibility criteria proposed by Bray and Sancio (2006)

The Boulanger & Idriss (2006) criteria, shown in Fig.1.13, classify soils as “sand-like” and “clay-like” based on PI, with a transition zone between these two categories. They accepted that fine-grained soil having a plasticity index higher than 7 like clay-like soil. If soil behaves sand-like, the soil is susceptible to liquefaction.

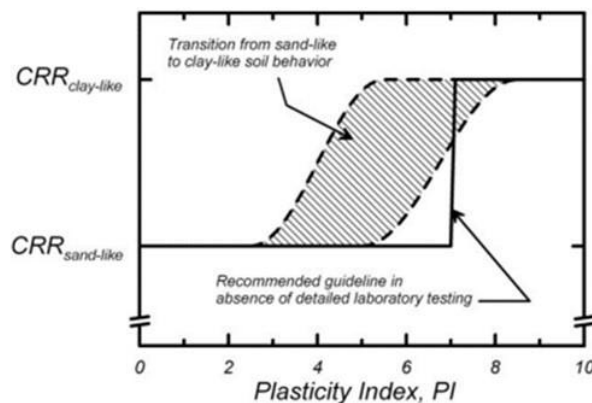


Fig 1.13 Schematic of the transition from sand-like to clay-like behaviour for fine-grained soils with increasing PI and recommended guideline for assigned cyclic resistance ratio (CRR) proposed by Boulanger & Idriss (2006).

The shape is also an important parameter; deposits having rounded shapes tend to become contracted while the occurrence of contraction is restricted to some extent by means of grain crushing in angular-shaped deposits (Terzaghi et al. 1996). Gradation is an important factor affecting liquefaction susceptibility. Depending on the void ratio, liquefaction potential is less for well graded soil as compared to poorly graded.

### 1.5.2 Relative density

Relative density is one of the most affecting factors in the liquefaction field for sand subjected to cyclic loading.

It is because of its effect on the nature of the cyclic response (liquefaction or cyclic mobility) and the value of the shear strength. Some authors have shown that increasing density decreases the liquefaction potential (Lee and Seed 1967, Seed and Idriss 1971, Seed 1979). In other words, the shear stresses to cause failure by one or the other of the two phenomena increases with the increase of the relative density.

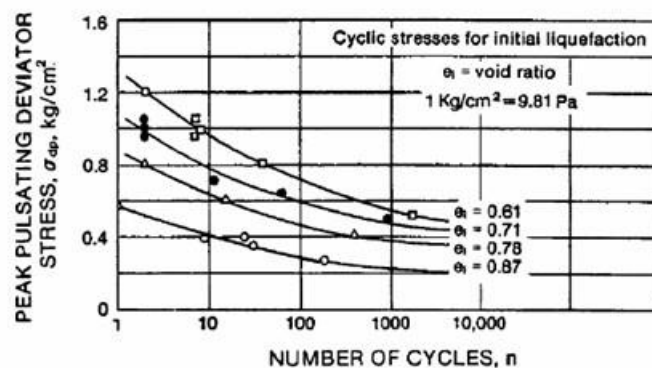


Fig 1.14 Influence of the void index on the cyclic shear strength (Lee and Seed, 1967)

### 1.5.3 Initial static shear stress

Soils are generally subjected to initial static shear stress due to overlying structures or the lithostatic stress of its layer. The effect of the initial static shear stress could lead an advantage or a disadvantage to stability of soils.



Lee and Seed (1967) and Seed (1979) showed that the resistance to liquefaction increases with the value of the initial stress deflector ( $K_c$ ). However, Yoshimi (1975) presented opposite results indicating that the presence of an initial deflector has a bad effect on the shear strength. This last observation was also found by Vaid and Finn (1979), Mohkam (1983) and Hyodo et al. (1994).

In a very detailed study on the influence of the presence of the initial static stress, Vaid and Finn (1979) and Vaid and Chern (1985) found that the resistance to cyclic loading could increase, decrease or remain unchanged as a function of the relative density, of the value of  $K_c$  and of the failure criterion retained (level of deformations allowed) (Fig.1.15).

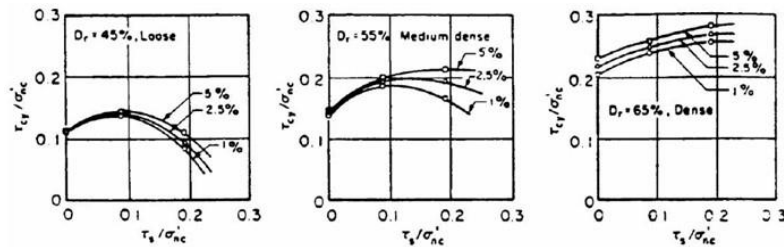


Fig 1.15 Effect of initial static stress on the cyclic stress ratio causing several levels of deformation in ten cycles (Vaid and Chern, 1983).

#### 1.5.4 Stress history

Another important parameter that could lead a soil deposit to liquefaction is the stress condition and density prior the earthquake. Finn et al (1970) show that when a sample of sand is subjected to a small shear deformation before applying cyclic loading, its resistance to liquefaction increases. However, if this pre-deformation is significant, its resistance reduces. A typical such property is the liquefaction strength of sandy soils. Shakings as a result of earthquakes is likely to improve the interlocking of sand grains. Careful analyses of liquefaction case histories have revealed that soils in regions prone to earthquakes have a higher resistance to liquefaction (Ishihara et al., 2015; Towhata et al., 2017; Yasuda et al., 2012). Dobry et al. (2014) compared young sand deposits in two sites in California where the sedimentation process at deposition created similar types of sand fabric. Heidari and Andrus (2012) also demonstrated the effects of small pre-shaking in enhancing the resistance of soils to liquefaction, based on case histories.

Seed et al (1977) in their experimental tests, applied cyclic loading to two different sample, one of which was preloaded; the experimental results demonstrate that the preloaded sample resistance to liquefaction was 1.5 times greater than that of sand without preloading (Fig.1.16).

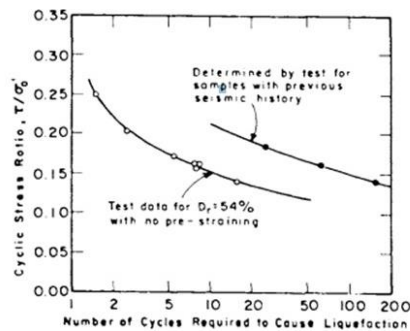
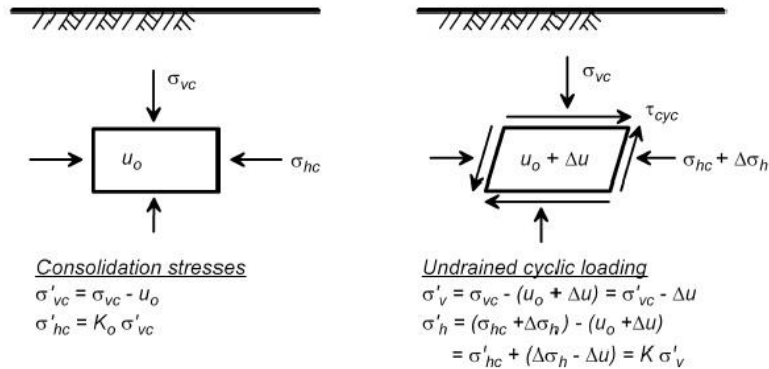


Fig 1.16 Effect of Previous Seismic History on Liquefaction Potential (Seed, et al. 1977).

## 1.6 Liquefaction triggering

If “predisponding” factors are related to the physical and mechanical characteristics of the soils and define their susceptibility (vulnerability) to the phenomenon, the “triggering” factors depend on the seismicity of the area in which the site is located (“danger”) and quantify the intensity of the seismic action necessary to activate the phenomenon (“triggering”).

During a seismic event, a soil element is subjected to dynamic loading (Fig.1.17) which can be described by means of released energy during it occurs. Even if mean factors affecting seismic intensity on the ground are spatial geometry, hypocentral distance and the way how wave is transmitted through rock, the response of site is a function of its own stiffness and damping properties.



**Fig 1.17 Schematic representation of static and dynamic stress**

## 1.7 Liquefaction severity index

A natural hazard means the probability of occurrence within a specified period of time and within a given area of a potentially damaging phenomenon. Risk means the degree of loss to a given element or set of elements at risk resulting from the occurrence of a natural phenomenon of given magnitude (Varnes 1984). The intensity of the liquefaction phenomenon and the effects on the stability of the foundation soil and the structures and infrastructure that exist on could be assess with liquefaction severity index, indicating the cumulative effect of liquefiable layers in the same deposit:

- Liquefaction Potential Index, LPI (Table 1-2), defined by Iwasaki in 1978, based on the width and depth of the liquefiable areas and on historical cases of liquefaction:

$$LPI = \int_0^{z_{crit}} F(z) * w(z) dz \quad \text{Eq. 1-1}$$

- $z_{crit}$  = maximum depth at with layer could be considered liquefiable; generally, 20m is the limit.
- $w(z)$  = function of depth, not linear; maximum value above the ground and zero in depth;
- $F(z)$  = function of Factor of Safety, from 0 to 1.

<b>LPI</b>	<b>Liquefaction risk</b>
LPI=0	Null
0<LPI≤2	Low
2<LPI≤5	Moderate
5<LPI≤15	High
LPI>15	Very high

**Table 1-2 The classes of liquefaction potential, according to the proposal Sonmez (2003)**

In addition, Toprak and Holzer in 2003, proposed a correlation of LPI values with the severity of surface effects for the Monterey Bay region during the Loma Prieta earthquake which result to be consistent with the severity scale proposed by Iwasaki 1982 (severe liquefaction likely for LPI>15 and not likely at LPI<5).

If probabilistic approach is followed, a probabilistic index is determined (Table 1-3):

$$LPbI = \int_0^{z_{crit}} P_L(z) * w(z) dz \quad \text{Eq. 1-2}$$

<b>LPbI</b>	<b>Probability</b>
LPbI≥85	Almost certain that it will liquefy
65≤LPbI≤85	Very likely to liquefy
35≤LPbI<65	Liquefaction and no liquefaction are equally likely
15≤LPbI<15	Unlikely to liquefy
LPbI<15	Almost certain that it will not liquefy

**Table 1-3 LPbI classification accordig to Chen e Juang, 2000**

- Liquefaction Settlement Index, LSI, provides us with an estimate of the subsidence occurring post-earthquake and thus of a reconsolidation of liquefiable layers:

$$LSI = \int_0^{z_{crit}} \varepsilon_v * dz \quad \text{Eq. 1-3}$$

- $z_{crit}$  = maximum depth at which layer could be considered liquefiable; generally, 20m is the limit;
- $\varepsilon_v$  = the calculated post-liquefaction volumetric reconsolidation strain for the soil sublayer  $z$  (Zhang et al. 2002).

- Lateral Spreading Index, LSpI, provides an estimate of the maximum potential horizontal displacement considering the maximum earthquake-induced shear deformation,  $Y_{max}$ :

$$LSpI = \int_0^{z_{crit}} Y_{max} * dz \quad \text{Eq. 1-4}$$

- Liquefaction severity number, LSN, defined by Tonkin & Taylor (2013) following the 2010-2011 New Zealand earthquake sequence:

$$LSN = 1000 \int_0^{20} \frac{\varepsilon_v}{z} \varepsilon_v * dz \quad \text{Eq. 1-5}$$

- $\varepsilon_v$  = the calculated post-liquefaction volumetric reconsolidation strain and entered as a decimal, and  $z$  is the depth below the ground surface in meters.

## Chapter 2

### 2 Methodological approach to liquefaction evaluation

#### 2.1 Approaches to task

Liquefaction is a phenomenon in which the strength and stiffness of soil is reduced by earthquake shaking or other dynamic loadings, leading soil to assume the mechanical behaviour characteristic of a liquid. Liquefaction has been responsible for tremendous amount of damage in historical earthquakes around the world, such as tilting or overturning of buildings, flow failure of steeply sloping ground such as dams and lateral spreading of softly to moderately sloping ground. For these reasons, dynamic analysis to predict soil behaviour in geotechnical structure has aroused much interest in last decades, from different points of view.

In this work, a procedure of analysis has been followed, based on two real cases of study; the main equipment for the geo-mechanical characterization of soils under dynamic stresses have been evaluated and simultaneously constitutive models has been analysed to better simulate liquefaction susceptibility of materials.

This project is built to define which is the best way to obtain an engineering forecast in liquefaction field, through the answer the following questions:

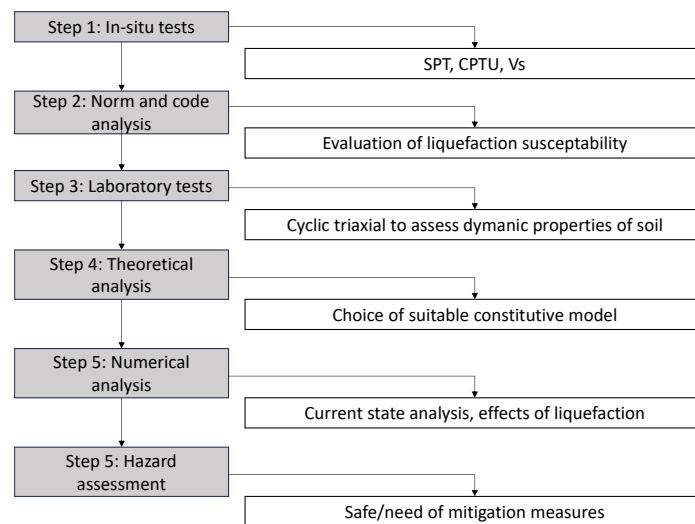
- 1) How can the phenomenon of liquefaction be reproduced in the laboratory?
- 2) Which are the best experimental tests?
- 3) Which are the adequate models to simulate soil liquefaction?
- 4) Is it possible to reproduce the tensile-deformative behaviour of geotechnical works susceptible to liquefaction with predictive numerical analyses?

The answer to the above questions will be based on two real cases which fully describe the listed issues.

Starting from this framework, it is interesting the synergy achievable with the company Matest in the development of new technologies in the field of dynamic triaxial and laboratory tests related to liquefaction, with

the aim of improving existing systems and implementing new equipment, applying the knowledge acquired in the study of the real cases dealt with in this project.

The research methodology adopted to investigate the objectives of the project is based on multiple kind of investigations: experimental (in-situ and in laboratory), theoretical (constitutive models) and numerical (finite element method).



**Fig 2.1 Flow chart of the methodological approach.**

A complete methodological approach is made of the six steps shown in Fig.2.1. In literature, Step#1 and #2 are usually considered as simplified approach, the others from Step #3 to #6 as advanced approach.

Generally, liquefaction evaluation is performed in two main steps: 1) in situ investigation or laboratory test analysis is used to evaluate the occurrence of soil liquefaction at a site during the design earthquake; 2) if the site is liquefied, the effects of liquefaction hazards on structures are evaluated through advanced mathematical constitutive models properly calibrated to predict liquefaction effects using numerical simulation. This work emphasizes the synergy between in situ, laboratory experimental analyses, and numerical simulations as a complete methodological approach. It offers a robust framework for evaluating liquefaction susceptibility and enables the design of targeted mitigation strategies to enhance the stability of geotechnical structures involved.

The novelty of this thesis is to apply the complete approach from step 1 to step 6 on two case studies.

## **2.2 Experimental approach**

In situ geognostic tests (CPTu, SPT) allow us estimating the lithologies involved, determining a safety factor for further analysis by means of laboratory machines to characterize the soil behaviour under dynamic stresses. Both SPT and CPTu present advantages and disadvantages for which further analyses are needed if the site is exposed to the danger of liquefaction, causing damage in structures. The national technical standards for construction (NTC18) suggests a list of requirements to assess liquefaction potential of the site. Their use is recommended at the design stage, to exclude (or consider necessary) any subsequent verification of liquefaction and to select the sites where to deepen the investigations through the engineering methods.

In this transition from simplified methods to advanced (engineering) methods, the understanding of the results from in situ tests, allows us to select the collected material to be tested in laboratory, by checking the safety factor ( $FS < 1$  or  $FS < 1.2$ ).

Cyclic triaxial tests are the most common tests performed to assess the cyclic behaviour of soil with regard of liquefaction, along with the cyclic simple shear test. In order to reproduce in situ conditions obtained by the combination of parameters obtained by SPT or CPTu (or both) and site seismic conditions, a series of cyclic triaxial tests have been performed. Laboratory tests have a dual purpose:

- assess liquefaction risk under determined seismic stresses: CPT test allows to check CRR (Cyclic resistance ratio) and CSR (Cyclic stress ratio) curve, an important starting point to define the cyclic loading to be applied to the sample during cyclic triaxial test
- obtain curves allowing the mathematical constitutive models to be calibrated: cyclic triaxial test allows us to assess one representative sample of the area under investigation; this is necessary for further analysis, it means constitutive model calibration to reproduce mathematically the real behaviour of the soil, with no dependence of the sample.



### **2.3 Theoretical and numerical approach**

Areas resulting positive to liquefaction analysis based geognostic test and NTC18 constitute a hazard quantified according to structure position and importance. Since engineering solutions aimed at securing those areas have significant costs, it's suggested to perform 2D dynamic modeling which will confirm or not the actual risk of liquefaction. Further considerations could be done since modelling based on geognostic test could underestimate or overestimate (in most of cases) the risk of liquefaction. For this reason, a modeling that uses constitutive models calibrated from real laboratory tests is chosen.

In order to dynamically simulate the behaviour of the soil and perform the tests to the liquefaction two main constitutive models have been used:

- The Mohr-Coulomb model simulates elastoplastic behavior. This behavioral hypothesis shows reliable results for nonlinear analysis of most soils.

- The Modified UBCSAND model simulates the trend of the effective stress for the prediction of the liquefaction behavior of the sands during a dynamic load (earthquake, human vibrations, ... ).

From a seismic point of view, according to the standard, a series of accelerograms is taken into account, along with a definition of project earthquake, to simulate correctly the seismic activity of the area.

Finite element model (FEM) is able to predict soil behaviour, in terms of expected deformations and subsidence on the work at the time of the earthquake along with pore pressure excess generated, highlighting the areas in which high liquefaction risk are detected, choosing better engineering solutions and therefore trying to reduce costs, if possible.

## Chapter 3

### 3 In situ investigations to assess liquefaction effects

#### 3.1 Introduction

In order to assess the causes of dynamic loading with respect to liquefaction, “simplified method” (Idriss & Seed, 1971) has been developed. This approach is the most commonly used technique in most parts of the world for estimating soil liquefaction due to earthquake loading. In this approach, there are two main terms, namely; cyclic shear stress caused by seismically generated loading and another cyclic shear stress related to liquefaction resistance (Seed & Idriss, 1971): “cyclic stress ratio” (CSR) is representative of loading term while “cyclic resistance ratio” (CRR) is an indicator of resistance term. The essential point of liquefaction assessment is the comparison of cyclic strength (CRR) and mobilized shear stress (CSR), which is presented in the equation:

$$FS = \frac{CRR}{CSR} \quad \text{Eq. 3-1}$$

#### 3.2 CSR - Earthquake-induced cyclic stress ratio

The determination of CSR is initially proposed by Seed and Idriss (1971). It depends on the maximum horizontal acceleration of the ground in the earthquake and several other parameters. The earthquake-induced CSR, at a given depth,  $z$ , within the soil profile, is usually expressed as a representative value (or equivalent uniform value) equal to 65% of the maximum cyclic shear stress ratio:

$$CSR = \frac{\tau_{media}}{\sigma'_{v0}} = \frac{0.65 * \tau_{max}}{\sigma'_{v0}} = 0.65 * \frac{a_{max}}{g} * \frac{\sigma_{v0}}{\sigma'_{v0}} * r_d \quad \text{Eq. 3-2}$$

- $\tau_{max}$  is the maximum cyclic shear stress;

- $a_{max}$ <sup>1</sup> is defined as the maximum acceleration peak expected at the surface for the seismic event considered;
- $\sigma_{v0}$  and  $\sigma'_{v0}$  are the total and effective vertical overburden stresses, respectively;
- $r_d$ <sup>2</sup> is a stress-reduction factor. For routine practice the values of  $r_d$  are estimated from the chart by Seed and Idriss as shown in Fig.3.1; this is defined as a parameter describing the ratio of cyclic stress for a flexible soil column to the cyclic stress for a rigid column:

$$r_d = \frac{(\tau_{max})_{deformable\ soil}}{(\tau_{max})_{rigid\ soil}} \quad \text{Eq. 3-3}$$

It is a function of the depth,  $z$ , and, in more recent formulations (Boulanger and Idriss, 2014), also of the moment magnitude of the seismic event considered,  $M_w$ , and of the peak horizontal maximum acceleration induced at the surface by that event,  $a_{max}$ .

---

<sup>1</sup> it is obtained from the analysis of the basic seismic hazard and quantifying the amplifying effects of the deposit (stratigraphic/topographic). The basic seismic hazard gives the value of the maximum expected horizontal acceleration,  $a_g$  in free field conditions on a rigid reference site with a horizontal topographic surface. The influence of stratigraphy ( $S_s$ ) and topography ( $S_T$ ) is quantified by empirical correlations:  $a_{max} = a_g * S_s * S_T$

<sup>2</sup> Stress-reduction factor or "non-linear shear mass participation factor" is a parameter defined empirically, linked to the variation of the stresses induced by the earthquake considering the deformability of the ground. Being a parameter calculated empirically, there are several interpretations depending on the simplified method used:  $r_d = f(z, M_w, a_{max})$

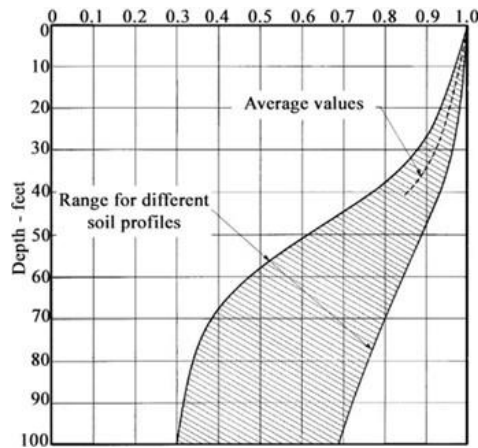


Fig 3.1 Stress reduction coefficient,  $r_d$ , according to Seed & Idriss (1971)

### 3.3 CRR- Cyclic resistance ratio

The CRR parameter is defined as the cyclic shear resistance of the ground,  $\tau_{cyc}$ , at a certain depth. It is obtained from empirical correlations based on the observation of cases of liquefaction linked to historical seismic events, starting from the Anchorage and Niigata earthquakes (1964).

First of all, a parameter, R, can be easily deduced from geotechnical tests on site (or in the laboratory) of current use, subsequently normalized  $R_{1N}$  and, where appropriate, corrected  $R_{1N_c}$  so that it can be representative of the liquefaction resistance of the soil.

In order to calculate R, on-site tests are generally used:

- from CPT tests with electric tip (or CPTU with piezocone) the peak resistance value  $q_c$  is obtained;
- SPT tests give the number of  $N_{SPT}$  blows,
- from down-hole and cross-hole tests the speed of the shear wave ( $V_s$ ) is obtained;

Generally, the methodologies based on SPT and CPT are mostly preferred for liquefaction resistance assessment, because of there are more extensive databases and experience, however,  $V_s$  have been becoming more familiar in the recent years.

Plotting the parameter R with respect to the seismic action identified with CSR, there is a curve that distinguishes the cases of liquefaction present from those in which the phenomenon has not occurred (Fig.3.2).

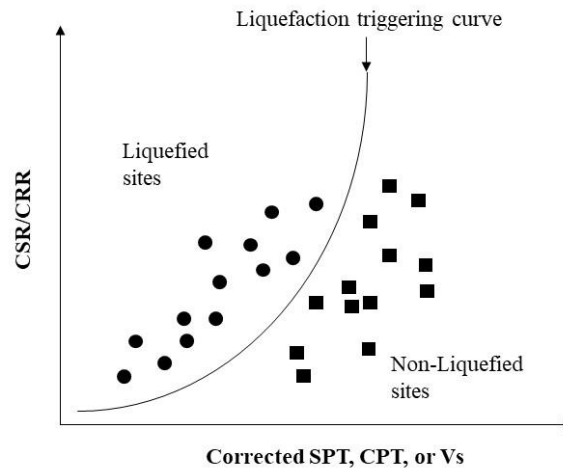


Fig 3.2 Liquefaction resistance curve

Initially, the liquefaction curves were obtained from a fairly homogeneous database (based on historical earthquakes), with clean sands (therefore with a percentage of fine material less than 5%) and values of  $M_w = 7.5$ . Corrective factors have been introduced in order to apply these correlations to different materials and boundary conditions.

#### ➤ Magnitude Scale Factor MSF

Generally, it is assumed as a value of  $M_w = 7.5$  but by grouping the data in relation to the energy of the seismic event that has activated (or not activated) the liquefaction, in classes of magnitude, it's possible to obtain different curves of resistance to liquefaction: for the same measured, normalised and corrected parameter R, resistance values decrease as the magnitude increases.

With this regard, CRR is corrected through the "Magnitude scale factor (MSF)", according to the following equation:

$$CRR_{M_w} = MSF * CRR_{M_w=7.5} \quad \text{Eq. 3-4}$$

MSF depends very much on the type of simplified model used, depending on the authors chosen (Fig.3.3).

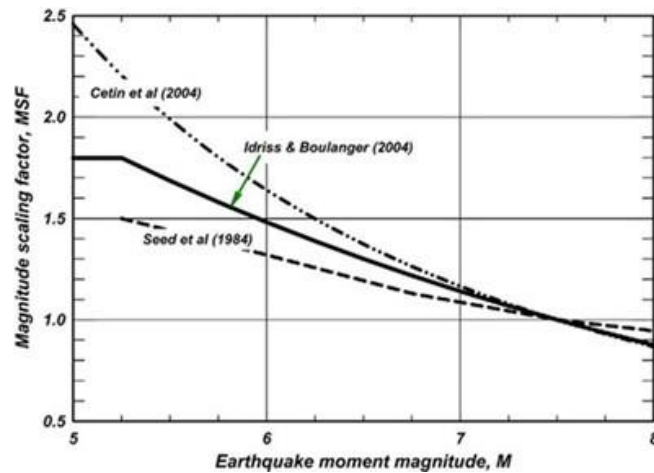


Fig 3.3 Magnitude scaling factors used by Seed et al. (1984), by Cetin et al. (2004), and by Idriss and Boulanger (2004)

➤ **Degree of saturation**

Generally, the phenomena of liquefaction occur in completely saturated soils, under water table, ( $S=1$ ) Skempton factor  $B=1$  ( $>0.9$ ). It may happen, however, that this condition is not completely satisfied, because of an oscillation of the water table itself for example; in these conditions, liquefaction can still occur, although the resistance to liquefaction is greater. Numerous studies have also revealed that partially saturated soil exhibits greater resistance to liquefaction than fully saturated soil depending on the degree of saturation (Sherif et al. 1977; Yoshimi et al. 1989; Grozic et al. 2000; Tsukamoto et al. 2002; Nakazawa et al. 2004; Okamura et al. 2006; Seid-Karbasi and Byrne 2006; Hatanaka and Masuda 2008). To overcome this problem, a corrective factor has been introduced (Fig.3.4):

$$CRR_S = K_S * CRR_{S=1} \qquad \text{Eq. 3-5}$$

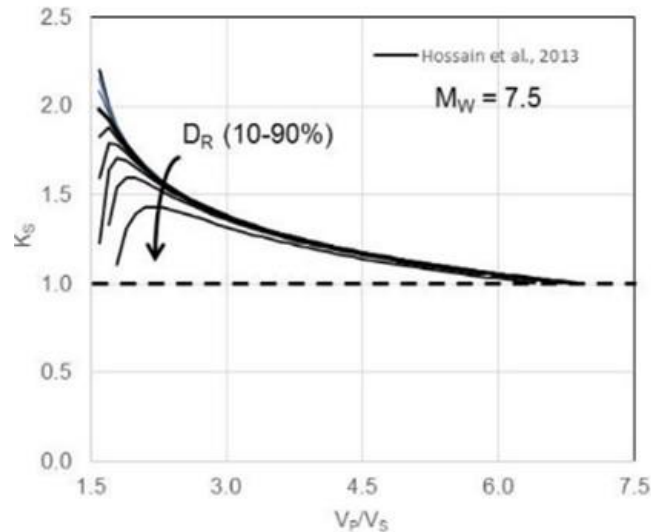


Fig 3.4 Correction factor  $K_S$  by Hossain et al., 2013

This correction factor should therefore be greater than 1 for  $S < 1$  and equal to 1 for  $S = 1$ .

➤ **Effective vertical stress**

Generally, cases of liquefaction in the literature occur at depths below 10m, with relative effective vertical stresses equal to 100kPa (1atm). The empirical correlations in the literature refer to this effective stress value, so a correction is provided to obtain CRR at the actual depth (and therefore vertical stress) to be investigated, also taking into account the initial conditions of the soil and its tensional history:

$$CRR_{\sigma'_{V0}} = K_{\sigma} * CRR_{\sigma'_{V0}=1} \quad \text{Eq. 3-6}$$

The corrective factor  $K_{\sigma}$  depends on the initial conditions of soil and on the tensional history (for example the degree of consolidation, OCR).

It is less than 1 for values of  $\sigma'_{V0} > 1$ , while it is taken precautionarily equal to 1 for lower values. Some authors, such as Boulanger and Idriss (2004), take the value 1.1 as the upper limit for K (Fig.3.5)

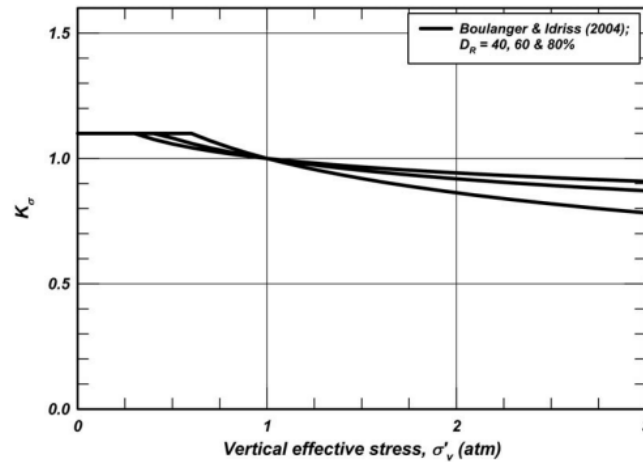


Fig 3.5  $K_{\sigma}$  values recommended by Idriss and Boulanger (2008) based on the relationships by Boulanger and Idriss (2004) for  $D_R = 40\%$ ,  $60\%$ , and  $80\%$ .

➤ **Effect of static shear stresses on cyclic strength**

The cyclic resistance of saturated sand or clay is affected by the presence of an initial static shear stress, as has been shown through numerous laboratory and physical modeling studies. These effects have been presented differently for sands and clays due to their differences in engineering behaviours.

The empirical correlations provided by the various authors are based on cases of liquefaction in the absence of loads, then in flat and free field conditions. Otherwise, in the presence of slight slopes or overloads (foundations for example), the CRR value should be corrected by a correction factor,  $K_{\alpha}$ , taking into account the initial stress state of the soil, through parameter  $\alpha = \tau_{st}/\sigma'_{v0}$  (the ratio between  $\tau_{st}$  related to initial static shear stresses pre-existing at earthquake and  $\sigma'_{v0}$  vertical effective stress) and the relative density. A correction factor is presented in the equation below:

$$CRR_{\alpha} = K_{\alpha} * CRR_{\alpha=0} \quad \text{Eq. 3-7}$$

It should be emphasized that the slopes and overloads that can be correlated with this parameter tend to be mild, since under worst-case



conditions (greater slopes and overloads) the liquefaction phenomenon would follow “flow liquefaction” patterns, which cannot be represented by the simplified methods under consideration. Example of curves proposed by Idriss and Boulanger are shown in Fig.3.6.

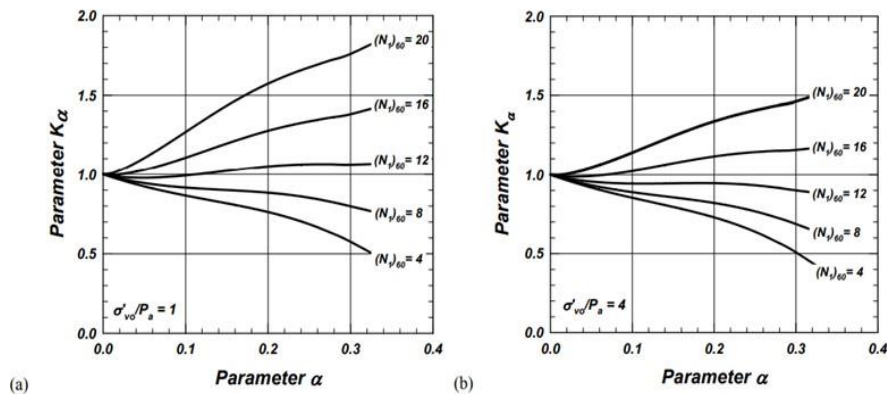


Fig 3.6 Variation of the static shear stress correction factor  $K_\alpha$  for sands at: (a) an effective overburden stress of 1 atm, and (b) an effective overburden stress of 4 atm (Idriss and Boulanger 2003)

### ➤ Soil deposit age

Data in the literature provide additional information about the liquefaction resistance: the age of the deposit may be important related to the amount of cementation which results in increased resistance. Empirical correlations are based on recent Holocene soils, but a factor is presented as a CRR correction:

$$CRR_{DR} = K_{DR} * CRR \quad \text{Eq. 3-8}$$

Hayati and Andrus (2009) have proposed a correlation for estimating  $K_{DR}$ :

$$K_{DR} = 0.13 * \log(t) + 0.83 \quad \text{Eq. 3-9}$$

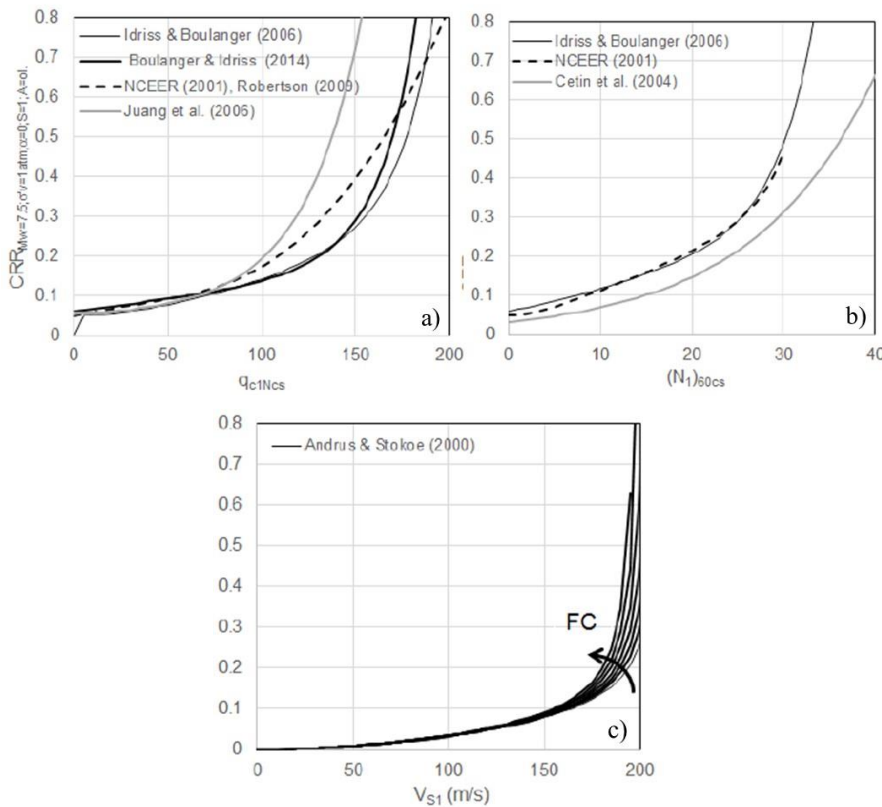
where  $t$  = geotechnical age of deposit in years. The geotechnical age of the deposit is the time because the most recent critical disturbance of the soil fabric, e.g., the time since the last episode of moderate-to-severe liquefaction that resulted in the loss of the particles' mechanical interlocking or breaking of chemical cementation at particles contacts, thus resetting the aging clock of the deposit (Rahimi et al., 2020).

Considering all the correction factors presented, cyclic resistance ratio CRR will finally be calculated as follows:

$$CRR = MSF * K_{\sigma} * K_{\alpha} * K_S * K_A * CRR_C \quad \text{Eq. 3-10}$$

$$CRR_C = CRR_{Mw=7.5; \sigma'_{V0}=1 \text{ atm}; \alpha=0; S=1; A=ol}$$

Where  $CRR_{Mw=7.5; \sigma'_{V0}=1 \text{ atm}; \alpha=0; S=1; A=ol}$  is a function of R parameter measured in site, normalized (ex.  $q_{c1N}$ ,  $(N_1)_{60}$ ,  $V_S$ ) and of the fine content, FC. Various correlations are provided by different authors, according to the simplified method used (it means the database of liquefaction cases assumed and the type of mathematical model adopted for the determination of the curve discriminated between cases of liquefaction and non-liquefaction). Fig. 3.7 shows some of the most recurring correlations used in the simplified methods that will be described later.



**Fig 3.7**  $CRR_{Mw=7.5; \sigma'_{V0}=1 \text{ atm}; \alpha=0; S=1; A=ol}$  for common simplified method: (a) CPT, (b) SPT, (c) Vs

### 3.3.1 Standard penetration test

Standard Penetration Test (Fig.3.8), SPT, consists in driving a standard thick-walled sample tube into the ground at the bottom of a borehole by blows from a slide hammer with standard weight and falling distance. The sample tube is driven 150 mm into the ground and then the number of blows needed for the tube to penetrate each 150 mm (6 in) up to a depth of 450 mm (18 in) is recorded.

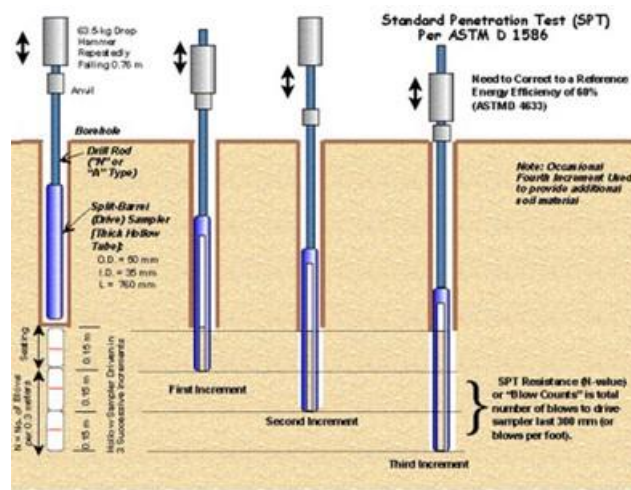


Fig 3.8 Schematic description of SPT test

The sum of the number of blows required for the second and third 6 in. of penetration is reported as SPT blow-count value, commonly termed "standard penetration resistance" or the "N-value", which should be normalized:

$$N_{60} = C_E * C_B * C_R * C_S * N_{SPT} \quad \text{Eq. 3-11}$$

The sample value is corrected by a series of parameters described below:

➤  $C_E = \frac{ER_M}{60}$  is related to the energy ratio  $ER_M$  released during the test;

Values suggested by Cetin (2018) are listed in Table 3-1:

Equipment	Approximate ER**	$C_E$ **
Safety Hammer	0.4 to 0.75	0.7 to 1.2
Donut Hammer	0.3 to 0.6	0.5 to 1.0
Donut Hammer*	0.7 to 0.85	1.1 to 1.4
Automatic-Trip Hammer (Donut or Safety Type)	0.5 to 0.8	0.8 to 1.4

\*With special Japanese "throw" release

\*\*The ranges shown can vary if equipment and/or monitoring and procedures are not good

**Table 3-1 Recommended corrections for SPT equipment (Cetin et al. 2018)**

- $C_B = 1.0 - 1.15$  is a correction factor related to the borehole diameter; value in accordance with to NCEER/NSF, Youd et al. (2001) are presented (Table 3-2):

Borehole diameter	$C_B$ **
65 to 115mm	1.00
150mm	1.05
200mm	1.15

**Table 3-2 Correction factor for borehole diameter (NCEER 2001)**

- $C_R = 0.75 - 1.0$  is a correction factor for the rod length; The rod length is the sum of the rod stick-up length (length above the ground surface) and the sampling depth. The values of  $C_R$  recommended in NCEER/NSF, Youd et al. (2001) given before by Seed, H. B. et al. (1984) and Skempton, A. W. (1986) are listed in the Table 3-3.

Rod length	$C_R$
Rod length < 3 m	0.75
Rod length 3-4 m	0.80
Rod length 4-6 m	0.85
Rod length 6-10 m	0.95
Rod length 10-30 m	1.00

**Table 3-3 Correction factor for Rod length (NCEER 2001)**

- $C_S = 1.0 - 1.3$  is the correction for no standardized sampler configuration. For standard sampler are set equal to unity. However, for samplers with an indented space for interior liners, but with liners omitted during sampling Seed, H. B. et al. (1985) recommend used the following expression:

$$C_S = 1 + \frac{(N_1)_{60}}{100} \quad \text{Eq. 3-12}$$

For  $10 \leq (N_1)_{60} \leq 30$

Sampling method	$C_s$
Standard sampler	1.0
Sampler without liners	1.1 to 1.3

**Table 3-4 Correction factor for sampling method (NCEER 2001)**

SPT N-values will increase with increasing effective overburden stress, and therefore an overburden stress correction factor should be considering Seed, H. B., and Idriss, I. M. (1982).

$$(N_1)_{60} = N_{60} * C_N \quad \text{Eq. 3-13}$$

This factor is commonly calculated from equation suggested by Liao, S. S. C. and Whitman, R. V. (1986):

$$C_N = \left(\frac{p_a}{\sigma'_{v0}}\right)^n \leq 1.7 \quad \text{Eq. 3-14}$$

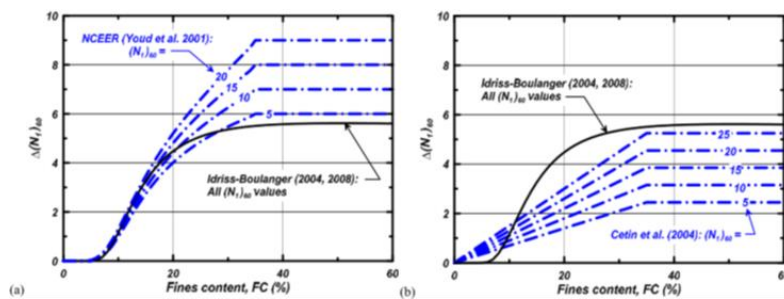
- $C_N$  is a normalization factor with respect to lithostatic stress ( $\sigma'_{v0}$ ), approximately 100 kPa (1 atm);

-  $n$  is a coefficient related to the type of soil ( $n = 1$  for clay,  $n = 0.5$  for sand) and to the relative density  $D_R$ .

$C_N$  should not exceed a value of 1.7 according to NCEER/NSF, Youd et al. (2001). There are other researches that have been recommended limits of 1.6 to 2.0 for  $C_N$ , as Cetin, K. O. et al. (2004), who suggest 1.6 as maximum value.

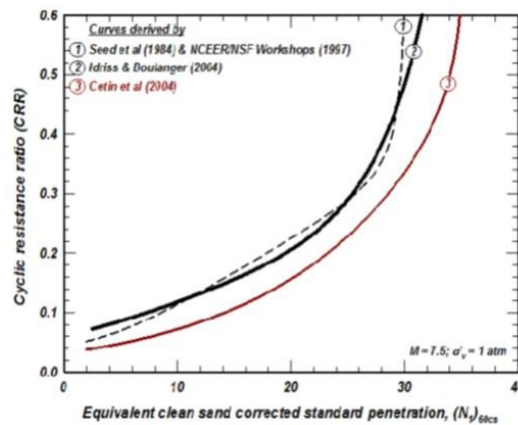
First recognized by Seed, H. B. et al. (1984), there is an increase of CRR with fines content, FC, where they reproduced curves of CRR for various

fines contents; then, a revised correction for fines contents was developed by NCEER/NSF, Youd et al. (2001); another proposed correlation for fines contents is suggested by Idriss, I. M. and Boulanger, R. W. (2004, 2008) and it is expressed in terms of equivalent clean sand ( $N_1$ )<sub>60cs</sub>. The resulting relationships are illustrated in Fig.3.9 along with: (a) the equivalent clean sand adjustments recommended by NCEER/NSF, Youd et al. (2001), based on the curves originally published by Seed, H. B. et al. (1984), and (b) the equivalent clean sand adjustments recommended in Cetin, K. O et al. (2004).



**Fig 3.9 Variation of  $\Delta(N_1)_{60}$  with fines content**

The function  $CRR(M=7.5, \sigma_v' = 1 \text{ atm and } (N_1)_{60cs})$  is shown in Fig.3.10, with the three liquefaction triggering correlations:



**Fig 3.10 SPT-based liquefaction triggering curves components**

### 3.3.2 Cone penetration test

The cone penetration test (CPT) (Fig.3.11) is a common in situ testing method used to determine the geotechnical engineering properties of soils and assessing subsurface stratigraphy. The testing apparatus consists of an instrumented still cone having a tip facing down, with a usual apex angle of  $60^\circ$  and cross-section area of  $1000 \text{ mm}^2$ . The cone is attached to an internal still rod than can run inside an outer hollow rod, which itself is attached to a sleeve.

Test consists of pushing a cylindrical steel cone shaped probe into the ground at a constant velocity with rate of  $20 \text{ mm/s}$  and measuring the resistance to penetration of the cone and of a surface sleeve. The cone resistance  $q_c$  is the force acting on the cone  $Q_c$  divided on the projected area of the cone  $A_c$ . The sleeve friction resistance  $f_s$  is the frictional force that turns on the friction sleeve,  $F_s$ , divided by its surface area,  $A_s$ . As well, the CPTu or piezocone allows us to measure the pore pressure.

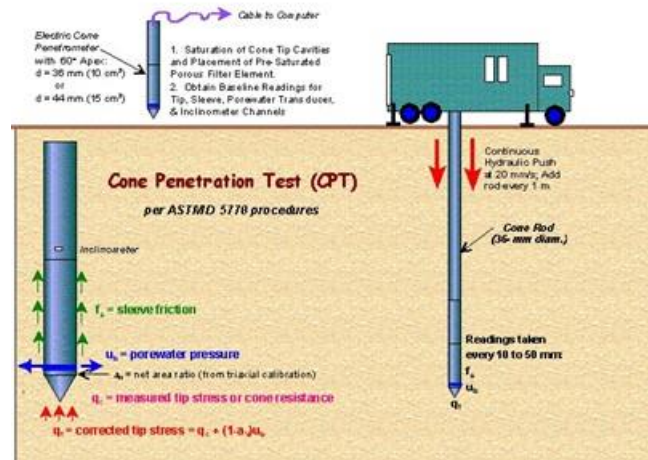


Fig 3.11 Schematic description of CPT test

The CPT has attracted more attention from many geotechnical researchers in the last 20 years since it is consistent, faster, and repeatable.

The development of CPT-based simplified methods came after the development of SPT-based methods. Many scholars (Robertson and Campanella, 1985; Seed and De Alba, 1986; Youd and Bennett, 1983; Kayen et al., 1992; Stark and Olsen, 1995) have proposed empirical

correlations between SPT and CPT penetration resistances to convert available SPT-based liquefaction triggering charts for use with CPT. Due to the lack of CPT case histories, the CPT-based cyclic resistance ratio (CRR) curves were developed based on those derived from SPT-based simplified methods or laboratory tests (Robertson, 1985; Seed and De Alba, 1986). With increasing numbers of CPT case histories, researchers (Shibata and Teparaksa, 1988; Stark and Olson, 1995; Suzuki et al., 1995) have developed CPT-based CRR curves following the framework of SPT-based simplified methods.

It should be noted that the current day of practice, three different updated methodologies are often being used to assess the potential of liquefaction trigger: Robertson (2009), Moss et al. (2006), Boulanger and Idriss (2016).

The CPT procedure requires normalization of tip resistance:

$$q_{c1N} = C_N * \left( \frac{q_c}{P_a} \right) \quad \text{Eq. 3-15}$$

$$C_N = \left( \frac{P_a}{\sigma'_{vo}} \right)^n$$

- $C_N$  = normalizing factor for cone penetration resistance;
- $P_a$  = 1 atm of pressure in the same units used for  $\sigma'_{vo}$ ;
- $n$  = exponent that varies with soil type (from 0.5 to 1)
- $q_c$  = field cone penetration resistance measured at the tip.

Different liquefaction strength curves, with increasing strength, at the same measured in situ and normalized value,  $q_{c1N}$ , as fine content increases could be obtained. As the case histories increase, adjustment to CRR curves has been done; Boulanger and Idriss proposed changes in the equivalent clean sand adjustment for the CPT. The deterministic version of the revised CPT-based correlation is shown in Fig.3.12 in terms of  $q_{c1N}$  for different values of FC, rather than in terms of the equivalent clean sand penetration resistances.



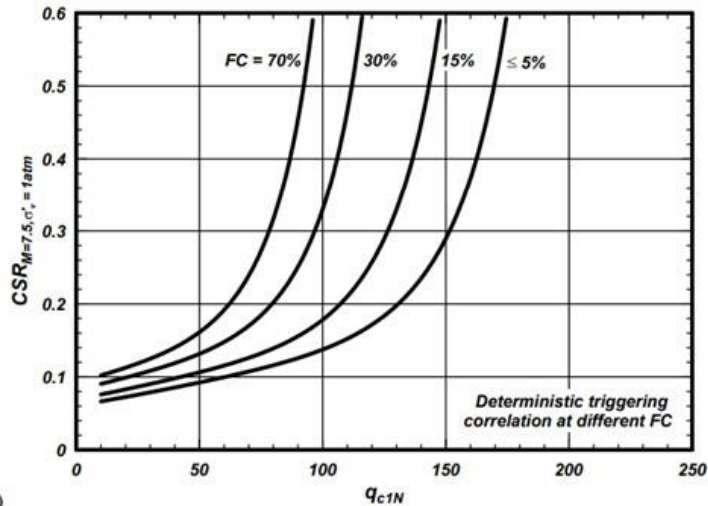


Fig 3.12 CPT -based soil liquefaction potential assessment and recommended boundary curves for soils with different fines content (FC).

Robertson introduced another concept, soil behavior type SBT which allows to differentiate soil types characterized as clays from soil types characterized as sands and silts. Robertson's SBT chart is a qualitative classification system that correlates soil behavior types with SPT N-values, overburden pressure, and soil type.

In the SBT chart, the  $I_c$  value refers to the "Soil Behavior Type Index," which combines parameters from the SPT N-value and the fines content of the soil, it helps classify soil behavior types into categories such as clay-like, silt-like, or sand-like, providing insights into how the soil might behave under various loading conditions. If the  $I_c$  calculated is  $>2.6$ , the soil is classified as clayey and is considered too clay-rich to liquefy, and the analysis is complete. However, soil samples should be retrieved and tested to confirm the soil type and liquefaction resistance.

If the calculated  $I_c$  is  $<2.6$ , the soil is most likely granular in nature.

$I_c$	Soil type
$I_c > 3.6$	Clay- organic soil
$2.95 < I_c \leq 3.6$	Clay- from silty clay to clay
$2.60 < I_c \leq 2.95$	Silt mixtures- from clayey silt to silty clay
$2.05 < I_c \leq 2.60$	Sand mixtures- from silty sand to sandy silt
$1.31 < I_c \leq 2.05$	Sand- from clean sand to silty sand
$I_c \leq 1.31$	From gravelly sand to dense sand

**Table 3-5 Robertson classification based on  $I_c$  value**

### 3.3.3 $V_s$

Over the past 30 years, in-situ measurement of small-strain shear-wave velocity  $V_s$  has been an alternative to the penetration-based approaches for compute liquefaction resistance due to it provides consistent information about soil resistance.

According to Andrus, R. D., and Stokoe, K. H., II. (2000), using  $V_s$  brings some advantages; of which can be mentioned the possibility of performed on small laboratory specimens, allowing direct comparisons between laboratory and field behavior; in addition, the measurements can be perform in soils that are hard to sample, such as gravelly soils where penetration tests may be unreliable. Moreover,  $V_s$  is a basic mechanical property of soil materials, directly related to small-strain shear modulus  $G_{max}$  by:

$$G_{max} = \rho V_s^2 \quad \text{Eq. 3-16}$$

where  $\rho$  = mass density of soil.

Making the contrast with  $V_s$ , SPT and CPT penetration methods have the advantage of correlating more directly with relative density, which has a strong effect on the cyclic behavior of saturated soil according to Idriss,

I.M. and Boulanger, R.W. (2008). On the other hand,  $V_s$  is considerably less sensitive to problems of soil compression and reduced penetration resistance when soil fines are present, compared with SPT and CPT penetration methods. Therefore,  $V_s$  requires only minor corrections for fines content (FC) (Kayen, R., et al. (2013)).

### 3.4 Simplified procedure to obtain Factor of safety

The calculation procedure and sequence are common to all methods and they are developed according to a series of easily implementable steps.

The required inputs are the following:

- the on-site measurements ( $q_c$  and  $f_s$ , or NSPT, or VS) and their depths from the campaign plane,  $z_i$ ;
- if available, the stratigraphy or index properties of the soil (particle size, fine content, FC, clay content, CF, plasticity index, PI) determined from samples taken from a nearby borehole or from the same borehole where the tests were carried out, in the case of SPT measures;
- the water table depth;
- seismic data related to the reference accelerogram, that is the maximum horizontal acceleration peak induced on the surface,  $a_{max}$ , and the moment magnitude, Mw.

The steps for the procedure are listed below:

- Correction, if required, of on-site measurements ( $q_c$ ,  $f_s$ , NSPT and  $V_s$ ).
- Calculation of total vertical stresses,  $\sigma_v$ , and effective,  $\sigma'_v$  with the exclusion, from subsequent calculations, of any strata above ground ( $z_i \leq z_w$ ).
- Exponential calculation  $n$  of the  $C_N$  normalization factor to be applied to the correct quantities to obtain the corresponding normalized values ( $q_{c1N}$ ,  $(N_1)_{60}$  and  $V_{s1}$ ). Any layer the lithology of which is not liquefiable (on the basis of the classification obtained indirectly from the available on-site measurements and/or using stratigraphy or laboratory measures, where available) are excluded from subsequent calculations.
- Calculation of the correction factor, if required, to be applied to  $q_{c1N}$  and  $(N_1)_{60}$  to determine the equivalent value for clean sands, that is, with a fine FC content of <5% (respectively  $q_{c1Ncs}$  and  $(N_1)_{60cs}$ ).
- Calculation of the cyclic resistance ratio  $CRR_{Mw=7.5; \sigma'_{v0}=1atm; \alpha=0; S=1; A=ol}$ . Exclusion from subsequent calculations of layers with values of resistance exceeding certain

predetermined thresholds ( $q_{c1Ncs} > 160$ ,  $(N_1)_{60cs} > 30$  and  $V_{s1} > 200$  m/s), considered not to be mechanically liquefiable.

- Calculation of corrective factors  $MSF$ ,  $K_\sigma$ ,  $K_S$ ,  $K_\alpha$ ,  $K_A$
- Calculation of reduction factor  $r_d$  of seismic action
- Calculation of the cyclic stress ratio CSR
- Calculation of the safety factor FSL or the probability of liquefaction, PL, from the value of FSL or directly.
- Deformation calculation  $\varepsilon_v$
- Calculation of  $\gamma_{max}$  deformations.

The assessment of the liquefaction hazard in the simplified procedure is undertaken by comparing the specific action effect at a given depth, designated as Cyclic Stress Ratio (CSR), induced by particular design earthquake with the soil resistance against liquefaction at that depth, designated as Cyclic Resistance Ratio (CRR). Hence, the ratio:

$$FSL = \frac{CRR}{CSR} = MSF * K_\sigma * K_\alpha * K_S * K_A * \frac{CRR_{Mw=7.5; \sigma'_{v0}=1atm; \alpha=0; S=1; A=ol}}{CSR} \quad \text{Eq. 3-17}$$

Where CRR is obtained by applying empirical correlations based on the parameter measured on site (suitably dimensioned and normalized) together with criteria for estimating corrective factors  $K_\sigma$ ,  $K_\alpha$ ,  $K_S$ ,  $K_A$ ,  $MSF$  to be assumed equal to one respectively for depths less than 10 m, initial static shear forces zero, saturated soils, Holocene soils and seismic events of magnitude 7.5.

## Chapter 4

### 4 Liquefaction susceptibility based on in-situ and norms: application on real case studies

In the following, the step 1 and 2 will be applied on the two case studies to evaluate liquefaction susceptibility. This is the equivalent to the so called “simplified procedure” proposed by Seed and Idriss in 1972 and it is considered a standard in professional analysis. In Italy it is performed according to the following regulatory context.

#### 4.1 Regulatory context

From the literature review, it can be seen that soil liquefaction can be induced by various reasons and circumstances. The damages caused by this phenomenon have a wide range of effects, causing damage not only economically but also culturally and humanly. Therefore, the regulations to prevent this phenomenon appear in the standards of many countries.

In Italy, NTC18 is the technical standard for construction that defines principles for the design, execution and testing of constructions, providing general safety criteria.

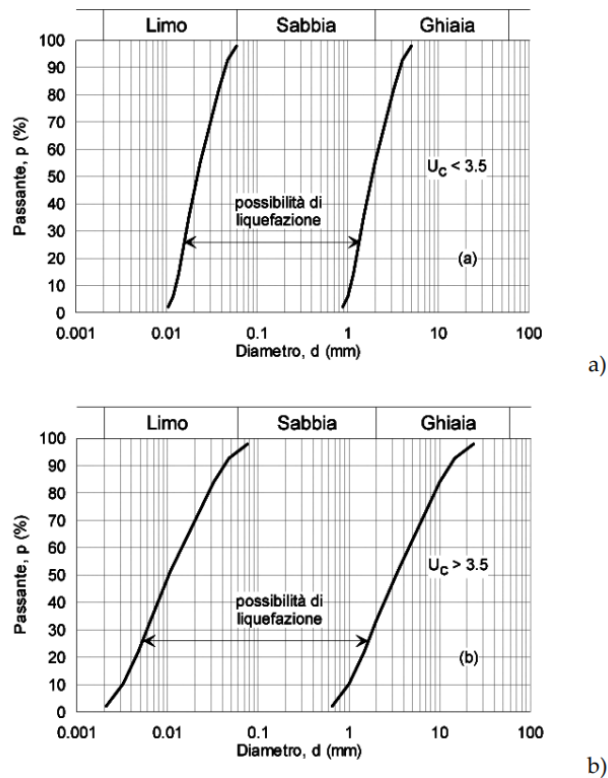
With regard to liquefaction, if the soil is susceptible to liquefaction and the consequent effects appear to affect the stability of slopes or structures, soil consolidation must be carried out and/or the load must be transferred to layers of likely to liquefy.

Chapter 7.11.3.4.2. is dedicated to liquefaction assessment. The liquefaction verification may be omitted where at least one of the following circumstances occurs:

- 1) Maximum expected accelerations at ground level in free field conditions less than 0.1g
- 2) Average seasonal water table depth greater than 15 m above ground level, for sub-horizontal ground level and structures with shallow foundations
- 3) Deposits consisting of clean sands with normalized penetrometric resistance  $(N_1)_{60} > 30$  or  $q_{c1Ncs} > 180$  where  $(N_1)_{60}$  is the value of resistance determined in dynamic

penetrometric tests (Standard Penetration Test) normalized to a vertical effective stress of 100 kPa and  $qc_{1N}$  is the value of resistance determined in static penetrometric tests (Cone Penetration Test) normalized to a vertical effective tension of 100 kPa;

- 4) Grain-size distribution outside the boundary shown in Fig.4.1. in the case of soils with uniformity coefficient  $U_c < 3.5$  and in the case of soils with uniformity coefficient  $U_c > 3.5$ .



**Fig 4.1 Grain-size distribution of liquefiable soil according to NTC18**

When none of the conditions are met and the foundation soil includes extensive layers or thick lenses of loose sand below the water table, the liquefaction safety coefficient at the depths where the potentially liquefiable soils are present must be evaluated. The liquefaction resistance can be evaluated based on the results of in situ tests or cyclic laboratory tests. The earthquake-induced stress is estimated through knowledge of the

expected maximum acceleration at the depth of interest. The maximum expected acceleration at the site can be estimated with the relationship:

$$a_{max} = a_g * S_S * S_T \quad \text{Eq. 4-1}$$

- $a_g$ =maximum expected horizontal acceleration at a rigid reference site.
- $S_S$ =a coefficient that consider the effect of stratigraphic amplification
- $S_T$ = a coefficient that consider the effect of topographic amplification

The design seismic action must be represented by time histories of accelerations. Accelerograms used in the analyses, no fewer than 7 in number, must be representative of the seismicity of the site, and their choice must be adequately justified.

The Standard requires analysis of the area through displacement method. The evaluation of stability conditions is carried out by comparing the displacement calculated for the critical collapse kinematism and the limit or threshold values of the displacement.

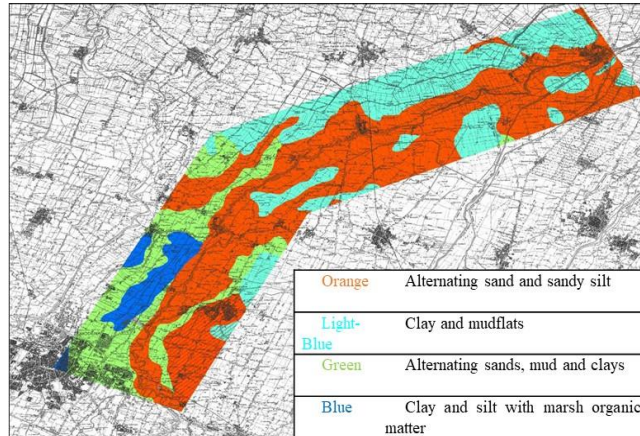
## **4.2 Case 1: Simulation of the dynamic behaviour of the Panaro embankments**

Following the structural and functional adjustment of the Panaro River embankment system (Province of Modena), a series of geognostic analyses (CPT, SCPTU) and geophysics analysis has been conducted to identify the main lithologies of the area and understand soil behaviour with respect to liquefaction phenomenon.

### **4.2.1 Geological and seismic setting**

The study area belongs entirely to the Po Valley and is in the Province of Modena. The lithologies encountered in outcrop and in the subsurface investigated, for the first 30 meters or so, consist of gravels (absent in the intervention areas), sands, silts and clays. The depositional environments belong to the conoid and floodplain.

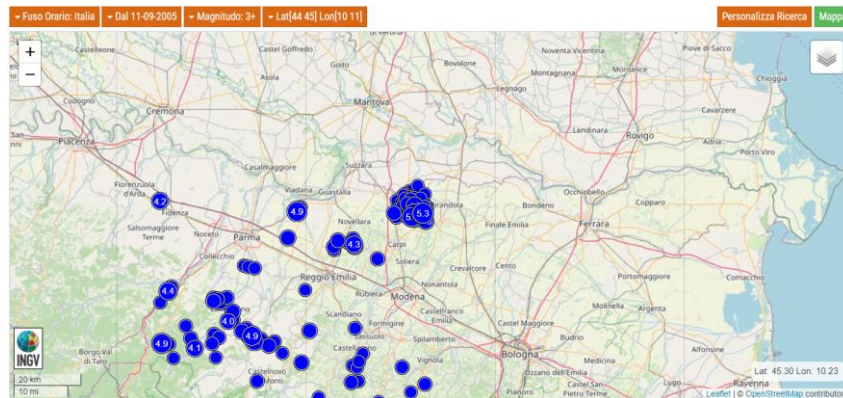
According to the CARG cartography of the area, different deposits are present (Fig.4.2):



**Fig 4.2 Deposition environment and lithologies (card 202-203 CARG)**

Regarding the water table depth, seasonality is extremely important, but generally its position is around 1-4 m; it's therefore plausible that if very rainy years or periods of intense and prolonged rains occur, the values of groundwater depth are very close to ground level.

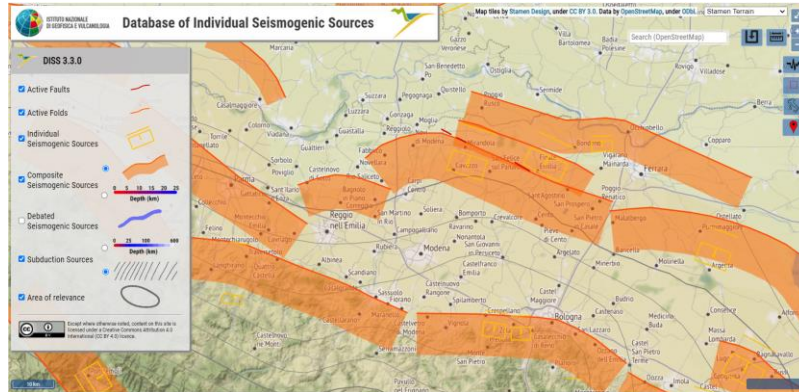
The area of interest has recorded numerous earthquakes with magnitude  $\geq 3$ , MCS scale (Locati, 2016) (Fig.4.3):



**Fig 4.3 Map of epicenters of major earthquakes with magnitude equal to or greater than 3 from 2005 to date (INGV, <http://cnt.rm.ingv.it/>)**

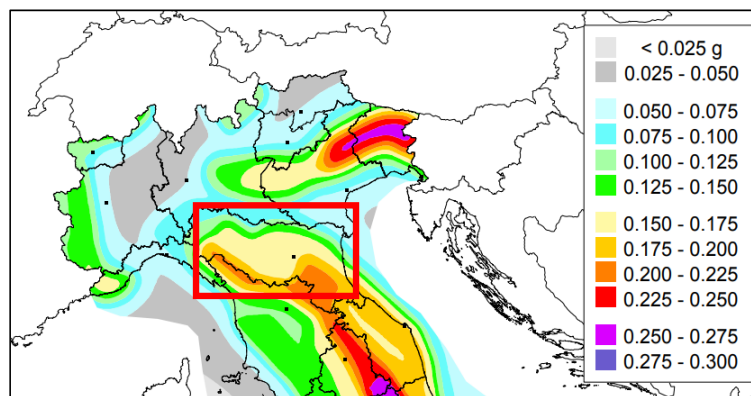
The seismogenic sources are described by the National Institute of Geophysics and Volcanology within the DISS3 Project (Fig.4.4):





**Fig 4.4 Seismic sources around the area of interest (INGV, <https://diss.ingv.it/diss330/dissmap.html> )**

In the northern part of the area, there are seismogenic sources classified as “ITCS049 Campeguine-Correggio” and “ITCS051: Novi-Poggio Renatico”; it means that earthquake magnitude of maximum 6.8 at epicentral depth 3-10 km can occur. In the southern part of the area, there are seismogenic sources classified as “ITCS047 “Castelvetro di Modena-Castel San Pietro Terme”; it means that earthquakes magnitude of maximum 6.8 at epicentral depth 3-10 km can occur. Generally, it’s important to define the basic seismic hazard of the area, checking the relative map at INGV site. It is needed to define peak acceleration values at ground for further analysis (Fig.4.5).



**Fig 4.5 Excerpt from the seismic hazard map (INGV, [http://zonesismiche.mi.ingv.it/documenti/mappa\\_opcm3519.pdf](http://zonesismiche.mi.ingv.it/documenti/mappa_opcm3519.pdf) )**

The area of interest falls in the class with  $0.150 < g < 0.175$ , according to Seismic hazard map of the national territory expressed in terms of

maximum ground acceleration with a 10% probability of exceedance in 50 years referring to rigid soils

#### 4.2.2 Geognostic investigations

For the geological, hydrogeological and seismic characterization of the area involved in this project, reference was made to a series of on-site tests, following the simplified procedure for liquefaction assessment:

- n°12 boreholes at depth of 20-30 m from ground level;
- n°65 CPT up to the depth of 20 m from ground level;
- n°5 SPT up to the depth of 30 m from ground level.
- electric tomography;
- seismic surface refraction.

The depth of 30 meters from ground level, allows us to calculate the parameter Vs30, fundamental for further analysis (NTC18 requirements).

In correspondence of Control section 82 and Control section 39-44 of the embankments, geognostic results certified a soil susceptibility to liquefaction (Fig.4.6).

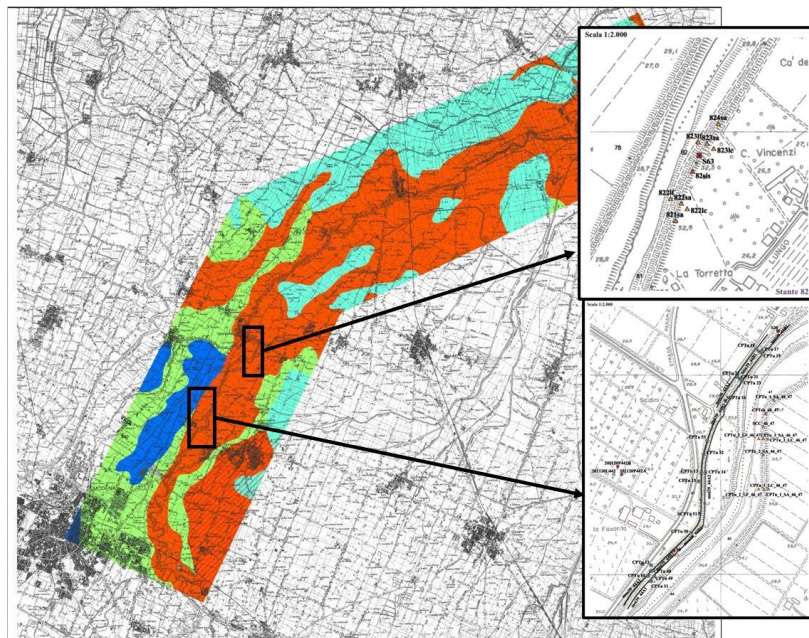
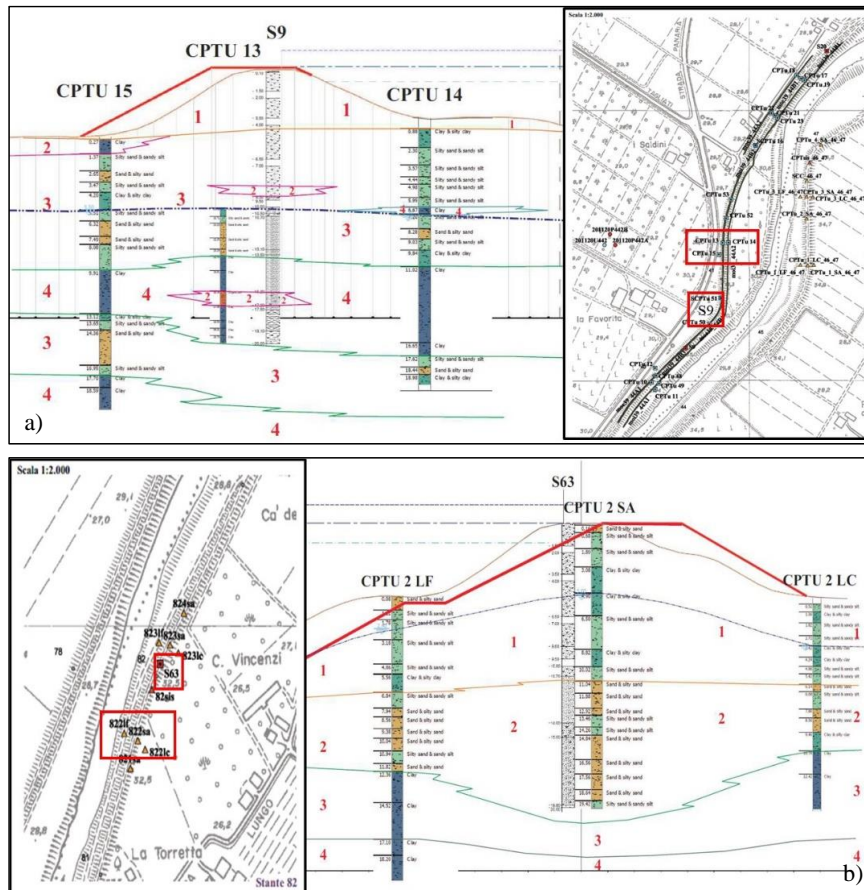


Fig 4.6 Location of the geognostic surveys at the resulting liquefaction-positive control sections

In these sections, lenses of fine and medium sands and silty sands occur, under the aquifer, probably linked to the presence of paleobeds (Fig.4.7).



**Fig 4.7 a) Technical-geological section of stand 39-44, b) Technical-geological section of stand 82**

All the penetrometric tests (CPT, CPT and SCPT) have been elaborated with a specific analysis software in order to obtain all the parameters of lithological characterization, resistance, deformability and permeability along the entire vertical test.

One of the key information taken from geognostic analysis for this project is the individuation of areas with Factor of Safety under the unit.

The elaboration of geognostic tests allows the individuation of critical area, checking Factor of Safety and also CRR/CSR graph.

Since the CSR is a result seismic demand placed on a soil layer, and CRR is the capacity of the soil to resist liquefaction, if CRR value recorded are less than CSR calculated, the area will be not stable and consequently the Factor of Safety will be under the unit. An example of this elaboration is presented in Fig.4.8.

Then, the elaboration of the parameter SBT (Soil Behaviour Type) and SBTn (normalized) of Robertson (2009) allows a first separation from sandy and clayey soil ( $I_c=2.6$ ).

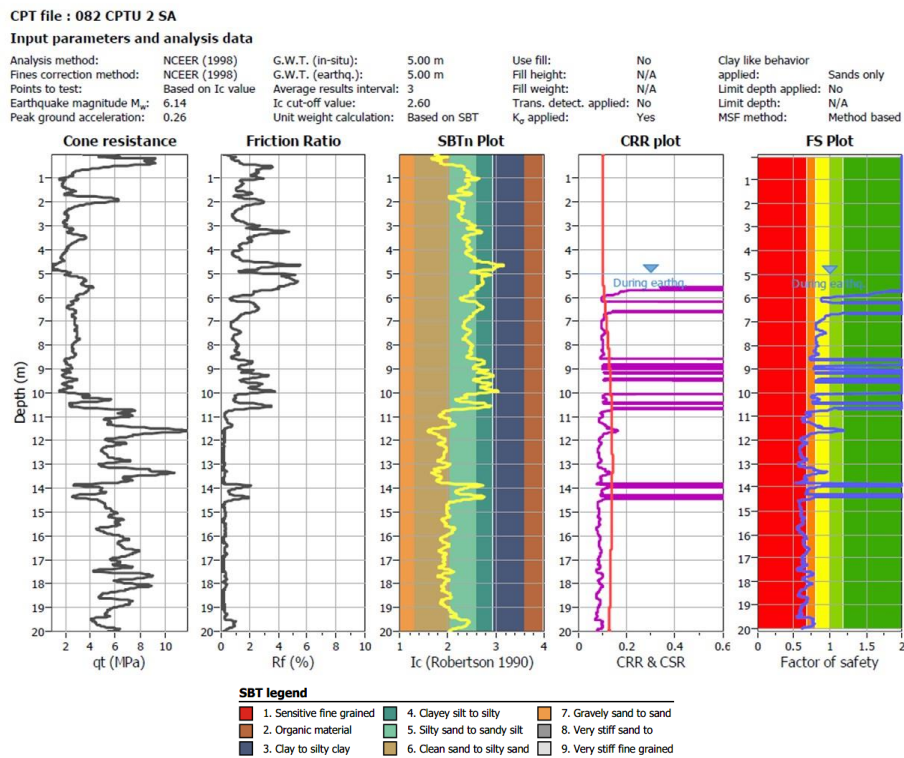


Fig 4.8 Input parameters and analysis data of CPTu2SA\_stand 39-44

### 4.2.3 NTC18 analysis

The assessment of site safety against liquefaction and overall stability is normed by NTC18 standard, which replace the previous version NTC08. It is the technical standard for construction in which is present a list of criteria to evaluate the liquefaction susceptibility of soil. Below a table with the results of NTC analysis for the case of study.

Chapter 7.11.3.4.2 Exclusion of liquefaction verification:

NTC18 requirements	Site value
1)Maximum expected accelerations at ground level in free field conditions less than 0.1g	$0.150g < a_g < 0.175g$
2)Average depth of the water table more than 15 m from ground level	~5 m
3)Deposits consisting of clean sands with normalized penetrometric resistance $(N_1)_{60} > 30$ or $q_{c1N} > 180$	$(N_1)_{60} < 30$ or $q_{c1N} < 180$
4)Grain-size distribution out of the the boundary	Grain-size distribution inside the boundary

Table 4-1 NTC18 requirements for Panaro river embankment case study

The risk of liquefaction may be considered as zero or negligible if at least one of the above conditions occurs. These criteria are only applicable in free field conditions, that is to say, in the horizontal ground level and in the absence of overloads.

According to these considerations the site needs further investigations with Advanced method (Laboratory test and Theoretical/Numerical analysis), since the Simplified method has confirmed liquefaction susceptibility of the area.

### 4.3 Case 2: the evaluation of the foundation system of the engineering work called Ponte Canale Ancona

Liquefaction susceptibility evaluation is a crucial point in seismic adaption of engineering works, especially following seismic events. This assumption is the starting point for the liquefaction analysis of this case of study, “Ponte Canale Ancona”, evaluating the expected safety conditions, the stability of the foundation and its resistant capacity under seismic loads.



### 4.3.1 Geological and seismic setting

The case work is located at km 119+500 of the A1 highway Milan - Parma, in the province of Lodi (Fig.4.9). CARG geological map, card n.60 “Piacenza” (Fig.4.10) is shown.



Fig 4.9 Geographical location of the case work

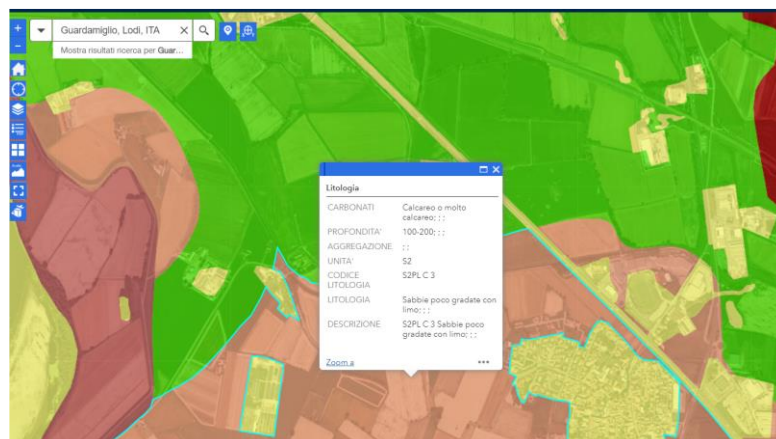
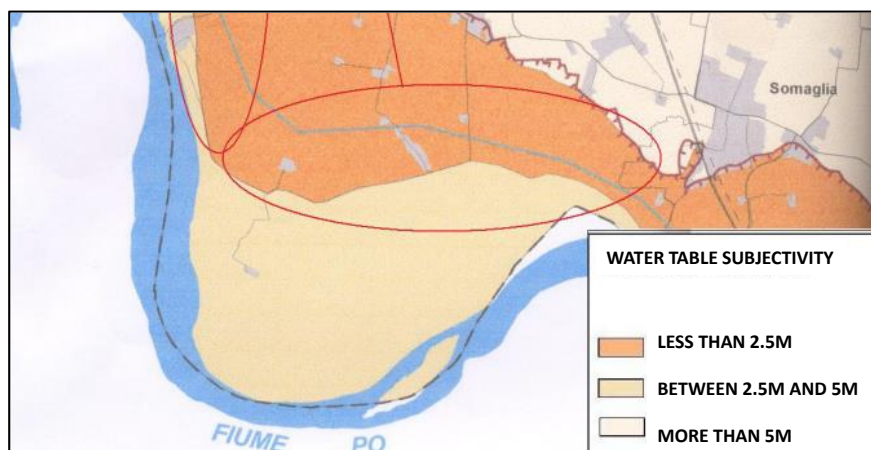


Fig 4.10 a) Extract of CARG card n.60 Piacenza; b) Viewer from Geoportale

The area of interest is located in the southern portion of the Lodi plain and it is part of the riverside band landscapes. It is characterized from the lithostratigraphic point of view by a powerful series of Pleistocene-Holocene alluvial deposits (Quaternary period). The main distinguishing feature of the subsoil is the extreme variability that lithographic facies present both vertically and horizontally thus reflecting environmental conditions of the fluvial-fluvioglacial continental type.

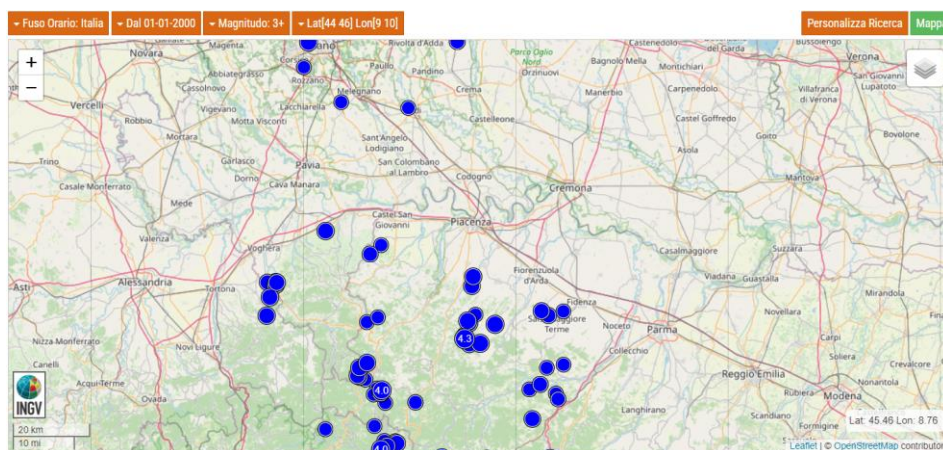
In relation to the local hydrogeological regime, it was identified a subsidence of the water table in the area of interest between 2.5 meters and

4 meters. In some periods of the year the depth of the aquifer may approximate the ground level or be distinguished from a very modest subsidence (Fig.4.11)



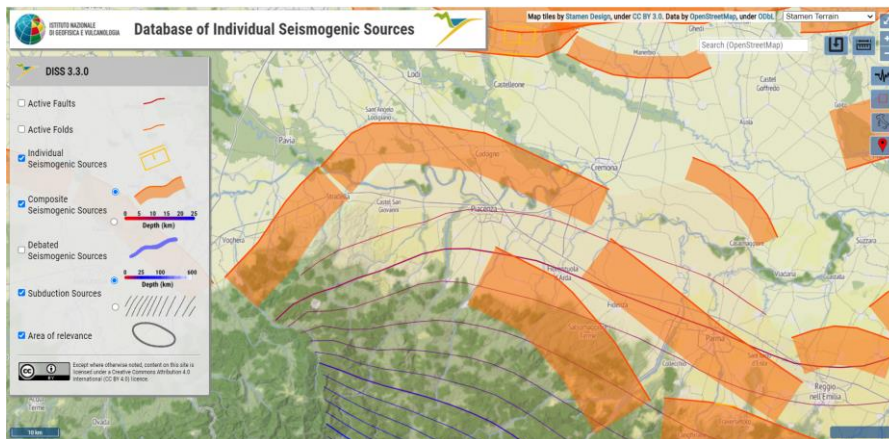
**Fig 4.11 Subjectivity of water table of the area under investigation (from <2.5m to 5m)**

The area of interest has recorded numerous earthquakes with magnitude  $\geq 3$ , MCS scale (Locati, 2016) (Fig.4.12):



**Fig 4.12 Map of epicenters of major earthquakes with magnitude equal to or greater than 3 from 2000 to date (INGV, <http://cnt.rm.ingv.it/>)**

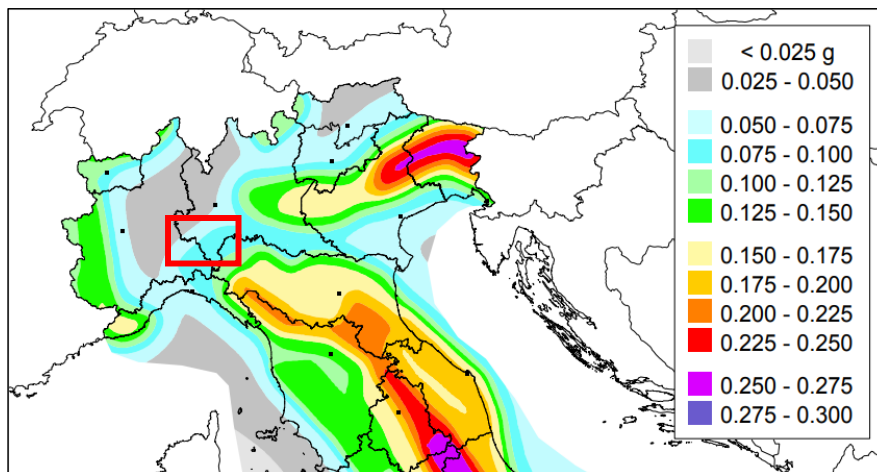
The seismogenic sources are described by the National Institute of Geophysics and Volcanology within the DISS3 Project (Fig.4.13):



**Fig 4.13 Seismic sources around the area of interest (INGV, <https://diss.ingv.it/diss330/dissmap.html> )**

The area is comprised within the seismogenic source classified as ITCS044, Portalbera-Cremona, it means that earthquakes magnitude of maximum 6.7 at epicentral depth 2-7 km can occur.

According to the Seismic hazard map of the national territory, the area falls into  $0.075g < a_g < 0.1g$  class (Fig.4.14).



**Fig 4.14 Excerpt from the seismic hazard map (INGV, [http://zonesismiche.mi.ingv.it/documenti/mappa\\_opcm3519.pdf](http://zonesismiche.mi.ingv.it/documenti/mappa_opcm3519.pdf) )**



### 4.3.2 Geognostic investigations

In order to verify the structure and in particular the foundational system, a geognostic investigation campaign was carried out at the end of 2021; the analyses were carried out in free field conditions, applying historical-empirical type methodologies in which the safety factor has been defined by the relationship between the available resistance to liquefaction and the stress induced by the design earthquake. Geognostic investigations are listed below (Fig.4.15):

- geognostic surveys (April 2021);
- MASW-HVSR seismic investigations (April 2021);
- measurement of piezometric levels in piezometers installed in boreholes;
- CPTU investigations (May 2022)
- SCPT investigations (March 2022)



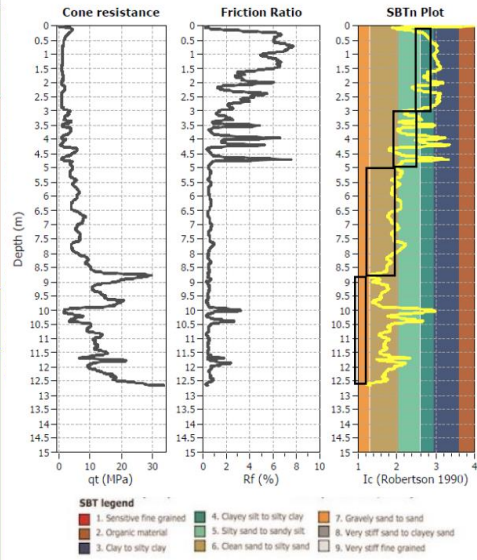
**Fig 4.15 Locations previous geognostic investigations (2021-2022)**

The results of the examination of the tests carried out, show the presence, in the first 4 meters of depth from the ground level, of silt-sandy deposits passing through more or less coarse average sand.

The following images show the results of SPT and CPT tests. Table 4-2 is a summary of geotechnical characterization of identified soils.

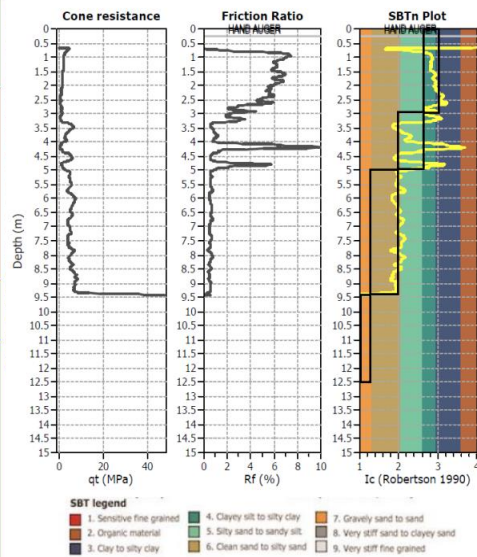
S2					
w.t.	lithology	prof	SPT	E (MPa)	φ (°)
	Silty and sandy silt	0.5		9.2	27.5
		1			
		1.5	5		
		2			
		2.5			
	Medium sand	3	4		
		3.5			
0		4			
0.5		4.5			
1		5			
1.5		5.5			
2		6	7		
2.5		6.5			
3		7			
3.5		7.5			
4	8				
4.5	8.5				
5	9	12			
5.5	9.5				
6	10				
6.5	Gravelly sand	10.5		34.8	33.3
7		11			
7.5		11.5			
8		12	19		
8.5		12.5			
9		13			
9.5		13.5			
10		14			
10.5		14.5			
11		15	26		
11.5	15.5		34.8	33.3	
12	16				
12.5	16.5				
13	17				
13.5	17.5				
14	18	20			
14.5	18.5				
15	19				
15.5	19.5				
16	20				

CPTU 1



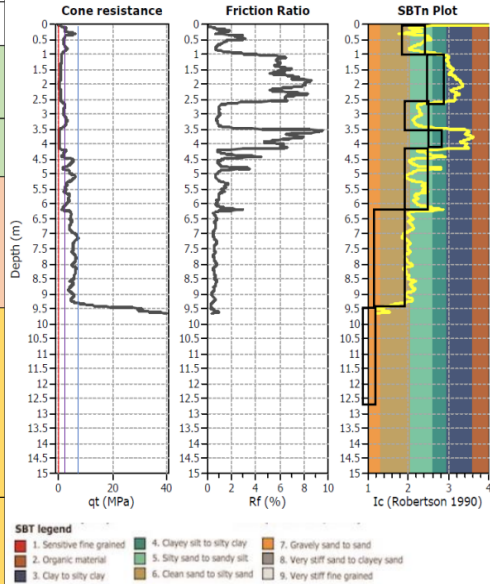
S2					
w.t.	lithology	prof	SPT	E (MPa)	φ (°)
	Silty and sandy silt	0.5		9.2	27.5
		1			
		1.5	5		
		2			
		2.5			
	Medium sand	3	4		
		3.5			
0		4			
0.5		4.5			
1		5			
1.5		5.5			
2		6	7		
2.5		6.5			
3		7			
3.5		7.5			
4	8				
4.5	8.5				
5	9	12			
5.5	9.5				
6	10				
6.5	Gravelly sand	10.5		34.8	33.3
7		11			
7.5		11.5			
8		12	19		
8.5		12.5			
9		13			
9.5		13.5			
10		14			
10.5		14.5			
11		15	26		
11.5	15.5		34.8	33.3	
12	16				
12.5	16.5				
13	17				
13.5	17.5				
14	18	20			
14.5	18.5				
15	19				
15.5	19.5				
16	20				

CPTU 2



S1					
w.t.	lithology	prof	SPT	E [MPa]	↓ [°]
	Medium coarse sand	0.5			
		1			
		1.5	4		
	Silty sand	2			
		2.5			
		3	8	10.2	28.5
0	Medium fine sand	3.5			
0.5		4			
1		4.5			
1.5	Medium coarse sand	5		10.2	28.5
2		5.5			
2.5		6	6		
3	Medium coarse sand	6.5			
3.5		7			
4		7.5			
4.5		8			
5		8.5		17.4	32.0
5.5		9	11		
6		9.5			
6.5	Gravelly sand	10			
7		10.5			
7.5		11			
8		11.5			
8.5		12	7		
9		12.5			
9.5		13			
10	Gravelly sand	13.5		35.8	33.6
10.5		14			
11		14.5			
11.5		15	22		
12		15.5			
12.5		16			
13		16.5			
13.5	Clean sand	17			
14		17.5			
14.5		18	26		
15		18.5		35.8	33.6
15.5		19			
16		19.5			
		20			

### CPTU 3



S1					
w.t.	lithology	prof	SPT	E [MPa]	↓ [°]
	Medium coarse sand	0.5			
		1			
		1.5	4		
	Silty sand	2			
		2.5			
		3	8	10.2	28.5
0	Medium fine sand	3.5			
0.5		4			
1		4.5			
1.5	Medium coarse sand	5		10.2	28.5
2		5.5			
2.5		6	6		
3	Medium coarse sand	6.5			
3.5		7			
4		7.5			
4.5		8			
5		8.5		17.4	32.0
5.5		9	11		
6		9.5			
6.5	Gravelly sand	10			
7		10.5			
7.5		11			
8		11.5			
8.5		12	7		
9		12.5			
9.5		13			
10	Gravelly sand	13.5		35.8	33.6
10.5		14			
11		14.5			
11.5		15	22		
12		15.5			
12.5		16			
13		16.5			
13.5	Clean sand	17			
14		17.5			
14.5		18	26		
15		18.5		35.8	33.6
15.5		19			
16		19.5			
		20			

### CPTU 4

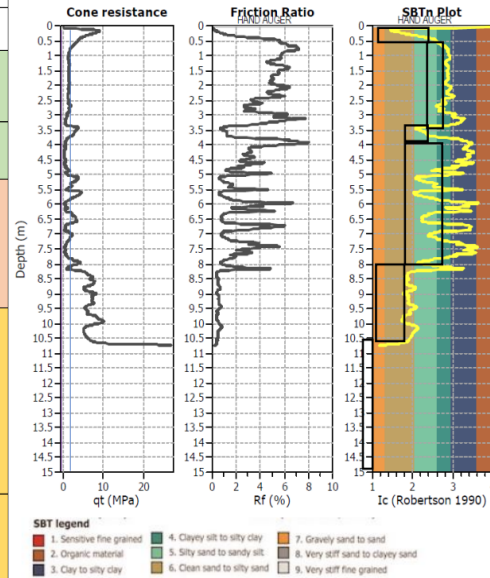


Fig 4.16 Results of CPT test and S1 and S2 boreholes

From [m]	To [m]	Geotechnical unit [-]	$\gamma$ [kN/m <sup>3</sup> ]	$\phi'$ [°]	$c'$ [kPa]
0.0	4.0	Silt and Sandy silt	19.5	10	4
4.0*	9.5	Medium sand	19.5	15	1
9.5	20	Coarse sand	19.5	33-24	2

**Table 4-2 Geomechanical characteristics of soil**

### 4.3.3 NTC18 analysis

During the preliminary checks carried out in April 2021, the analysis of the investigations led to the following results, in accordance with NTC18 requirements.

Chapter 7.11.3.4.2 Exclusion of liquefaction verification:

NTC18 requirements	Site value
1)Maximum expected accelerations at ground level in free field conditions less than 0.1g	0.150g < $a_g$ < 0.175g
2)Average depth of the water table more than 15 m from ground level	~4 m
3)Deposits consisting of clean sands with normalized penetrometric resistance $(N_1)_{60} > 30$ or $q_{c1N} > 180$	deposits consist of predominantly sandy sediments distinct from $(N_1)_{60} < 30$
4)Grain-size distribution out of the boundary	Grain-size distribution inside the boundary

The risk of liquefaction may be considered as zero or negligible if at least one of the above conditions occurs. These criteria are only applicable in free field conditions, that is to say, in the horizontal ground level and in the absence of overloads.

According to these considerations the site needs further investigations with Advanced method (Laboratory test and Theoretical/Numerical analysis), since the Simplified method has confirmed liquefaction susceptibility of the area.

## Chapter 5

# 5 Laboratory tests to support advanced procedure for liquefaction effect on geotechnical structures

### 5.1 Introduction

The measurement of dynamic soil properties is a critical task in the solution of geotechnical earthquake engineering problems. A wide variety of laboratory techniques is available each with different advantages and limitations with respect to different problems. In order to be able to predict such phenomena a deep understanding of the soil behaviour under cyclic loading is mandatory. It can be stated that nowadays, although many aspects still remain to be clarified, our knowledge of soil behaviour has advanced to a point where constitutive modeling can be reliably employed to allow for accurate prediction in engineering practice.

In general, the simplified liquefaction analysis or the cyclic tests used in the first step combined with the numerical simulation analysis used in the second and third steps become the most used approaches in practice.

Several researchers have conducted strain-controlled and stress-controlled laboratory investigations employing regular harmonic excitations for the dynamic characterization of soils (Seed and Lee 1966; Dobry et al. 1982; Ishihara 1993; Lombardi et al. 2014; Chattaraj and Sengupta 2016). It has been reported that when saturated soil deposits are subjected to regular harmonic loading, either by strain- or stress-controlled manner, the generated variations in the excess pore-water pressure (PWP) are primarily responsible to alter the strength characteristics of the soil (Matasovic and Vucetic 1992). Seed and Idriss (1972) and Dobry et al. (1982) were the pioneering researchers to introduce the cyclic stress- and strain-controlled approach, respectively, to qualify the liquefaction resistance of soils with the variations in excess PWP.

In this Chapter a literature review about advanced procedure focusing on equipment is presented.

## 5.2 Laboratory equipment

A challenge in liquefaction laboratory testing is the selection and operation of testing equipment. There are various types of equipment available, such as cyclic simple shear, cyclic triaxial, cyclic torsional shear, or centrifuge models, each with its own advantages and limitations. For example, cyclic simple shear apparatus can simulate the horizontal shear stress induced by earthquakes, but it cannot capture the effects of confining pressure or vertical drainage. Cyclic triaxial apparatus can apply both vertical and horizontal stresses, but it may induce non-uniform strain distribution or sample disturbance. Centrifuge models can simulate the gravity and scale effects of field conditions, but they are expensive and complex to operate. Therefore, there is a need to compare and evaluate the performance and accuracy of different testing equipment and develop guidelines for their selection and calibration. Another challenge in liquefaction laboratory testing is the determination and control of testing parameters, such as cyclic stress ratio, frequency, number of cycles, drainage conditions, and pore pressure measurements. These parameters can affect the onset, development, and consequences of liquefaction, as well as the interpretation and extrapolation of test results.

Dynamic behavior of soils is traditionally represented using strain dependent dynamic soil properties and liquefaction potential. Dynamic soil properties include initial shear modulus- $G_{max}$ , normalized shear modulus reduction ( $G/G_{max}$ ) and damping ratio ( $D$ ) variation. Such properties can either be obtained by in situ testing or by laboratory testing. In-situ testing can only provide the dynamic soil properties at low strain range and is not always feasible, while laboratory tests can furnish the required properties over wide strain range and varying loading conditions. Laboratory testing apparatus such as resonant column (RC), bender element (BE), cyclic torsional shear (CTS), cyclic triaxial (CTX), dynamic simple shear (DSS), etc. have been used to determine the dynamic soil properties (Kramer 1996; Towhata 2008); each apparatus is unique in its application.

In this project cyclic triaxial equipment has been mostly analysed (Controls and Matest made), then cyclic simple shear equipment (GDS made).

### 5.2.1 Cyclic triaxial test

In most studies of the liquefaction phenomenon, the load was chosen with the aim to reproduce similarly the load appearing during earthquakes. During an earthquake, the waves do not propagate in a single direction but in several directions. In one direction, the earthquake wave includes two elements: the horizontal wave and the vertical wave. Seed and Idriss (1982) recognized that the waves propagating as vertical direction are predominant. Under these earthquake waves, the soil grains tend to move closer together, the void between grains decreases and water in the void tend to drain. However, the earthquake waves usually impact a very large area; thus, the water cannot drain in a short period of time during the earthquake. This happens even with sandy soils, which have good permeability. To simulate these conditions one method is used: to apply the cyclic load to the sample in the triaxial cell in the undrained condition.

Several researches are available about liquefaction assessment based on strain-controlled and stress-controlled triaxial tests. It was reported that the increase of excess PWP in saturated sand deposits, during earthquake/cyclic loading, results in the reduction in internal friction and consequent loss of strength, thereby leading to liquefaction.

Cyclic triaxial tests have been widely used to axes soil liquefaction potential since the early 1960s because they are simple enough and rather common. In undrained cyclic triaxial tests, the imposed cyclic stress ratio CSR is defined as the ratio between the shear stress  $q$  and the normal effective stress  $\sigma'_{ref}$ , acting on the plane of maximum shear stress:

$$CSR = \frac{q}{2\sigma'_{ref}} \quad \text{Eq. 5-1}$$

Where  $q$  is the deviatoric stress and  $\sigma'_{ref}$ :

$$\sigma'_{ref} = \frac{\sigma'_1 + \sigma'_3}{2} \quad \text{Eq. 5-2}$$

Where  $\sigma'_1$  and  $\sigma'_3$  are the maximum and minimum effective stress acting on the specimen at the end of the consolidation phase. In case of isotropically consolidated test,  $\sigma'_{ref}$  is equal to consolidation pressure. Soil liquefaction should be identified as the condition of null effective stress. In cyclic triaxial tests is usually assumed that liquefaction is attained

at conventional stress or strain thresholds. The stress-based approach refers to the pore pressure ratio,  $Ru = \Delta u / \sigma'_c$ , between the cyclically induced pore pressure increment  $\Delta u$  and the confining stress  $\sigma'_c$ . The strain-based approach typically assumes a limit value for the double amplitude axial strain  $\varepsilon_{DA}$ .

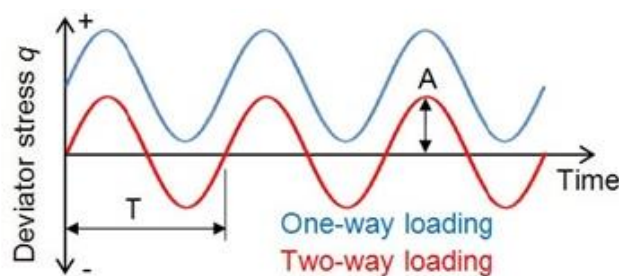
There are broadly two main aspects of dynamic cyclic loading that differentiate the soil response from traditional static behaviour. These are:

- The reversal of applied stress
- The rate-dependency of soil response

(i) Reversal of applied stress

Reversing the stress applied to a soil element refers to variation in sign of the rate of stress increase. More simply for triaxial testing, this typically means oscillating between increasing and decreasing values of deviator stress  $q$  applied to a soil test specimen.

Examples of two cyclic loading patterns that may be used during a cyclic triaxial test are displayed in Fig.5.1- here one-way loading refers to cases in which the applied stress does not change sign (e.g. remains positive at all times), while two-way loading corresponds to cases in which the applied stress does change sign (i.e. alternates between positive and negative values). Note the time taken for loading to complete one cycle is given by the loading period,  $T$ , while the magnitude of loading is described by the amplitude,  $A$ .



**Fig 5.1 One-way and two-way cyclic loading patterns in cyclic triaxial test**

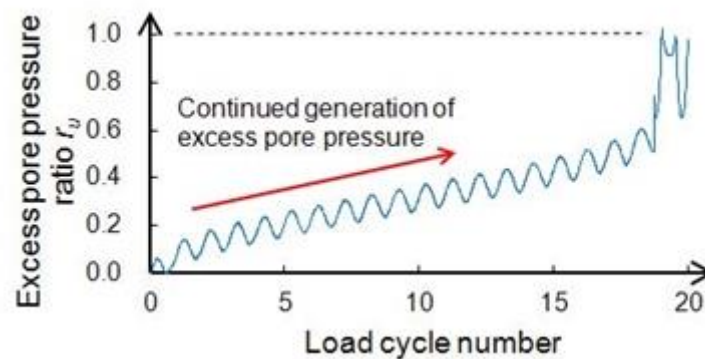
Two principal features of soil response when undergoing stress reversal are: (1) the accumulation of plastic shear strain; (2) generation of excess pore water pressure. Importantly, these features only occur once the soil behaviour becomes elasto-plastic, which approximately corresponds to



applied shear strains in the order of 0.01 % or larger (Ishihara, 1996). At shear strains below 0.01 % most soil behaviour tends to be purely elastic.

Excess pore water pressure generation refers to the change in pore pressure that occurs within a saturated soil as a load is applied. In practice a build-up of excess pore pressure reduces the effective stress applied to a soil deposit, which in some cases may trigger complete failure of the soil. A well-known example of this is the liquefaction of sand deposits - here the rapid cyclic loading produced by an earthquake causes the pore pressure to rise more quickly than it can be dissipated, even though sand is a relatively permeable material. Once the effective stress of the sand approaches zero the ability of the soil to resist shear loading is lost, resulting in significant soil deformations.

To quantify pore pressure build-up during a triaxial test, the excess pore pressure ratio  $r_u$  is often used. Therefore, when  $r_u = 0$  the pore pressure is equal to the applied back pressure, while when  $r_u = 1$  the pore pressure is equal to the confining pressure and the effective stress has reduced to zero. Such response is displayed in Fig.5.2, which details the generation of excess pore pressure during an undrained cyclic test on a sand specimen. Note the ratio may also be expressed as a percentage.



**Fig 5.2 Generation of excess pore water pressure during an undrained cyclic loading test on a sand specimen.**

(ii) Rate-dependency of soil response

The rate at which loading is applied has been shown to significantly affect the response of a soil. In general, faster loading rates result in stiffer and stronger response for cohesive soils, an observation that has been made when testing specimens under monotonic (loading in one direction only) and cyclic conditions.

Interestingly the rate-dependency of soil response is due to two factors. The first is the effect of inter-particle viscosity, and the second is the effect the loading rate has on a soil's ability to dissipate excess pore pressure.

Although dynamic cyclic triaxial tests may be used to investigate many aspects of the dynamic cyclic response of soils, two commonly-used test standards are:

- ASTM D3999-11 (Determination of the Modulus and Damping Properties of Soils Using the Cyclic Triaxial Apparatus)
- ASTM D5311-11 (Load Controlled Cyclic Triaxial Strength of Soil)

ASTM D3999-11 is primarily used to determine the degradation in secant Young's modulus  $E$ , and increase in damping coefficient  $D$ , of a soil specimen as the applied axial strain  $\epsilon_a$  is increased. Note estimates for the shear modulus  $G$  and applied shear strain  $\gamma$  may also be obtained through use of Poisson's ratio  $\mu$ , which is equal to 0.5 for undrained conditions.

ASTM D5311-11 is used to determine the cyclic strength of a soil specimen by loading the soil under undrained conditions until a given failure criterion is reached. Typically, failure is defined by the excess pore pressure ratio  $ru$  reaching 1.0, or some limiting value of double amplitude (DA) axial strain  $\epsilon_a$  being exceeded (20 % is specified in the test standard, although 5 % is often used for liquefaction studies). If multiple specimens are tested with different cyclic stress ratios applied, then cyclic strength curves like those shown in Fig.5.3 may be generated.

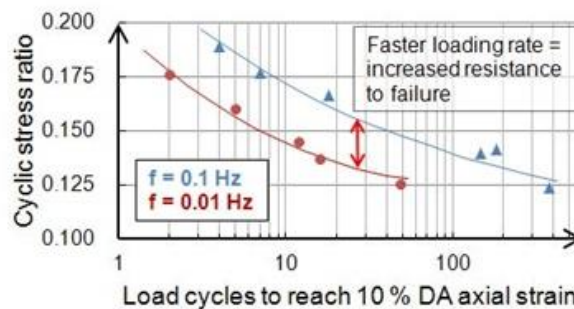


Fig 5.3 Cyclic strength curves of Kaolin specimens for loading frequencies equal to 0.1 Hz and 0.01 Hz (data from Özyaydin and Erguvanli, 1980).

Each of the above test standards importantly specifies that cyclic loading must be applied dynamically to the test specimens. Here ASTM D3999-11 states loading must be carried out at frequencies between 0.5 Hz to 1 Hz, while ASTM D5311-11 allows for loading frequencies between 0.1 Hz to 2 Hz.

### 5.2.2 Cyclic simple shear test

Cyclic simple shear is probably the most popular laboratory test to investigate the dynamic behaviour of soils after the cyclic triaxial testing. Cyclic loading mechanism in simple shear test resembles the earthquake loading conditions better compared to the cyclic triaxial test.

Consolidation in simple shear is anisotropic, and can be assumed to represent at rest condition in the field. Also, specimen preparation is relatively easier compared to that for triaxial testing.

Liquefaction is usually defined on the basis of either the pore pressure ratio or the axial/shear strain. In the cyclic direct simple shear test, a specimen is deemed to have liquefied when a single amplitude of the shear strain exceeds 3.75% or the excess pore pressure ratio exceeds 90%.

Sample for cyclic simple shear test is placed on the interior area of a number of rings, which can move freely to the desired direction, so the shear strains  $\gamma$  are distributed to the whole area of the sample (Fig.5.4).

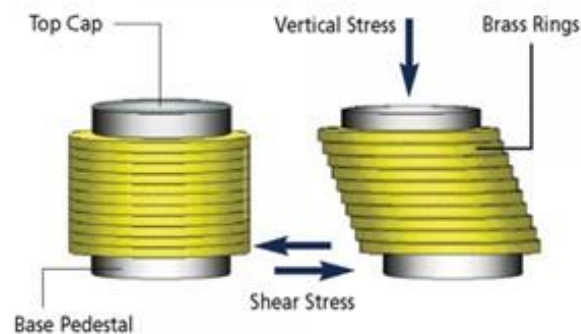


Fig 5.4 Scheme of sample in cyclic simple shear equipment

In the CSS test, the stress conditions (Fig.5.5) in the horizontal plane (or the plane of maximum shear stress) can be considered to be identical

to those at the in-situ soil surface, as previously explained. A vertical effective stress ( $\sigma'_{v0}$ ) is applied to the horizontal plane and the horizontal deformation is constrained by a wire-reinforced membrane or Teflon-coated stacked aluminium rings. Additionally, a cyclic shear stress ( $\tau_{cyc}$ ) is applied to the horizontal plane to simulate the vertically propagating shear wave generated by earthquake loading. Therefore, Cyclic stress ratio (CSR) in the CSS test is defined as:

$$CSR = \frac{\tau_{cyc}}{\sigma'_{v0}} \quad \text{Eq. 5-3}$$

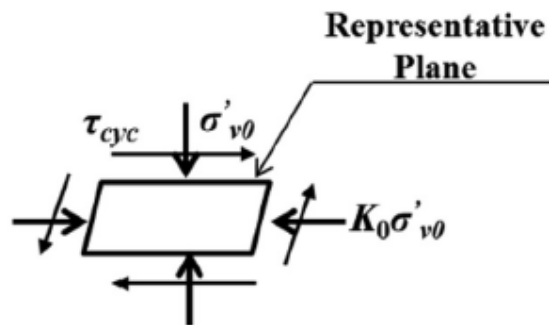


Fig 5.5 Stress condition in CSS test

Some researchers have performed cyclic simple shear test keeping the vertical stress constant (Dyvik et al. 1987), while some others have performed test keeping the consolidated height of the specimen constant during shearing (Chang, 2008; Hazirbaba, 2009; Jafarzadeh, 2012). Regardless, the specimens are sheared in undrained conditions and the generated excess pore pressures are measured with a pore pressure transducer.

Cyclic simple shear test could be conducted in drained and undrained condition. In drained constant volume simple shearing, specimens are sheared in drained conditions in such a way that the volume of the specimens is kept constant during the entire shearing stage. Since, volumetric strain is equal to the axial strain in a simple shear test, constant volume is preserved by adjusting the magnitude of the vertical stress on the specimen so that the height of specimen does not change during shearing. Because drainage is allowed, no pore pressure is measured with

a transducer, and the change of vertical stress is used to predict the excess pore pressures in an equivalent undrained test (Bjerrum, 1966).

Then, in undrained condition, Dyvik et al. demonstrated on normally consolidated clay that pore pressures measured is identical with the pore pressures predicted from a drained constant volume simple shear test.

Montoya et al. (2013) conducted CSS test on dry sample under drained constant volume conditions and the corresponding undrained pore pressure is calculated from the loss of the measured axial stress. Researches on drained constant volume cyclic simple shear tests on clean and silty sand specimens have shown that liquefaction potential of those soils could also be determined via dry samples. This is an important observation, since dry specimens are much easier to prepare and less time consuming compared to their saturated counterparts, as the demanding saturation process is eliminated. This approach has been used by several studies including Monkul et al. (2015) and Porcino and Diano (2016).

Furthermore, to investigate dynamic properties of soil performing cyclic simple shear test, ASTM standard is used:

- ASTM D8296 - Standard Test Method for Consolidated Undrained Cyclic Direct Simple Shear Test under Constant Volume with Load Control or Displacement Control

According to the standards, equipment specifications and testing procedures for the measurement of constant volume strength and stress-strain characteristics of cohesive soils after one-dimensional consolidation using a constant rate of simple shear deformation mode of loading are defined. Then, the constant volume condition is equivalent to the undrained condition for saturated specimens.

Considering the relative quality of laboratory techniques for measuring dynamic soil properties, the cyclic simple shear tests provide a good estimate of shear modulus, material damping, and the effect of the number of cycles on the dynamic properties.

More company are able to provide Cyclic simple shear apparatus, as GDS, Controls, VJtech, Geocomp.

### 5.2.3 Resonant column test

The resonant column test is particularly useful for studying the behaviour of soils in response to dynamic loads and assessing their liquefaction potential. This test is a well-established medium-frequency wave propagation technique for the dynamic characterization of soils; the resonant frequency is the frequency at which the soil specimen exhibits maximum amplitude of oscillation in response to cyclic shear loading. Cyclic loading is applied to the cylindrical specimen by subjecting it to repeated cycles of torsional shear deformation while maintaining constant volume. The soil specimen is subjected to cyclic loading at different frequencies while measuring the corresponding shear stress response. This helps evaluate how the soil's dynamic properties change with varying loading frequencies. The cyclic loading simulates the ground shaking experienced during an earthquake.

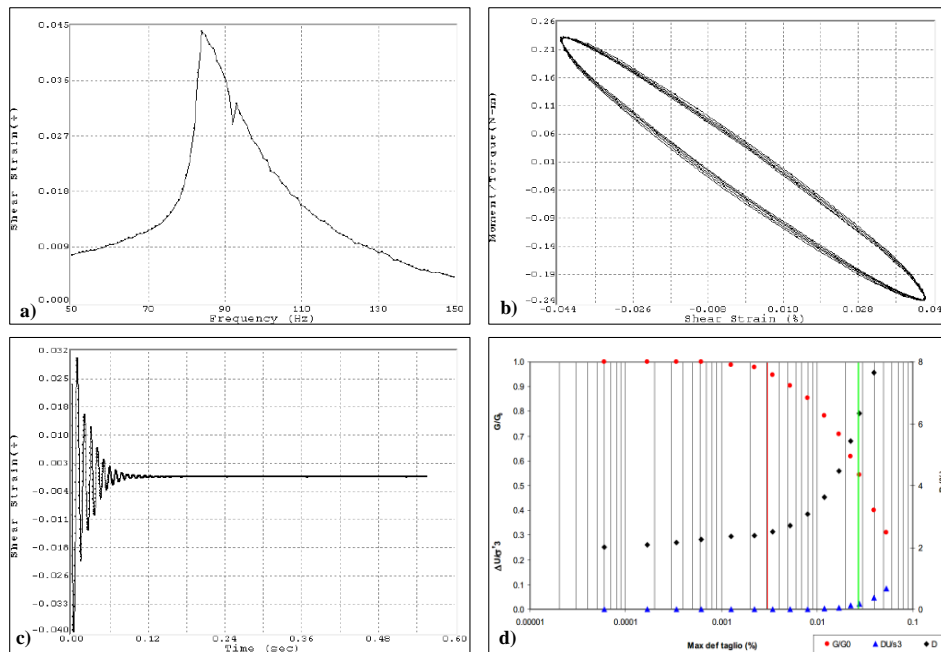
Test consists in applying a sinusoidal-shaped torque to the top of a fixed-free cylindrical specimen (fixed base and top free to rotate) enclosed in a triaxial cell, gradually increasing the frequency; the resonant frequency of the specimen is determined as the frequency at which the maximum shear strain is obtained.

The test is used to determine the dynamic properties of the soil, including its shear modulus ( $G$ ) and damping ratio ( $D$ ). These properties are essential for assessing how the soil responds to dynamic loading.

1. Shear Modulus ( $G$ ): Applying the theory of elastic wave propagation in a cylindrical specimen, it's possible to calculate the VS and then the value of the shear modulus  $G = \rho * V_s^2$ . The shear modulus represents the stiffness of the soil specimen. It is measured at various frequencies and shear strain levels to assess the soil's dynamic properties under different loading conditions.

2. Damping Ratio ( $D$ ): The damping ratio represents the energy dissipation characteristics of the soil during cyclic loading. It is typically measured at various frequencies and shear strain levels to evaluate how well the soil dissipates energy during loading.

Typical results of resonant column test are shown in Fig.5.6.



**Fig 5.6 Typical results of resonant column test: a) range of frequencies investigated; b) Hysteresis loop  $t-\gamma$  under conditions of forced oscillations; c) strain decay (damping) by free oscillations; d) Decay law of normalized shear modulus ( $G/G_0$ ), damping ( $D$ ) and pore pressure ratio ( $RU$ ) with respect to the logarithm of the strain of shear  $\gamma$**

## 5.2.4 Centrifuge test

Geotechnical materials such as soil and rock have nonlinear mechanical properties that depend on the effective confining stress and stress history. The centrifuge applies an increased “gravitational” acceleration to physical models in order to produce identical self-weight stresses in the model and prototype.

The one-to-one scaling of stress enhances the similarity of geotechnical models and makes it possible to obtain accurate data to help solve complex problems such as earthquake-induced liquefaction, soil-structure interaction and underground transport of pollutants such as dense non-aqueous phase liquids.

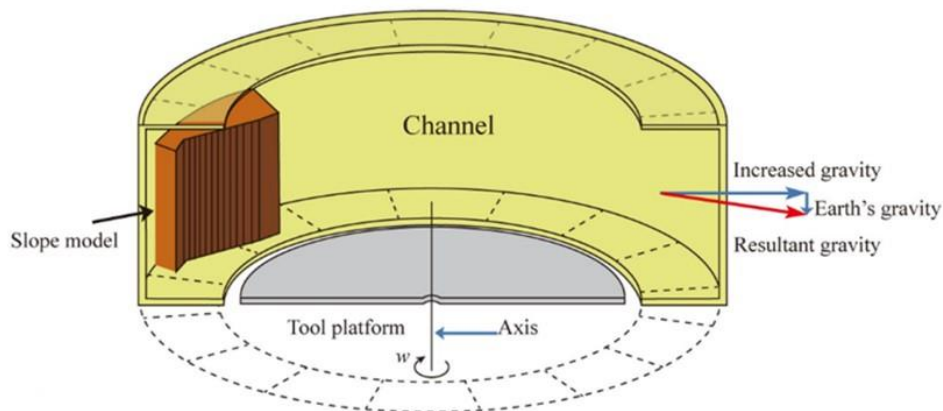
Centrifuge modelling is a valuable tool for studying the effects of ground shaking on critical structures without risking the safety of the public. The centrifuge can recreate a wide range of field phenomena and

environments under laboratory conditions, generating realistic data to verify and validate computer simulations and engineering analyses.

Several researchers have used centrifuge tests to study the seismic performance of relatively deep and uniform deposits of saturated, loose-to-medium dense, clean sand (e.g., Liu and Dobry 1997 and Hausler 2002). Physical modelling offers an opportunity to test soil in real site conditions with controlled variables (soils, slopes, stratification etc.). The principles and essential features of centrifuge modelling involve replicating the prototype slope behaviour within a small model by increasing the acceleration from 1g condition to  $ng$ , which provides identical stress and strain in the model and the prototype at corresponding points.

Commercially two model of centrifuge exist, drum and beam.

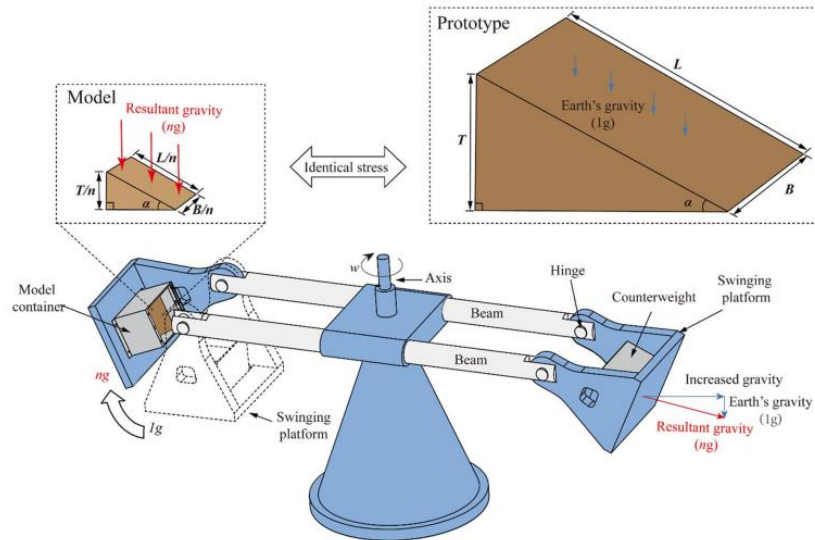
In a drum centrifuge, the drum is rotated around the whole edge of a cylinder that is spinning around its axis, as shown in Fig.5.7. The drum centrifuge consists of a main channel, in which the model is built or placed, and a tool platform, where actuators and sensors can be mounted together with the data acquisition systems.



**Fig 5.7 Schematic view of the drum centrifuge (modified from Morales, 2013)**

The beams are those that are composed of a beam that rotates around an axis and at the ends of which there are, either two tilting baskets or a tilting basket and a counterweight depending on the design. The model, which is prepared outside the centrifuge machine, is placed in the tilting basket. Beam centrifuges, made up of a rotating arm and swinging platform, are the majority of the centrifuges with longer radiuses, Fig.5.8 (Kim et al., 2009; López et al., 2021).





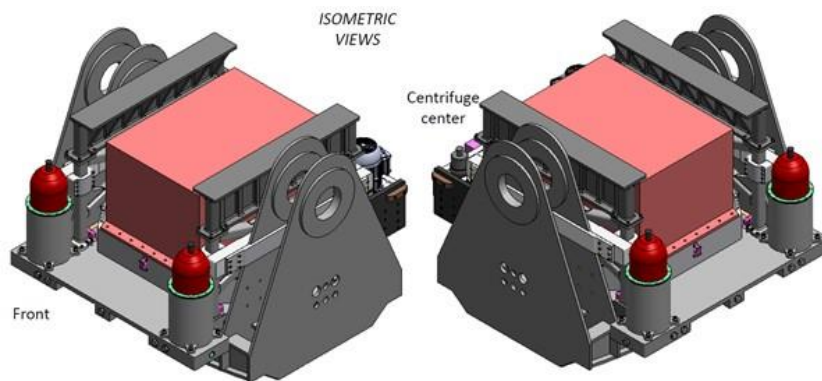
**Fig 5.8 Schematic view of the beam centrifuge (Kyoto University) from a plan view**

Based on the designs, sizes, and machine components of the two centrifuges, in a drum centrifuge test, the soil model is prepared inside the channel of the drum centrifuge (Morales Peñuela, 2013; Yin et al., 2019). In contrast, in a beam centrifuge test, the soil containers used are rigid boxes or laminar boxes (Fig.5.9), depending on the objectives and requirements of the tests. For beam centrifugation, soil models are typically constructed in a rectangular rigid chamber with one transparent boundary under both static and dynamic conditions (Higo et al., 2015; Miao et al., 2018; Pipatpongsa et al., 2020).



**Fig 5.9** Box container of Dundee university's centrifuge

In beam centrifuge, earthquake loading is applied using a servo-hydraulic Systems in-flight earthquake simulator (Fig.5.10)



**Fig 5.10** Example of Schematic of the Actidyn on-board earthquake simulator.

## Chapter 6

### 6 Laboratory results on the two case studies

#### 6.1 Research method

Laboratory equipments are essential for assessing the liquefaction potential of soil samples, which is crucial for making informed decisions in geotechnical engineering and construction, especially in areas prone to seismic activity.

In situ geognostic tests (CPTu, SPT) allow to estimate the lithologies involved, determining a safety factor for further analysis by means of laboratory machines to characterize the soil behaviour under dynamic stresses ( $FS < 1$  or  $FS < 1.2$ ).

In this Chapter, a series of laboratory tests is presented. Cyclic simple shear (Case1) and cyclic triaxial test (Case1 and Case2) have been performed to investigate soil behaviour under different dynamic stress. Cyclic triaxial tests has been performed considering the parameters obtain by SPT or CPTu (or both) and site seismic condition.

Cyclic simple shear tests have been performed in order to find the characteristic curve, testing sample under different value of CSR.

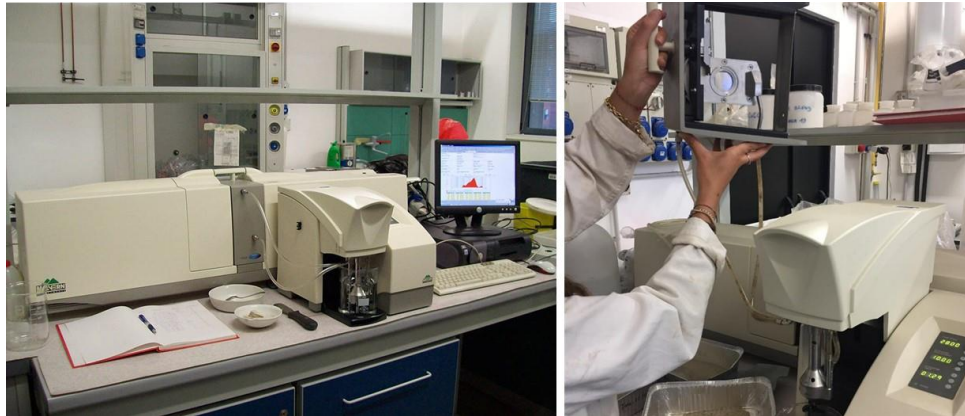
Laboratory tests have a dual purpose: assess liquefaction risk under determined seismic stress and obtain curves allowing the mathematical constitutive models to be calibrated.

Triaxial apparatus is a Controls equipment, whereas Simple shear apparatus is a GDS equipment.

##### 6.1.1 Geotechnical soil classification

The grain-size distribution curve of the material to be tested is an important starting point in liquefaction evaluation (also taking into account the NTC18 requirements) along with the minimum and maximum void ratio calculated.

A Malvern Mastersize 2000E (Fig.6.1) laser granulometer was used for particle size analysis.



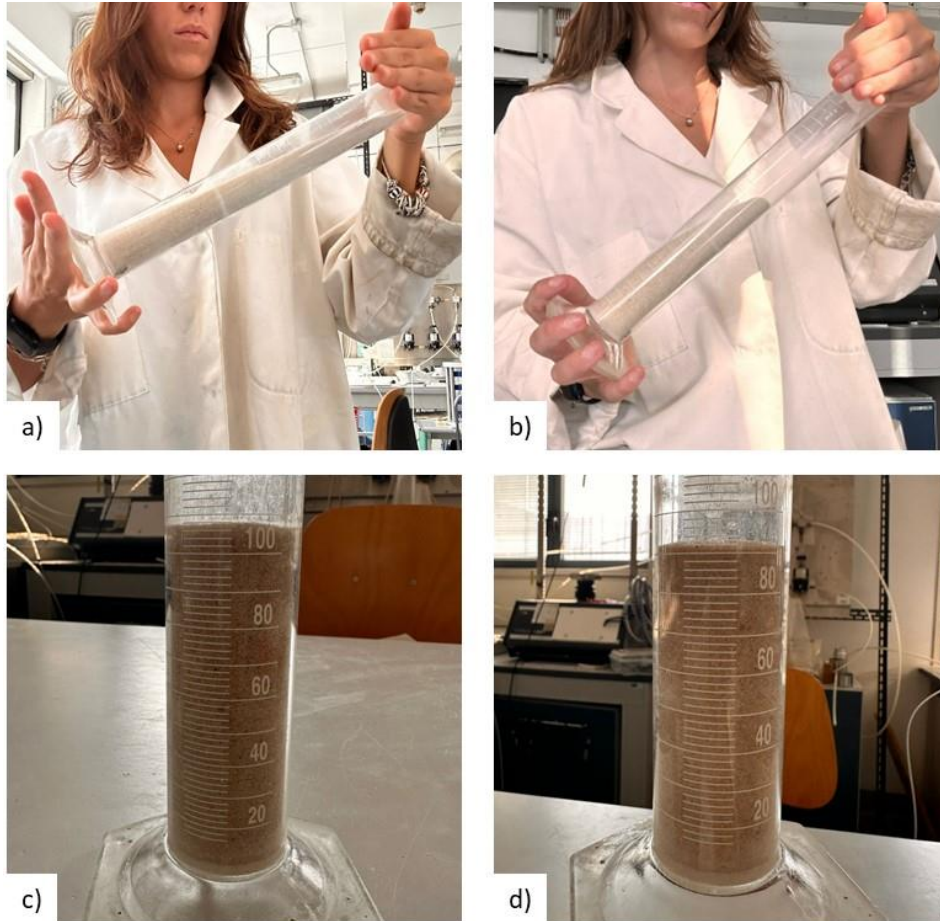
**Fig 6.1 Malvern Mastersize 2000E located in Bicocca laboratory**

With the Mastersizer 2000E it is possible to perform particle size analysis for materials between 1 mm and 0.1 microns, obtaining particle size curves of extreme detail.<sup>3</sup>

The index of maximum voids was determined by the free fall of the material in a graduated cylinder, the volume of which is known (Fig.6.2.). Reading the label on the cylinder, it's possible to calculate the maximum index of voids (Fig.6.2). Then, by vibrating and rotating the material several times, the minimum index of voids was determined. In figure below, an example of this application with Hostun sand, which is standardized, to double-check the method reliability.

---

<sup>3</sup> The Mastersizer 3000 uses the technique of laser diffraction to measure the particle size and particle size distribution of materials. It does this by measuring the intensity of light scattered as a laser beam passes through a dispersed soil sample. This data is then analyzed to calculate the size of the particles that created the scattering pattern.

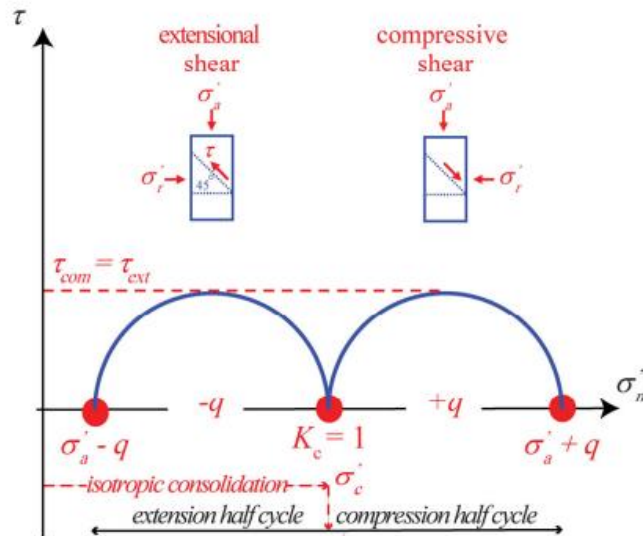


**Fig 6.2 Void ratio index evaluation with technique of vibrating and rotating the material: a) displace the sand on all the length of the cylinder; b) start to rotate and tilt the cylinder trying to disperse the grains in their natural position; c) maximum void index; d) minimum void index**

### 6.1.2 Cyclic triaxial test

Regarding engineering earthquake simulation in laboratory research, cyclic triaxial apparatuses certainly play a prevailing role (Tsukamoto and Ishihara 2022) since they are capable of producing a sequence of deviator stresses, very similar to seismic loading. The test specimens should be isotropically consolidated with consolidation stress ratio  $K_c = 1$  ( $K_c = \sigma'_a / \sigma'_r$  where  $\sigma'_a$  and  $\sigma'_r$  stand for axial and radial effective stress,

respectively) (Fig.6.3). Under cyclic triaxial conditions, it is usual to take either the excess pore water pressure ratio  $r_u$  or axial strain  $\epsilon_a$  as a yardstick to recognize the outset of liquefaction.



**Fig 6.3 Schematic representation of undrained cyclic loading for isotropically consolidated sample, under cyclic triaxial test**

Sand liquefaction behaviour, as studied in cyclic triaxial test, corresponds to two main phenomena according to the density index of sand matrix: cyclic mobility in both medium-dense and dense states and true liquefaction (or flow liquefaction) in very loose state.

### 6.1.2.1 Equipment

The real picture of the apparatus for dynamic triaxial tests used in this study is shown in Fig.6.4. The dynamic (cyclic) triaxial testing system DYNATRIAX EmS provided by Controls includes a dynamic controller to generate and control dynamic parameters, i.e. force, displacement and pore water pressure. It is capable of providing fully automatic high frequency and load dynamic triaxial testing.

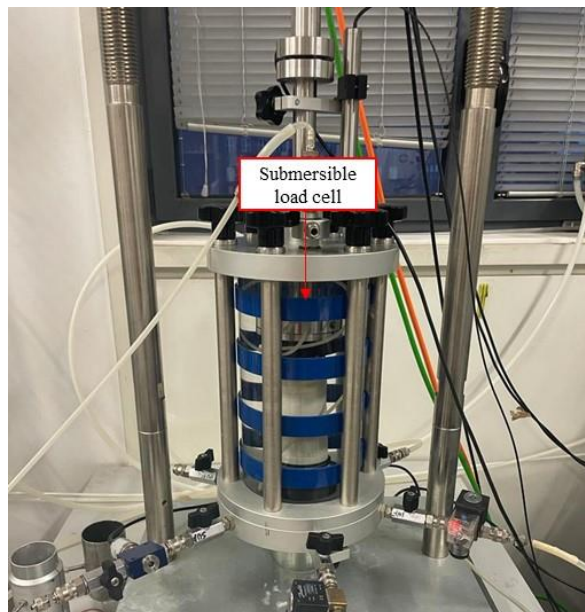




**Fig 6.4 DYNATRIAX EmS- dynamic triaxial apparatus**

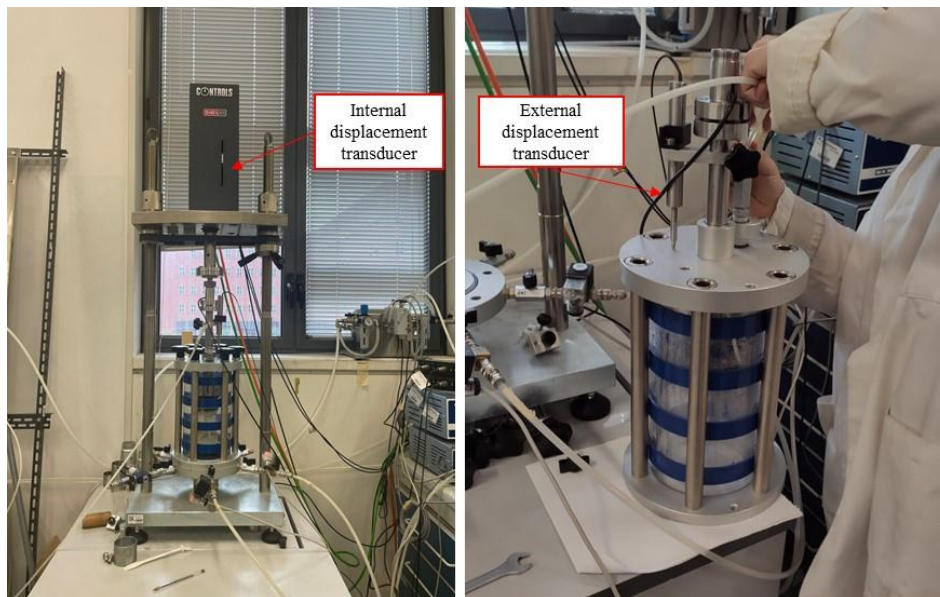
The axial load with the maximum value of 15 kN is applied on top of the sample. The load is generated by an electro-mechanical actuator placed on the top of the load frame.

A submersible load cell is used to measure the load transmitted to the sample (Fig.6.5), because deleting the effect of connections and the inertia of the piston, contrary to the presence of an external load cell.



**Fig 6.5 Axial load measurement: submersible cell 10 kN**

The axial strain varies during the test and it is measured by two transducers (Fig.6.6). One is integrated with the electro-mechanical actuator. The axial strain measured by this transducer has low accuracy due to the errors caused by the connections between parts of the device. The other transducer is fixed to the piston. This transducer allows measuring the relative movement between the piston and the cell ceiling. It is more exact than the first transducer because the errors caused by the connections have been eliminated.



**Fig 6.6 Axial measurement system of cyclic triaxial equipment**

The cell pressure and back pressure are transmitted to the cell and sample through an Air-Water Interface (Fig.6.7), controlled by pneumatic automatic pressure control, 1000kPa is the maximum value for both pressure line.





**Figure 6.1 Pressure and volume change control: air-water bladder and automatic volume change apparatus**

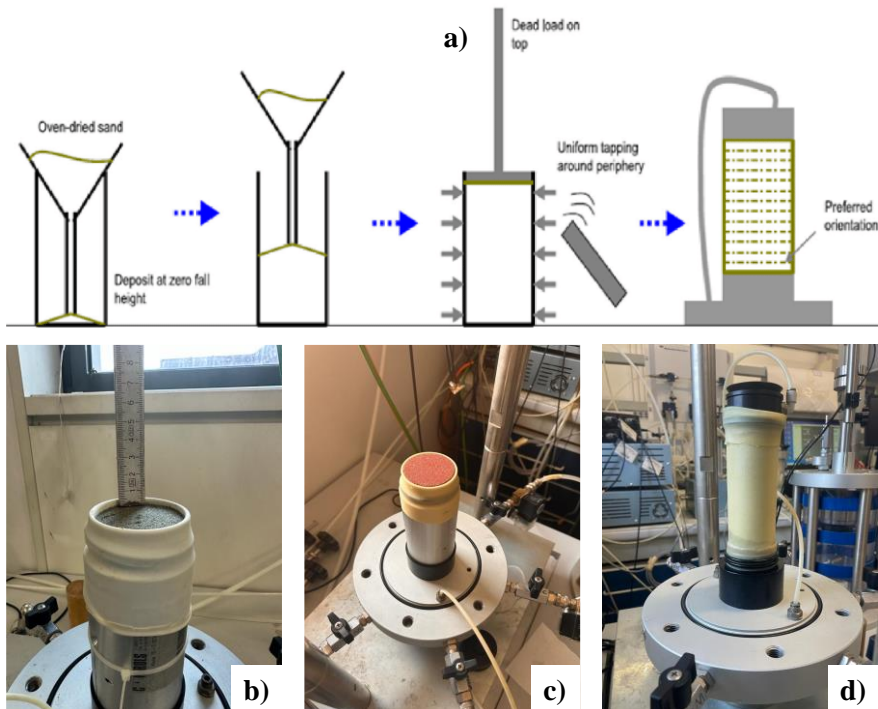
Back pressure is applied on bottom of the sample, while the pore water pressure is measured at the top of the sample. Porous stone and filter paper are installed at both ends of the sample, to help drainage and in preventing the soil particles from entering the back pressure line system. De-air water is usually used to circulate the samples, because the remaining air bubbles after the first stage of sample saturation dissipate into the de-aired water easier than tap water.

#### **6.1.2.2 Test procedure**

Triaxial tests were performed on cylindrical specimens measuring 100 mm by 50 mm ( $H/D = 2$ ) at desired density.

##### ➤ *Sample preparation*

From the literature review (Dang 2019), there are three methods often used to reconstitute samples: wet tamping, dry deposition, and water sedimentation; in this study dry deposition method (Fig.6.7a) has been choose to reconstitute sample at desired void ratio. Air trapped between the membrane and the mould was sucked out by application of vacuum which leaves no void between the membrane and the mould wall. The membrane conforms to the exact shape and volume of the mould. Dry sand was deposited in a funnel, the lower end of which was placed at the bottom of the mould and then slowly rose in circular motions to the upper end of the mould, tamping if necessary; vacuum was applied to the base of triaxial cell before removing the mould, -5kPa, since the sample was remoulded.



**Fig 6.7 Sample preparation: a) dry air pluviation; b)-c)-d) sequence of sample preparation with vacuum applied from the bottom of the base**

➤ *Sample saturation*

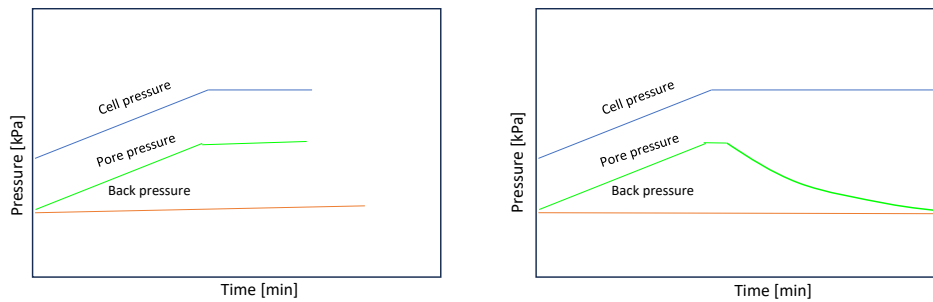
The technique adopted to saturate the sample consists in flushing of de-aired water through the sample, from the bottom to the top. In a first phase, drainage to the top of the sample was opened to allow the pouring of water; secondary, a flushing of CO<sub>2</sub> (carbon dioxide) was performed for 15 minutes in order to reduce saturation (Arab et al. 2016) which is very long, generally. As flushing was finished, cell pressure and back pressure were increased in step. Skempton's coefficient B was used to check the saturation of the samples. To check it, first, the back pressure valve was closed and the cell pressure was increased. This growth of cell pressure results in an increase in the pore water pressure. The ratio between the measured pore pressure increase and the cell pressure is the Skempton's coefficient B, and it's defined as below:

$$B = \frac{\Delta u_w}{\sigma_3} = \frac{(\text{Pore pressure final} - \text{Pore pressure initial})}{(\text{Cell pressure final} - \text{Cell pressure initial})} \quad \text{Eq. 6-1}$$

Sample is considered fully saturated when  $B=1$ , however for sand material also 0.98 is a good value to achieve.

➤ *Sample consolidation*

Sample consolidation consists in two steps. Firstly, back pressure line was closed and cell pressure line was increased to reach a difference between cell and back pressure equal to consolidation pressure, about 100 kPa, which reflects the geostatic stress<sup>4</sup>. Increasing the cell pressure, the pore pressure will increase of the same amount. Then, back pressure valve was opened to allow drainage of excess of pore pressure. Consolidation stops when pore pressure lies on back pressure value and in the meantime no change in volume is recorded (Fig.6.8).



**Fig 6.8 Schematic representation of consolidation in terms of pressure versus time. Consolidation stops when pore pressure is equal to back pressure**

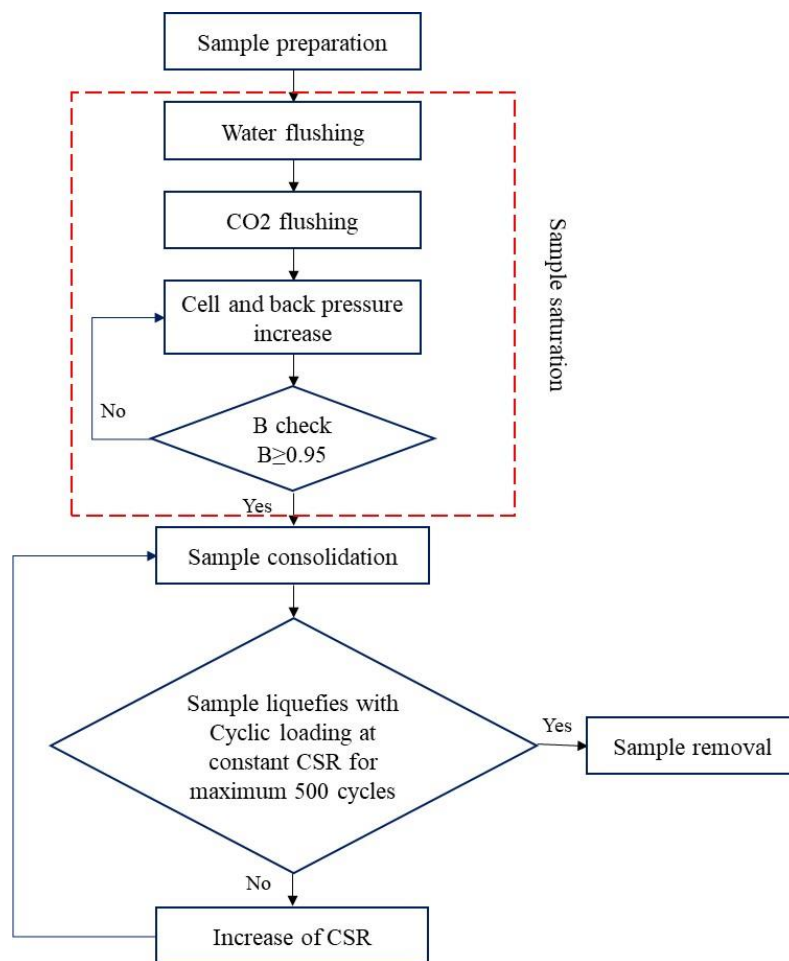
➤ *Cyclic loading*

The triaxial test, performed with static and dynamic loadings, provides a convenient and versatile method for assessing soil behaviour in the laboratory, with regard of liquefaction phenomenon. To investigate soil response under seismic condition, the parameters to be considered during the experiment include the cyclic loading wave, the load frequency, and the value of the cyclic stress ratio (CSR). These parameters are aimed to reproduce similarly the real earthquake of the area. Generally, for earthquake simulations, frequency of 1Hz is considered. In this study tests

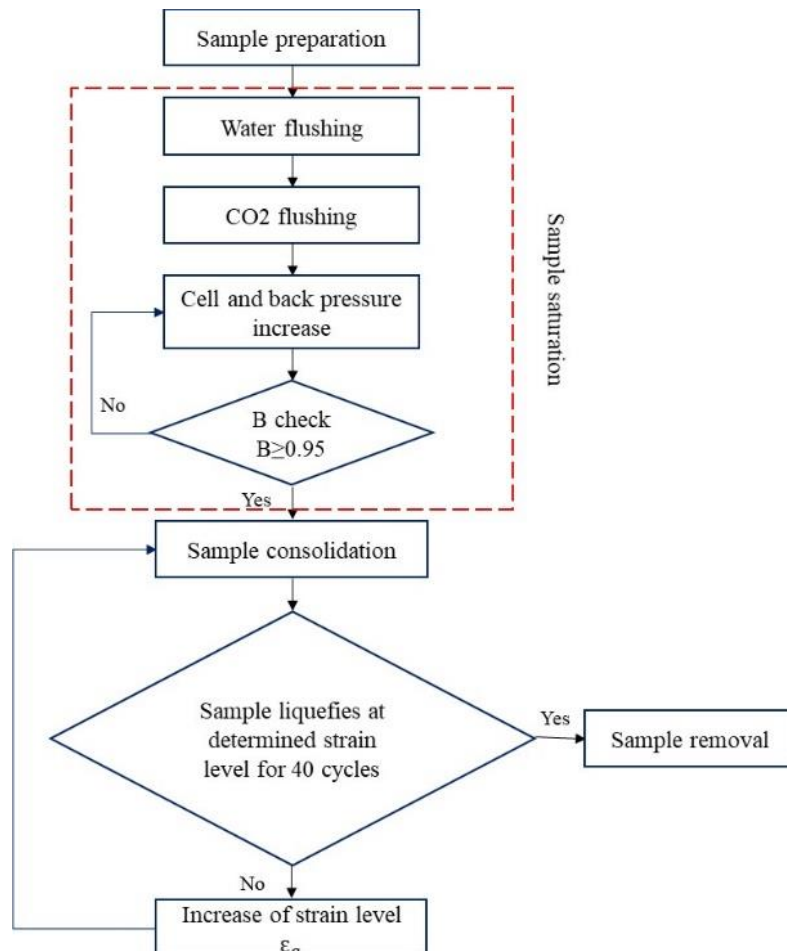
<sup>4</sup> Liquefaction occurs at lower depth, not more than 15m, for this reason an average value for real geostatic stress is about 100kPa

are performed at 1.5Hz. Sample were subjected to cyclic loading for maximum 500 cycles; if liquefaction didn't occur, cyclic loading (CSR) was increased for other 500 cycles, until reaching liquefaction.

The protocol applied for these tests (according to the standard) is explained in Fig.6.9 and Fig.6.10.



**Fig 6.9 Test procedure for cyclic triaxial test (ASTMD5311)**



**Fig 6.10 Test procedure for cyclic triaxial test (ASTMD3999)**

### 6.1.3 Cyclic simple shear test

The simple shear test is used for routine work for undersea structures, landslips and earthquake performance studies.

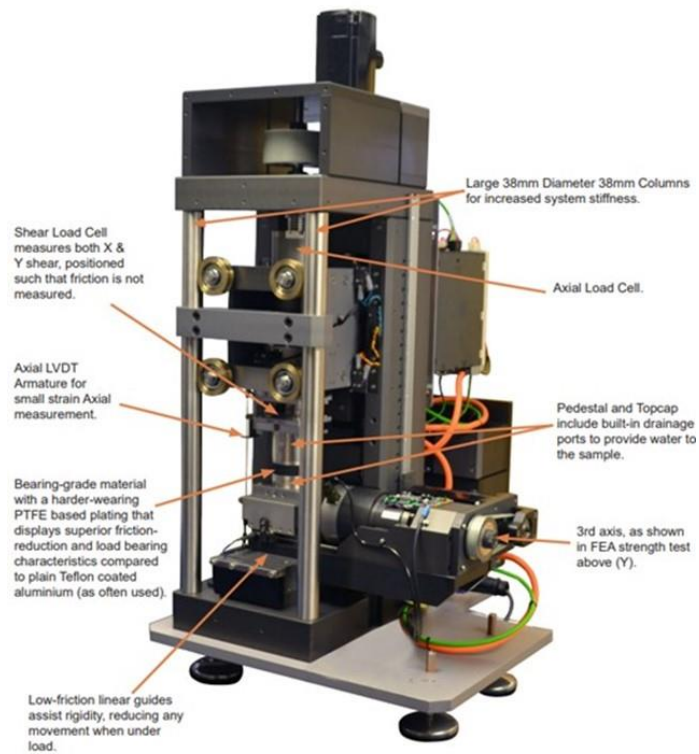
The cyclic simple shear tests were conducted using an electro-mechanical GDS Instruments Variable Direction Dynamic Simple Shear Device (VDDCSS) as shown in Fig.6.11-6.12. The system controls the axial (vertical) force on the soil specimen when applying combinations of shear (horizontal) forces in two directions, this is achieved by having a secondary shear actuator that acts at 90 degrees to the primary shear actuator. When used as a variable direction machine, the secondary shear

axis can be used independently of the other shear axis or in conjunction with it. For this testing programme only one horizontal axis was used.



**Fig 6.11 Variable Direction Dynamic Simple Shear Device (VDDCSS) located at Dundee's University**

The machine is equipped with two 2 kN load cells (one for each horizontal axis) allowing independent  $\pm 10$  mm travel in each direction, whereas the axial force is applied to the specimen through an electro-mechanical actuator via a 5 kN load cell. Loading frequencies of up to 1 Hz are possible on all axes.



**Fig 6.12 Schematic representation of Variable Direction Dynamic Simple Shear Device (VDDCSS)**

Tests have been conducted on dry specimens which are much easier to prepare and less time consuming compared to their saturated counterparts, since the saturation process is eliminated. Test procedure has followed the equivalent undrained method described by Montoya et al. (2013) where the CSS tests are conducted under drained constant volume conditions and the corresponding undrained pore pressure is calculated from the loss of the measured axial stress.

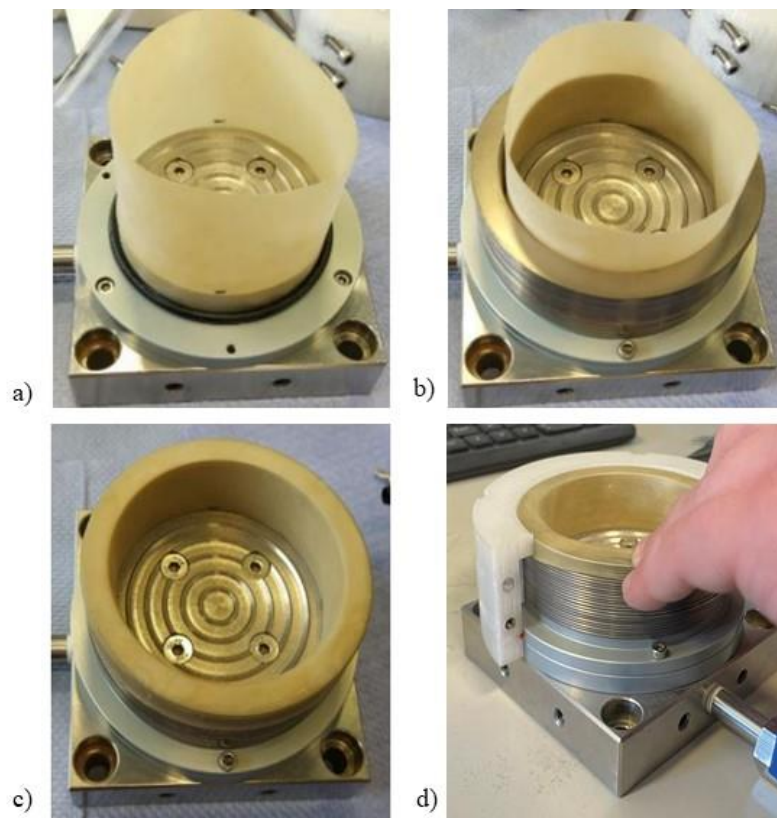
### **6.1.3.1 Test procedure**

Cyclic simple shear tests were performed on cylindrical specimens measuring 70mm diameter and 24 mm height.



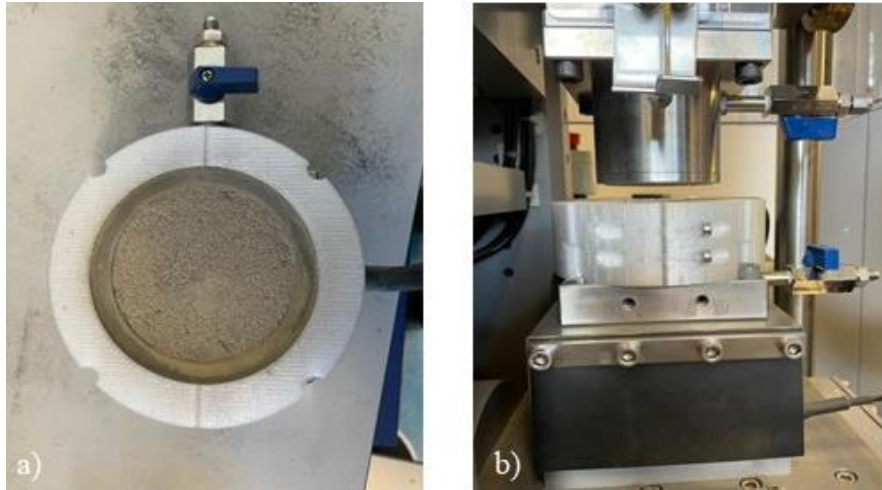
➤ *Sample preparation*

The specimen preparation with dry funnel deposition technique was used in this study, placing the sand within a series of thin coated steel rings surrounding a latex membrane (Fig.6.13-6.14).



**Fig 6.13 Sample preparation for cyclic simple shear test: a) place the membrane and oring to fix it at the base of the mould; b) place the aluminium rings; c) fold the membrane on the aluminium rings, applying vacuum at the base of the mould to stretch the membrane on the rings; d) place the Teflon mould to fix the aluminium rings in sample deposition**

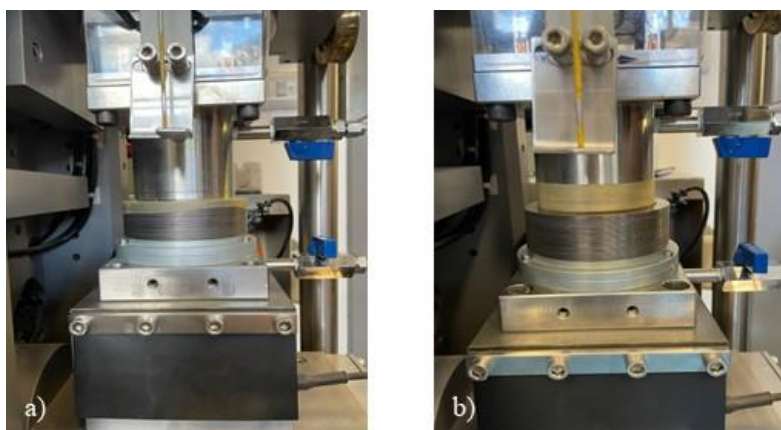




**Fig 6.14 Mounting sample: a) fill the mould with the dry sample with Teflon mould attached and vacuum open; b) disconnect the vacuum and place the sample with Teflon mould in the machine**

➤ *Sample consolidation*

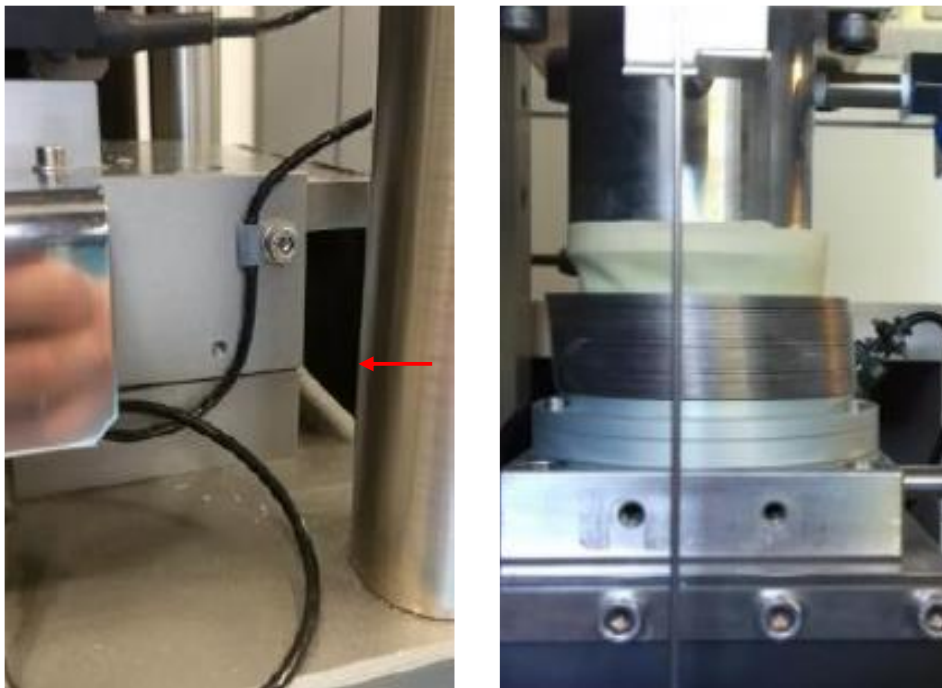
Sample consolidation (Fig.6.15) is the first phase of test: it consists of placing the load cell close to the sample, controlling the axial displacement; successively, the axial load target is applied to the sample and when the cell load is touching the sample holding the axial load, the plastic mould can be removed. Test stops when no change in volume is recorded.



**Fig 6.15 Consolidation phase: a) when vertical stress is reached, the Teflon mould can be removed; b) stretch the membrane upward to free aluminium rings**

➤ Cyclic loading

To investigate soil response under seismic condition, the parameters to be considered during the cyclic loading phase are the normal stress, it means axial load, the shear stress, consequently the CSR, the frequency and deformation, from LVDTs of which machine is equipped (Fig.6.16). These parameters are aimed to reproduce similarly the real earthquake of the area. In this study tests are performed at 0.01Hz.



**Fig 6.16 Cyclic loading phase: a) a check of the alignment of the moving platform and the stable base; b) sample at the end of the cyclic phase**

## 6.2 Results research

### 6.2.1 Case 1: Simulation of the dynamic behaviour of the Panaro embankments

Following the observations made in the preliminary in situ analysis, a series of laboratory tests, especially cyclic triaxial tests, have been carried out on remoulded soil in correspondence of borehole S36 (control section 82) (Fig.6.17) and S9 (control section 44) (Fig.6.18), taking in account the in situ relative density, in order to better characterize the soil considered liquefiable according to previous analysis.

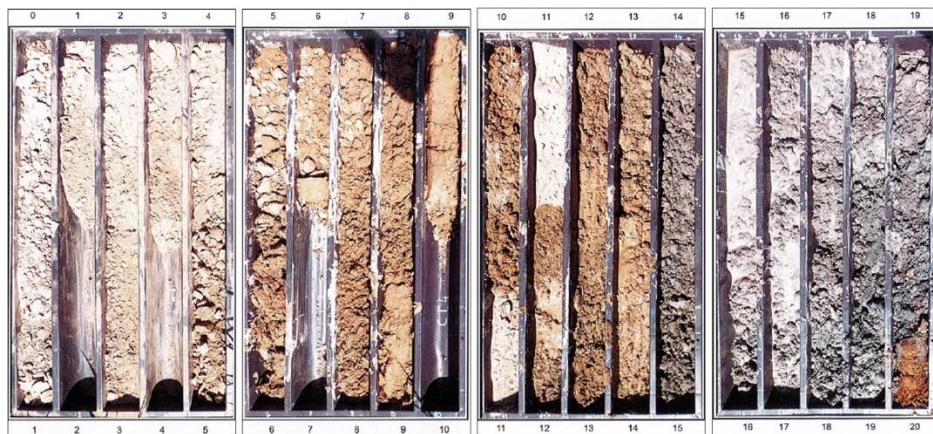


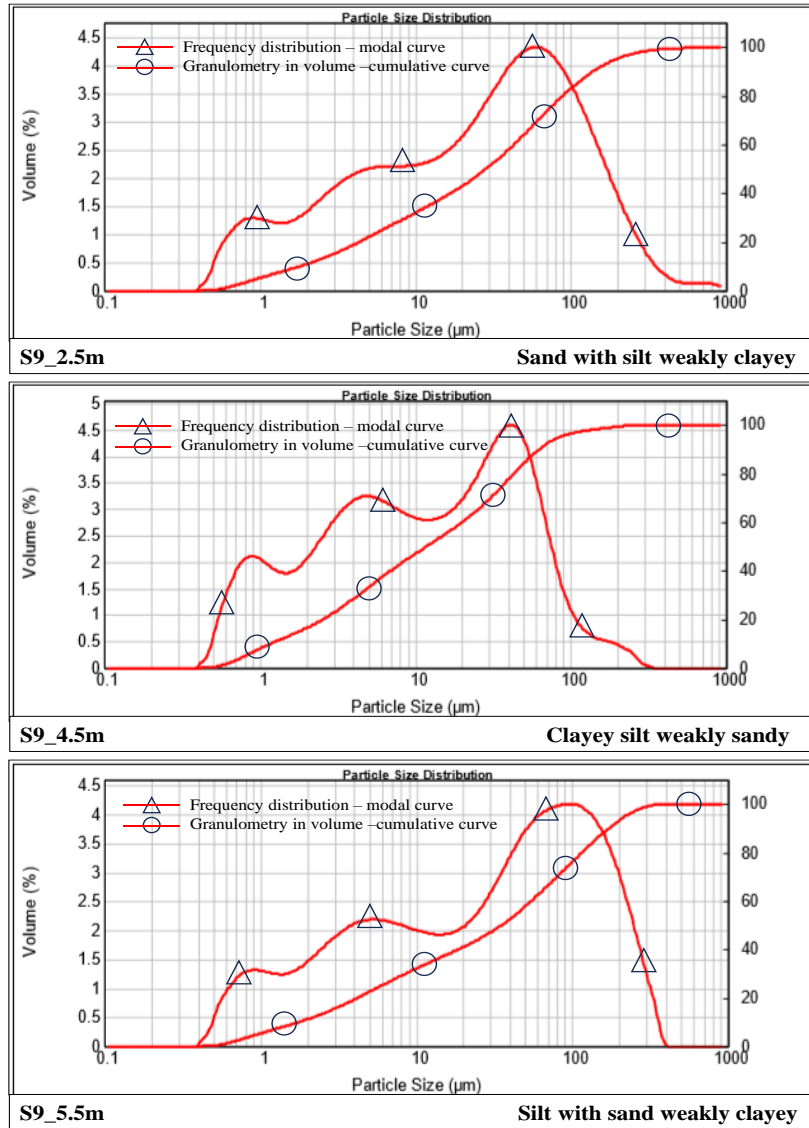
Fig 6.17 Control section 82\_S63 borehole 0-20 m

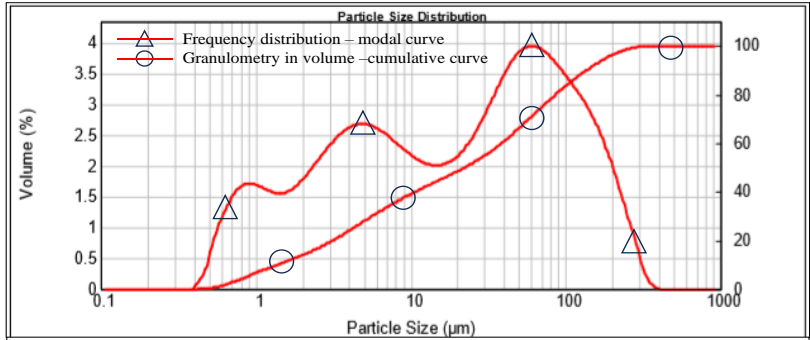


Fig 6.18 Stante 44\_S9 borehole 0-20m

## 6.2.2 Material

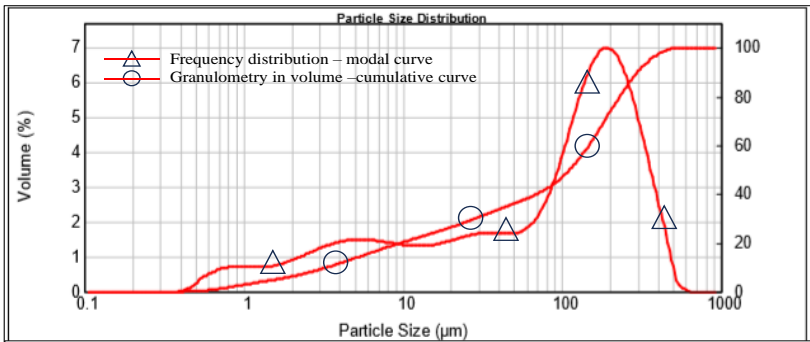
Grain size analysis of soil under investigation is shown in Fig.6.19 for borehole S63 and Fig.6.20 for borehole S9.





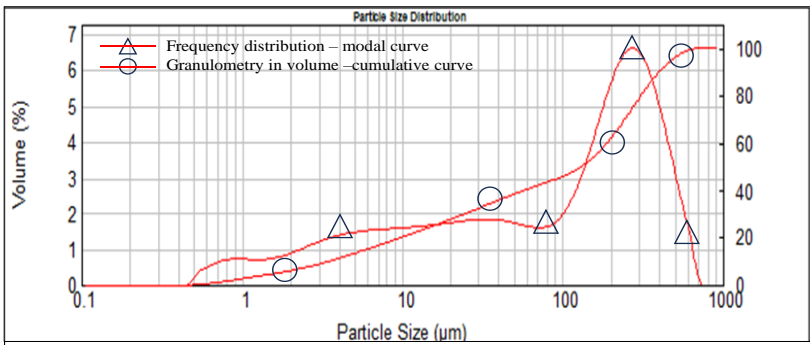
**S9\_8.5m**

**Silt with sand clayey**



**S9\_10.5m**

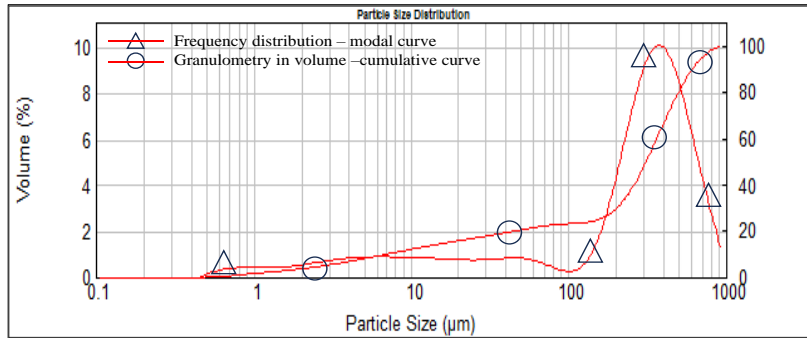
**Silt with sand clayey**



**S9\_12.5m**

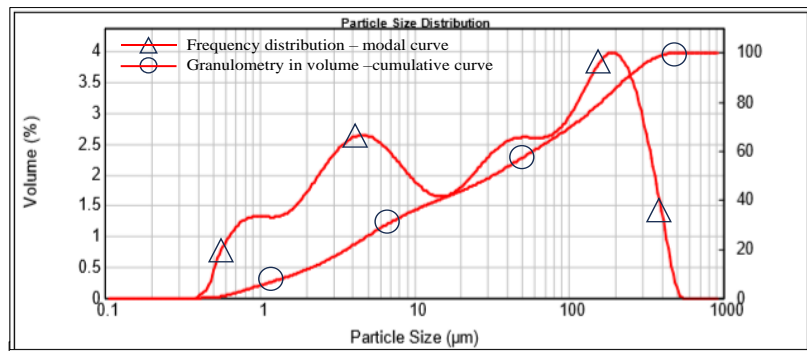
**Sand with silt weakly clayey**





S9\_15.5m

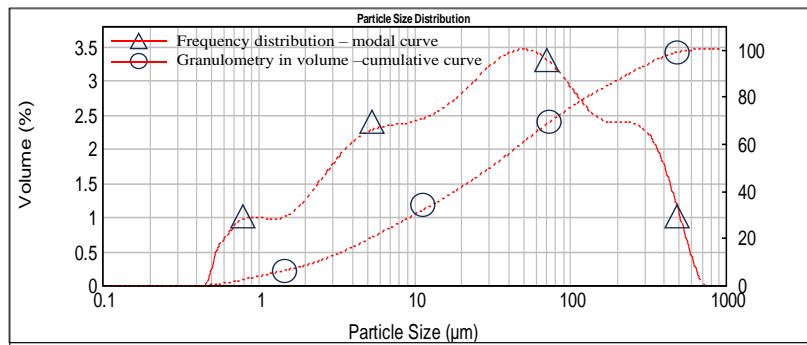
Sand with silt weakly clayey



S9\_17.2m

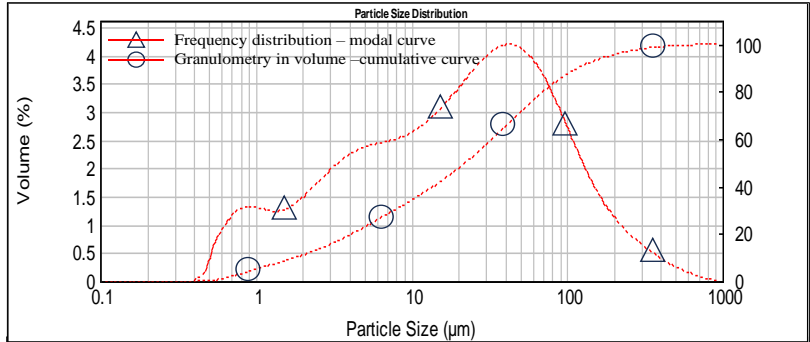
Silt with sand clayey

Fig 6.19 Gran-size distribution of S9 soil



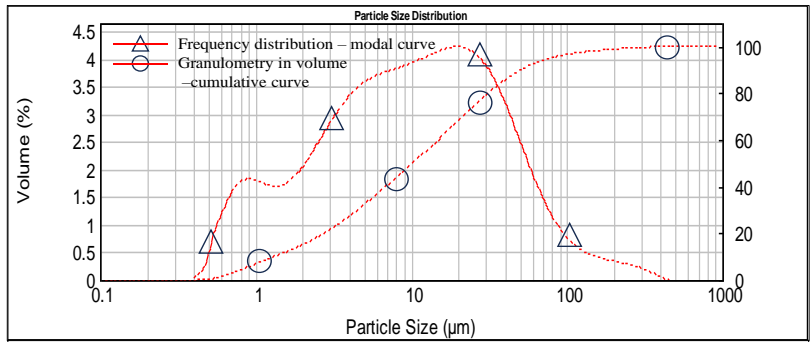
S63\_2.5m

Silt with sand weakly clayey



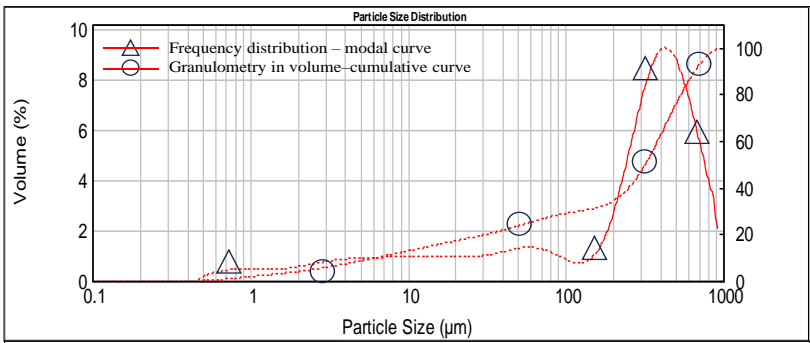
**S63\_4.5m**

**Sandy silt weakly clayey**



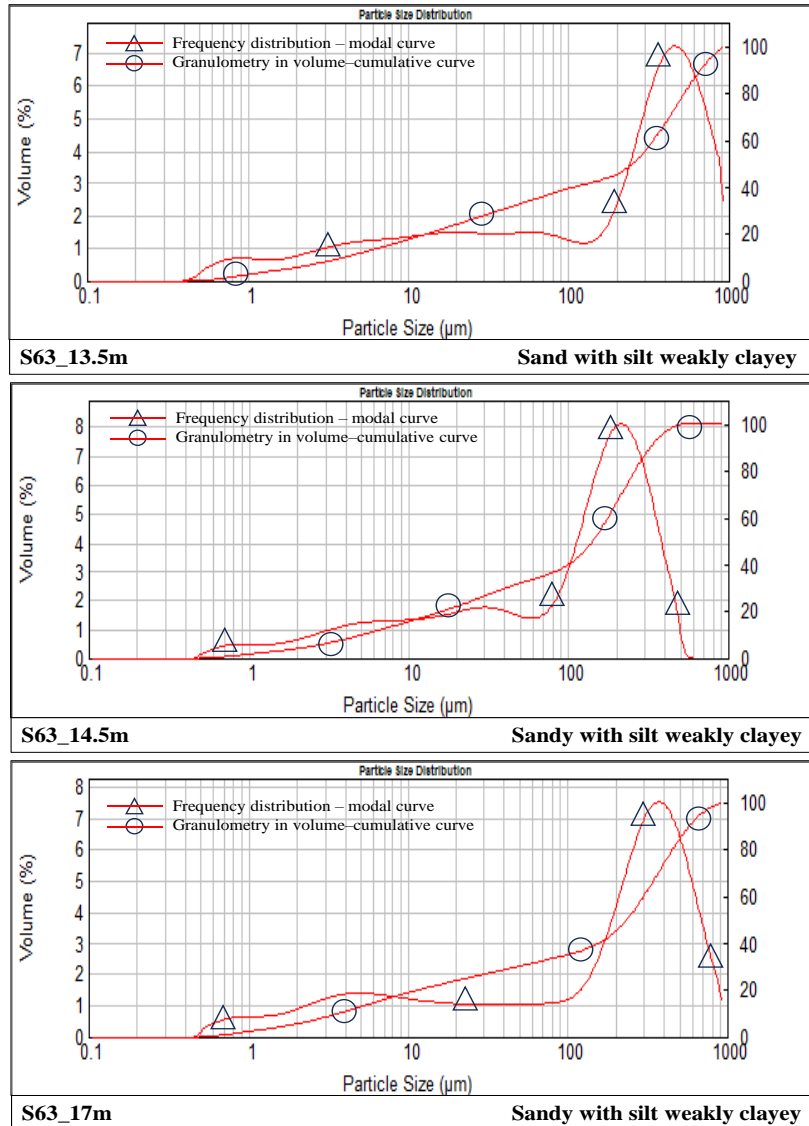
**S63\_6.5m**

**Sandy silt weakly clayey**



**S63\_11m**

**Silty sand weakly clayey**



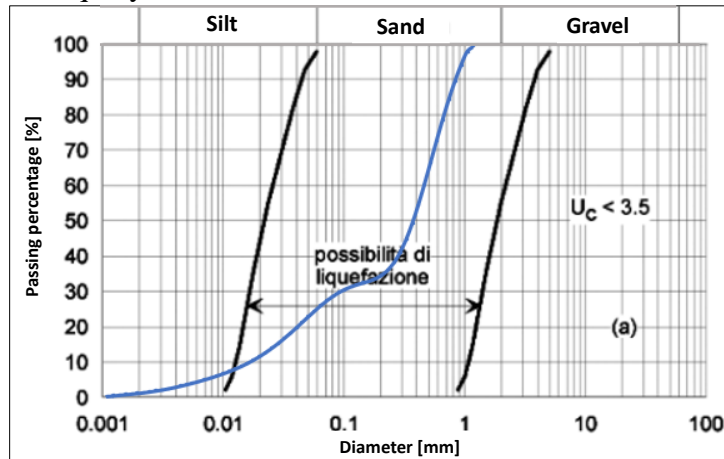
**Fig 6.20 Gran-size distribution of S63 soil**

According to the stratigraphic profile, in correspondence of the borehole S63 it's possible to distinguish more silty levels on the surface and more sandy levels at greater depths. As regards the S9 borehole, the soils analysed can be classified as sands.

Regarding grain-size distribution, regulation (NTC18) previously mentioned, suggests limiting curves to single out potentially liquefying



soils. In Fig.6.21. an example is shown; it can be noted that sample can be expected to liquefy, since the curve is within the boundaries.



**Fig 6.21 Grain size distribution of soil (S63\_11.4-11.6) along with the boundaries of liquefaction susceptible soil according to NTC (2018).**

According to the particle size curves, Atterberg limits (Table 6-1) were only applied to the most superficial samples with a predominantly silty grain size.

Campione	LL (limite liquido)	LP (limite plastico)	Wn (contenuto acqua nat.)	IP (indice di plasticità)
S9_2,5mt	30	19	12	11
S9_4,5mt	32	17	12	15
S9_5,5mt	26	15	6	11
S9_8,5mt	29	16	19	13
S9_17,5mt	66	23	27	43
S63_2,5mt	26	17	3	9
S63_4,5mt	31	19	\	12
S63_6,5mt	31	11	5	20

**Table 6-1 Atterberg limits value for superficial layers of S9 and S63 boreholes**

The void index of soil has been calculated with procedure explained in previous paragraph, results are shown in the table below (Table 6-2):

SAMPLE	mass (g)	V(cm <sup>3</sup> )	$\gamma_d$ (g/cm <sup>3</sup> )	$\gamma_s$ (g/cm <sup>3</sup> )	n	e	
S9_10,80- 11,00 m	182	137.23	1.33	2.65	0.50	1.00	$e_{max}$
	182	112.28	1.62	2.65	0.39	0.63	$e_{min}$
S9_13,75-14 m	183	158.78	1.15	2.65	0.57	1.30	$e_{max}$
	183	129.29	1.42	2.65	0.47	0.87	$e_{min}$
S9_14,8-15,00 m	183	123.62	1.48	2.65	0.44	0.79	$e_{max}$
	183	102.07	1.79	2.65	0.32	0.48	$e_{min}$
S9_15,40- 15,60 m	20.24	15.89	1.27	2.65	0.52	1.08	$e_{max}$
	20.24	12.94	1.56	2.65	0.41	0.69	$e_{min}$
S63_7,40-7,60 m	183	153.11	1.20	2.65	0.55	1.22	$e_{max}$
	183	117.95	1.55	2.65	0.41	0.71	$e_{min}$
S63_11,40- 11,60 m	181	117.95	1.53	2.65	0.42	0.73	$e_{max}$
	181	106.61	1.70	2.65	0.36	0.56	$e_{min}$
S63_13,40- 13,60 m	183	124.75	1.47	2.65	0.45	0.81	$e_{max}$
	183	104.34	1.75	2.65	0.34	0.51	$e_{min}$
S63_17,40- 17,60 m	183	129.29	1.42	2.65	0.47	0.87	$e_{max}$
	183	104.34	1.75	2.65	0.34	0.51	$e_{min}$

Table 6-2 Geotechnical characterization of soil

## 6.2.3 Cyclic triaxial test

### 6.2.3.1 Test program

A series of cyclic triaxial test load controlled (Table 6-3), compliant with ASTM D5311 standard were carried out on saturated and consolidated sample, in order to define the liquefaction behaviour under determined condition: 1.5Hz frequency and  $\pm 60N$  as cyclic load applied to the sample ( $\pm 30kPa$  as deviatoric stress), testing specimen at different depth of boreholes, except for the last two tests.

Identification code	Borehole	Depth (m)	Initial porosity	Initial deviatoric stress (kPa)
<b>TXD1_ S63_11.4_P100</b>	S63	11.4-11.6	0.38	60
<b>TXD2_ S63_11.4_P100</b>	S63	11.4-11.6	0.38	0
<b>TXD3_ S9_10.8_P100</b>	S9	10.8-11	0.43	0
<b>TXD4_ S9_13.75_P100</b>	S9	13.75-14	0.38	0
<b>TXD5_ S9_14.8_P100</b>	S9	14.8-15	0.37	0
<b>TXD6_ S9_15.4_P100</b>	S9	15.4-15.6	0.45	0
<b>TXD8_ S63_13.4_P100</b>	S63	13.4-13.6	0.38	0
<b>TXD9_ S63_17.4_P100</b>	S63	17.4-17.6	0.39	0
<b>TXD10_ S63_11.4_P100</b>	S63	11.4-11.6	0.38	0
<b>TXD11_ S63_11.4_P100</b>	S63	11.4-11.6	0.38	0

**Table 6-3 Cyclic triaxial test performed**

In a typical cyclic triaxial test, various parameters and results are obtained to assess the cyclic behavior and liquefaction potential of soils under cyclic loading conditions. The samples were subjected to a constant CSR cyclic loading until liquefaction. Sample is considered liquefied if at least one the following condition is verified:

- Double amplitude (of axial strain) reaches 5%
- Excess pore water pressure equals to cell pressure, it means effective stress equals to zero.

Cyclic shear stress represents the shear resistance of the soil under cyclic loading conditions. It is measured during the test and plotted against the number of loading cycles.


Axial strain represents the deformation in the axial direction of the soil specimen due to cyclic shear loading. It is measured and plotted against the number of cycles to assess how the soil's volume changes during cyclic loading. Excess pore water pressure ( $u$ ) is monitored during the test and is typically observed to increase with each cycle of loading. The magnitude

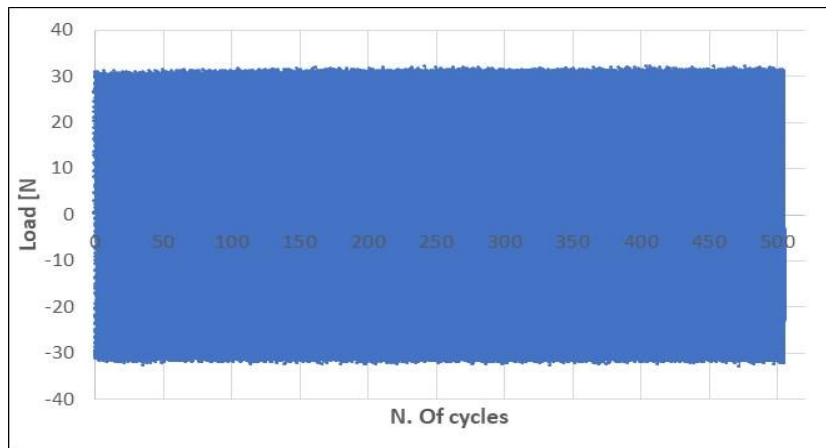
and rate of pore water pressure buildup are important for assessing liquefaction susceptibility.

### 6.2.3.2 Results

Each single test will be shown in detail on the following pages.

#### ➤ TXD1\_S63\_11.4\_P100

	Height (mm)	100
	Diameter (mm)	50
	Base area (mm <sup>2</sup> )	1962.5
	Volume (mm <sup>3</sup> )	196250
	Mass (g)	320.5
	Density (kg/mc)	1633
	Initial porosity	0.38
	Confining pressure (kPa)	100
	Final B test	0.96
	Initial deviatoric stress (kPa)	60KPa



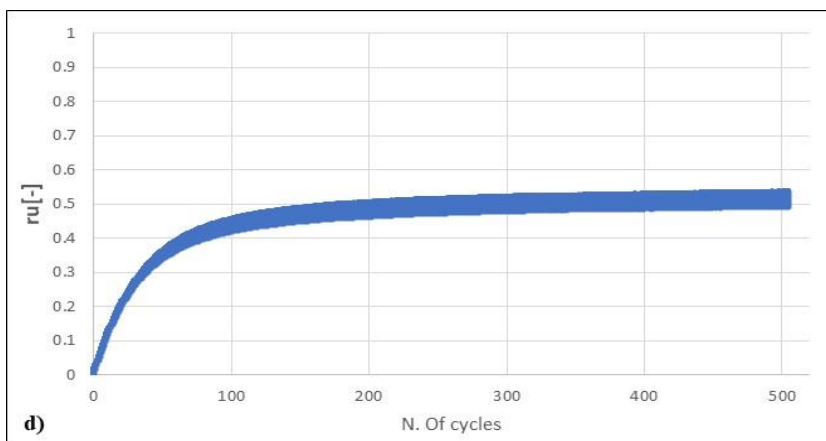
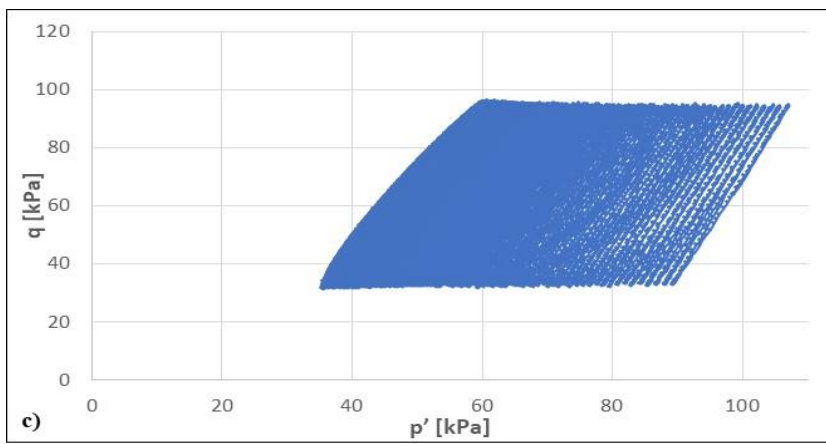
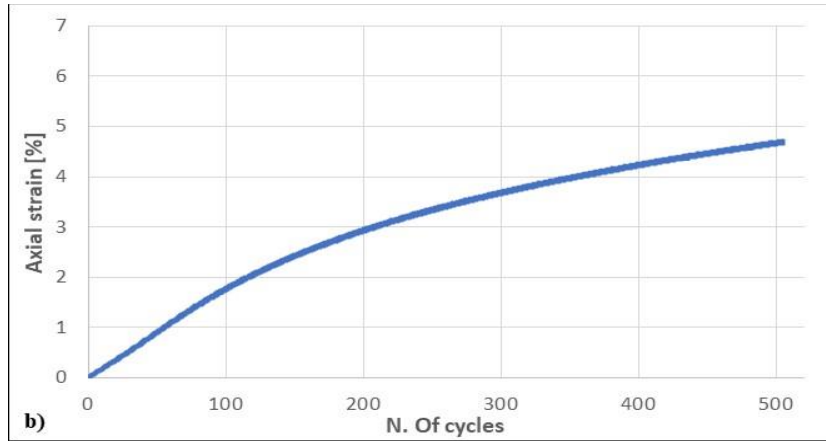
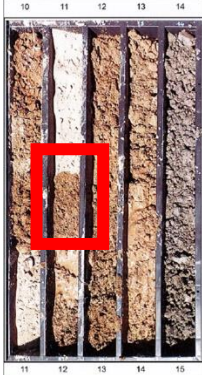
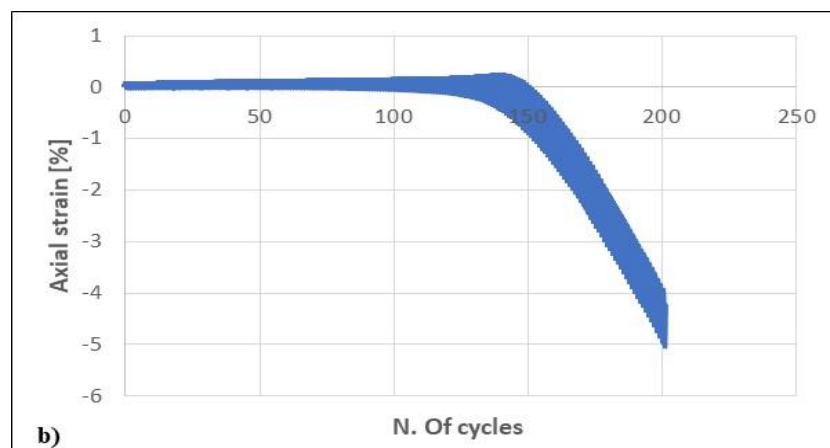
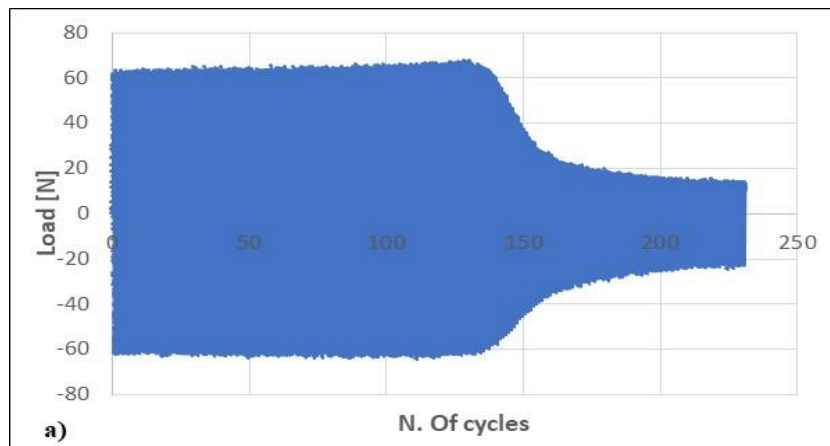
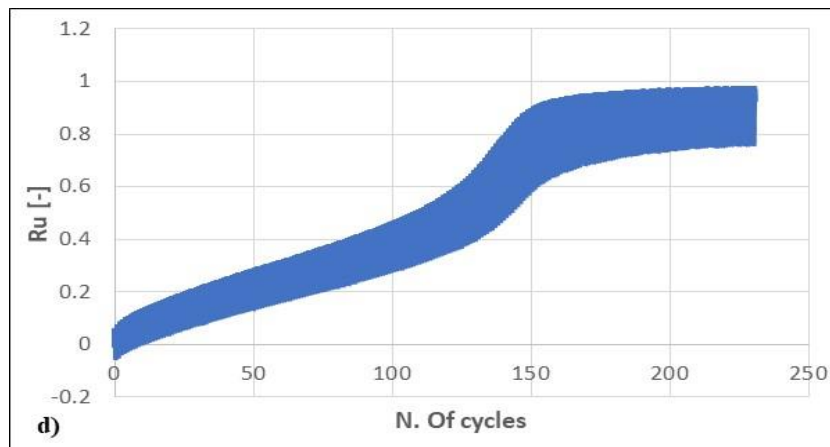
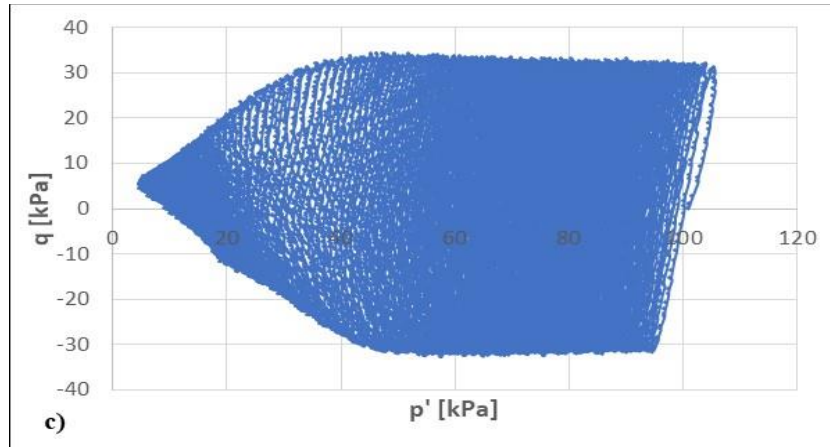


Fig 6.22 TXD1\_S63\_11,4 test results: a) load versus cycles; b) axial strain versus cycles; c) stress path ( $q$ - $p'$ ); d)  $ru$  versus cycles

➤ TXD2\_S63\_11.4\_P100


	Height (mm)	100
	Diameter (mm)	50
	Base area (mm <sup>2</sup> )	1962.5
	Volume (mm <sup>3</sup> )	196250
	Mass (g)	320.5
	Density (kg/mc)	1633
	Initial porosity	0.38
	Confining pressure (kPa)	100
	Final B test	0.96
	Initial deviatoric stress (kPa)	0kPa

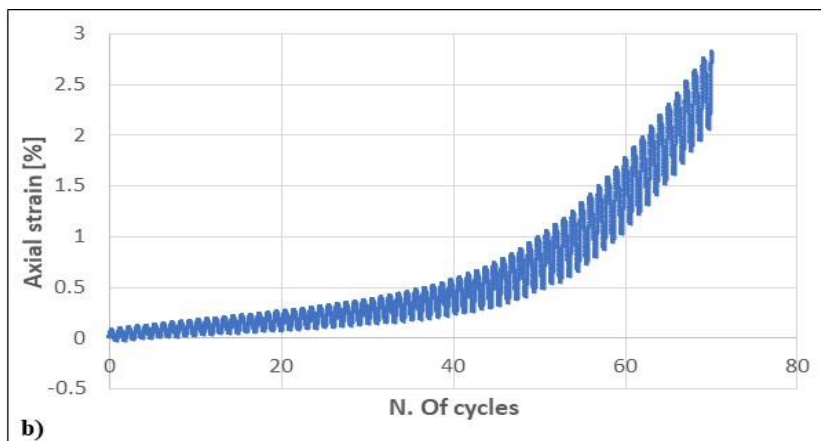
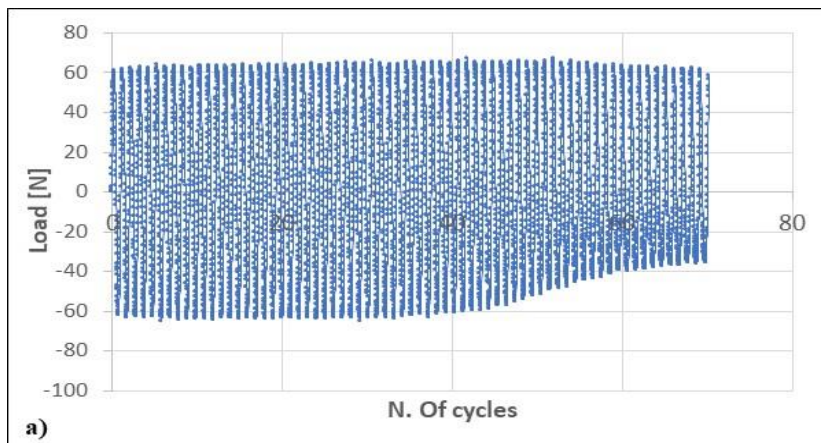




**Fig 6.23 TXD2\_S63\_11,4 result: a) load versus cycles; b) axial strain versus cycles; c) stress path (q-p'); d) ru versus cycles**

➤ TXD3\_S9\_10.8\_P100

	Height (mm)	100
	Diameter (mm)	50
	Base area (mm <sup>2</sup> )	1962.5
	Volume (mm <sup>3</sup> )	196250
	Mass (g)	295.1
	Density (kg/mc)	1504
	Initial porosity	0.43
	Confining pressure (kPa)	100
	Final B test	0.94
	Initial deviatoric stress (kPa)	0





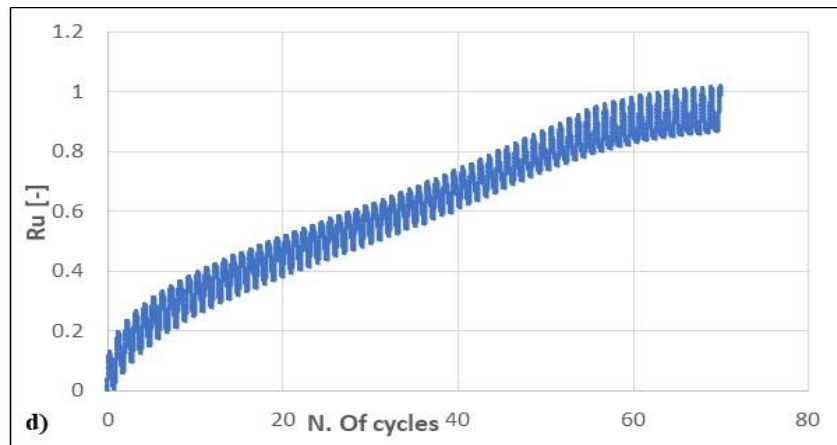
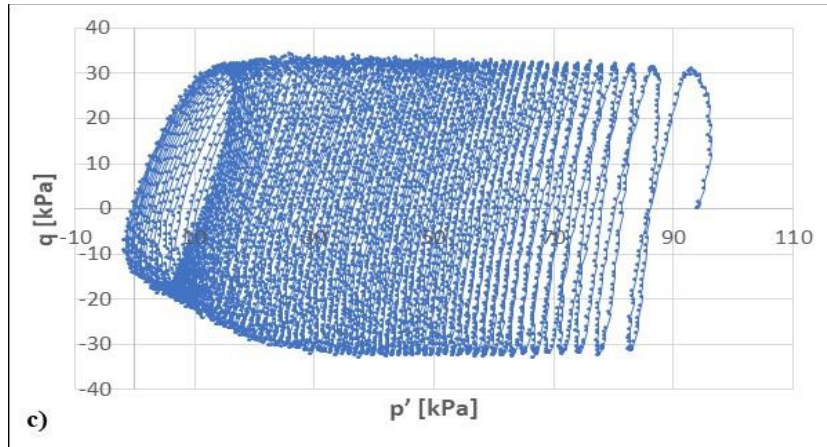

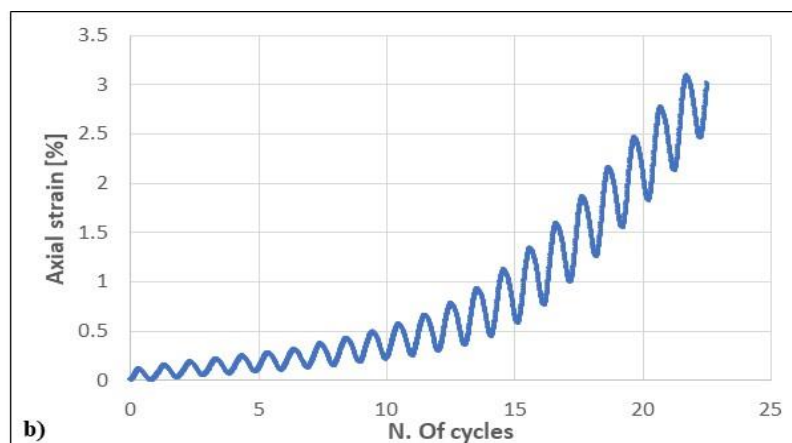
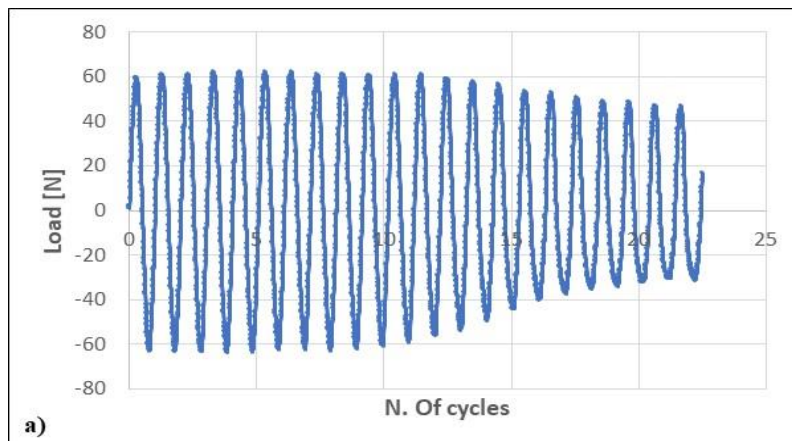


Fig 6.24 TXD3\_S9\_10,8: a) load versus cycles; b) axial strain versus cycles; c) stress path (q-p'); d) ru versus cycles

➤ TXD4\_S9\_13.75\_P100

	Height (mm)	100
	Diameter (mm)	50
	Base area (mm <sup>2</sup> )	1962.5
	Volume (mm <sup>3</sup> )	196250
	Mass (g)	321
	Density (kg/mc)	1636
	Initial porosity	0.38
	Confining pressure (kPa)	100
	Final B test	0.96
	Initial deviatoric stress (kPa)	0



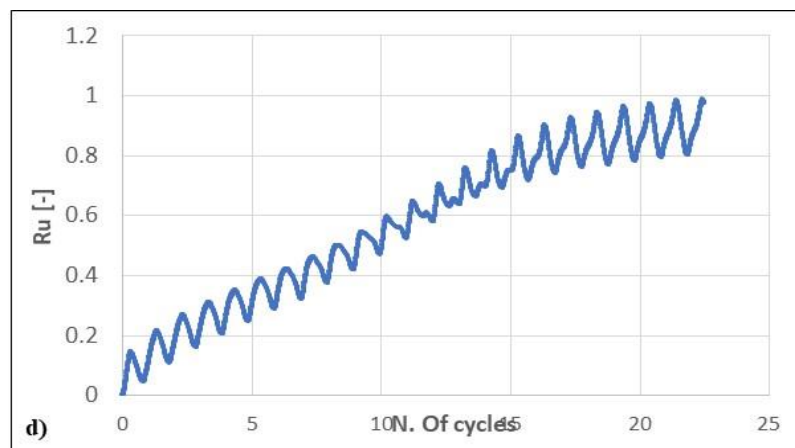
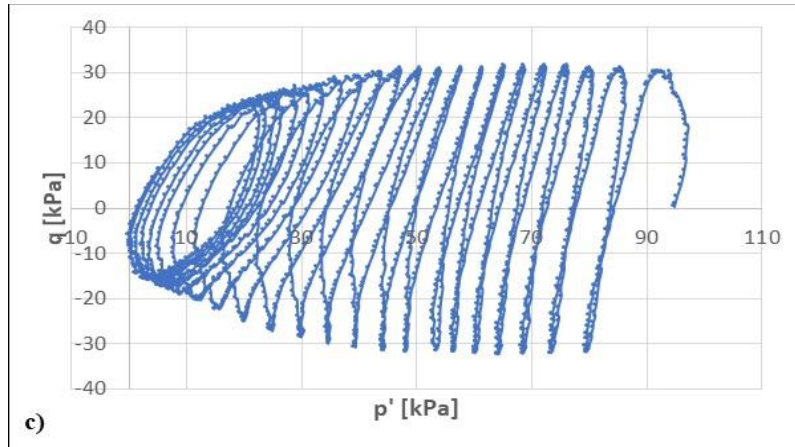

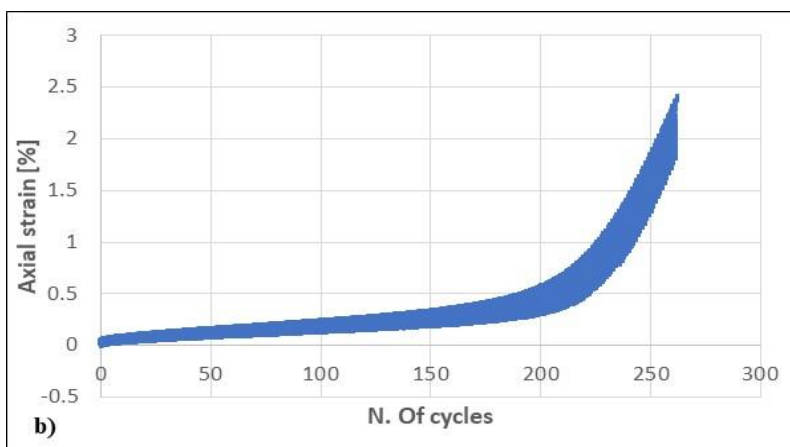
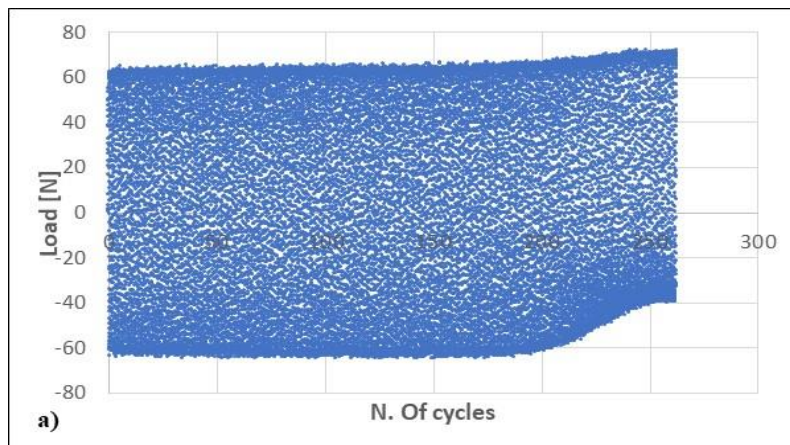


Fig 6.25 TXD4\_S9\_13,75: a) load versus cycles; b) axial strain versus cycles; c) stress path (q-p'); d) ru versus cycles

➤ TXD5\_S9\_14.8\_P100

	Height (mm)	100
	Diameter (mm)	50
	Base area (mm <sup>2</sup> )	1962.5
	Volume (mm <sup>3</sup> )	196250
	Mass (g)	327.5
	Density (kg/mc)	1667
	Initial porosity	0.37
	Confining pressure (kPa)	100
	Final B test	0.80
	Initial deviatoric stress (kPa)	0



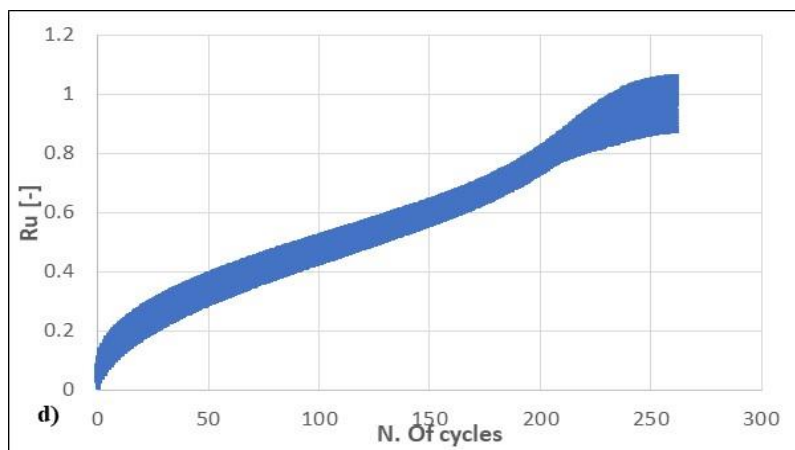
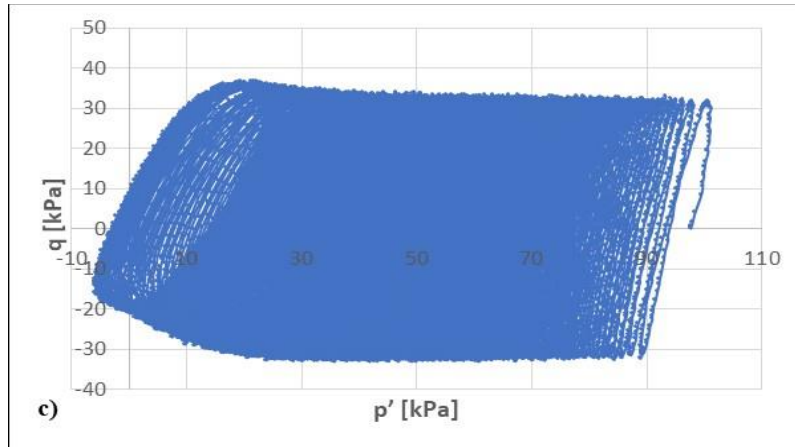

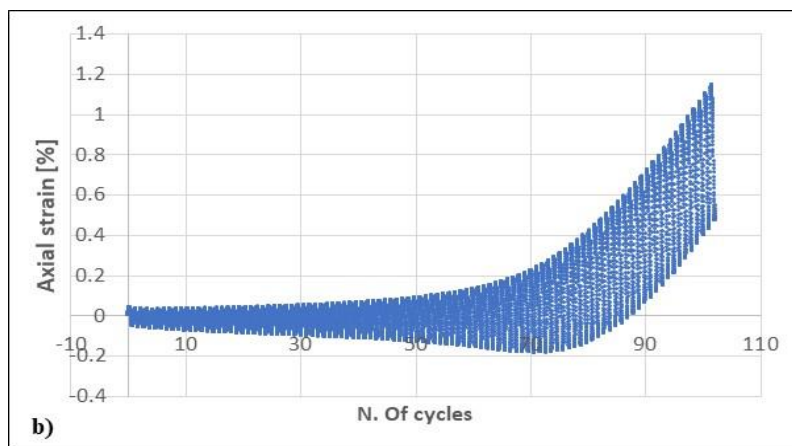
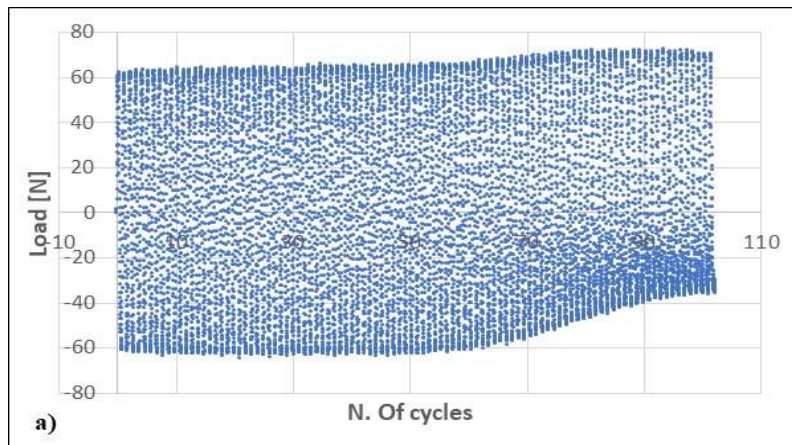


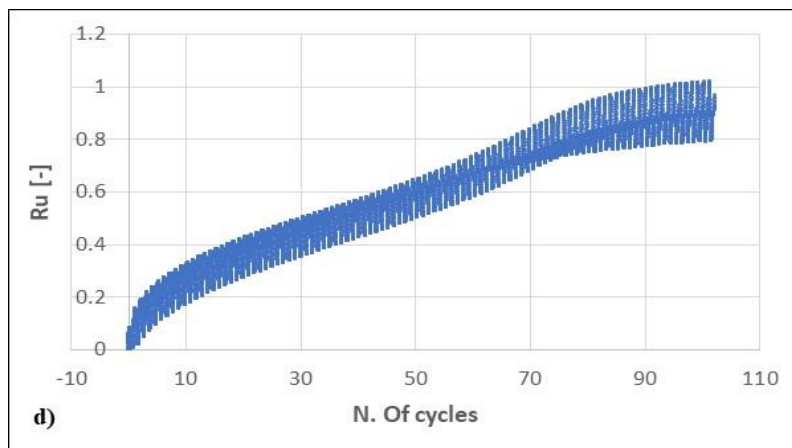
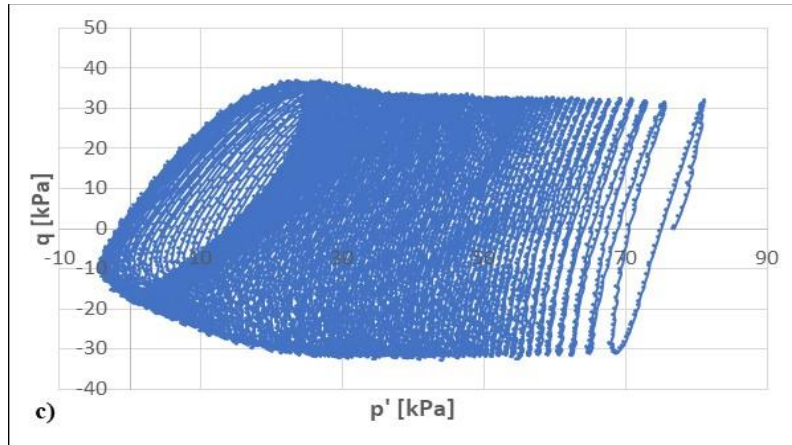
Fig 6.26 TXD5\_S9\_14,8: a) load versus cycles; b) axial strain versus cycles; c) stress path ( $q$ - $p'$ ); d)  $r_u$  versus cycles

➤ TXD6\_S9\_15.4\_P100

	Height (mm)	100
	Diameter (mm)	50
	Base area (mm <sup>2</sup> )	1962.5
	Volume (mm <sup>3</sup> )	196250
	Mass (g)	288
	Density (kg/mc)	14667
	Initial porosity	0.45
	Confining pressure (kPa)	100
	Final B test	0.96
	Initial deviatoric stress (kPa)	0

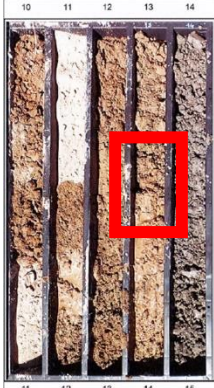


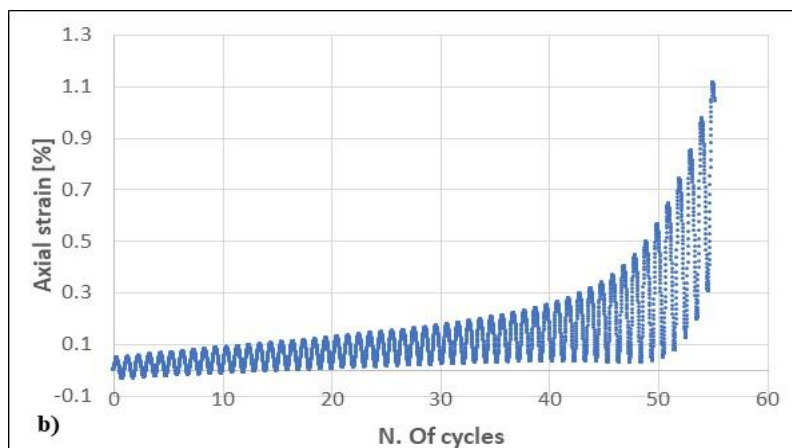
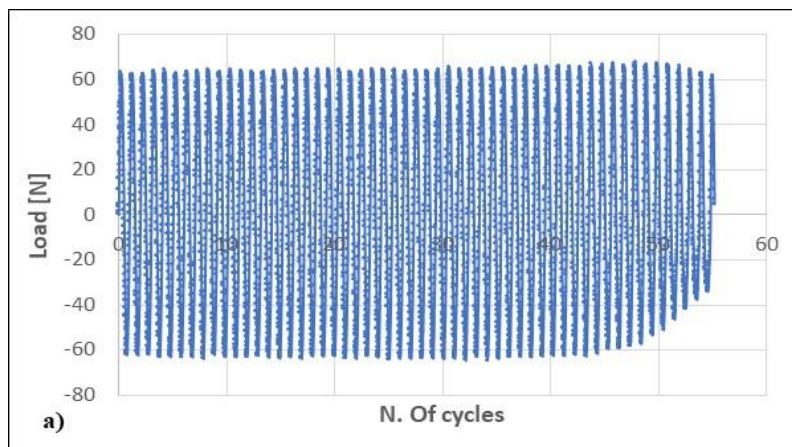




**Fig 6.27 TXD6\_S9\_15,4: a) load versus cycles; b) axial strain versus cycles; c) stress path ( $q$ - $p'$ ); d)  $ru$  versus cycles**

➤ TXD8\_S63\_13.4\_P100

	Height (mm)	100
	Diameter (mm)	50
	Base area (mm <sup>2</sup> )	1962.5
	Volume (mm <sup>3</sup> )	196250
	Mass (g)	322
	Density (kg/mc)	1641
	Initial porosity	0.38
	Confining pressure (kPa)	100
	Final B test	0.88
	Initial deviatoric stress (kPa)	0





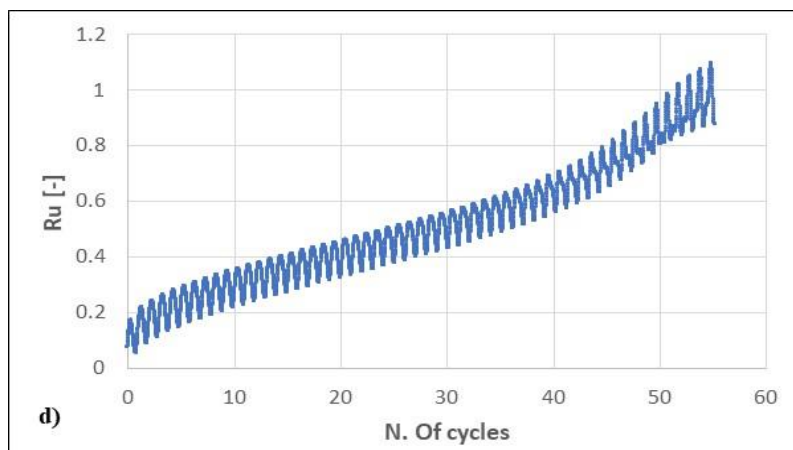
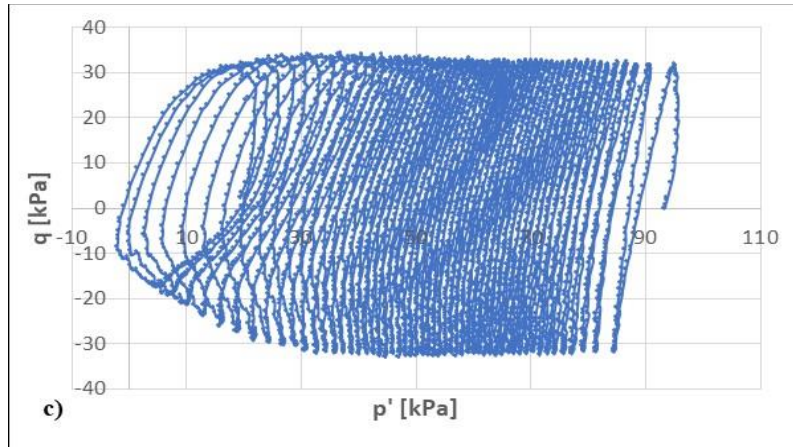
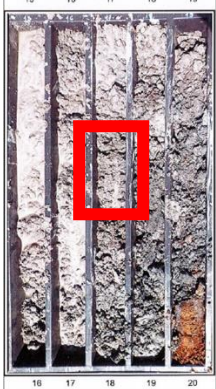
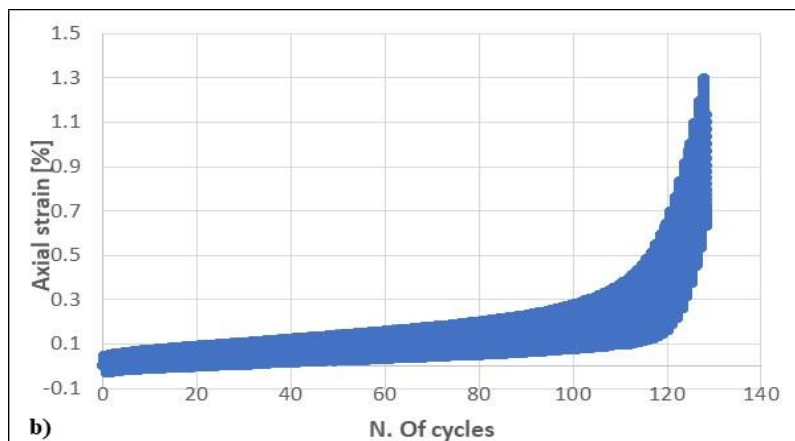
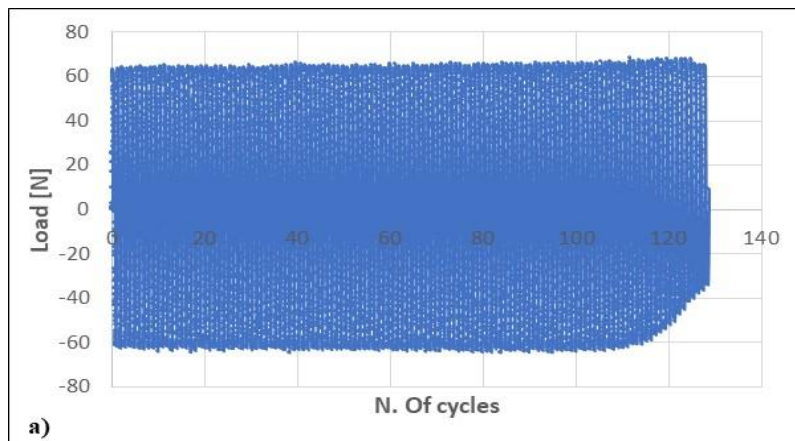


Fig 6.28 TXD8\_S63\_13,4: a) load versus cycles; b) axial strain versus cycles; c) stress path ( $q$ - $p'$ ); d)  $ru$  versus cycles

➤ TXD9\_S63\_17.4\_P100

	Height (mm)	100
	Diameter (mm)	50
	Base area (mm <sup>2</sup> )	1962.5
	Volume (mm <sup>3</sup> )	196250
	Mass (g)	318
	Density (kg/mc)	1620
	Initial porosity	0.39
	Confining pressure (kPa)	100
	Final B test	0.93
	Initial deviatoric stress (kPa)	0



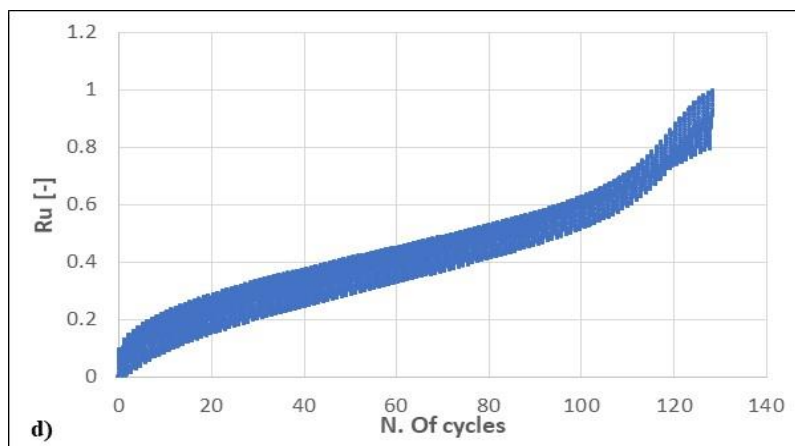
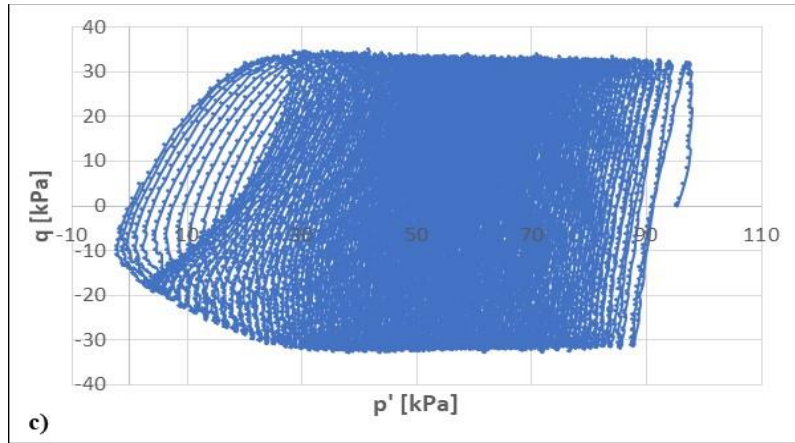

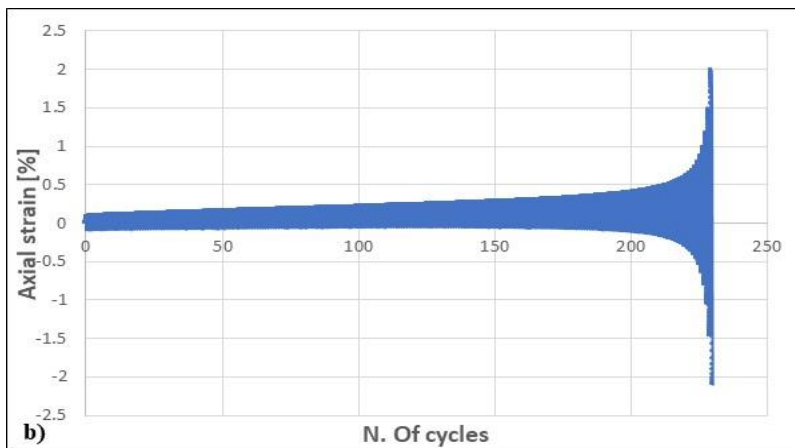
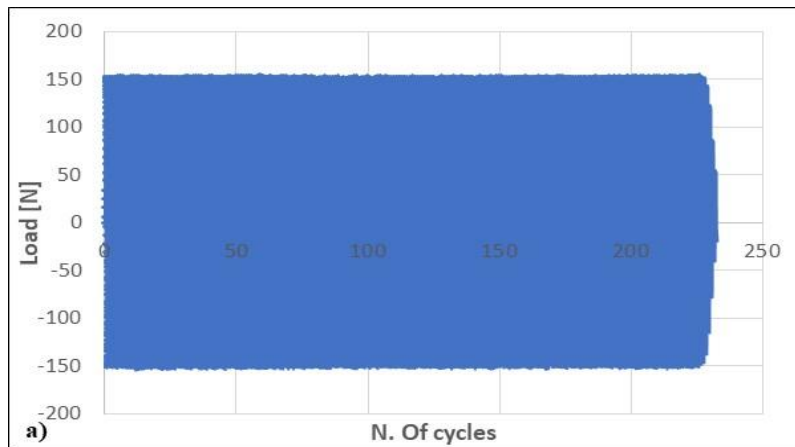


Fig 6.29 TXD9\_S63\_17,4: a) load versus cycles; b) axial strain versus cycles; c) stress path ( $q$ - $p'$ ); d)  $ru$  versus cycles

➤ TXD10\_S63\_11.4\_P100

	Height (mm)	100
	Diameter (mm)	50
	Base area (mm <sup>2</sup> )	1962.5
	Volume (mm <sup>3</sup> )	196250
	Mass (g)	320.5
	Density (kg/mc)	1633
	Initial porosity	0.38
	Confining pressure (kPa)	100
	Final B test	0.96
	Initial deviatoric stress (kPa)	60KPa



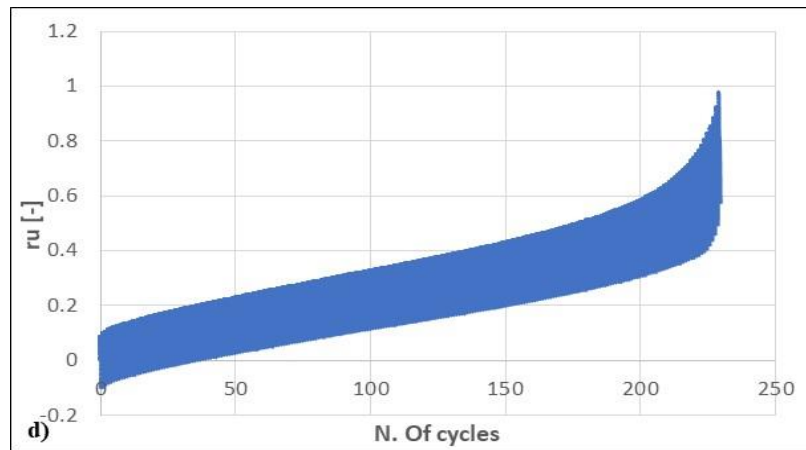
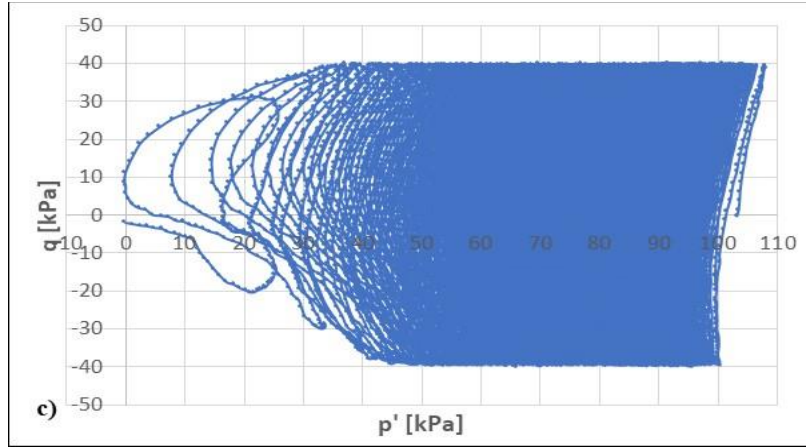

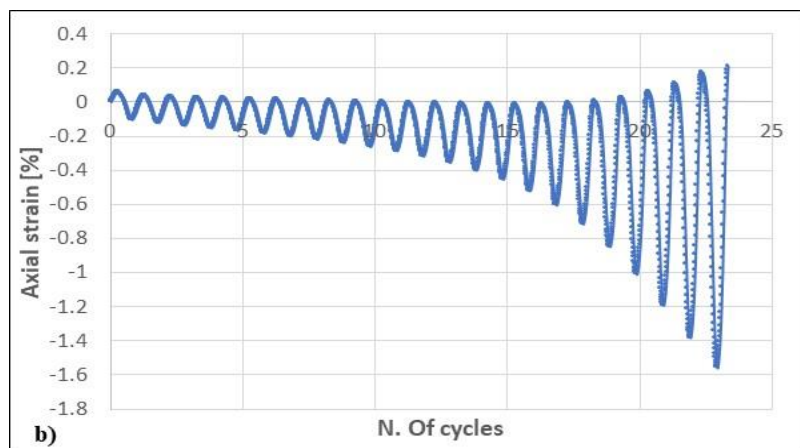
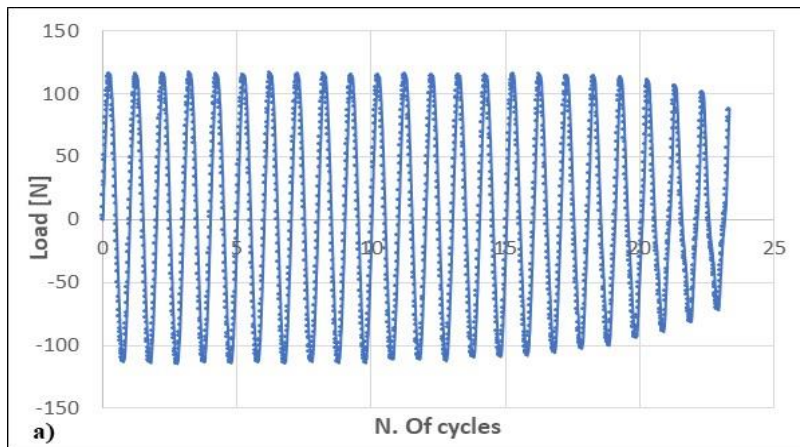
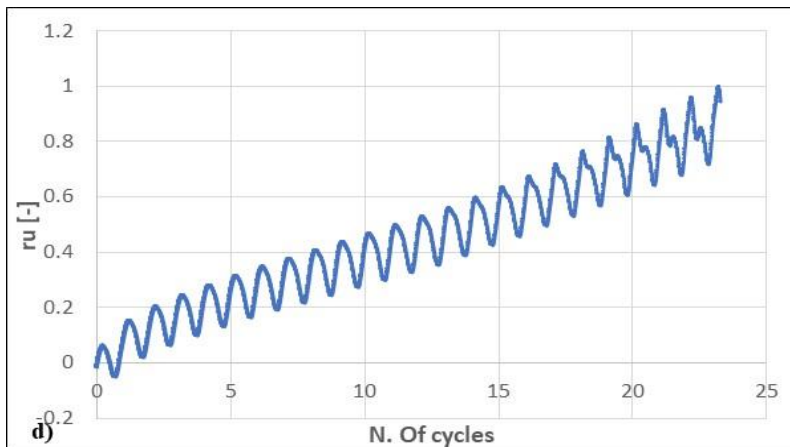
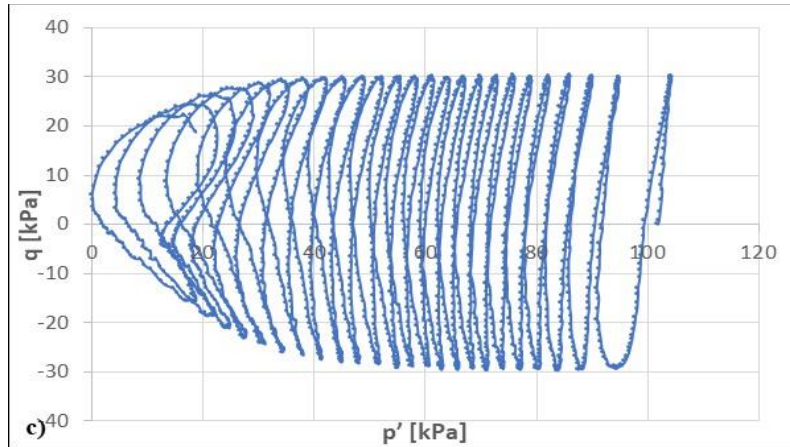


Fig 6.30 TXD10\_S63\_11.4: a) load versus cycles; b) axial strain versus cycles; c) stress path ( $q$ - $p'$ ); d)  $ru$  versus cycles

➤ TXD11\_S63\_11.4\_P100

	Height (mm)	100
	Diameter (mm)	50
	Base area (mm <sup>2</sup> )	1962.5
	Volume (mm <sup>3</sup> )	196250
	Mass (g)	320.5
	Density (kg/mc)	1633
	Initial porosity	0.38
	Confining pressure (kPa)	100
	Final B test	0.96
	Initial deviatoric stress (kPa)	60KPa



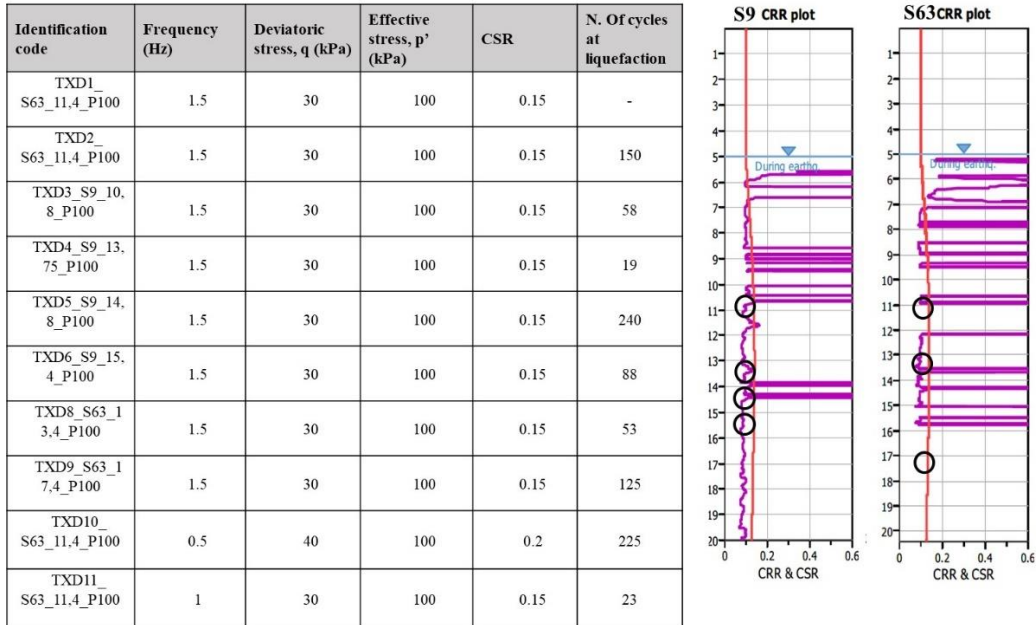


### 6.2.3.3 Discussion

A series of cyclic triaxial test has been performed on Panaro sand, in order to study its behaviour under cyclic stress and to find the geotechnical parameters for further analysis with constitutive model.

Samples from different depth have tested with same condition, resulting in different number of cycles at liquefaction. A summary of results (Fig.6.29) is shown in table below along with CPT result. The red line is referred to the CSR as seismic demand, instead the violet line is the result of CPT, in terms of CRR; as known FS is less than the unit if CRR is minor than CSR, and in fact the depths in which this condition is verified are of our interest. CSR value is about 0.15, and in these tests this condition was reproduced.





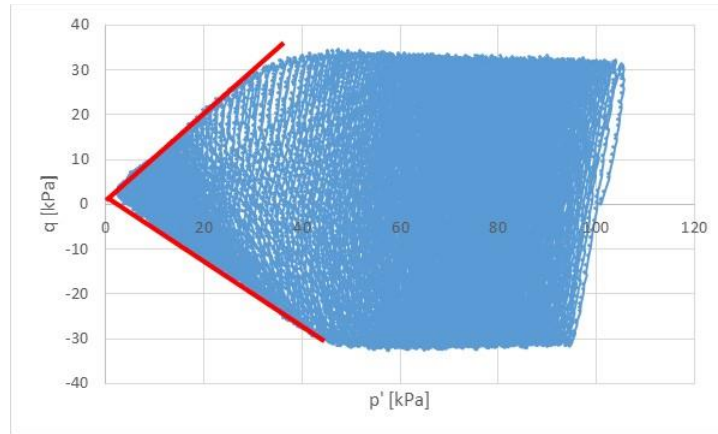
**Fig 6.31 Summary of test results on the left; on the right CPT results in correspondence of the two boreholes investigated**

All the specimens reached liquefaction condition when one or both conditions were verified, except for the first test where initial deviatoric stress was different to 0, it means anisotropic condition; in that case liquefaction was not reached and this is in line with expected result, since an increase of deviatoric stress before cyclic phase, could produce an increase of shear strength.

The relationship between the mean effective stress and the deviator stress of the tests are presented in figure. The Fig.6.30 is butterfly shape, a characteristic of the cyclic mobility phenomenon. The q-p' curve approaches the failure criteria lines (q is the deviator stress and p' is the effective mean stress). The relationship between the slope of the failure criterion lines and the friction angle is shown in equations:

- $M = \frac{6 \cdot \sin \varphi}{3 - \sin \varphi}$  in compression
- $M = -\frac{6 \cdot \sin \varphi}{3 + \sin \varphi}$  in extension



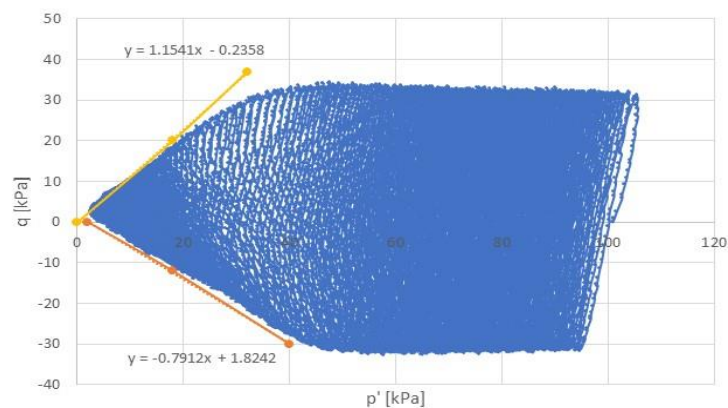


**Fig 6.32 Stress path of TXD2\_S63\_11,4 showing the butterfly shape**

Comparison was done with the friction angle deduced from the cyclic test (Fig.6.31) in this study (TXD2\_S63\_11,4) with the one derived from a direct shear test on the same material (Table 6-4):

Sample	Type of test	M compression	M extension
S63_11.4	Direct shear test	1.14	-0.82
S63_11.4	Cyclic triaxial test	1.15	-0.79

**Table 6-4 Comparison results of M between direct shear and cyclic triaxial test**



**Fig 6.33 Stress path graph of TXD2\_S63\_11,4 with calculated M**

The butterfly shape is well explained in the test shown; unfortunately, not all the tests show the same shape, but according to our aim, specimens

are considered liquefied, because in every test (except for TXD1)  $r_u$  reaches 1.

## 6.2.4 Cyclic simple shear test

### 6.2.4.1 Test program

Cyclic simple shear tests have been performed on Panaro sand (Fig.6.32), with different CSR ratio, in order to find the characteristic curve studying a different equipment and its feature.

For each borehole, S63 and S9, one level has been chosen:

- S63\_11,40-11,60m;
- S9\_13,75-14m.



Fig 6.34 Panaro sand tested with cyclic simple shear test, in the box (Bicocca university) and in the bags (Dundee University)

The testing program is shown in Table 6-5, explicating the normal and shear stress applied in order to obtain desired CSR ratio.

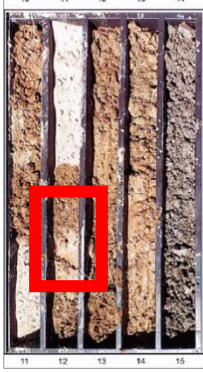
Tests are conducted in dry condition and taking advantages from the “constant volume” procedure. Shear stress is applied horizontally recording also the axial load value decreasing. A loss of about 90% in axial load will correspond to an increase of pore pressure leading to  $r_u$  value equal to 1, it means liquefaction.

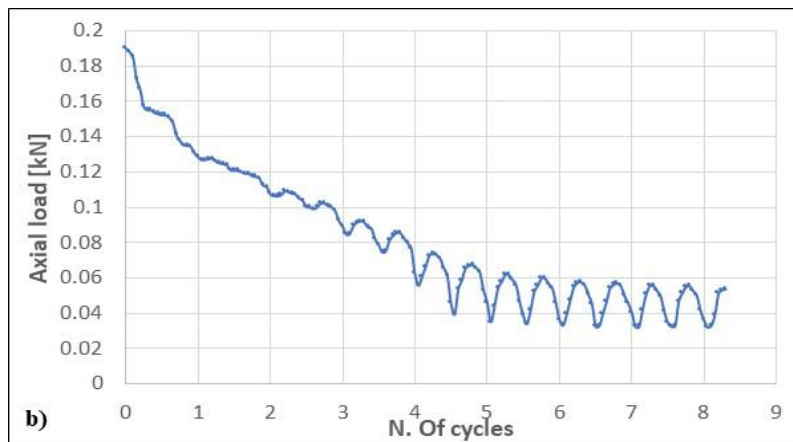
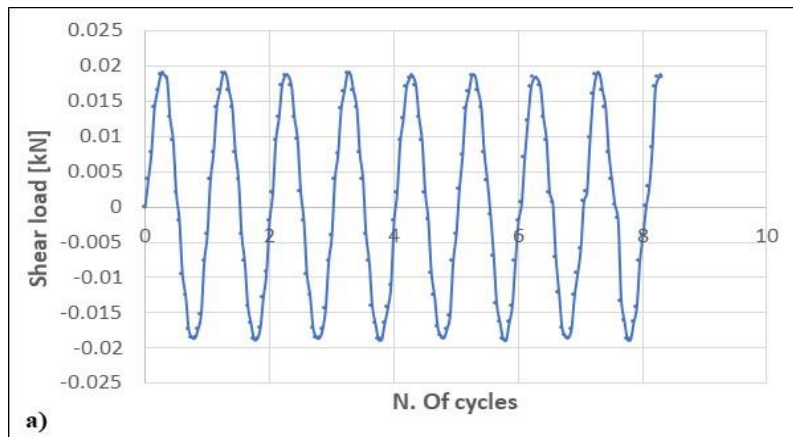
Test n.	Sample	Dr (%)	$\sigma'_v$ (kPa)	$\tau$ (kPa)	CSR	N. of cycles at liquefaction
CSS 1	S63	60	50	5	0.1	5.5
CSS 2	S63	60	100	10	0.1	20
CSS 3	S63	60	50	3.75	0.075	52
CSS 4	S63	60	100	7.5	0.075	37
CSS 5	S63	60	50	2.5	0.05	ND
CSS 6	S63	60	100	5	0.05	ND
CSS 7	S9	15	100	7.5	0.075	ND
CSS 8	S9	15	50	5	0.1	63
CSS 9	S9	15	100	10	0.1	ND
CSS 10	S9	15	50	6	0.12	20
CSS 11	S9	15	50	11	0.22	1

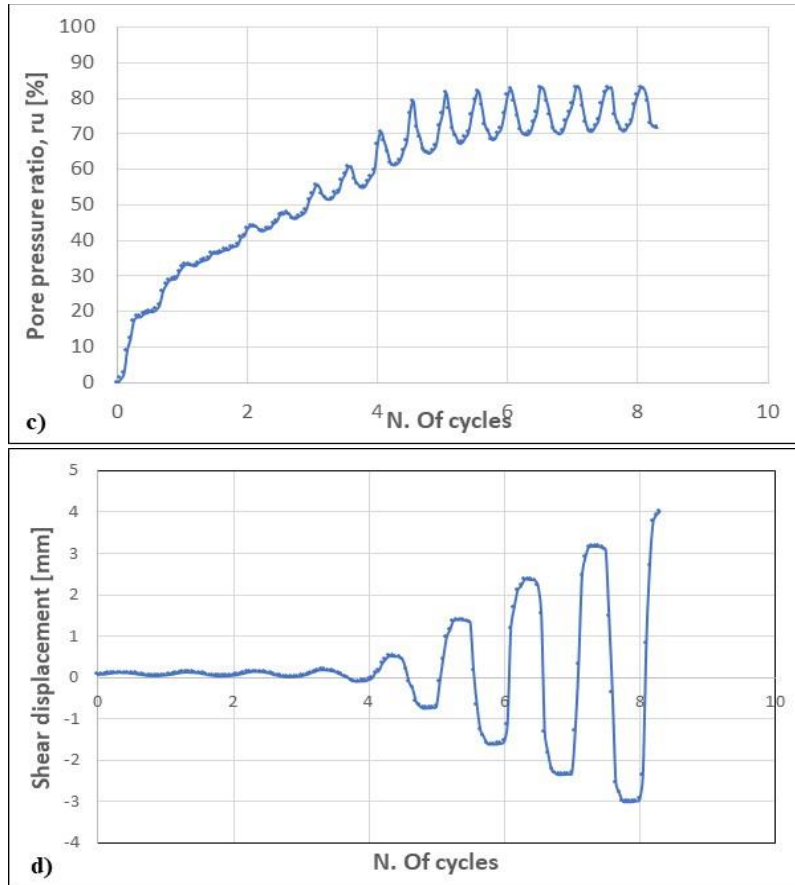
Table 6-5 Programme of Cyclic Simple Shear (CSS) testing

### 6.2.4.2 Results

#### ➤ CSS 1

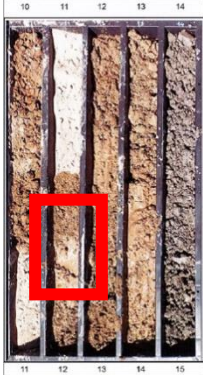
	Height (mm)	22.8
	Diameter (mm)	70
	Base area (mm <sup>2</sup> )	3879.54
	Volume (mm <sup>3</sup> )	88453.5
	Mass (g)	137.68
	Density (kg/mc)	1633
	Initial porosity	0.38
	Normal stress (kPa)	50
	Shear stress (kPa)	5
	CSR	0.1

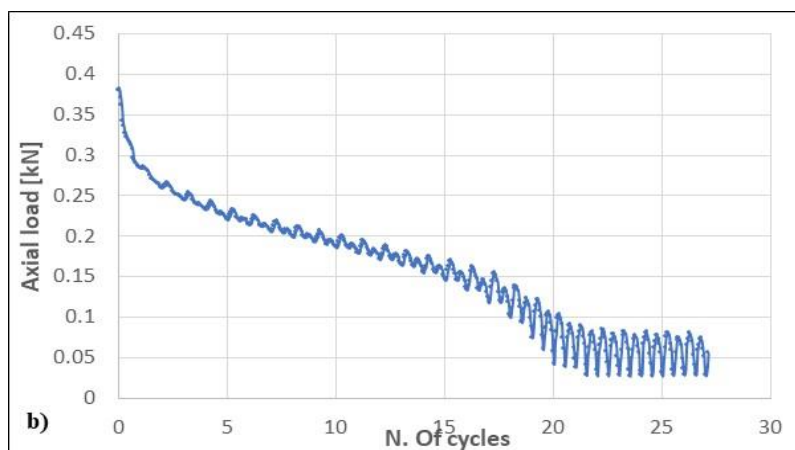
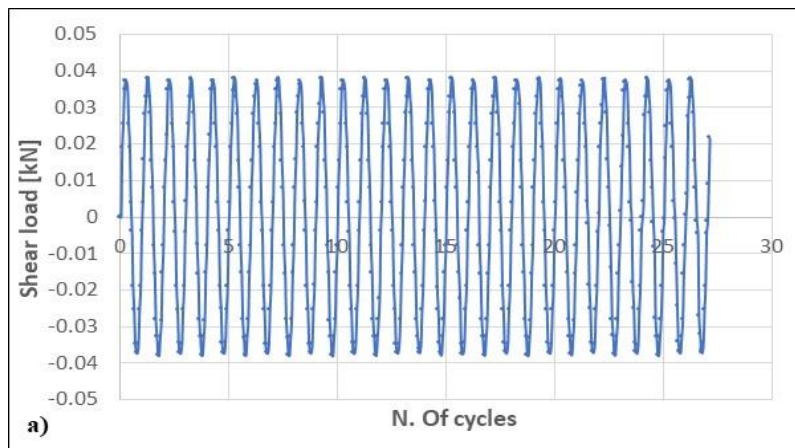


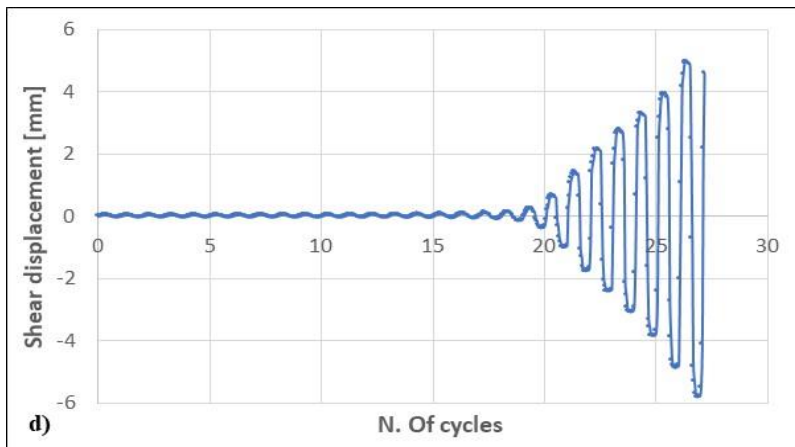
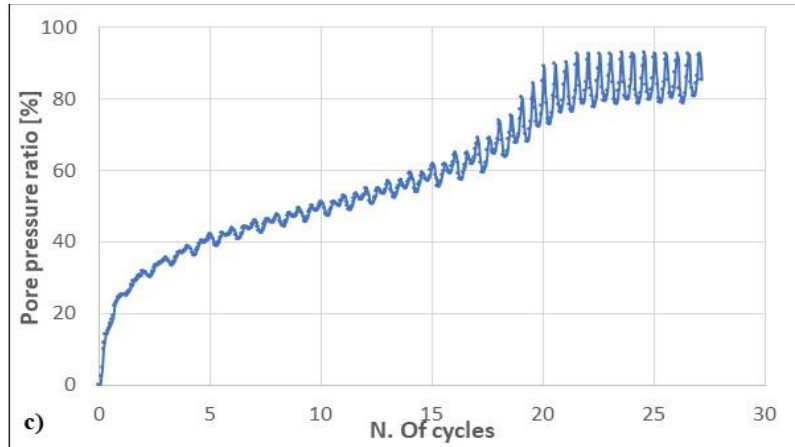


**Fig 6.35 CSS1 results: a) Shear load versus cycles; b) Axial load versus cycles; c) Pore pressure ratio versus cycles; d) shear displacement versus cycles**

➤ CSS 2

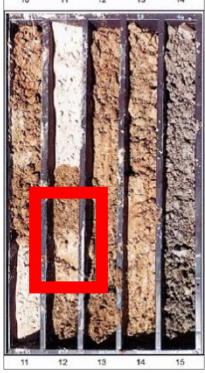
	Height (mm)	22.8
	Diameter (mm)	70
	Base area (mm <sup>2</sup> )	3879.54
	Volume (mm <sup>3</sup> )	8922.94
	Mass (g)	138.45
	Density (kg/mc)	1552
	Initial porosity	0.47
	Normal stress (kPa)	100
	Shear stress (kPa)	10
	CSR	0.1

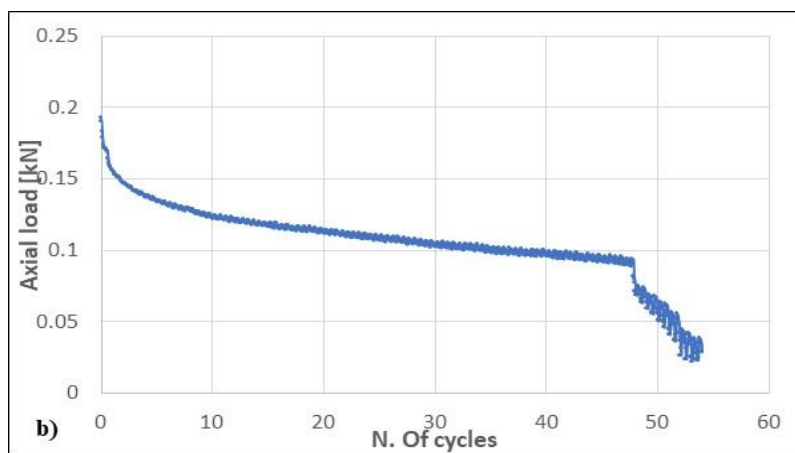
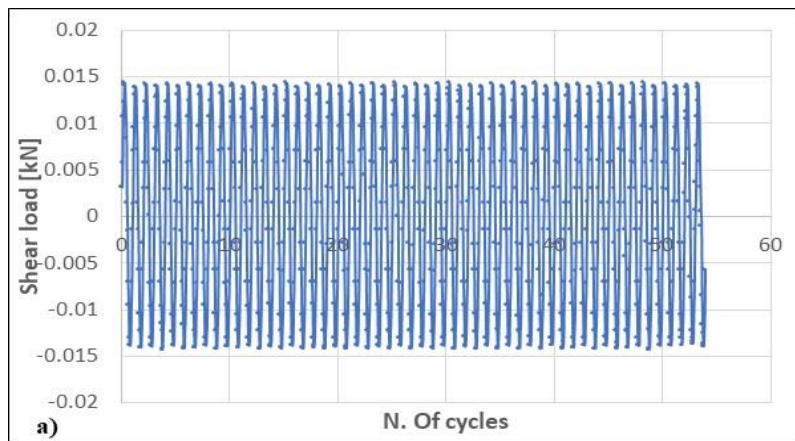




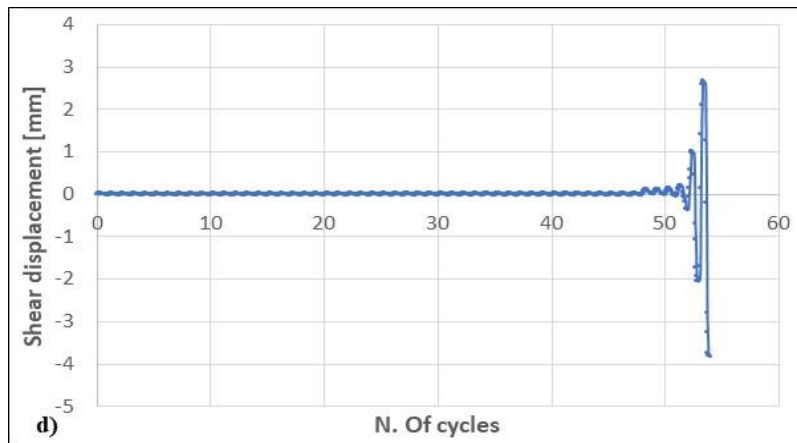
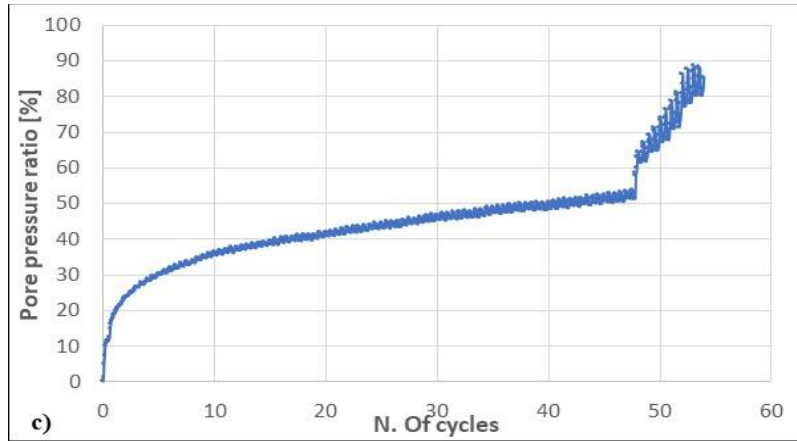
**Fig 6.36 CSS2 results: a) Shear load versus cycles; b) Axial load versus cycles; c) Pore pressure ratio versus cycles; d) shear displacement versus cycles**

➤ CSS 3

	Height (mm)	21.5
	Diameter (mm)	70
	Base area (mm <sup>2</sup> )	3879.54
	Volume (mm <sup>3</sup> )	83410.12
	Mass (g)	134.05
	Density (kg/mc)	1607
	Initial porosity	0.39
	Normal stress (kPa)	50
	Shear stress (kPa)	3.75
	CSR	0.075

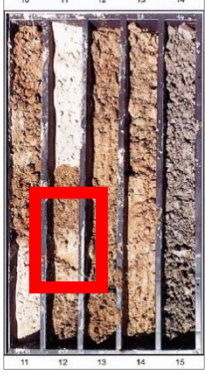


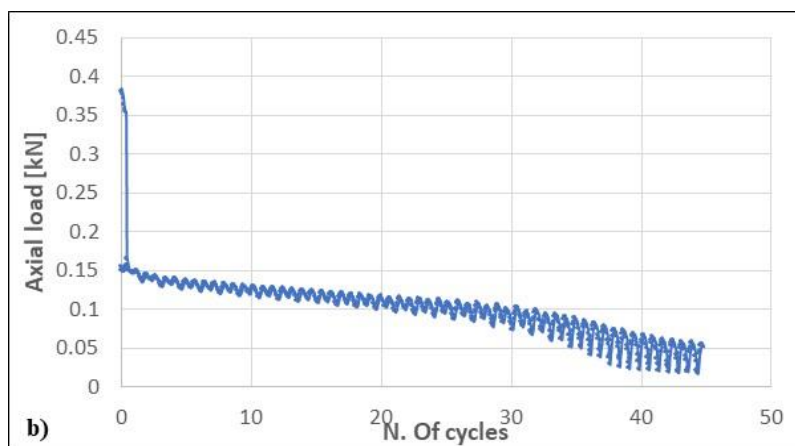
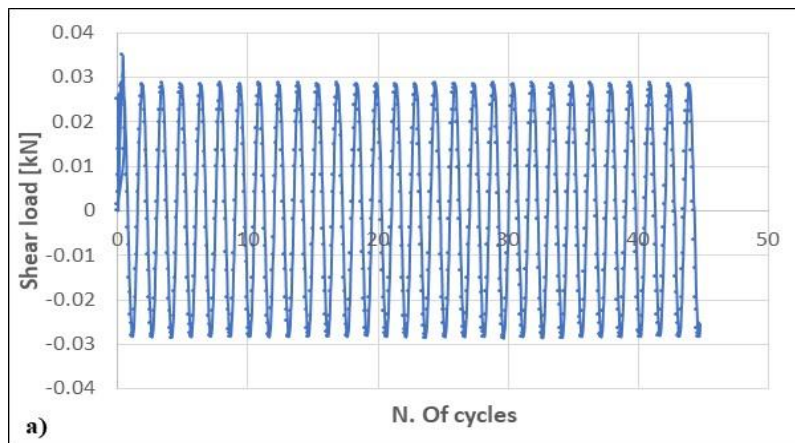


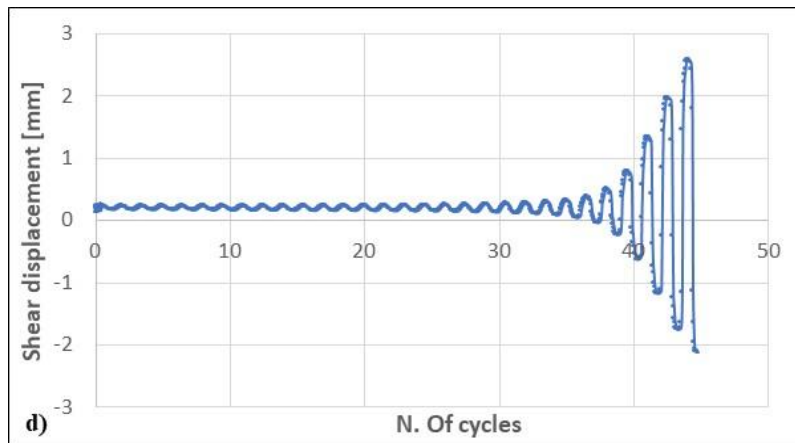
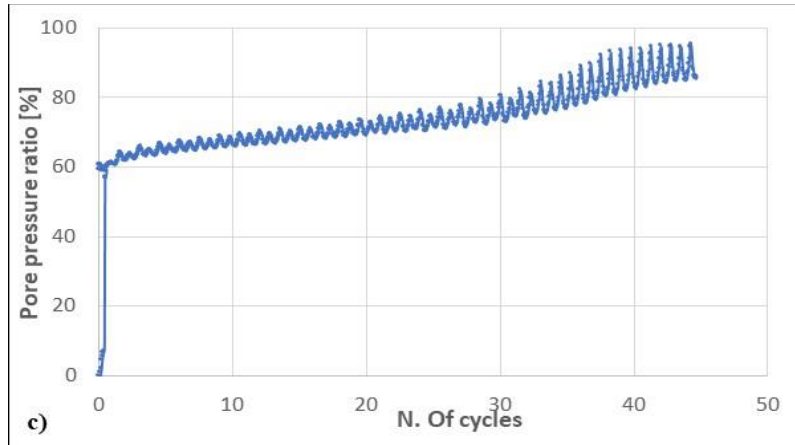


**Fig 6.37 CSS 3: a) Shear load versus cycles; b) Axial load versus cycles; c) Pore pressure ratio versus cycles; d) shear displacement versus cycles**

➤ CSS 4

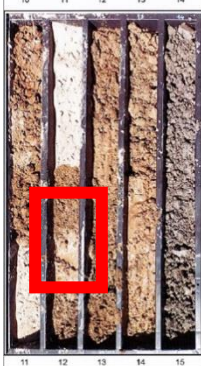
	Height (mm)	22
	Diameter (mm)	70
	Base area (mm <sup>2</sup> )	3879.54
	Volume (mm <sup>3</sup> )	85349
	Mass (g)	134.1
	Density (kg/mc)	1571
	Initial porosity	0.41
	Normal stress (kPa)	100
	Shear stress (kPa)	7.5
	CSR	0.05

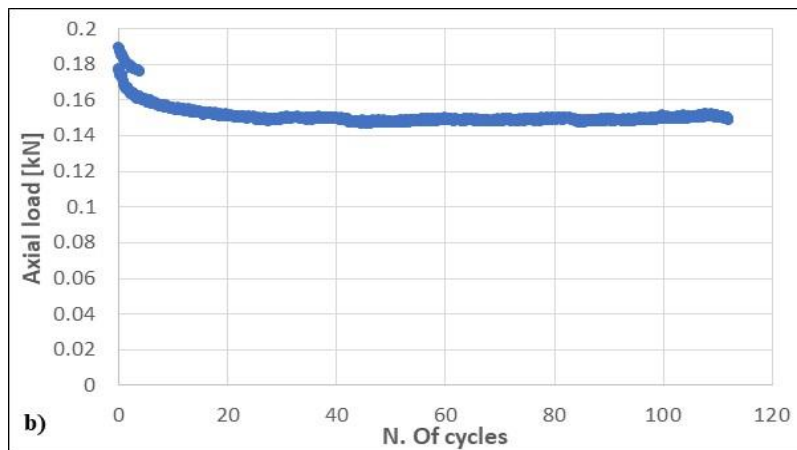
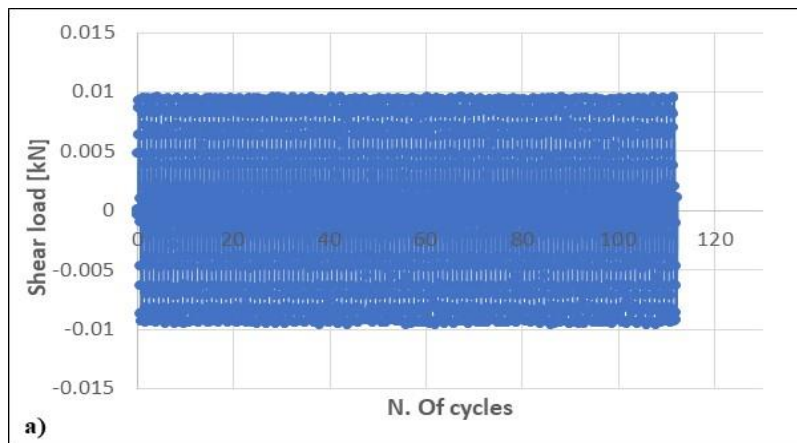


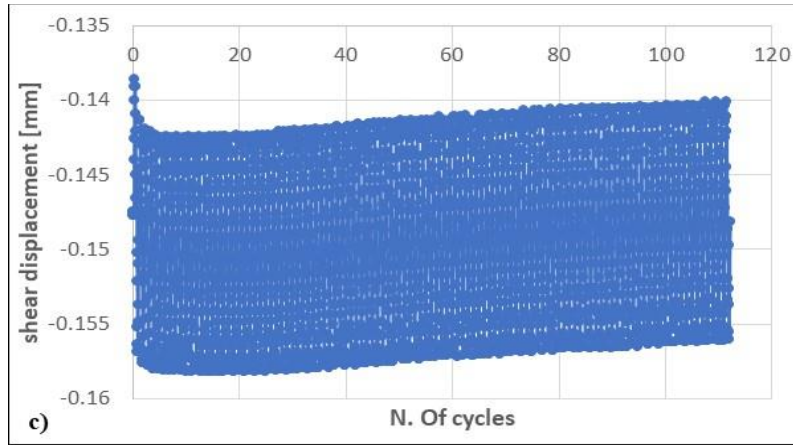


**Fig 6.38 CSS 4 results: a) Shear load versus cycles; b) Axial load versus cycles; c) Pore pressure ratio versus cycles; d) shear displacement versus cycles**

➤ CSS 5

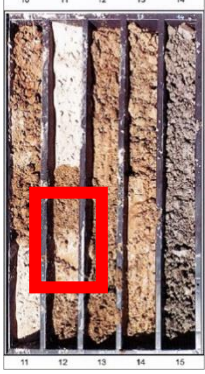
	Height (mm)	22
	Diameter (mm)	70
	Base area (mm <sup>2</sup> )	3879.54
	Volume (mm <sup>3</sup> )	85349
	Mass (g)	134.1
	Density (kg/mc)	1571
	Initial porosity	0.41
	Normal stress (kPa)	50
	Shear stress (kPa)	2.5
	CSR	0.05

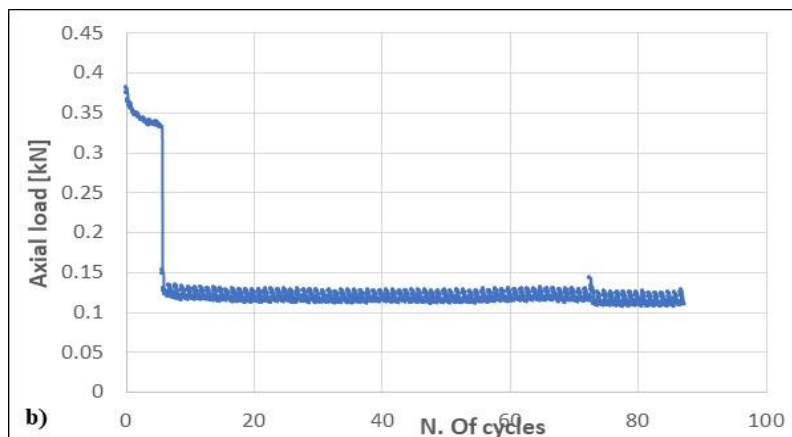
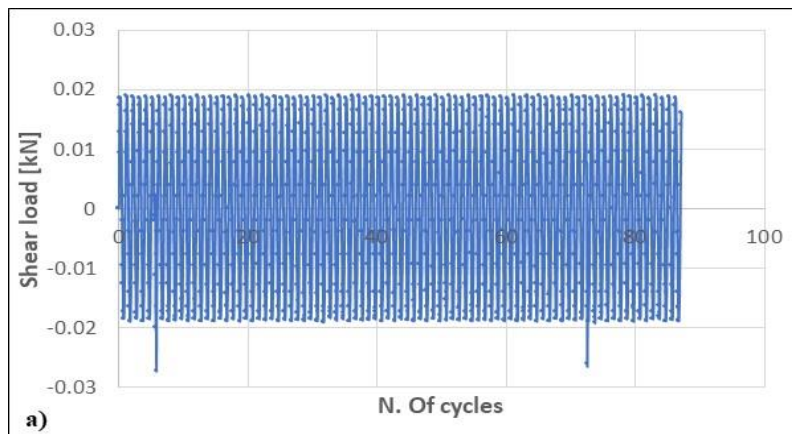


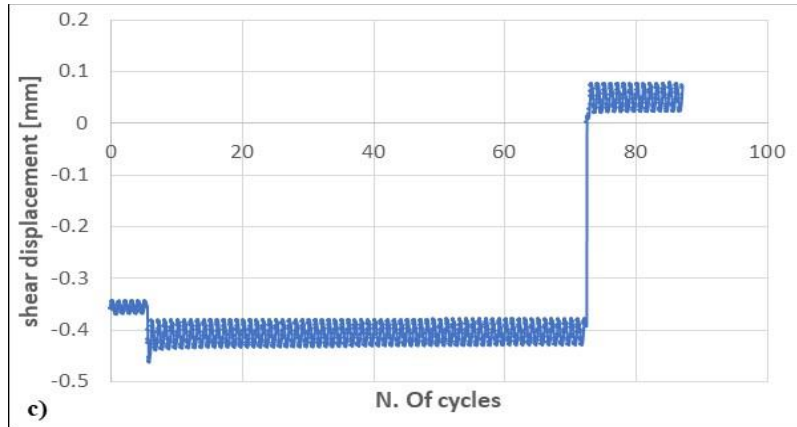


**Fig 6.39 CSS 5 results: a) Shear load versus cycles; b) Axial load versus cycles; c) shear displacement versus cycles**

➤ CSS 6


	Height (mm)	24
	Diameter (mm)	70
	Base area (mm <sup>2</sup> )	3879.54
	Volume (mm <sup>3</sup> )	93109
	Mass (g)	143.6
	Density (kg/mc)	1542
	Initial porosity	0.42
	Normal stress (kPa)	100
	Shear stress (kPa)	5
	CSR	0.05

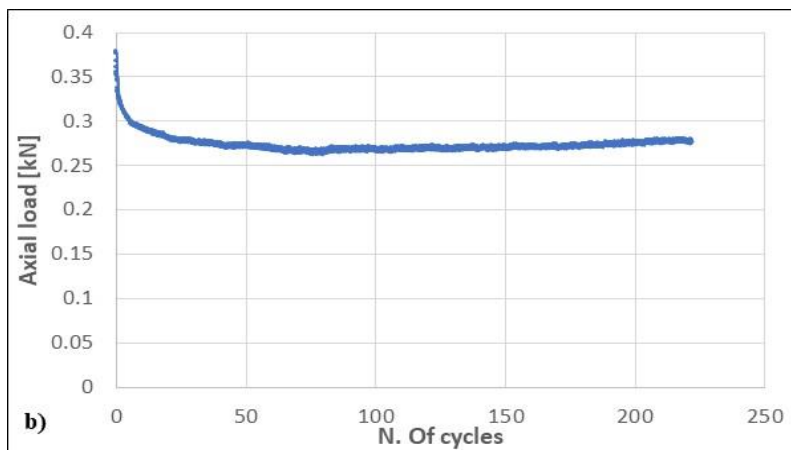
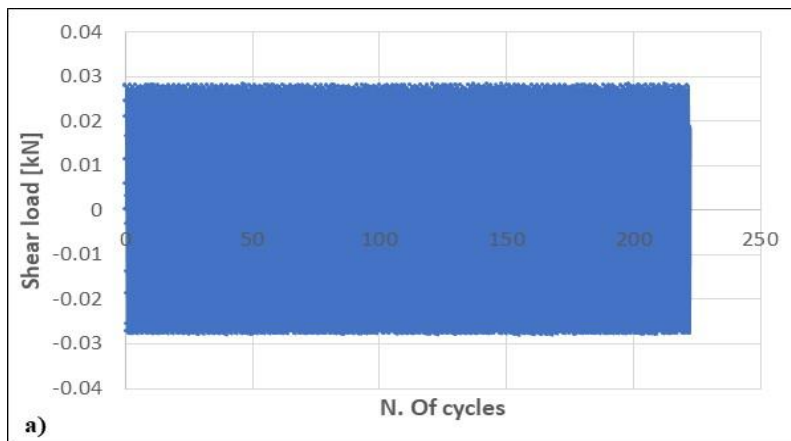




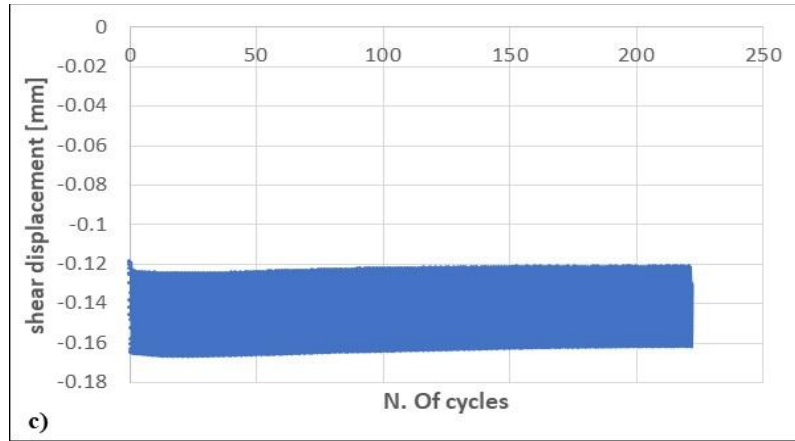
**Fig 6.40 CSS 6 results: a) Shear load versus cycles; b) Axial load versus cycles; c) shear displacement versus cycles**

➤ CSS 7

	Height (mm)	24
	Diameter (mm)	70
	Base area (mm <sup>2</sup> )	3879.54
	Volume (mm <sup>3</sup> )	93109
	Mass (g)	123.44
	Density (kg/mc)	1326
	Initial porosity	0.50
	Normal stress (kPa)	100
	Shear stress (kPa)	7.5
	CSR	0.075




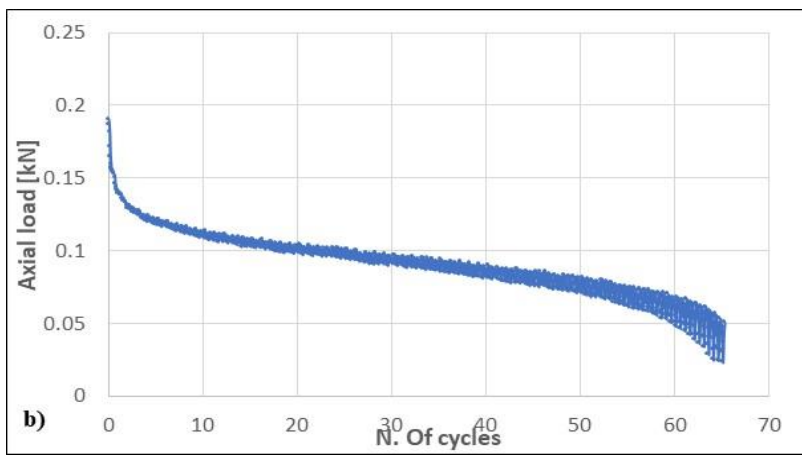
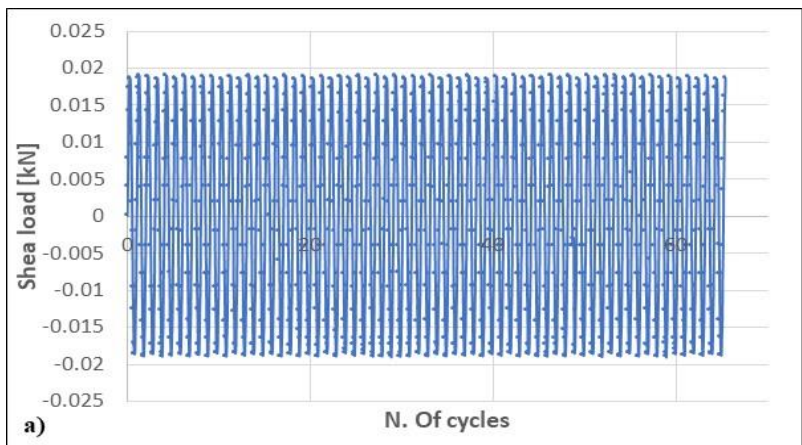


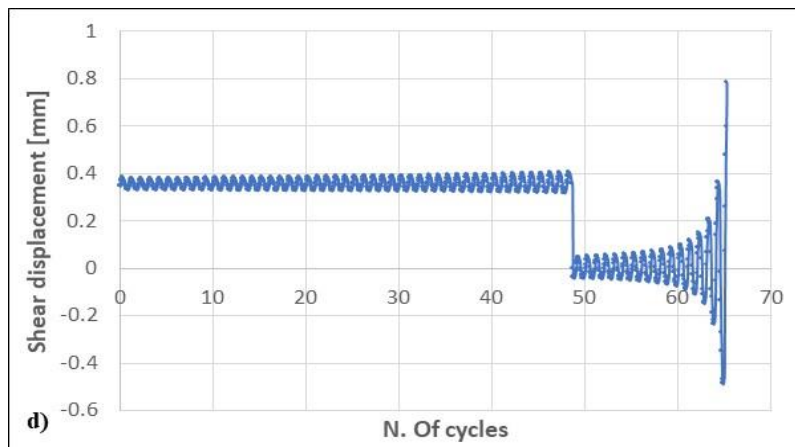
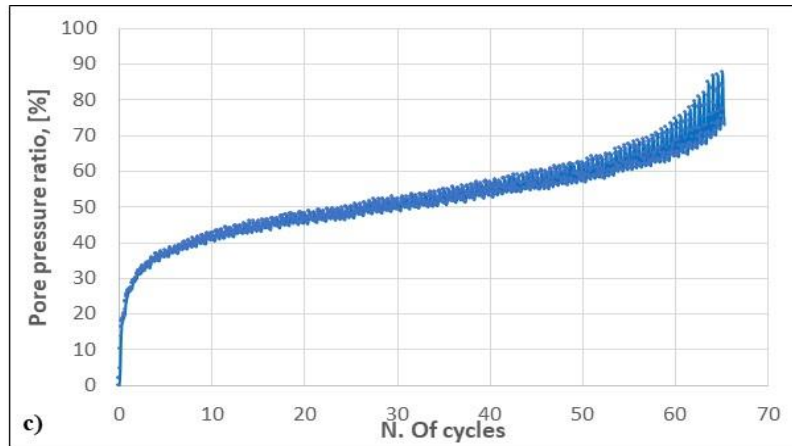


**Fig 6.41 CSS7 results: a) Shear load versus cycles; b) Axial load versus cycles; c) shear displacement versus cycles**

➤ CSS 8


	Height (mm)	24
	Diameter (mm)	70
	Base area (mm <sup>2</sup> )	3879.54
	Volume (mm <sup>3</sup> )	93109
	Mass (g)	123.44
	Density (kg/mc)	1326
	Initial porosity	0.50
	Normal stress (kPa)	50
	Shear stress (kPa)	5
	CSR	0.1

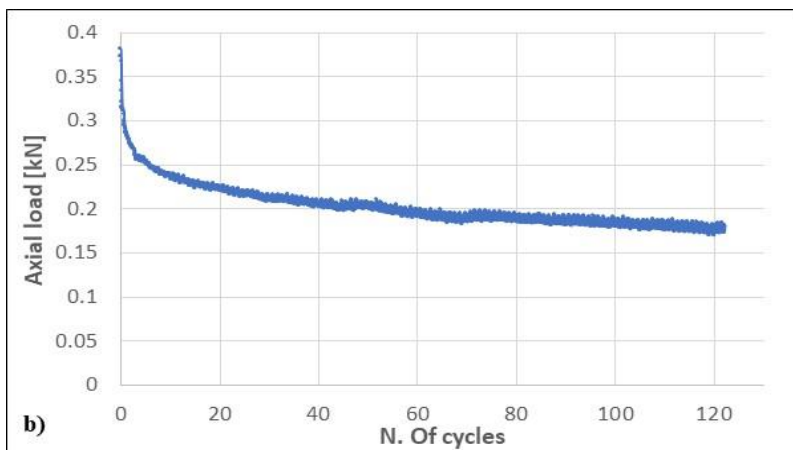
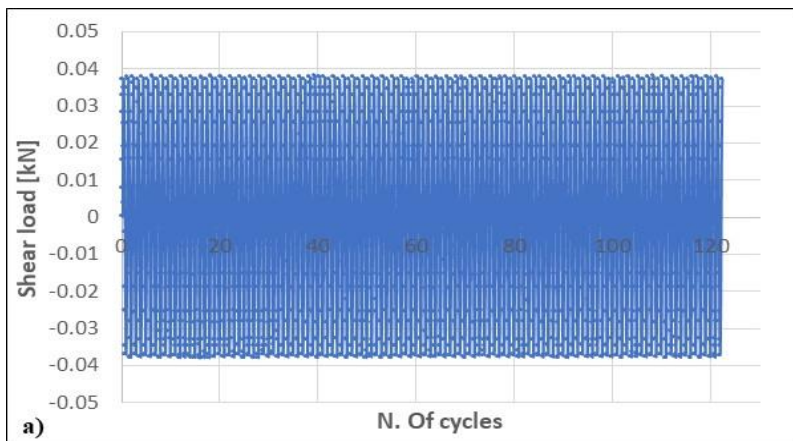


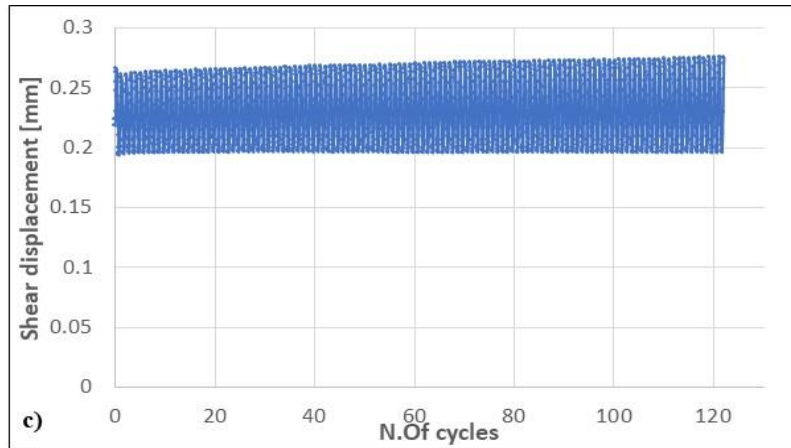


**Fig 6.42 CSS8 results: a) Shear load versus cycles; b) Axial load versus cycles; c) Pore pressure ratio versus cycles; d) shear displacement versus cycles**

➤ CSS 9


	Height (mm)	24
	Diameter (mm)	70
	Base area (mm <sup>2</sup> )	3879.54
	Volume (mm <sup>3</sup> )	93109
	Mass (g)	123.44
	Density (kg/mc)	1326
	Initial porosity	0.50
	Normal stress (kPa)	100
	Shear stress (kPa)	10
	CSR	0.1

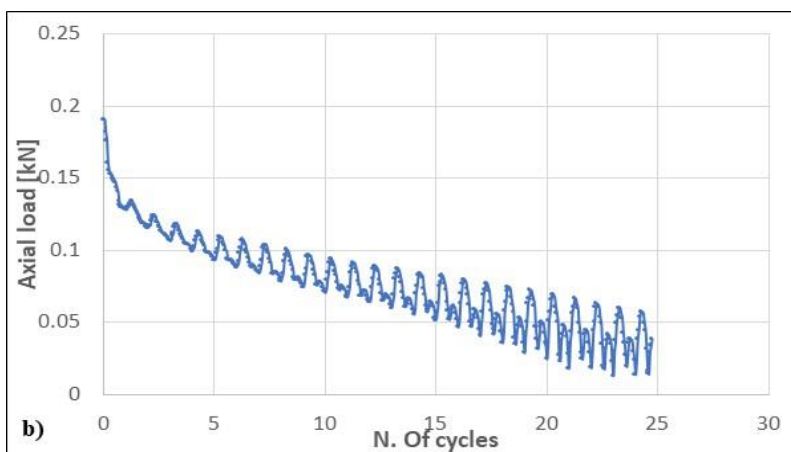
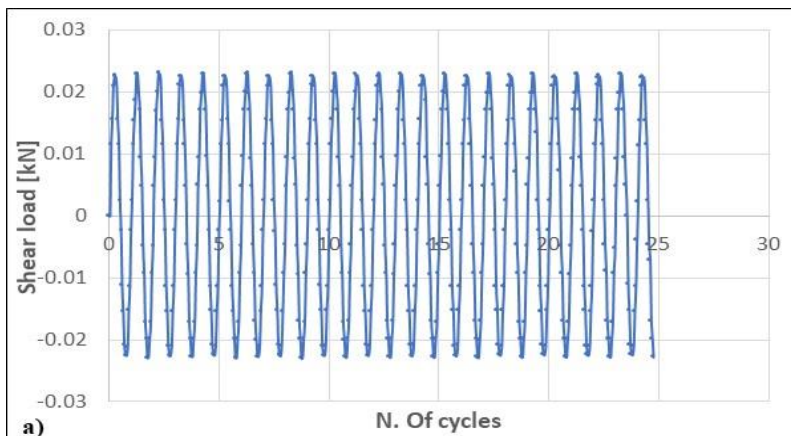


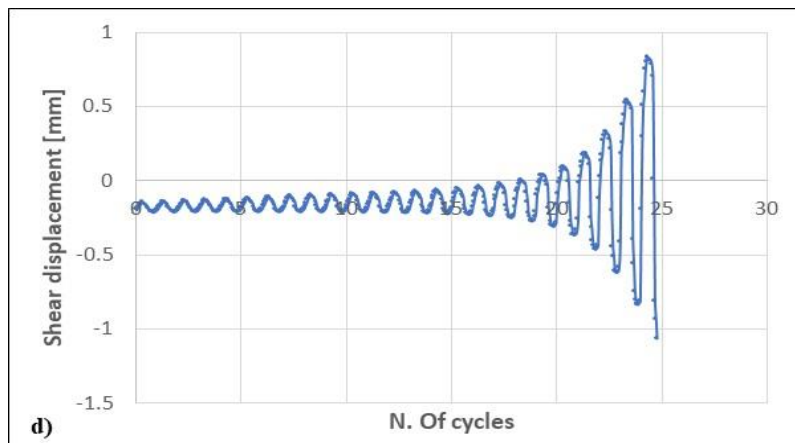
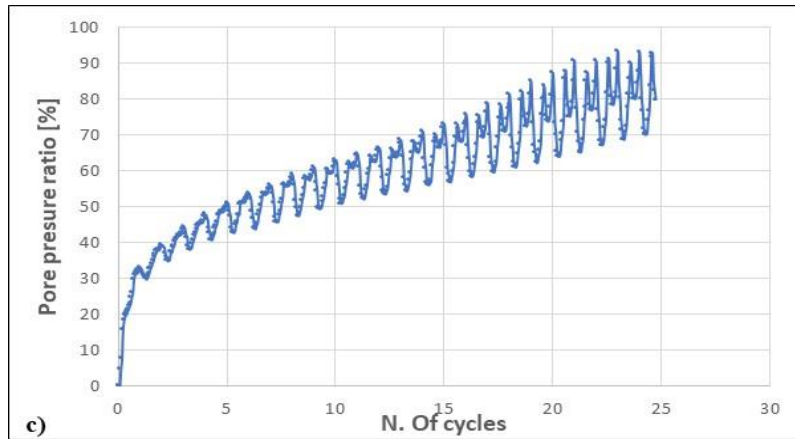


**Fig 6.43 CSS9 results: a) Shear load versus cycles; b) Axial load versus cycles; c) shear displacement versus cycles**

➤ CSS 10


	Height (mm)	24
	Diameter (mm)	70
	Base area (mm <sup>2</sup> )	3879.54
	Volume (mm <sup>3</sup> )	93109
	Mass (g)	123.44
	Density (kg/mc)	1326
	Initial porosity	0.50
	Normal stress (kPa)	50
	Shear stress (kPa)	6
	CSR	0.12

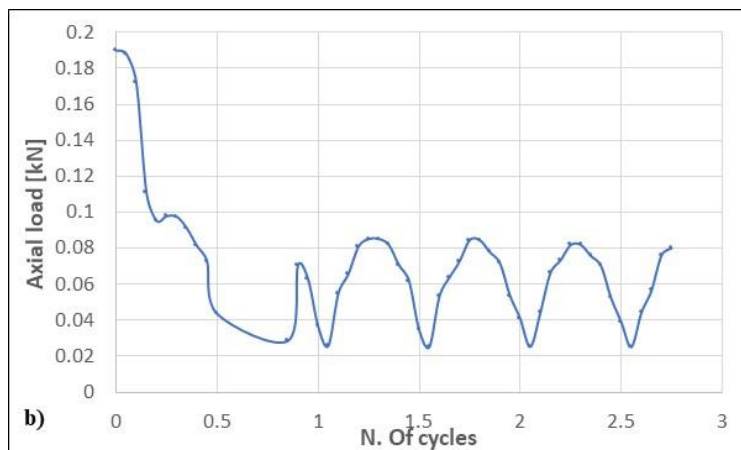
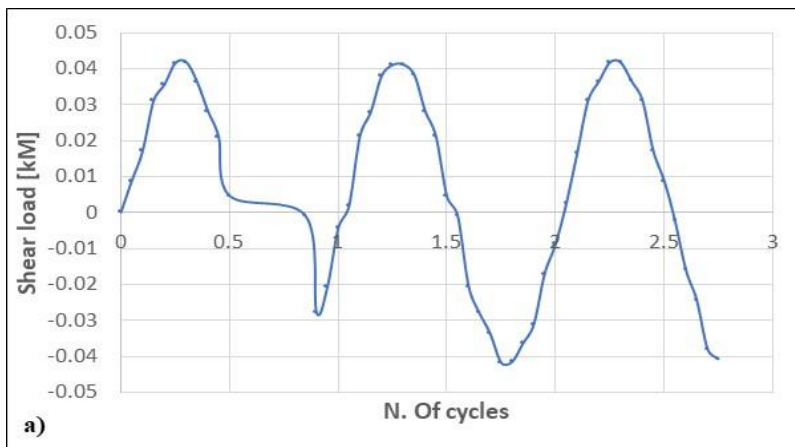




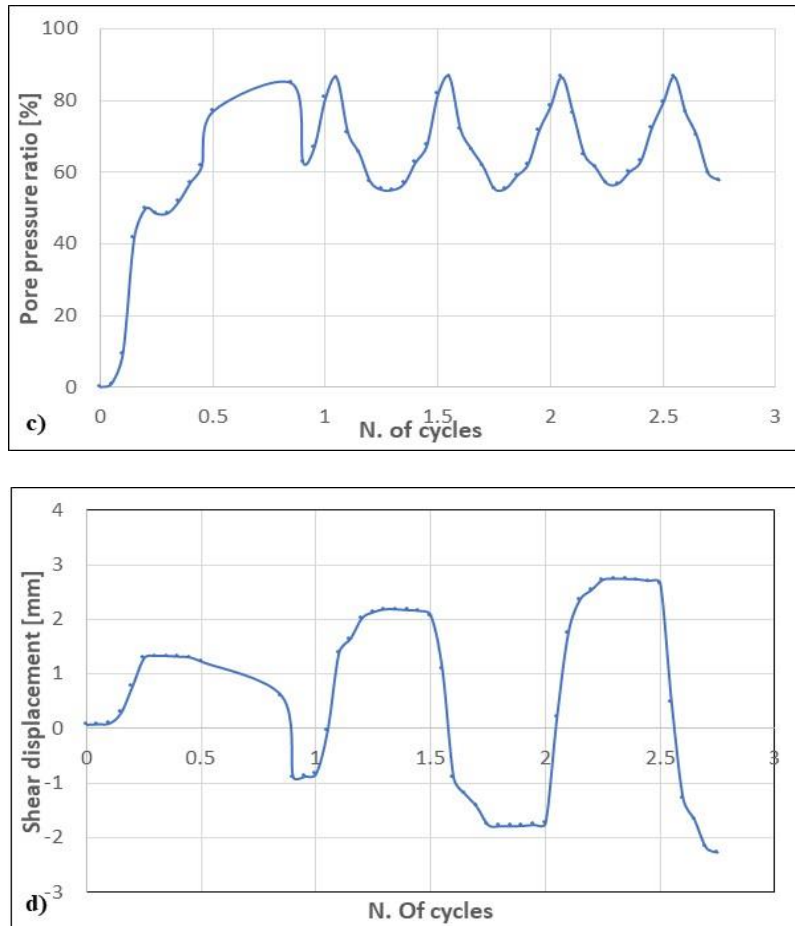
**Fig 6.44 CSS 10 results: a) Shear load versus cycles; b) Axial load versus cycles; c) Pore pressure ratio versus cycles; d) shear displacement versus cycles**

➤ CSS 11

	Height (mm)	24
	Diameter (mm)	70
	Base area (mm <sup>2</sup> )	3879.54
	Volume (mm <sup>3</sup> )	93109
	Mass (g)	123.44
	Density (kg/mc)	1326
	Initial porosity	0.50
	Normal stress (kPa)	50
	Shear stress (kPa)	11
	CSR	0.22





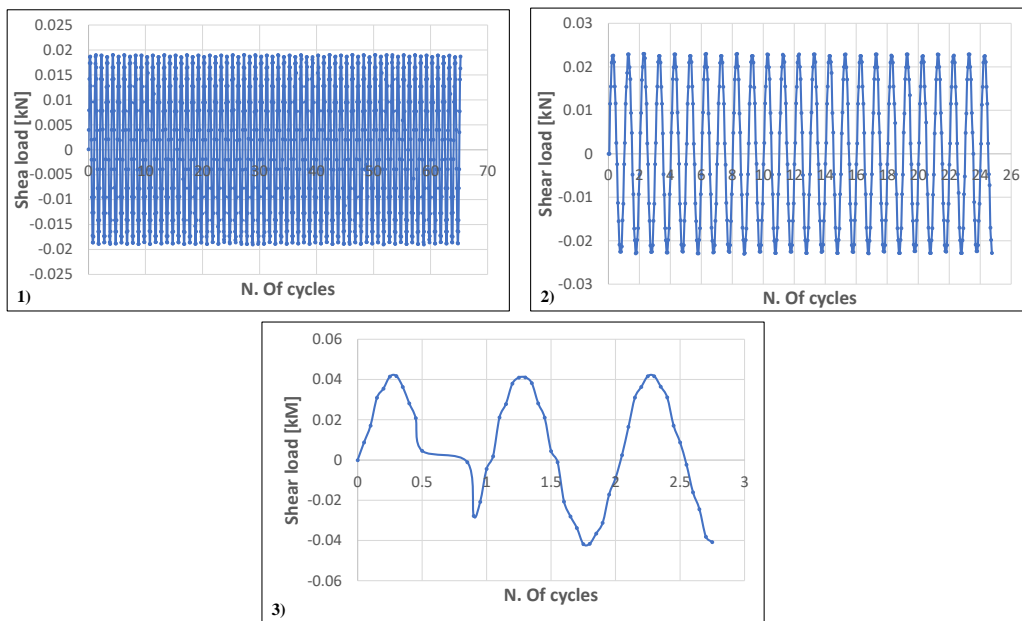


**Fig 6.45 CSS 11 results: a) Shear load versus cycles; b) Axial load versus cycles; c) Pore pressure ratio versus cycles; d) shear displacement versus cycles**

### 6.2.4.3 Discussion

Cyclic simple shear tests are able to provide reliable results with regard of liquefaction in less time than a cyclic triaxial test and this could be considered an advantage, considering no saturation of the sample.

Fig.6.46 shows the variation of the shear load versus the number of cycles in three tests, having the similar density but subjected to different CSR cyclic loading, increased from 0.1 to 0.22.

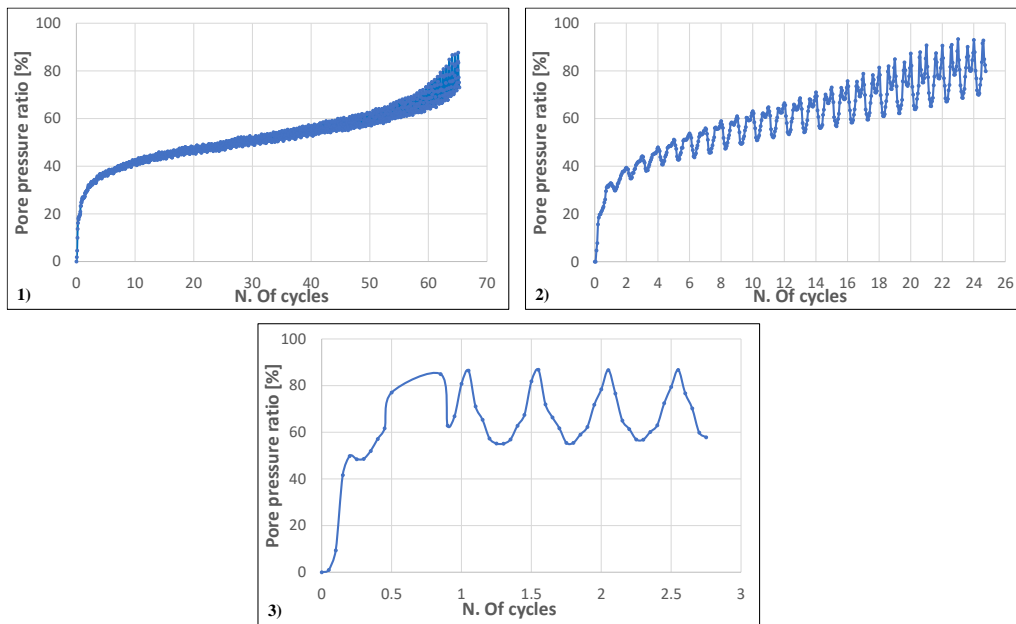


**Fig 6.46 Comparison of shear load for same material with different CSR**

In the Fig.6.45, the horizontal lines appear in the graph at the beginning. This phenomenon shows good agreement with the analysis of cyclic mobility phenomenon. Under lower CSR, the test appears to be more stable. The decrease of CSR results in the increase of the number of cycles causing liquefaction.

The pore water pressure increment of tests is presented in Fig.6.47. In tests with the initial CSR of 0.12-0.22, the two-peak mechanism appears. This is a characteristic of cyclic mobility as mentioned by some other authors (Benahmed 2001, Vernay et al. 2019, etc.). The presence of the two peaks mechanism in a cyclic simple shear liquefaction test can be a significant indicator of the potential for liquefaction. The first peak represents the initial strengthening of the soil due to shear stress, while the

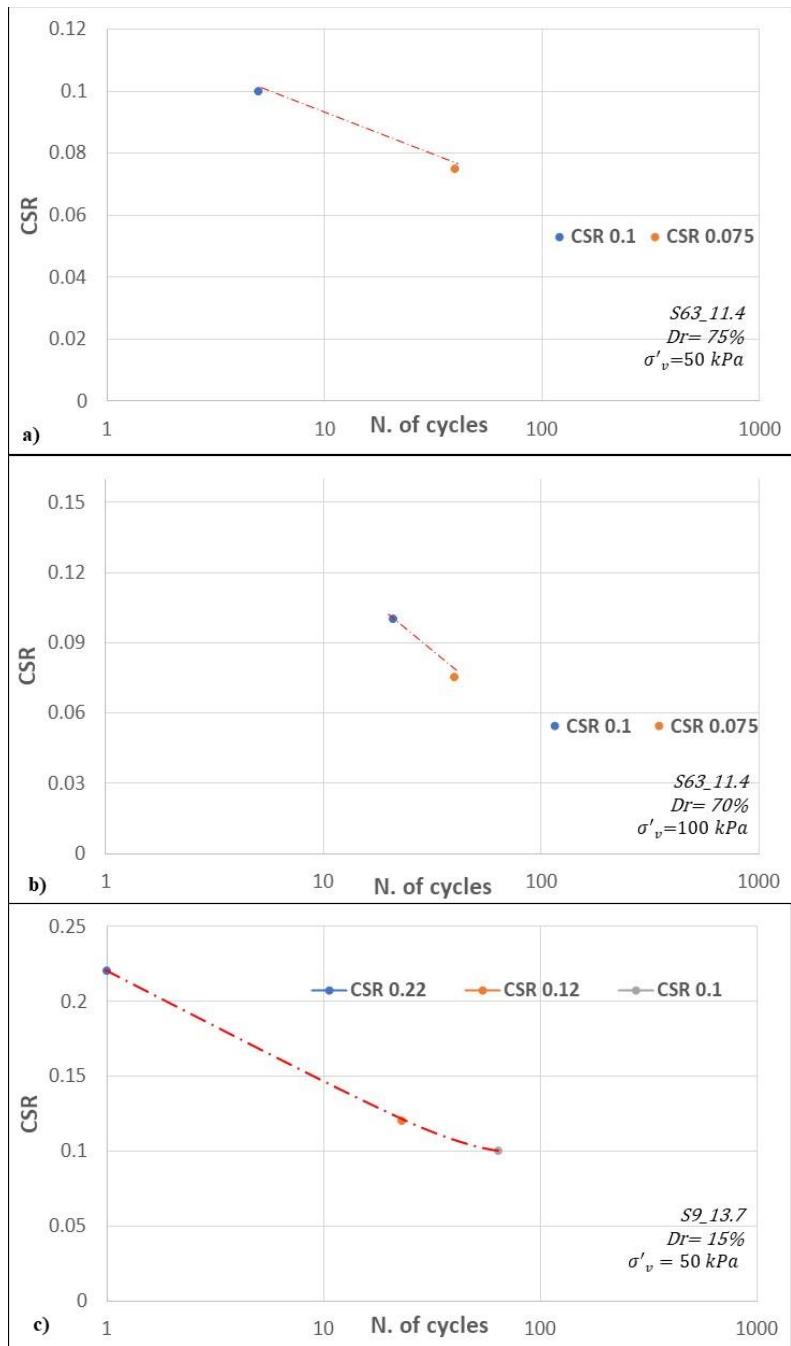
secondary peak suggests the soil's potential to regain strength after initial weakening due to pore pressure buildup and reconsolidation.



**Fig 6.47 Comparison of pore pressure ratio ( $r_u$ ) for same material with different CSR**

Plotting CSR versus number of cycles at liquefaction, it's possible to define the cyclic resistance curve of the material, at different CSR and at same normal stress; this curve is unique. Since tests with CSR 0.05 didn't reach liquefaction, only two points are available for S63 material; taking into account this aspect, S9 material has been tested with higher CSR value, obtaining a curve passing to at least three points.

Liquefaction resistance curves of Panaro sand under unidirectional cyclic loading, according to the axial stress are shown in Fig.6.48.



**Fig 6.48** Liquefaction resistance curve resulting from CSS test: a) S63 material normal stress 50 kPa; b) S63 material normal stress 100 kPa; c) S9 material normal stress 50 kPa

### 6.3 Case 2: Ponte canale Ancona

On the basis of the investigations carried out in 2021/2022 with historical-empirical procedure/methodologies under free-field conditions, the susceptibility to liquefaction of the deposits has been confirmed.

In November 2022, a new survey (S1) in correspondence of previous S2 (Fig.6.49) has been conducted.

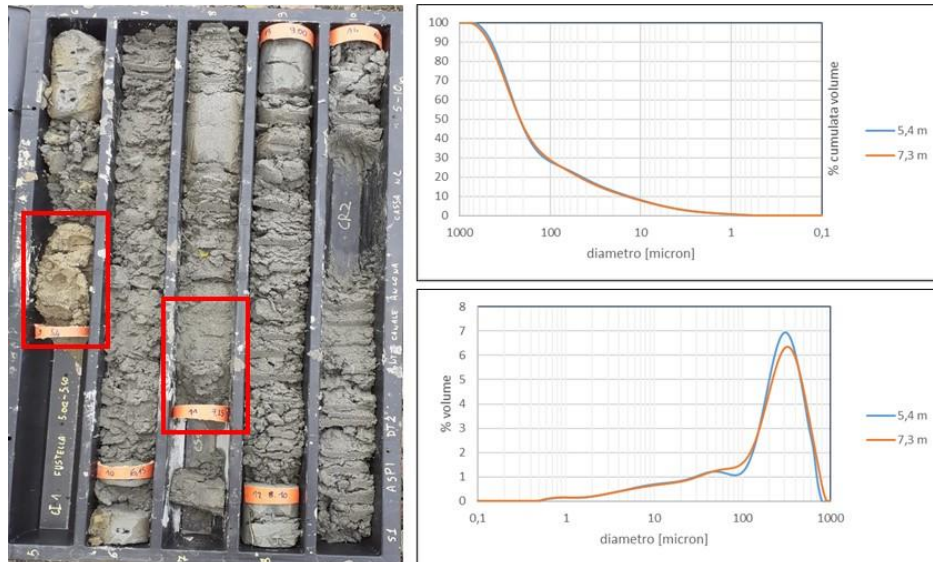


Fig 6.49 Material taken from borehole S1 (previous S2) in November 2022

#### 6.3.1 Materials

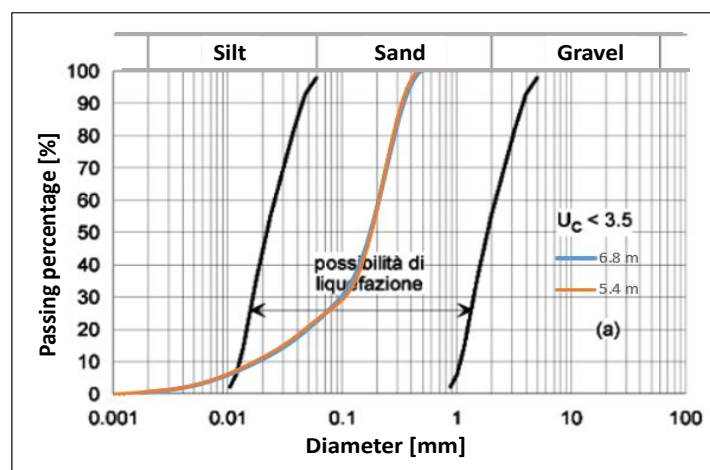
Firstly, the grain-size distribution curve of the material taken from boreholes is presented in Fig.6.50, providing an initial evaluation of granulometric class. For this study, materials taken from two depth were under laboratory investigations.

Granulometric analysis has been conducted to better characterize soil at depths of 5.4m and 7.3m. A Malvern Mastersize 2000E laser granulometer was used for the particle size analysis. The two samples are very similar and can be classified as sand with weakly clayey silt.



**Fig 6.50 Grain-size analysis for sample at 5.4m and 7.3m to be tested, on the left the material in the box**

Regarding grain-size distribution, regulation (NTC18) previously mentioned, suggests limiting curves to single out potentially liquefying soils. In Fig.6.51 an example is shown; it can be noted that samples can be expected to liquefy, since the curve is within the boundaries.



**Fig 6.51 Ranges of grain size distribution of soil along with the boundaries of liquefaction susceptible soil according to NTC (2018).**

The in-situ density was estimated by sampling two undisturbed core pieces with a cylindrical die in situ and on the samples used for dynamic testing. The maximum voids index (Table 6-6) was determined by the free fall of the material in a graduated cylinder, the volume of which is known. Then by vibrating and rotating the material several times, the minimum voids index was determined.

depth [m]	die volume [cm <sup>3</sup> ]	wet weight [g]	$\gamma_n$ [g/cm <sup>3</sup> ]	dry weight[g]	$\gamma$ dry [g/cm <sup>3</sup> ]	Wn %	$\gamma_s$ [g/cm <sup>3</sup> ]	n	e
4.3	39.25	73.66	1.88	58.8	1.50	25.27	2.65	0.43	0.77
4.7	39.25	79.13	2.02	60.77	1.55	30.21	2.65	0.42	0.71
5.4	39.25	72.17	1.84	57.7	1.47	25.08	2.65	0.45	0.80
7.3	39.25	83.6	2.13	68.33	1.74	22.35	2.65	0.34	0.52

**Table 6-6 Maximum and minimum void index calculations for sample taken in situ and for sample to be tested in laboratory**

### 6.3.2 Cyclic triaxial test

In order to model the dynamic behaviour of the soil as closely as possible, cyclic laboratory tests on remoulded sample were carried out with Wykeham-Farrance apparatus, Dynatriax Ems-Tech.

#### 6.3.2.1 Test program

Several cyclic triaxial test have been carried out in order to better characterize soil response under cyclic condition.

Test according to ASTM D3999 and D5311 standard and no standard were performed on both stratigraphic levels. The list is presented in Table 6-7.

	Freq [Hz]	Double Amplitude		Freq [Hz]	Double Amplitude
TXD1_liqu_5.4_1	1.5	60N	TXD11_liqu_5.4_6	1.5	0.15
TXD1_liqu_5.4_2	1.5	90N	TXD11_liqu_5.4_7	1.5	0.175
TXD2_liqu_5.4_1	1.5	20N	TXD1_damping_5.4_1	0.5	0.5mm
TXD2_liqu_5.4_2	1.5	40N	TXD1_damping_5.4_2	0.5	0.64mm
TXD3_liqu_5.4_1	1.5	30N	TXD1_damping_5.4_3	0.5	0.8mm
TXD3_liqu_5.4_2	1.5	60N	TXD1_damping_5.4_4	0.5	1mm
TXD4_liqu_7.3	1.5	60N	TXD1_damping_5.4_5	0.5	1.1mm
TXD5_liqu_5.4	1.5	100N	TXD1_damping_5.4_6	0.5	1.24mm
TXD6_liqu_5.4_1	0.5	30N	TXD1_damping_5.4_7	0.5	1.36mm
TXD6_liqu_5.4_2	1	50N	TXD1_damping_5.4_8	0.5	1.46mm
TXD6_liqu_5.4_3	1.5	60N	TXD1_damping_5.4_9	0.5	1.8mm
TXD7_liqu_5.4_1	1.5	0.1mm	TXD1_damping_5.4_10	0.5	2.4mm
TXD7_liqu_5.4_2	1.5	0.4mm	TXD2_damping_7.3_1	0.1	0.02mm
TXD7_liqu_5.4_3	1.5	0.6mm	TXD2_damping_7.3_2	0.1	0.04mm
TXD8_liqu_7.3	1.5	60N	TXD2_damping_7.3_3	0.1	0.08mm
TXD9_liqu_7.3	1.5	100N	TXD2_damping_7.3_4	0.1	0.1mm
TXD10_liqu_7.3	1.5	120N	TXD2_damping_7.3_5	0.1	0.14mm
TXD12_liqu_7.3	1.5	50N	TXD2_damping_7.3_6	0.1	0.2mm
TXD11_liqu_5.4_1	1.5	0.03mm	TXD2_damping_7.3_7	0.1	0.24mm
TXD11_liqu_5.4_2	1.5	0.055mm	TXD2_damping_7.3_8	0.1	0.4mm
TXD11_liqu_5.4_3	1.5	0.08mm	TXD2_damping_7.3_9	0.1	0.6mm
TXD11_liqu_5.4_4	1.5	0.1mm	TXD2_damping_7.3_10	0.1	0.8mm
TXD11_liqu_5.4_5	1.5	0.135mm	TXD2_damping_7.3_11	0.1	0.9mm

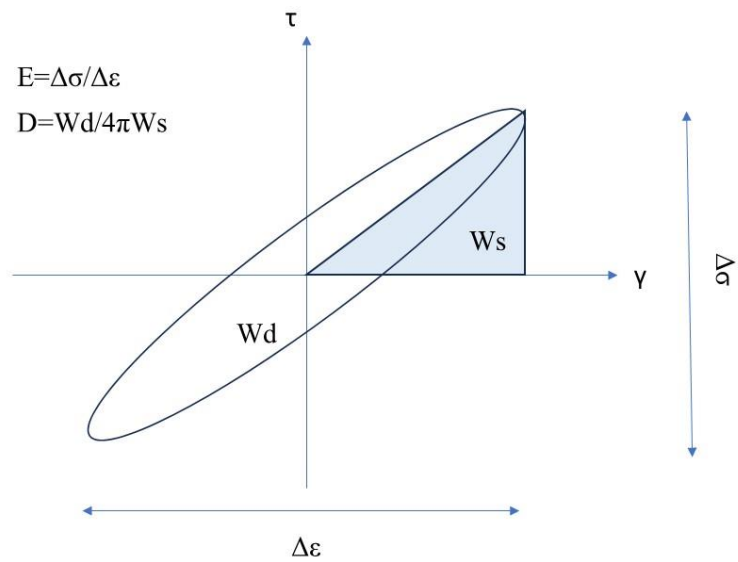
**Table 6-7 Cyclic triaxial test performed on material at 5.4m and 7.3m depth**

ASTM D5311 standard load-controlled test and non-standard strain-controlled tests have the same aim, it means to investigate sample behaviour under cyclic stress with regard to liquefaction, checking stress path and  $r_u$  value most of all; load controlled test will lead to increase deformation to maintain the target, while strain-controlled test will lead to load decreasing as a consequence of the maintaining of the target imposed.

In a cyclic triaxial test according to ASTM D3999, damping and elastic modulus are important parameters used to assess the dynamic behaviour of soils subjected to cyclic loading conditions (Fig.6.52). These parameters




provide insights into how a soil specimen dissipates energy and deforms under cyclic shear loading.

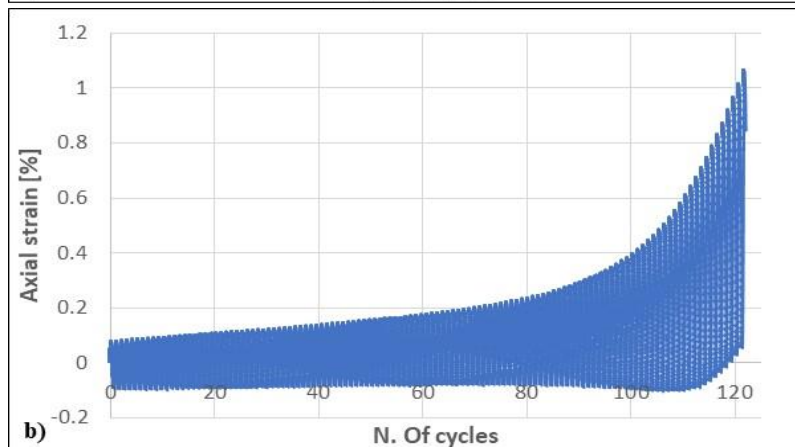
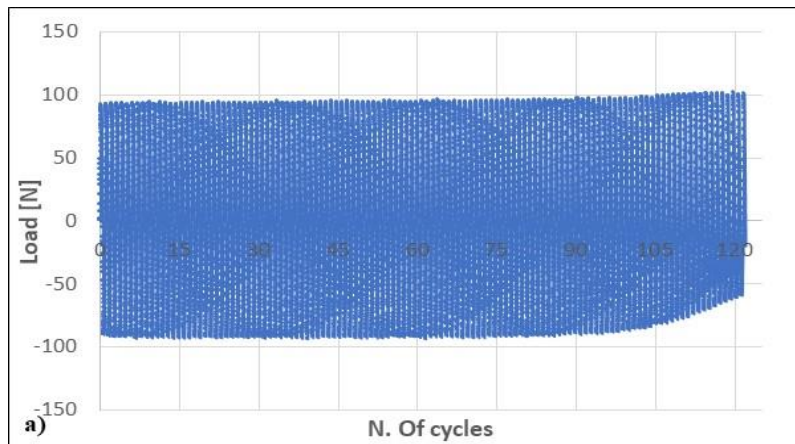


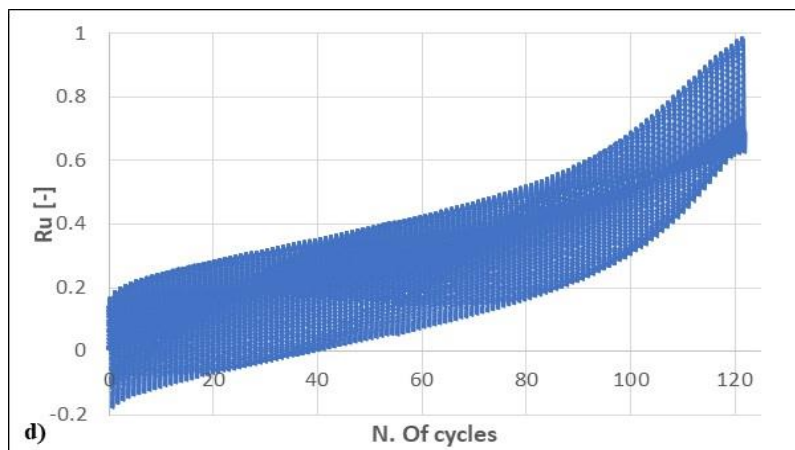
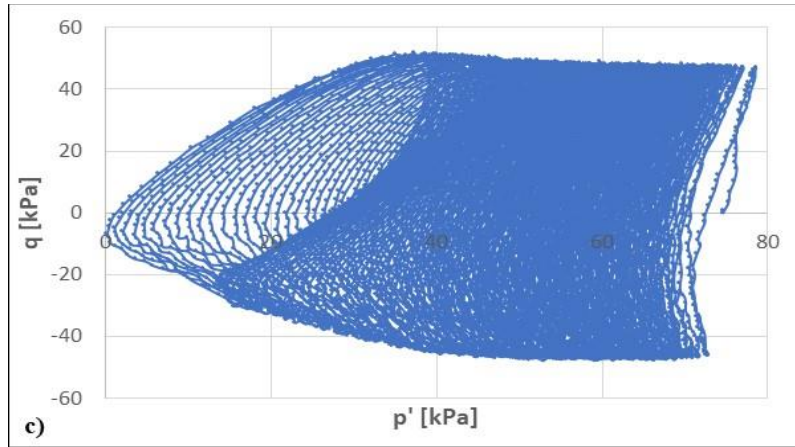
**Fig 6.52 Hysteresis loop of a single cyclic strain level test with schematic representation of Damping and Elastic modulus calculation**

### 6.3.2.2 Results

#### ➤ TXD1-ASTM D5311


	Height (mm)	100
	Diameter (mm)	50
	Base area (mm <sup>2</sup> )	1962.5
	Volume (mm <sup>3</sup> )	196250
	Mass (g)	288.48
	Density (kg/mc)	1469
	Initial porosity	0.45
	Confining pressure (kPa)	70
	Final B test	0.95
	Initial deviatoric stress (kPa)	0

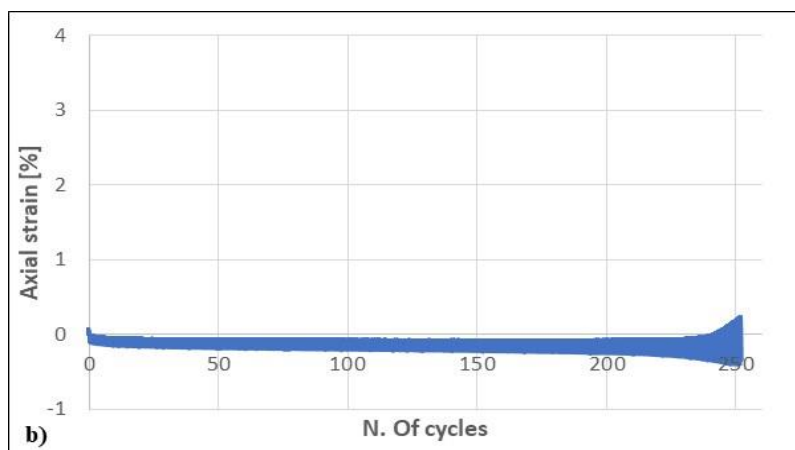
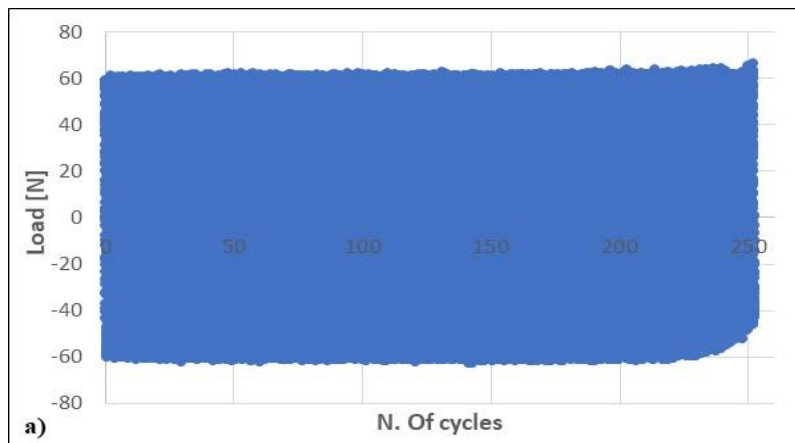


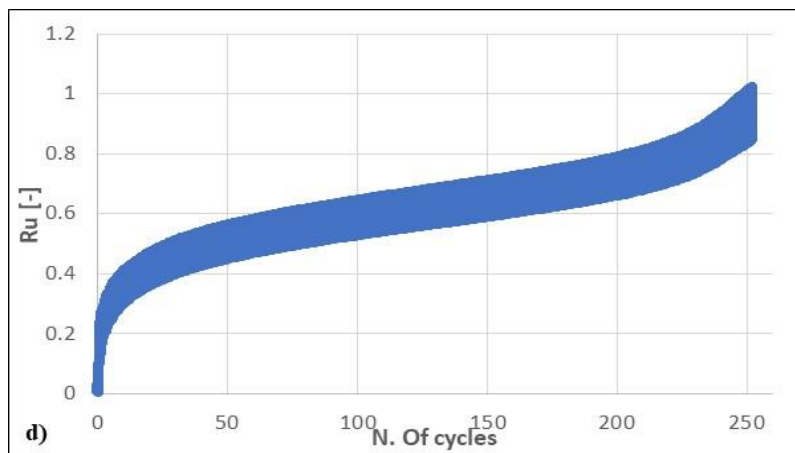
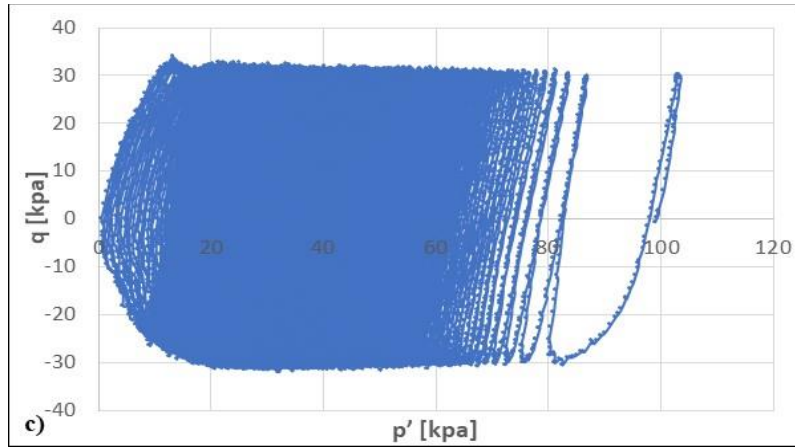


**Fig 6.53 TXD1-ASTMD5311 results: a) load versus cycles; b) axial strain versus cycles; c) stress path ( $q$ - $p'$ ); d)  $ru$  versus cycles**

➤ TXD2-3-(ASTM D5311)


	Height (mm)	100
	Diameter (mm)	50
	Base area (mm <sup>2</sup> )	1962.5
	Volume (mm <sup>3</sup> )	196250
	Mass (g)	288.8
	Density (kg/mc)	1467
	Initial porosity	0.44
	Confining pressure (kPa)	95
	Final B test	0.96
	Initial deviatoric stress (kPa)	0

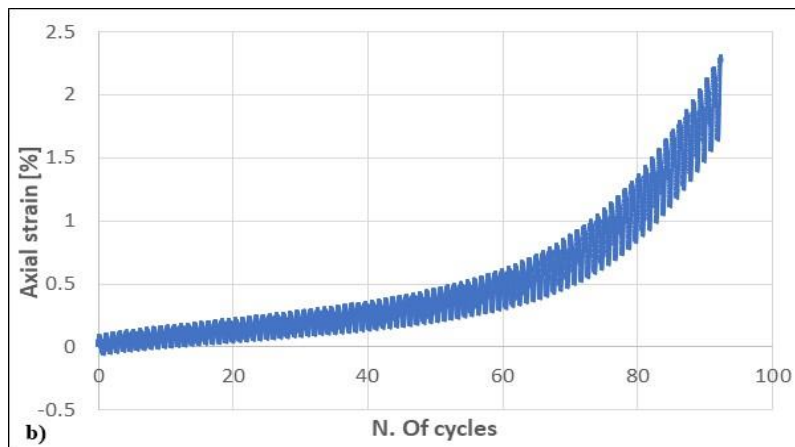
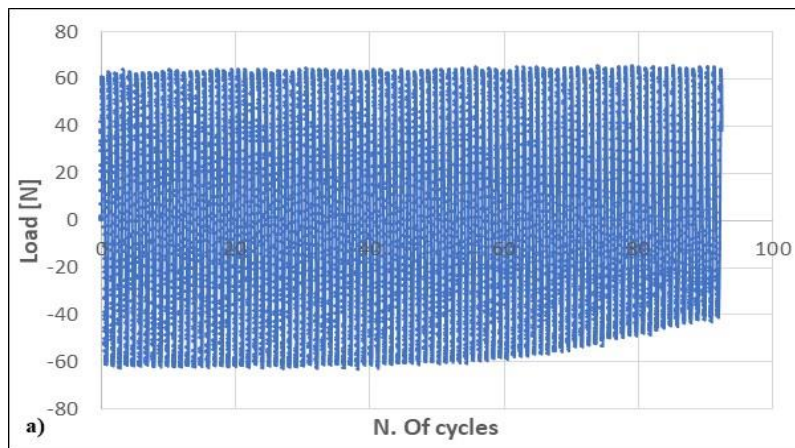


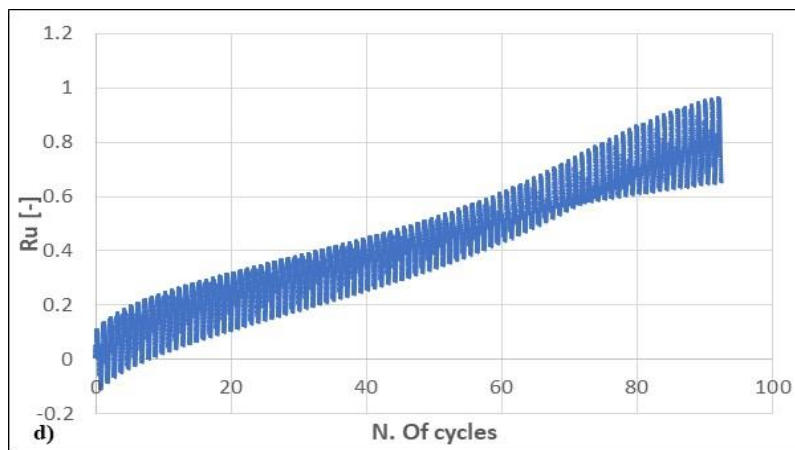
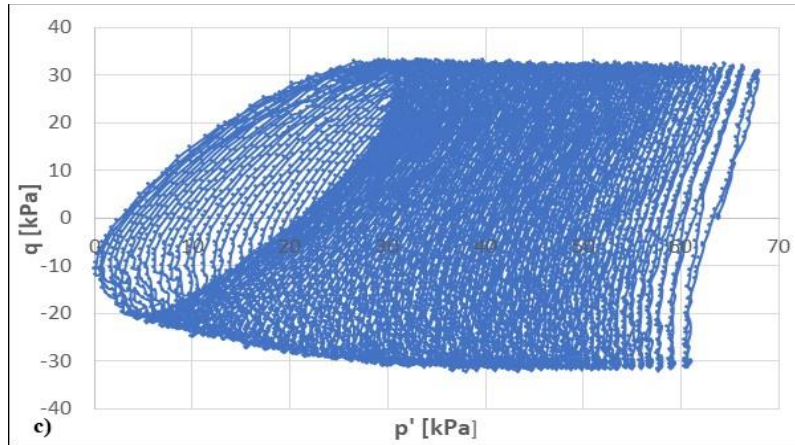


**Fig 6.54 TXD2-3-ASTMD5311 results: a) load versus cycles; b) axial strain versus cycles; c) stress path ( $q$ - $p'$ ); d)  $r_u$  versus cycles**

➤ TXD3-(ASTM D5311)


	Height (mm)	100
	Diameter (mm)	50
	Base area (mm <sup>2</sup> )	1962.5
	Volume (mm <sup>3</sup> )	196250
	Mass (g)	288.8
	Density (kg/mc)	1467
	Initial porosity	0.44
	Confining pressure (kPa)	95
	Final B test	0.96
	Initial deviatoric stress (kPa)	0

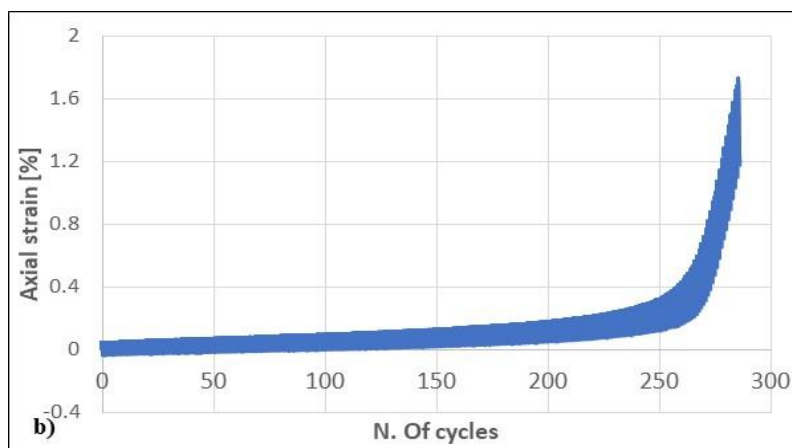
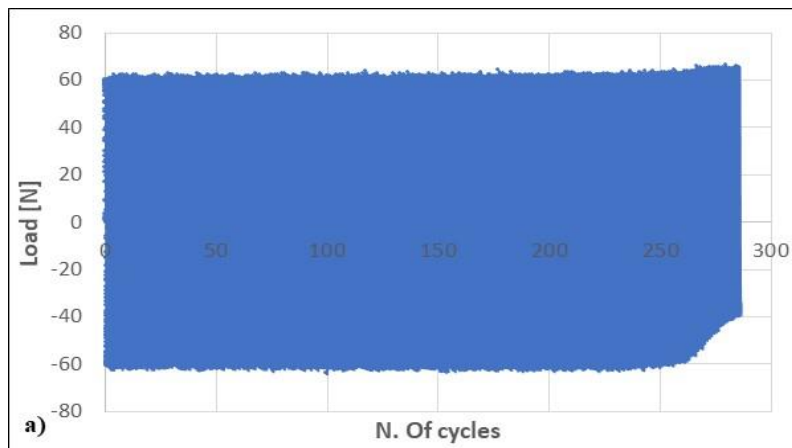




**Fig 6.55 TXD3-ASTMD5311 results: a) load versus cycles; b) axial strain versus cycles; c) stress path (q-p'); d) ru versus cycles**

➤ TXD4-(ASTM D5311)

	Height (mm)	100
	Diameter (mm)	50
	Base area (mm <sup>2</sup> )	1962.5
	Volume (mm <sup>3</sup> )	196250
	Mass (g)	341
	Density (kg/mc)	1737.57
	Initial porosity	0.34
	Confining pressure (kPa)	100
	Final B test	0.93
	Initial deviatoric stress (kPa)	0





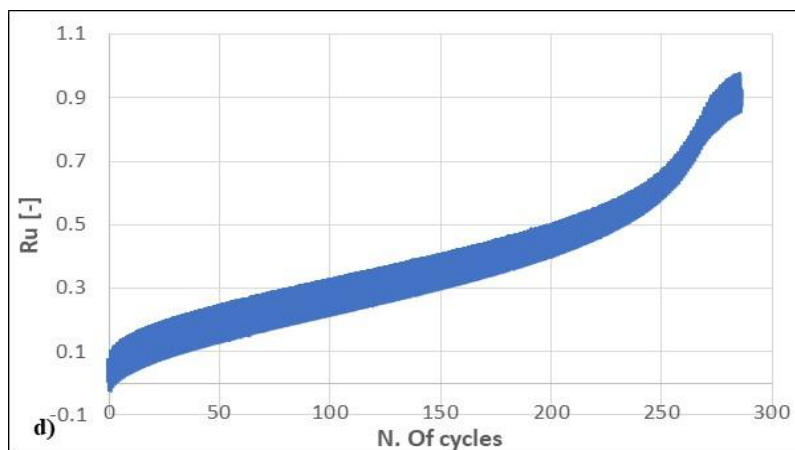
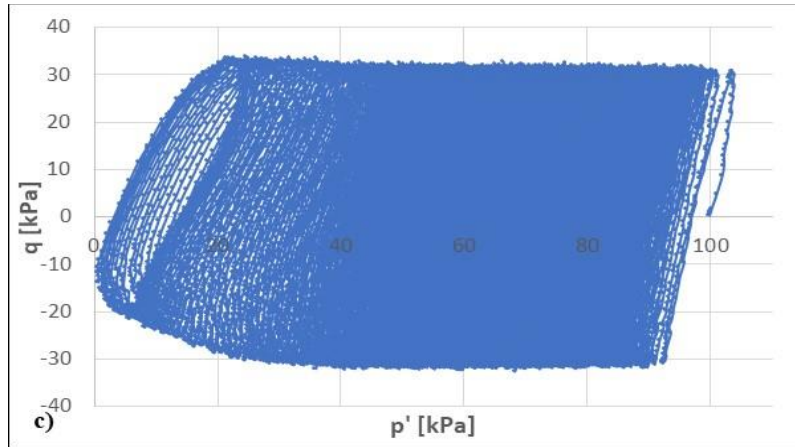

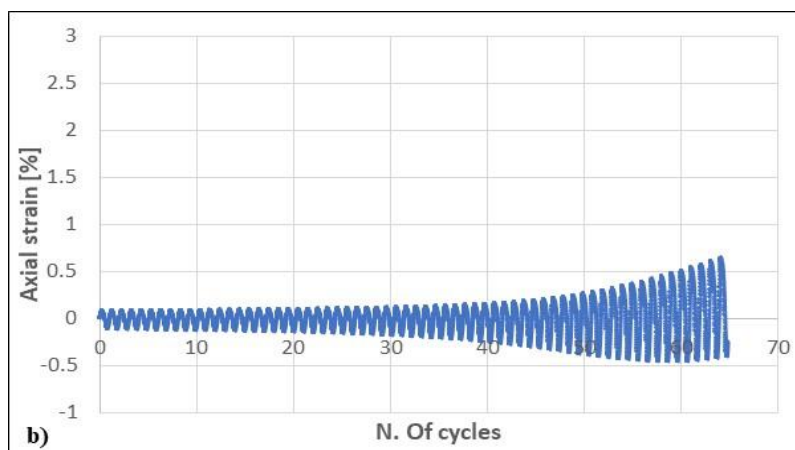
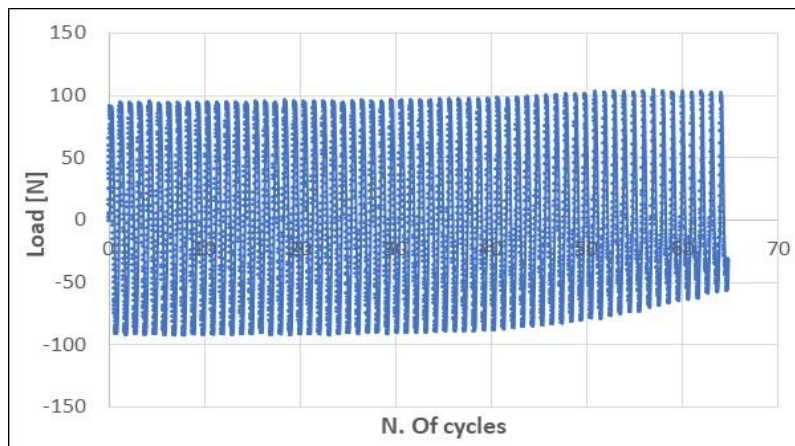
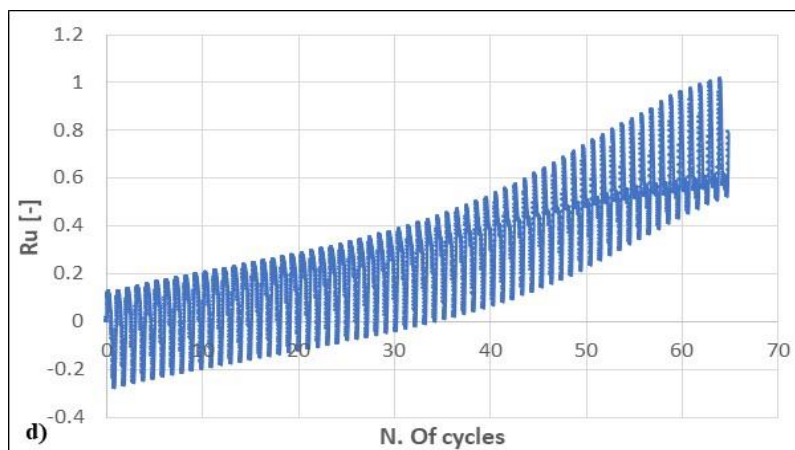
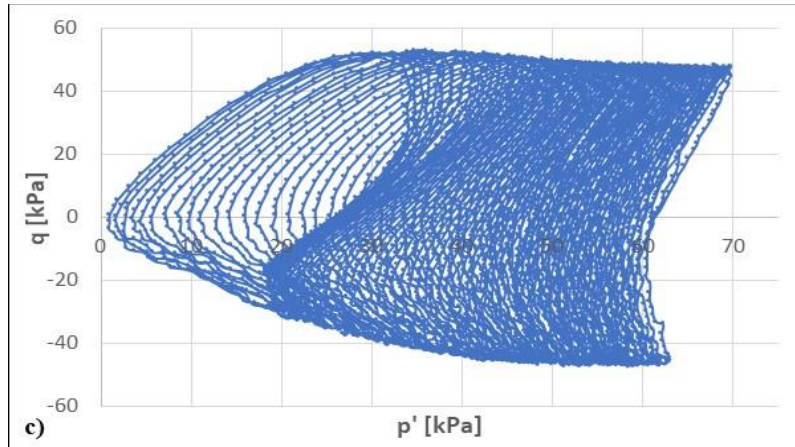


Fig 6.56 TXD4-ASTMD5311 result: a) load versus cycles; b) axial strain versus cycles; c) stress path ( $q$ - $p'$ ); d)  $r_u$  versus cycles

➤ TXD5-(ASTM D5311)


	Height (mm)	100
	Diameter (mm)	50
	Base area (mm <sup>2</sup> )	1962.5
	Volume (mm <sup>3</sup> )	196250
	Mass (g)	280
	Density (kg/mc)	1426
	Initial porosity	0.46
	Confining pressure (kPa)	60
	Final B test	0.97
	Initial deviatoric stress (kPa)	0

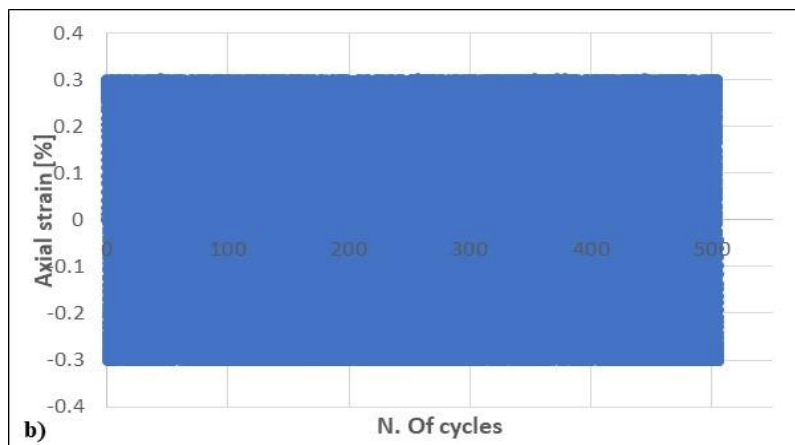
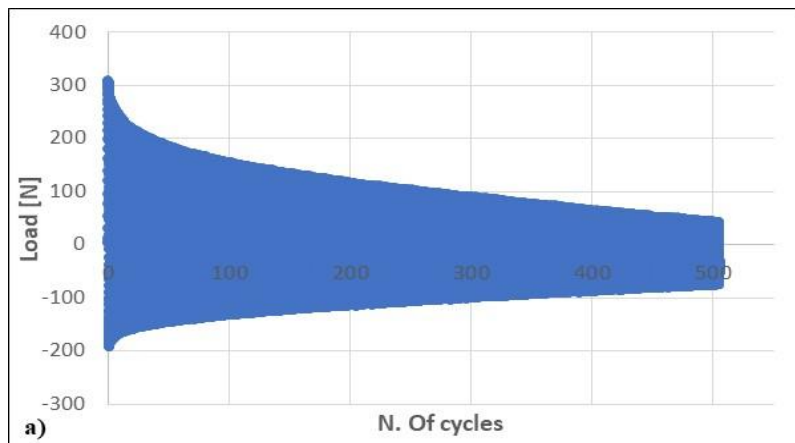


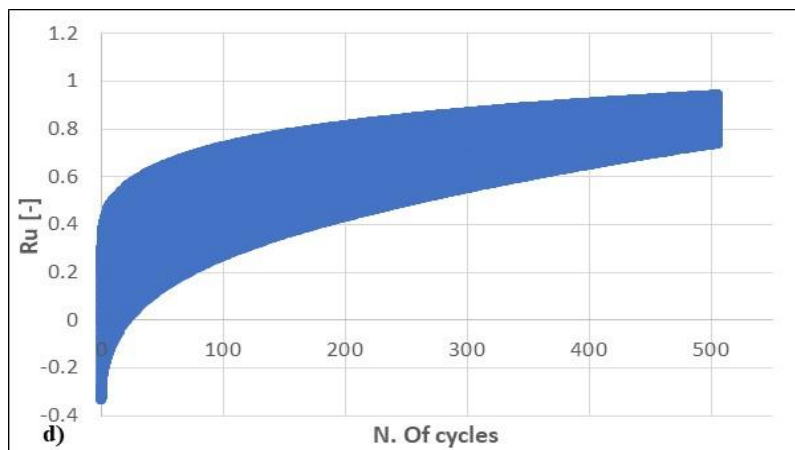
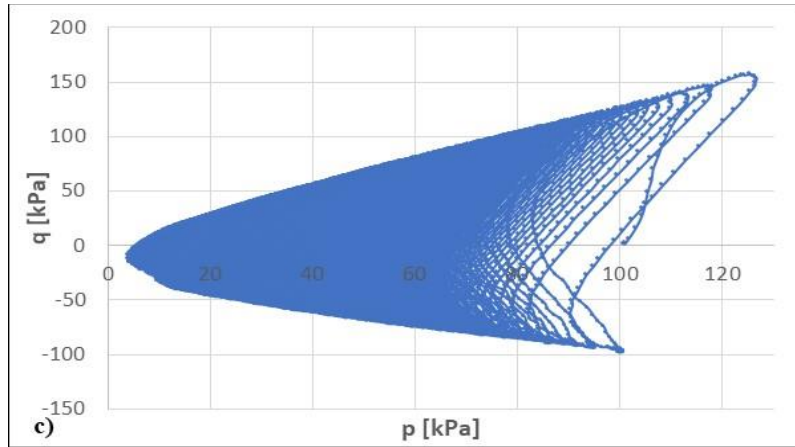


**Fig 6.57 TXD5-ASTMD5311 results: a) load versus cycles; b) axial strain versus cycles; c) stress path ( $q$ - $p'$ ); d)  $r_u$  versus cycles**

➤ TXD7-(NON-STANDARD)


	Height (mm)	100
	Diameter (mm)	50
	Base area (mm <sup>2</sup> )	1962.5
	Volume (mm <sup>3</sup> )	196250
	Mass (g)	286
	Density (kg/mc)	1457
	Initial porosity	0.45
	Confining pressure (kPa)	95
	Final B test	0.98
	Initial deviatoric stress (kPa)	0

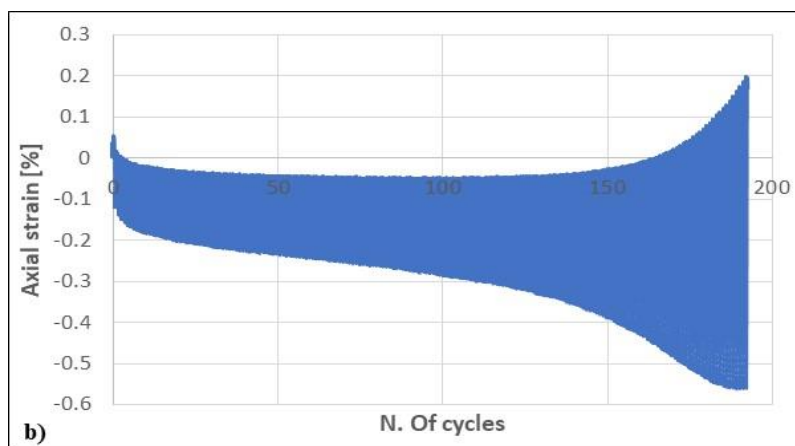
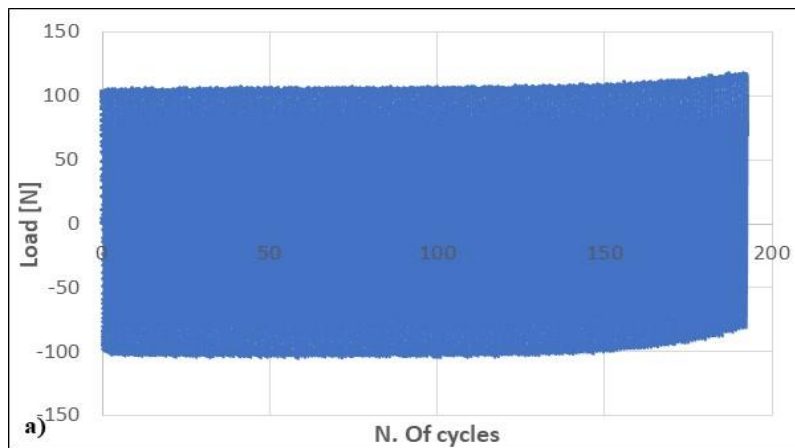


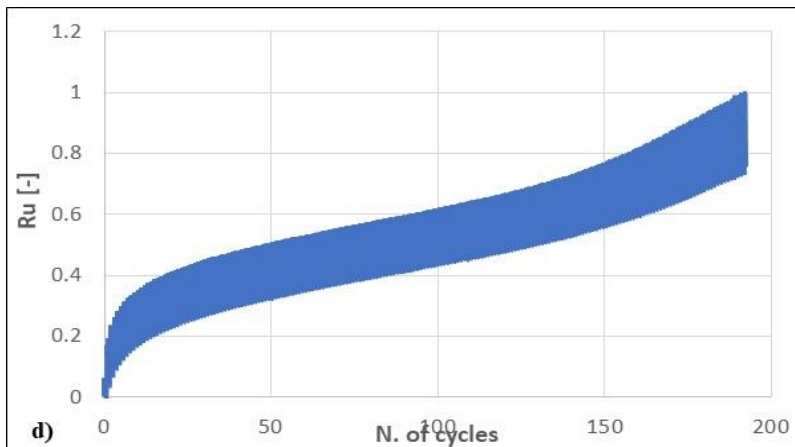
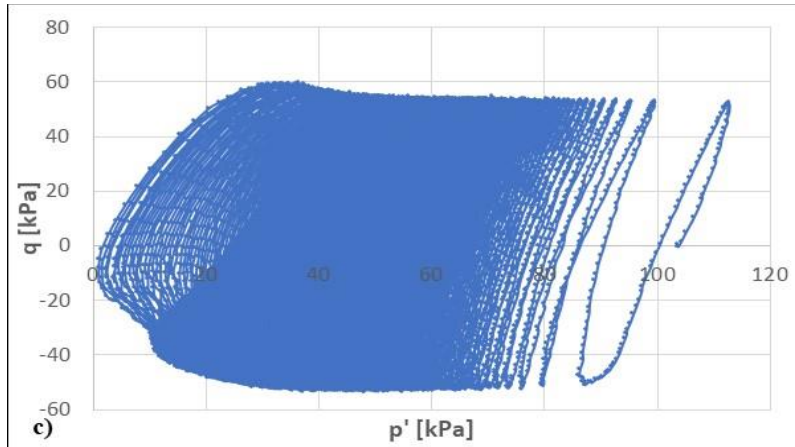


**Fig 6.58 TXD7-NON -STANDARD: a) load versus cycles; b) axial strain versus cycles; c) stress path ( $q$ - $p$ ); d)  $r_u$  versus cycles**

➤ TXD9- (ASTM D5311)

	Height (mm)	100
	Diameter (mm)	50
	Base area (mm <sup>2</sup> )	1962.5
	Volume (mm <sup>3</sup> )	196250
	Mass (g)	288.8
	Density (kg/mc)	1467
	Initial porosity	0.44
	Confining pressure (kPa)	100
	Final B test	0.95
	Initial deviatoric stress (kPa)	0

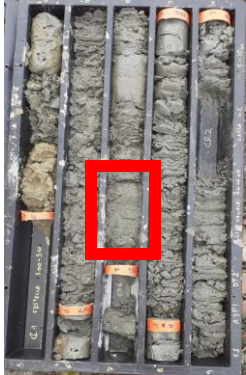


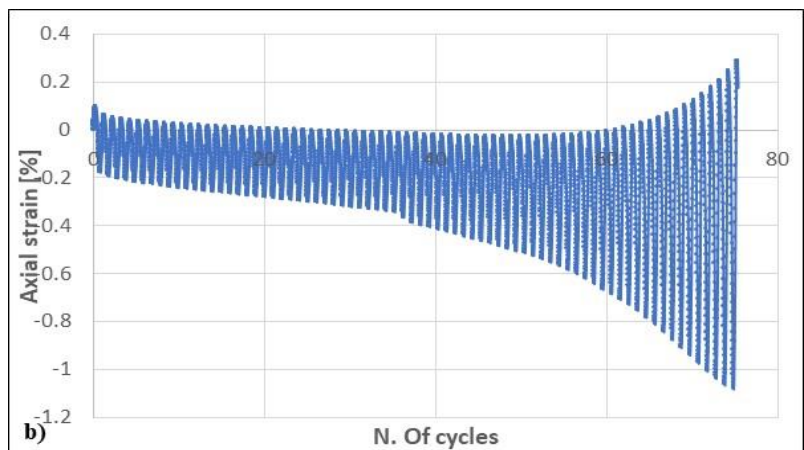
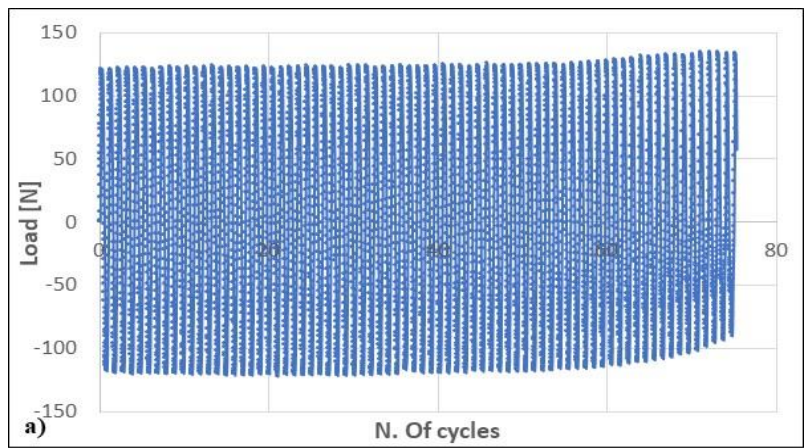


**Fig 6.59 TXD9-ASTMD5311 results: a) load versus cycles; b) axial strain versus cycles; stress path (q-p'); d) ru versus cycles**

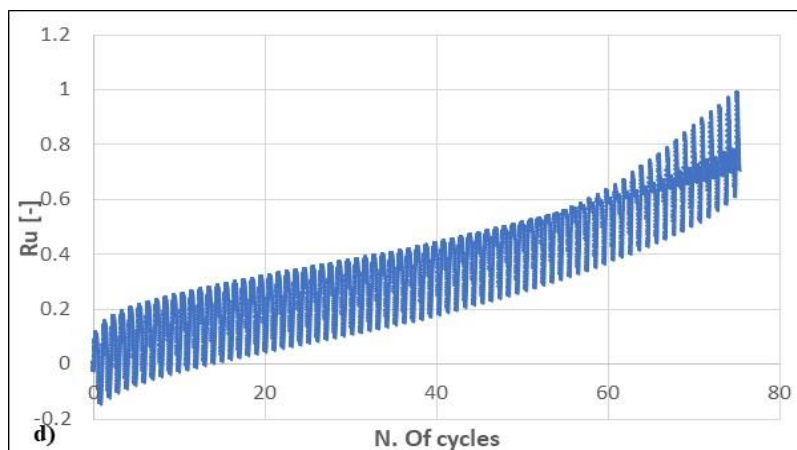
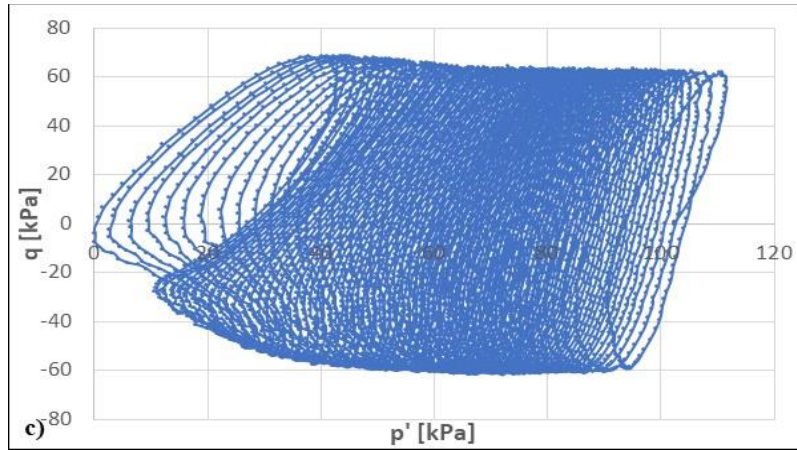


➤ TXD10-(ASTM D5311)

	Height (mm)	100
	Diameter (mm)	50
	Base area (mm <sup>2</sup> )	1962.5
	Volume (mm <sup>3</sup> )	196250
	Mass (g)	293
	Density (kg/mc)	1492
	Initial porosity	0.43
	Confining pressure (kPa)	100
	Final B test	0.97
	Initial deviatoric stress (kPa)	0




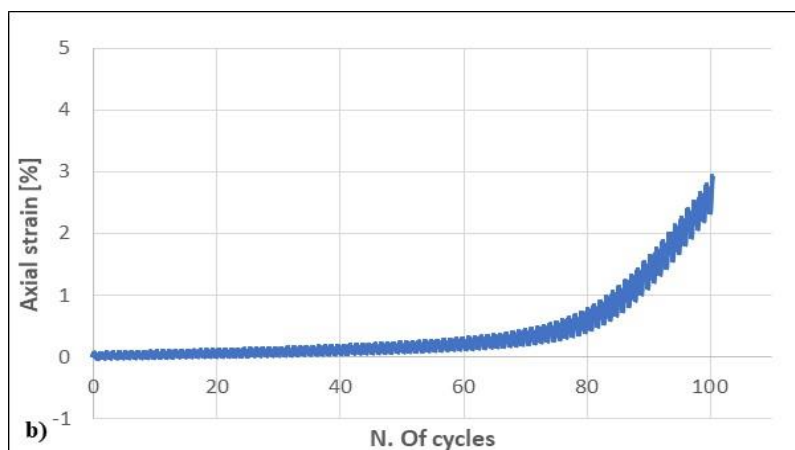
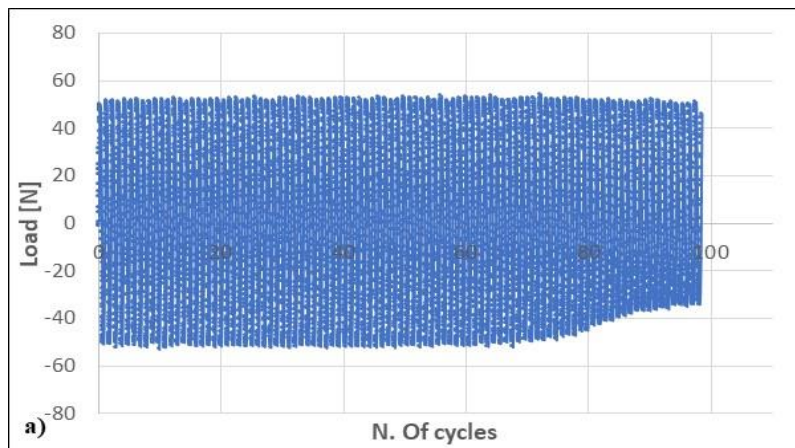


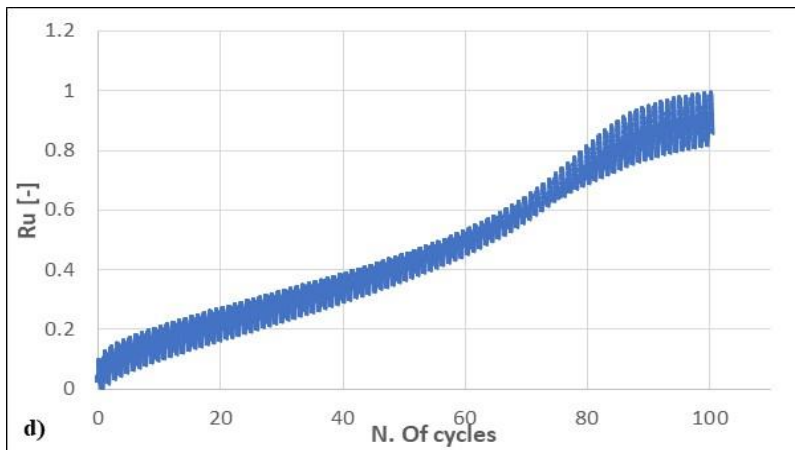
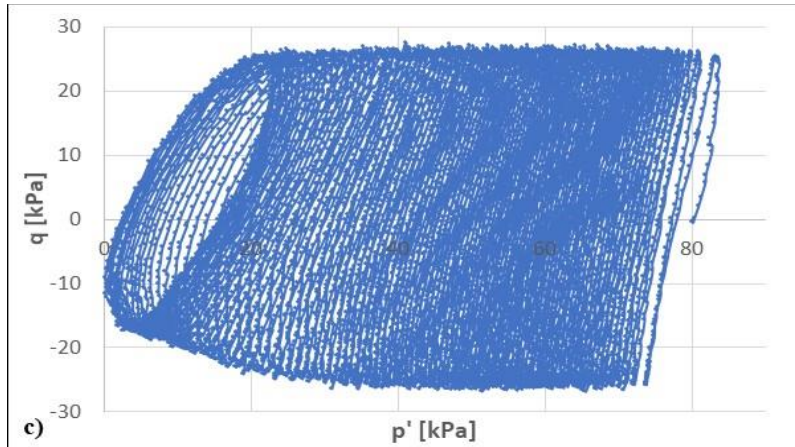


**Fig 6.60 TXD10-ASTMD5311 results: a) load versus cycles; b) axial strain versus cycles; stress path ( $q$ - $p'$ ); d)  $r_u$  versus cycles**

➤ TXD12-(ASTM D5311)


	Height (mm)	100
	Diameter (mm)	50
	Base area (mm <sup>2</sup> )	1962.5
	Volume (mm <sup>3</sup> )	196250
	Mass (g)	294.04
	Density (kg/mc)	1498
	Initial porosity	0.43
	Confining pressure (kPa)	80
	Final B test	0.90
	Initial deviatoric stress (kPa)	0





**Fig 6.61 TXD12-ASTMD5311 results: a) load versus cycles; b) axial strain versus cycles; stress path ( $q$ - $p'$ ); d)  $r_u$  versus cycles**

➤ TXD1-(ASTMD3999)

	Height (mm)	100
	Diameter (mm)	50
	Base area (mm <sup>2</sup> )	1962.5
	Volume (mm <sup>3</sup> )	196250
	Mass (g)	288
	Density (kg/mc)	1467
	Initial porosity	0.44
	Confining pressure (kPa)	100
	Final B test	0.97
	Initial deviatoric stress (kPa)	0

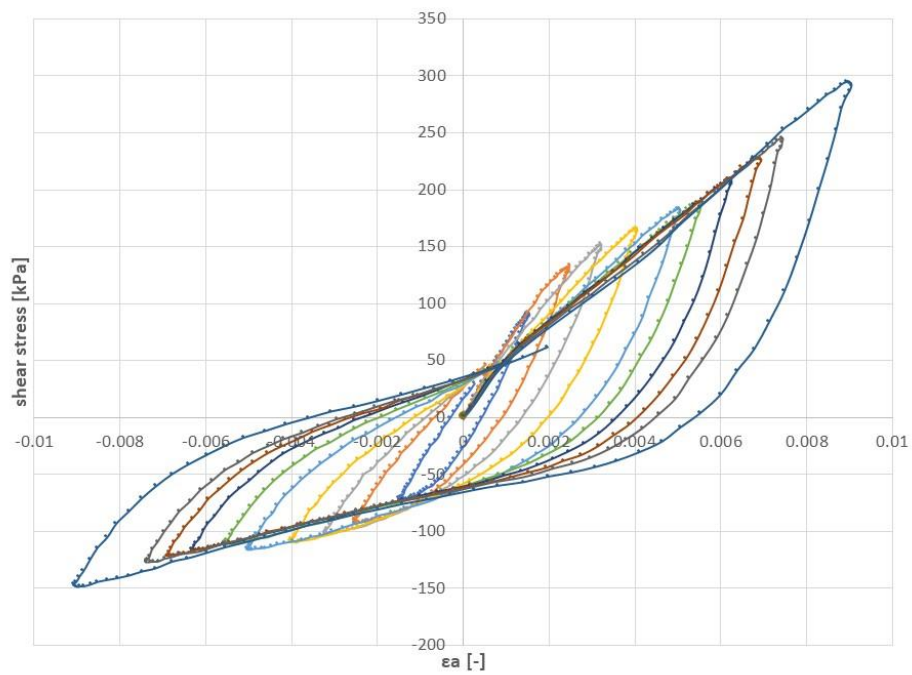
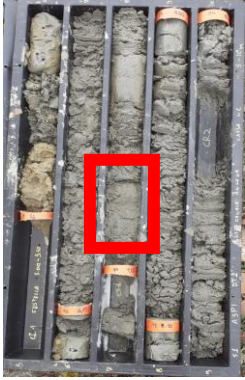


Fig 6.62TXD1-ASTMD3999 results: hysteresis loop of cycle n.1 for each strain level

➤ TXD2-(ASTMD3999)

	Height (mm)	100
	Diameter (mm)	50
	Base area (mm <sup>2</sup> )	1962.5
	Volume (mm <sup>3</sup> )	196250
	Mass (g)	297
	Density (kg/mc)	1513
	Initial porosity	0.45
	Confining pressure (kPa)	100
	Final B test	0.96
	Initial deviatoric stress (kPa)	0

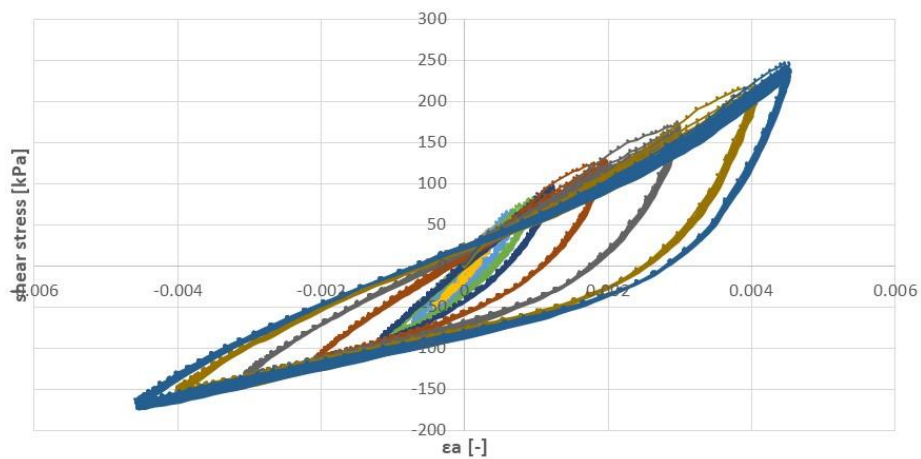


Fig 6.63 TXD2-ASTMD3999 results: hysteresis loop of cycle n.1 for each strain level

### 6.3.2.3 Discussion

A series of cyclic triaxial test has been performed on sand under investigation taken from Ponte Canale Ancora site, in order to study its behaviour under cyclic stress and to find the geotechnical parameters for further analysis with constitutive model.

Specimen from two different depths have been tested with under different stress condition and frequency. The same specimen, if not liquefied, has been subjected to increased CSR in order to reach liquefaction condition (as suggested by test protocol).

A summary of results compliant to ASTM D5311 is shown in Fig.6.64 along with CPT result. The red line is referred to the CSR as seismic demand, instead the violet line is the result of CPT, in terms of CRR; as known FS is less than the unit if CRR is minor than CSR, and in fact the depths in which this condition is verified are of our interest. CSR value is about 0.15, and in these tests a range of CSR has been investigated, in accordance to the specimen's answer to cyclic load applied.

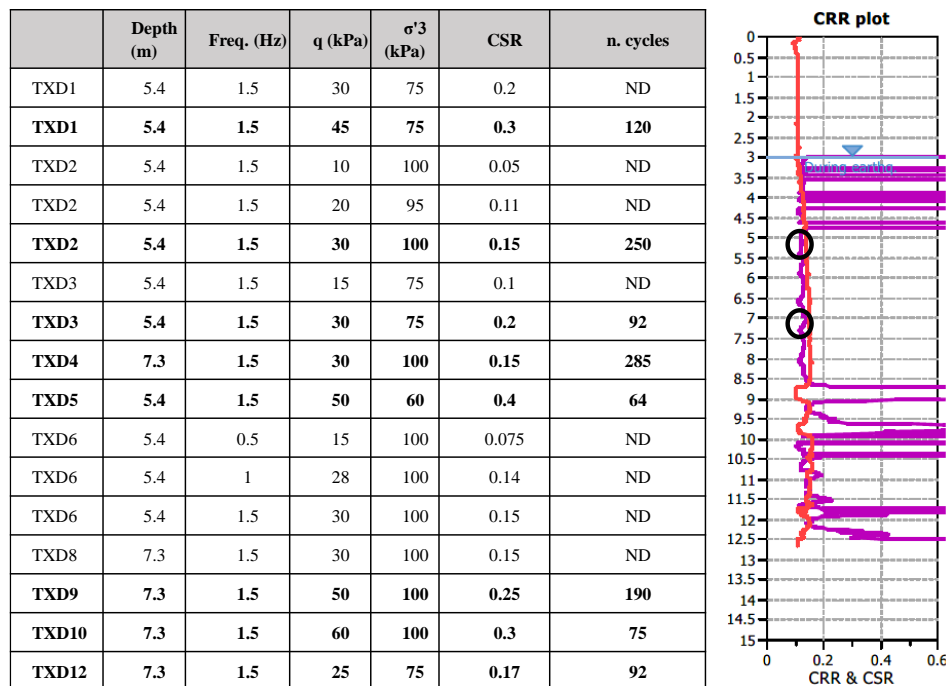


Fig 6.64 Summary of test results on the left; on the right CPT results in correspondence of the two depths investigated

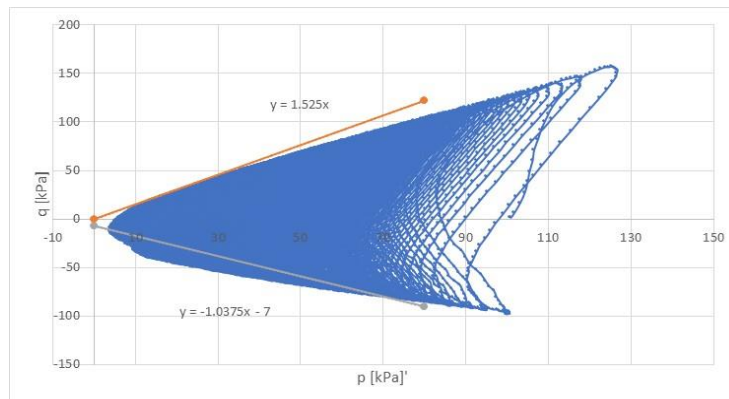
From these tests emerge that liquefaction is not always verified, and higher CSR are needed to liquefy.

In these tests the butterfly shape is not so evident, even if liquefaction is identified by the excess of pore pressure.

To investigate sample under different condition, non-standard test, it means strain-controlled tests, have been performed. Sample is liquefied when subjected at cyclic strain level with a double amplitude equal to 0.6mm (TXD7\_5.4); stress path resulting, presents a similar butterfly shape (Fig.6.65). From a comparison with the internal friction angle obtained from in situ test (Table 6-8), M coefficient is recalculated:

Sample	Type of test	M compression	M estension
5.4m	SPT (Schertmann)	1.55	-1.02
5.4m	Cyclic triaxial test	1.57	-1.03

**Table 6-8 Comparison results of M between SPT and cyclic triaxial test**



**Fig 6.65 Stress path of TXD7 test with butterfly shape**

Along with test compliant with ASTM D5311, standard and non-standard, tests compliant with ASTM D3999 have been performed for Damping and Elastic modulus evaluation.

The secant Young's modulus was determined as the ratio between the peak-to-peak deviatoric stress and the peak-to-peak axial strain along with each cycle. The Young's modulus decreases with increasing strain level.

The damping ratio was calculated from a hysteresis loop and is shown versus shear strain. Damping ratio increase as the shear strain increase. It quantifies how effectively the soil dissipates energy as heat during each loading cycle. The damping ratio is typically expressed as a decimal or percentage. High damping indicates that the soil dissipates a significant amount of energy during each cycle, leading to more pronounced energy



loss and reduced amplitude in subsequent cycles. Low damping indicates that the soil dissipates less energy, resulting in less energy loss and higher amplitude in subsequent cycles.

The elastic modulus represents the stiffness or stiffness recovery of the soil specimen under cyclic loading. It is also known as the shear modulus and is a measure of how well the soil recovers its stiffness during the unloading phase of each loading cycle. High elastic modulus indicates that the soil recovers its stiffness effectively during each cycle, demonstrating a strong ability to regain its original shape and resist deformation. Low elastic modulus suggests that the soil undergoes significant permanent deformation and experiences stiffness degradation during cyclic loading.

Tests have been performed in strain control condition, applying deformation to the sample ( $\epsilon_a$ ) according to the standard. Results are in line with expected ones, it means an increase of Damping ratio and a decrease of Elastic modulus as cyclic strain levels increase (Fig.6.66, Fig.6.67).

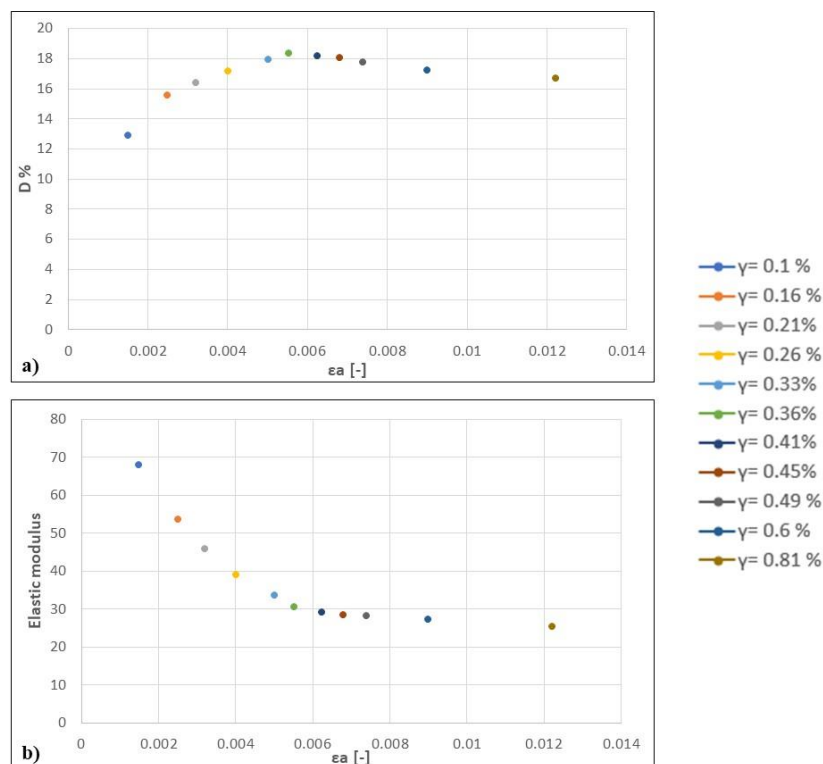
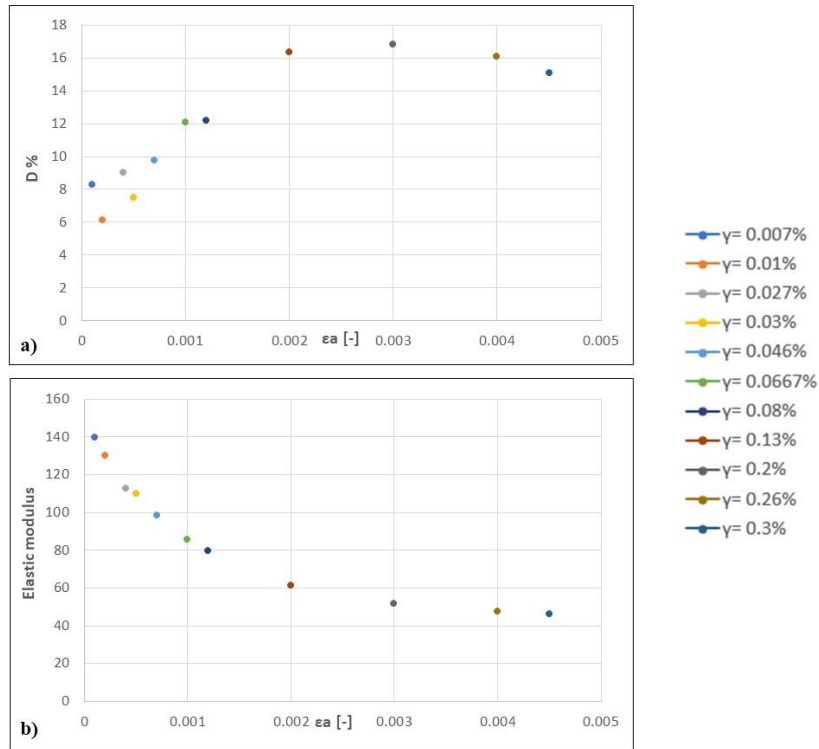


Fig 6.66 TXD1-ASTMD3999 elaboration: a) Damping versus  $\epsilon_a$ ; b) Elastic modulus versus  $\epsilon_a$





**Fig 6.67 TXD2-ASTMD3999 elaboration: a) Damping versus  $\epsilon_a$ ; b) Elastic modulus versus  $\epsilon_a$**

# 7 Constitutive model and numerical analysis: application on case studies

## 7.1 Introduction

This chapter will present the theoretical and numerical study developed in collaboration with Eg4Risk at Milano-Bicocca University.

Advanced computer-based methods in liquefaction evaluation are widely used in last few decades to numerical modelling of liquefaction typically involves the use of constitutive models, helping to capture the stress-strain response and pore pressure generation in soils. Liquefaction constitutive models were improved from loose coupled effective stress models (e.g., Finn model) to fully coupled effective stress models (e.g., UBCSAND model and PM4SAND model).

Advanced constitutive model UBCSAND has been chosen in this study to predict the phenomenon of liquefaction. Specifically, the model was implemented in the most widely used finite element numerical calculation code in geotechnical engineering, FEANX, in order to calibrate its parameters and to perform dynamic numerical analyses to study the behaviour of a soil susceptible to liquefaction in response to dynamic and cyclic stress and to evaluate the effects induced by liquefaction as the distance from the epicentre changes.

When conducting liquefaction analysis using numerical models, it is essential to calibrate the models using laboratory testing data or field observations. Model parameters, such as soil properties and earthquake input motions, should be carefully selected and validated to ensure accurate simulations of liquefaction phenomena. Additionally, sensitivity analyses and validation against real-world case studies are common practices in numerical liquefaction modelling to enhance the reliability of predictions. The input parameters of for the analysis are: the geotechnical parameters to model liquefiable and not liquefiable strata of soil and the project seismic input, based on real earthquake of the area.

## 7.2 UBCSAND

In geotechnical engineering, a constitutive model is a mathematical representation of how soils and other materials respond to various stresses and strains. Constitutive models for soil liquefaction are used to simulate and predict how soils will behave under different loading conditions, such as earthquake-induced stresses.

The UBCSand Liquefaction Model, also known as the Seed-Idriss Model, is a well-known constitutive model used in geotechnical engineering to assess the liquefaction potential of sandy soils during seismic events. It was developed by Professor Harry Bolton Seed and Professor I.M. Idriss at the University of California, Berkeley.

This model provides a mathematical framework for estimating how the pore water pressure in sandy soils changes during an earthquake. It is important to understand how changes in pore water pressure can affect the soil's behavior, developing the “banana loops” in the shear stress versus shear strain plot once liquefaction occurs (e.g., Beaty and Byrne 1998, Park and Byrne 2004).

Realistic soil responses are obtained by independently controlling the accumulation of permanent shear strains and volumetric strains in the model. This model includes two yielding surfaces to model the cyclic behavior of soils:

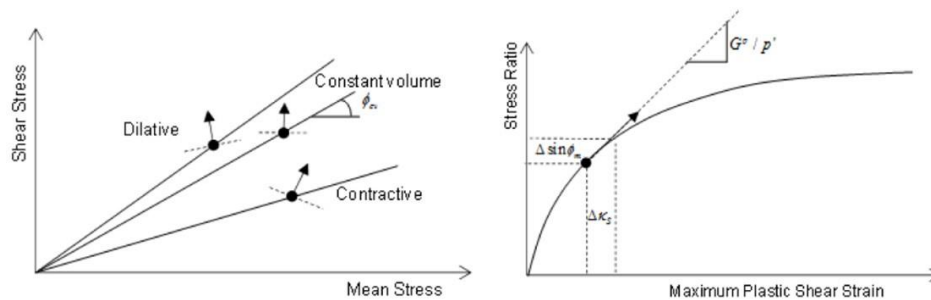
- the primary yielding surface with which an isotropic work hardening law is associated;
- the secondary yielding surface to which is associated a work hardening law kinematics that allows us to model the fact that as the number of cycles at a constant amplitude of distortional strain there is a reduction in volume and an increase in stiffness (soil thickening).

As previously mentioned, such a constitutive model simulates the trend of effective stresses for predicting the liquefaction behavior of sands during a dynamic load (earthquake, anthropogenic vibrations, ...). In this case in the region of elastic behavior, a nonlinear one is allowed, where the elastic modulus changes as a function of the applied effective stress.

$$G^e = K_G^e p_{ref} \left( \frac{p' + p_t}{p_{ref}} \right)^{ne} \quad K^e = \frac{2(1+\nu)}{3(1-2\nu)} G^e \quad \text{Eq. 7-1}$$

In the plastic region, the behavior is defined by three functions: shear (shear hardening), compression (cap hardening) and pressure cut-off. In

general, shear stress induces a plastic expansion that is a function of the difference between the mobilized friction angle ( $\phi_m$ ) and the constant volume friction angle ( $\phi_{cv}$ ). The plastic shear deformation is related to the ratio of final and initial shear strains (at  $t = 0$ ) by a hyperbolic function (Fig.7.1).



**Fig 7.1 Dilative and contractile behavior of the envelope at linear failure and hyperbolic trend function stress ratio and maximum plastic shear deformation**

The model, depends on many parameters, the complete list is represented below (Fig.7.2) with a brief description of the individual parameters and the empirical formula, if any, for calculating them from the parameter  $(N_1)_{60}$ , which can be identified for each unit from standard geotechnical tests, in particular from SPTs (Standard Penetration Tests).

Parameter	Description	Reference
Pref	Reference Pressure	In-situ horizontal stress at mid-level of soil layer
Elastic (Power Law)		
$K_G^e$	Elastic shear modulus number	Dimensionless
$ne$	Elastic shear modulus exponent	Dimensionless
Plastic / Shear		
$\phi_p$	Peak Friction Angle	Failure parameter as in MC model
$\phi_{cv}$	Constant Volume Friction Angle	-
C	Cohesion	Failure parameter as in MC model
$K_G^p$	Plastic shear modulus number	Dimensionless
$np$	Plastic shear modulus exponent	Dimensionless
$R_f$	Failure ratio ( $q_f / q_a$ )	0.7–0.98 (< 1), decreases with increasing relative density
$F_{post}$	Post Liquefaction Calibration Factor	Residual shear modulus
$F_{den}$	Soil Densification Calibration Factor	Cyclic Behavior
Advanced parameters		
Pcut	Plastic/Pressure Cutoff (Tensile Strength)	-
$K_G^c$	Cap Bulk Modulus Number	-
$mp$	Plastic Cap Modulus Exponent	-
OCR	Over Consolidation Ratio	Normal stress / Pre-overburden pressure

$$K_G^e = 21.7 \times 20.0 \times (N_1)_{60}^{0.333}$$

$$30^\circ < \phi_p < 34^\circ$$

$$\nu = 0.0163$$

$$K_G^p = K_G^e (N_1)_{60}^{-2} \times 0.003 + 100.0$$

$$ne = 0.5$$

$$np = 0.4$$

$$\phi_p = \begin{cases} \phi_{cv} + (N_1)_{60} / 10.0 & ((N_1)_{60} < 15.0) \\ \phi_{cv} + (N_1)_{60} / 10.0 + \max\left(0.0, \frac{(N_1)_{60} - 15}{5}\right) & ((N_1)_{60} \geq 15.0) \end{cases}$$

$$R_f = 1.1 \times (N_1)_{60}^{-0.15}$$

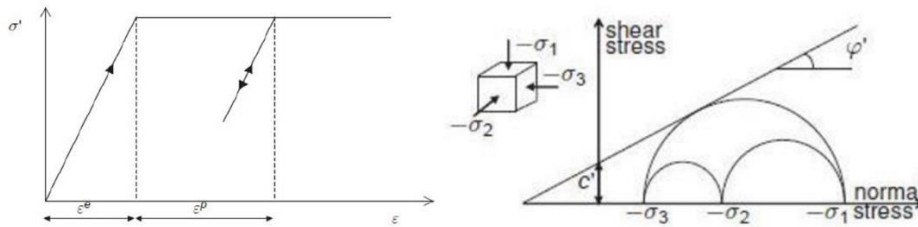
[Parameters and Equations for Calibration]

**Fig 7.2 UBCSAND modified parameters with description and empirical formulas for their calculation from SPT tests.**

To estimate liquefaction in quantitative terms, the Pore Pressure Ratio (PPR, otherwise denoted by  $ru$ ) is used.

### 7.3 Mohr-Coulomb

Mohr-Coulomb model simulates elasto-plastic behavior (Fig.7.4). This behavioral hypothesis shows reliable results for nonlinear analysis of most soils.



**Fig 7.3 Elasto-plastic stress behaviour as a function of deformation and linear break envelope.**

While the linear region is only a function of the soil's elastic modulus (or Young's modulus), infinite deformation plasticization occurs when shear and normal stress meet the well-known Mohr-Coulomb equation:

$$\tau' = c' + \sigma' \tan \phi' \quad \text{Eq. 7-2}$$

This model is used for modelling all the units present less the liquefiable one. Therefore, the main parameters required by the model to characterize the activation of the plastic deformation are the cohesion (intercept of the break envelope), the friction angle (angle of inclination of the break envelope), dilatancy angle (a low value of this parameter is considered in favour of safety) tensile strength.

## 7.4 Numerical analysis

Numerical analyses were performed using the MIDAS FEA NX computational program. The computational program allows complex 2D and 3D models by performing advanced geotechnical finite element numerical analyses and in the field of soil-structure interaction. Coupled multidisciplinary analyses allow a variety of geotechnical design applications to be handled. Midas FEA NX is currently one of the best software for advanced 3D geotechnical finite element analyses and in the field of soil-structure interaction. Coupled multidisciplinary analyses allow the full range of geotechnical design applications to be handled in a single environment, particularly foundations, bulkhead excavations, tunnels, underground structures, filtration analysis, soil consolidation, dams, seismic analysis, and slope stability.

The graphical user interface is simple and intuitive, enabling the creation of complex 2D and 3D models with unparalleled levels of accuracy and efficiency.

Midas FEA NX has an extensive library of finite elements that allows modelling both the ground domain and all types of structures, from buildings to all infrastructures.

The FEA NX platform is also complemented by a 3D CAD environment capable of creating and managing geometric functions without limits of complexity and of importing geometries from all major CAD formats; in particular, with the Terrain Geometry Maker function it is able to import satellite topographic maps, defining a new standard in the simulation of reality. The powerful post-processor automatically generates contours, diagrams, graphs and tables related to all types of results that allow quickly and efficiently to identify the critical points of the project to be included in the final report.

The primary steps involved in this process may include:

- **Geometric Modeling:** Create a 2D or 3D model of the site, including the soil layers, the structures, and other relevant components.
- **Material Properties:** Define the material properties of the soil layers, including properties related to liquefaction susceptibility.
- **Boundary Conditions:** Apply appropriate boundary conditions to represent the interactions between the soil and structures, considering both static and dynamic conditions.

- **Loading Conditions:** Specify the dynamic loading conditions that simulate an earthquake event. This may include ground motion data.
- **Analysis Settings:** Set up the FEA analysis with parameters such as time-stepping methods, damping, and analysis duration.
- **Simulation:** Run the FEA analysis to simulate the behaviour of the soil and structures during the earthquake. The software will calculate factors such as stresses, displacements, and pore water pressure changes.
- **Liquefaction Assessment:** Use the analysis results to assess the potential for soil liquefaction in different areas of the site.
- **Post-Processing:** Examine and interpret the analysis results to understand how the structures and soil layers respond to dynamic loading, with a focus on areas prone to liquefaction.

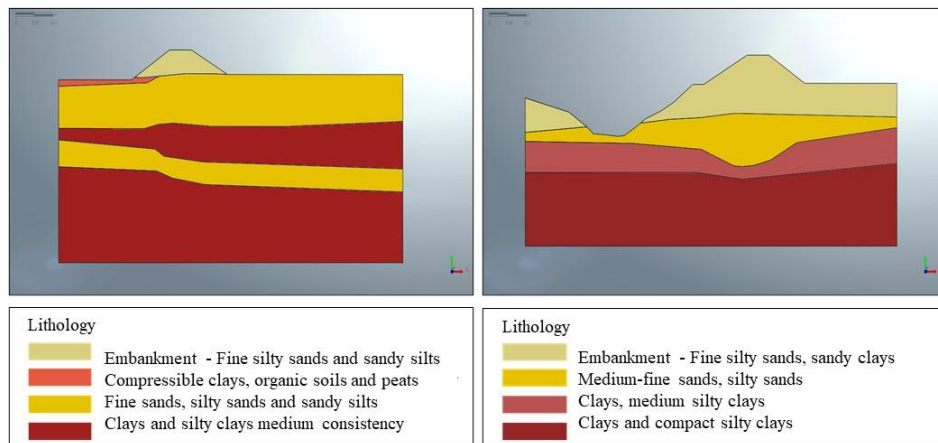
The following section will present the results of advanced analysis of Case1 and Case2 as a final step of a complete liquefaction assessment. In situ test along with laboratory test, cyclic triaxial test, provide the identification of geotechnical parameters to dynamically simulate the geotechnical structures involved.

## **7.5 Case 1: Simulation of the dynamic behaviour of the Panaro embankments**

The topographic profile of the project in correspondence of the two critical area, Control section 82 and Control section 39-44 are shown in Fig.8.1, without the inclusion of any of the engineering works for the embankment adjustment:

- Control section 82: mainly composed by the stratigraphic succession of four lithotypes. The only unit found vulnerable to liquefaction is unit 2, located at the base of the embankment
- Control section 39-44: composed of four typical riverbed lithologies; in this embankment portion, unit 3, the sandy unit with the greatest propensity for liquefaction, results in depositional alternation with lithotypes that are decidedly more cohesive.

A viscous constraint is applied to the side of model (in dynamic analysis a fixed constraint cannot be applied, as in static analysis). A kinematic constraint of embedding has been applied to the base of the model, against which the seismic input is applied. The damping ratios used in the code are 5% (default value suggested by the code).



**Fig 7.4 2D CAD section of the control section 39-44 sx and 82 dx with relative lithological geometries**

### 7.5.1 Calibration of the parameters of the UBC SAND constitutive model

In order to dynamically simulate the behaviour of the embankment in correspondence of Control section 82 and Control section 39-44, previously defined as potentially liquefiable, two main constitutive models have been used:

- Mohr-Coulomb for non-liquefiable lithological units
- Modified UBCSAND, for liquefiable lithological units

Based on the geognostic investigations carried out, it's possible to characterize the geotechnical parameters of the identified lithological units. With regard to friction angle, cohesion and permeability of non-liquefiable units, the most conservative ones derived from laboratory tests, were included in the models. The elastic moduli for each layer were derived from the weighted average of the values identified by CPTu. In

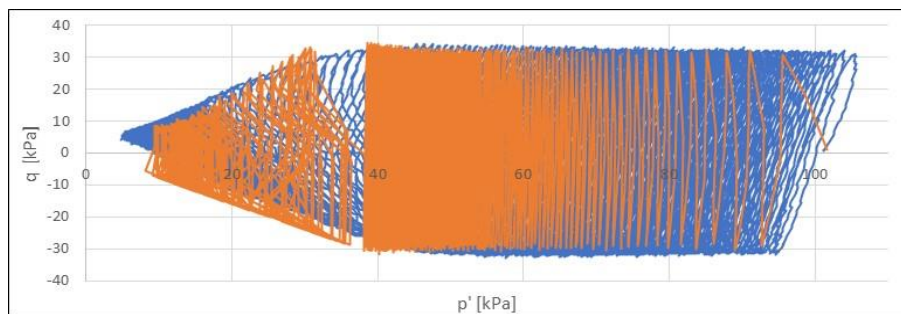


addition, from these, the coefficient  $N_{60}$ , was calculated indirectly using CPTu interpretation software.

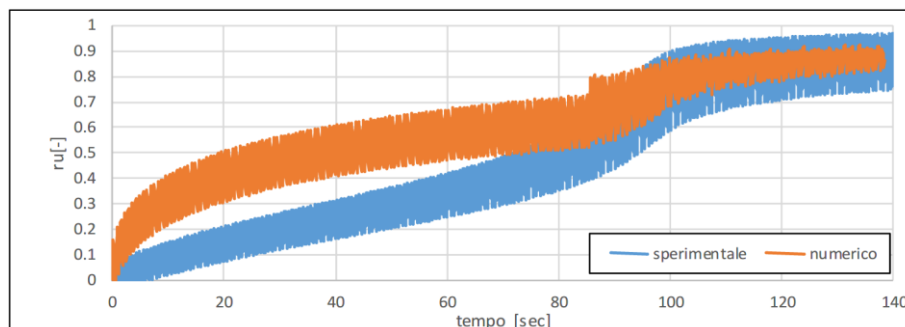
In a previous analysis, having the trend of  $N_{60}$  with depth available, its normalized  $(N_1)_{60}$  was calculated at the in-situ stress state, and finally, once corrected, a weighted average of these values was taken over the depths inherent in the liquefiable level, to arrive at defining the appropriate  $(N_1)_{60}$ , from which to derive all the parameters needed for the modified UBCSAND. For both Control sections, a  $(N_1)_{60}$  of 14 was calculated.

In this work, the parameters  $F_{dens}$  and  $F_{post}$ , concerning, respectively, the main hardening parameter induced by soil densification during stress cycles and the secondary hardening parameter occurring during the liquefaction process were calibrated from the results of dynamic triaxial test, for Control section 82.

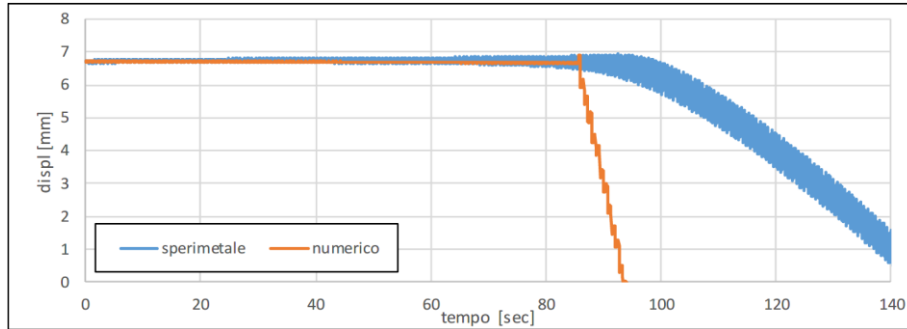
The calibration of the constitutive parameters  $F_{dens}$  and  $F_{post}$  is shown in Fig.7.5-7.7:



**Fig 7.5 calibration of UBCSAND parameters with dynamic triaxial test: deviatorial stress and effective pressure**



**Fig 7.6 calibration of UBCSAND parameters with dynamic triaxial test: ru versus time**



**Fig 7.7 calibration of UBCSAND parameters with dynamic triaxial test: vertical displacement versus time**

The following tables summarize the parameters used in the modelling, excluding those parameters set as standard in modified UBCSAND, namely:

<i>ne</i>	<i>np</i>	<i>pre<sub>f</sub></i> [kPa]
0.5	0.4	100

	MOHR-COULOMB			UBCSAND
	Unit 1	Unit 2	Unit 4	Unit 3
<b><i>E</i></b> [kPa]	53535	11471	42541	49893
<b><i>v<sub>u</sub></i></b>	0.3	0.3	0.35	0.49
<b><i>γ</i></b> [kNm <sup>3</sup> ]	18.5	16	19	19
<b><i>K<sub>0</sub></i></b>	0.484962	0.741181	609269	<i>K<sub>0</sub>(S)</i>
<b><i>γ<sub>sat</sub></i></b> [kNm <sup>3</sup> ]	19	17	20	20
<b><i>e<sub>0</sub></i></b>	0.3	0.3	0.3	0.73
<b><i>K<sub>xyz</sub></i></b> [m/s]	7.00E-07	8.00E-09	3.00E-08	5.00E-06
<b><i>C</i></b> [kPa]	4	1	2	0
<b><i>φ</i></b>	31°	15°	23°	-
<b><i>φ<sub>cv</sub></i></b>	-	-	-	34
<b><i>φ<sub>p</sub></i></b>	-	-	-	35.4
<b><i>K<sub>G</sub><sup>e</sup></i></b>	-	-	-	1045.1
<b><i>K<sub>G</sub><sup>p</sup></i></b>	-	-	-	714.5
<b><i>R<sub>f</sub></i></b>	-	-	-	0.74
<b><i>F<sub>post</sub></i></b>	-	-	-	0.7
<b><i>F<sub>dense</sub></i></b>	-	-	-	1

**Table 7-1 •Control section 39-44 parameters**

	MOHR-COULOMB			UBCSAND (SPT)	UBCSAND (CTX)
	Unit 1	Unit 3	Unit 4	Unit 2	Unit 2
<b>E [kPa]</b>	36400	7000	1000	48130	48130
<b><math>\nu_u</math></b>	0.3	0.3	0.35	0.49	0.49
<b><math>\gamma</math> [kNm<sup>3</sup>]</b>	19	19	19	19	19
<b>K0</b>	0.484962	0.741181	609269	K0(S)	K0(S)
<b><math>\gamma_{sat}</math> [kNm<sup>3</sup>]</b>	20	20	20	20	20
<b><math>e_0</math></b>	0.61	0.5	0.5	0.73	0.73
<b><math>K_{xyz}</math> [m/s]</b>	2.00E-07	9.00E-08	1.00E-07	7.00E-06	7.00E-06
<b>C [kPa]</b>	5	2	4	0	0
<b><math>\phi</math></b>	32°	24°	27°	-	-
<b><math>\phi_{cv}</math></b>	-	-	-	33	30
<b><math>\phi_p</math></b>	-	-	-	34.4	31.4
<b><math>K_G^e</math></b>	-	-	-	1045.1	1045.1
<b><math>K_G^p</math></b>	-	-	-	714.5	714.5
<b><math>R_f</math></b>	-	-	-	0.74	0.74
<b><math>F_{post}</math></b>	-	-	-	0.7	0.7
<b><math>F_{dense}</math></b>	-	-	-	1	0.485

Table 7-2 •Control section 82 parameters

## 7.5.2 Numerical modelling

Numerical analysis has been conducted considering four scenarios described in Table 7-3. The simulations of case A and case B, as regards the liquefiable layer, use parameters of the geological relationship resulting from field geotechnical surveys and surveys. For cases C and D it has been assumed to increase the value of the stiffness of the liquefiable layer by 25% by changing the value of the elastic modulus (E); an increase in stiffness is expected to correspond to more critical results for the liquefiable layer.

Another sensitive parameter referring to the liquefiable unit is the constant K of proportionality between horizontal and vertical stress. For cases A and D a K value of 0.46 has been set (mean value generating a linear variation of vertical effective forces with depth) whereas for cases B and C a unit K corresponding to an isotropic condition of initial effort in any direction has been assumed:

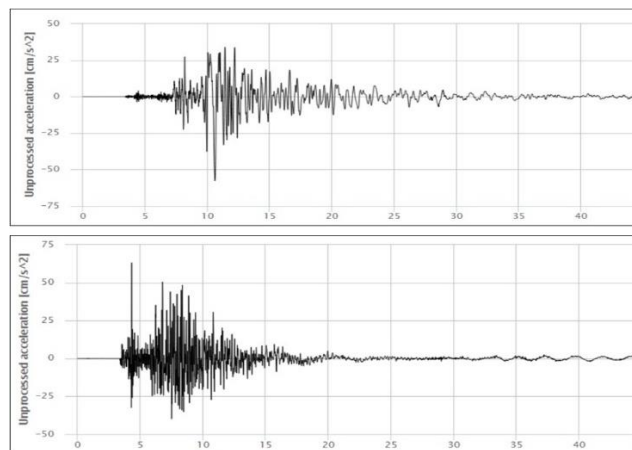
	CASE A	CASE B	CASE C	CASE D
	geotechnical report parameters	geotechnical report parameters	Young modulus increased of 25%	Young modulus increased of 25%
	$K_0 = 0.46$	$K_0 = 0.46$	$K_0 = 1$	$K_0 = 1$
	Design earthquake	Design earthquake	Emilia 29-05-12 earthquake	Emilia 29-05-12 earthquake
Control section 82	x	x	x	x
Control section 39-44	x	x	x	x

**Table 7-3 Summary of the modelling cases performed**

In this scenario, the worst case is represented by case D for Control section 82, for which UBCSAND has been calibrated with parameters obtained from cyclic triaxial test shown above.

#### 7.5.2.1 Dynamic input loads and seismic modelling

When performing dynamic modelling, as in this case, it is extremely important to perform the seismic characterization of the system under study. The site under study was hit by the earthquake of 29 May 2012, suffering no particular damage except some slight subsidence of the order of centimetres. It was decided to simulate the phenomenon that occurred to have real evidence of what happened some years ago. From the INGV (Istituto Nazionale di Geofisica e Vulcanologia) databases, the earthquake's seismogram (Fig.7.8) was extracted:



**Fig 7.8 Top: EW component earthquake 29 May 2012 recorded in the IT.RAV0 station of the INGV. At the bottom Up Down component of the same. In axis X time in seconds.**

Given the very high sampling (traces of 24000 samples each, sampling time of 0.5 ms) to minimize the calculation time of the software, it was necessary to resample the same at 25 Hz (40 ms). Such sampling is allowed by Nyquist's law, which allows resampling a signal with a minimum frequency twice the dominant frequency of the signal. It was also checked that the frequency spectrum of the resampled signal did not vary from the initial one. However, not reaching the maximum number of samples decided by the software architecture, it was decided to simulate only the arrival of the S wave in the two components East West (EW) and Up Down (UD). Another important element was to define the local scaling of the accelerations: also, from the INGV website it was possible to download the shakemap of the Emilia event of 29 May. This map contains the contour of the acceleration peaks as a function of the latitude and longitudinal position (Fig.7.9). The chosen point was the one with GPS coordinates as much as possible close to the locality Bomperto (MO), common where the control section affected by the modeling are located.

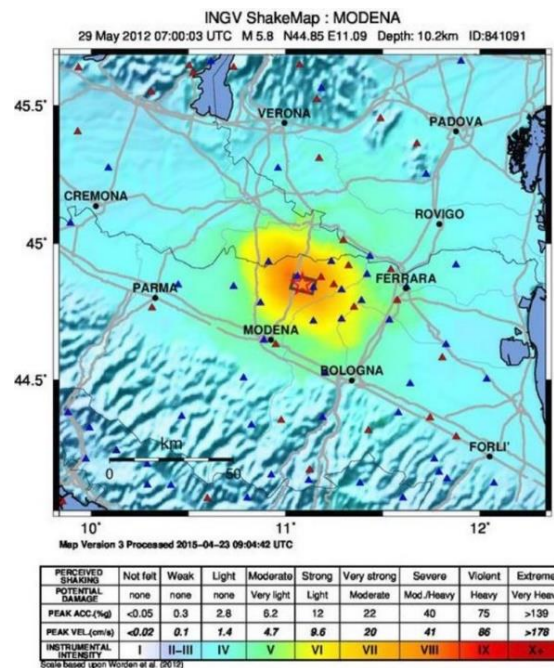
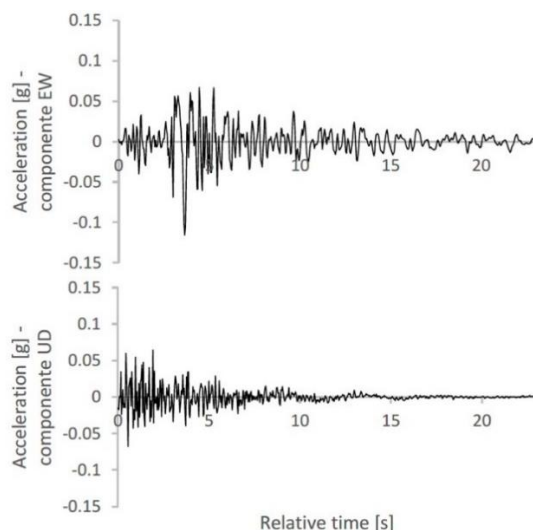


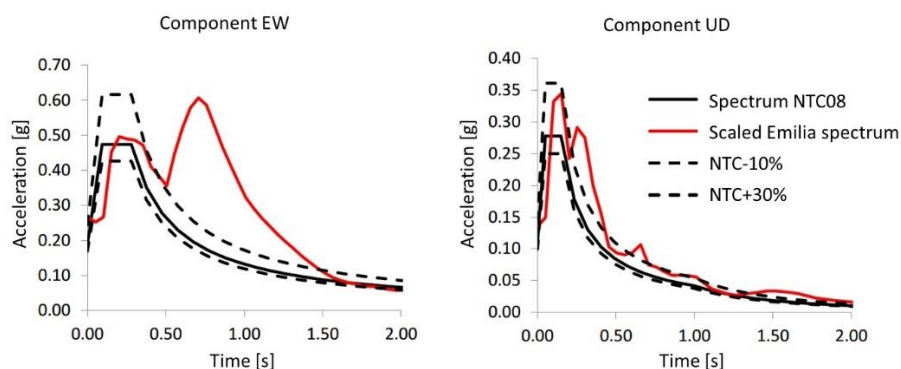
Fig 7.9 Shakemap published by INGV three years after the earthquake.

The calculated peak ground acceleration (PGA) value was 0.1154g. By then scaling the waveforms for this value, the final input signal is shown in Fig.7.10:



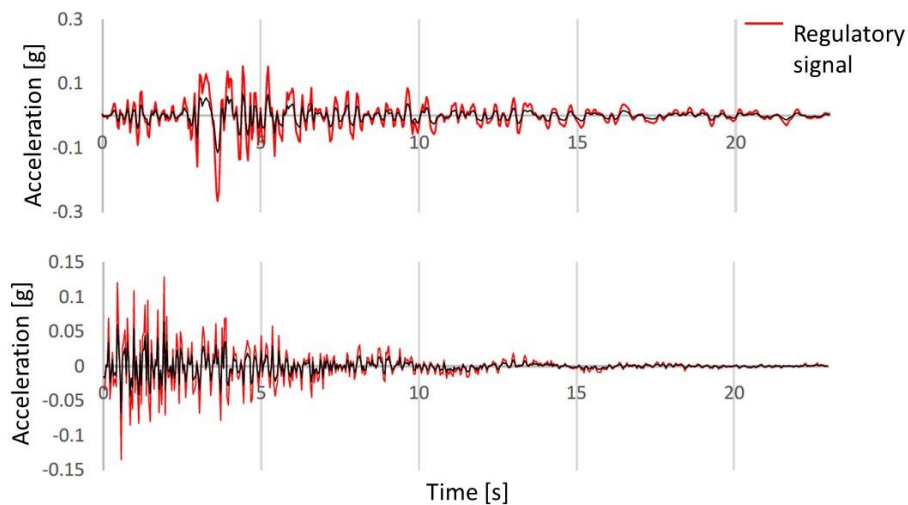
**Fig 7.10 EW component (top) and UD component (bottom) resampled and scaled to the PGA calculated for the Bomporto site.**

The Technical Standards for Construction NTC2018 provide that in the design phase is taken into account a seismic signal whose spectrum complies with those in the ministerial decree. Then considering the signals in Fig.7.11, their spectra have been calculated and scaled to those of the standard.



**Fig 7.11 EW component (left) and UD component (right) resampled and scaled to the PGA calculated for the Bomporto site.**

After that, the signals with the spectrum conforming to the decree were regenerated: the maximum acceleration induced by the design earthquake is amplified 2 times in the component x and 2.3 times in the component y, as can be seen in the following Fig.7.12. The simulations will be carried out both with the project earthquake and with that of 29 May 2012.



**Fig 7.12 Comparison of components EW (top) and UD (bottom) between the processed earthquake (black) and that scaled to the regulatory spectrum (red)**

### 7.5.3 Results

In previous analysis, it was decided to perform simulations in four different cases for each of the two control sections in question having a total of 8 analyses, based on in situ test.

In this work, it has decided to conduct a single analysis using the new constitutive parameters of the UBC SAND model, calibrated from cyclic dynamic triaxial test TXD2, taking into consideration the most unfavourable condition, represented by scenario D for control section 82.

The following figures (Fig.7.13-7.17) shown the results analysis.

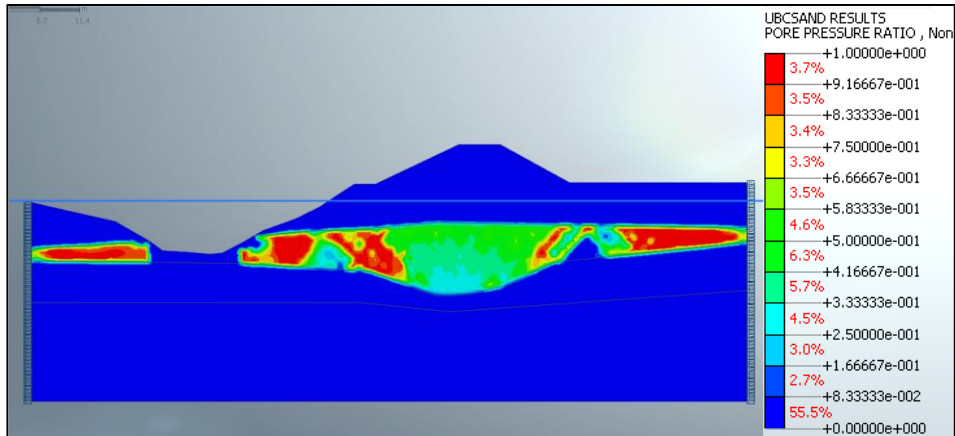


Fig 7.13 Control section 82 – case D- ru evaluation

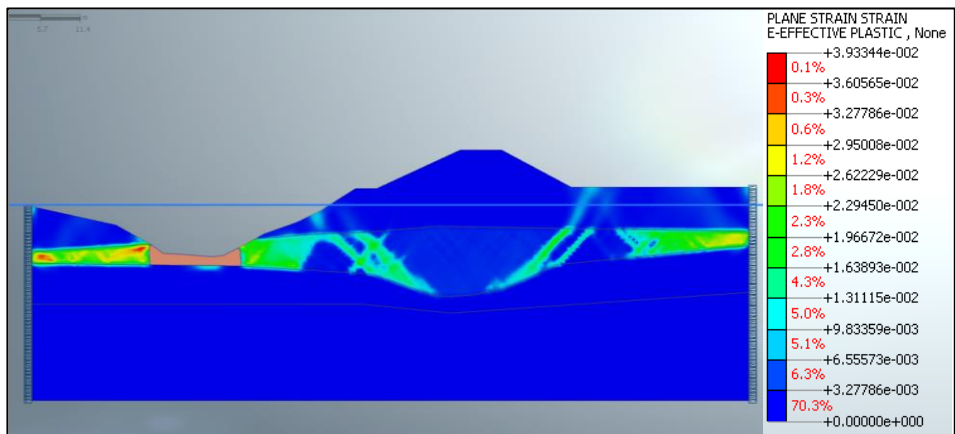


Fig 7.14 Control section 82 – case D – plastic deformation evaluation

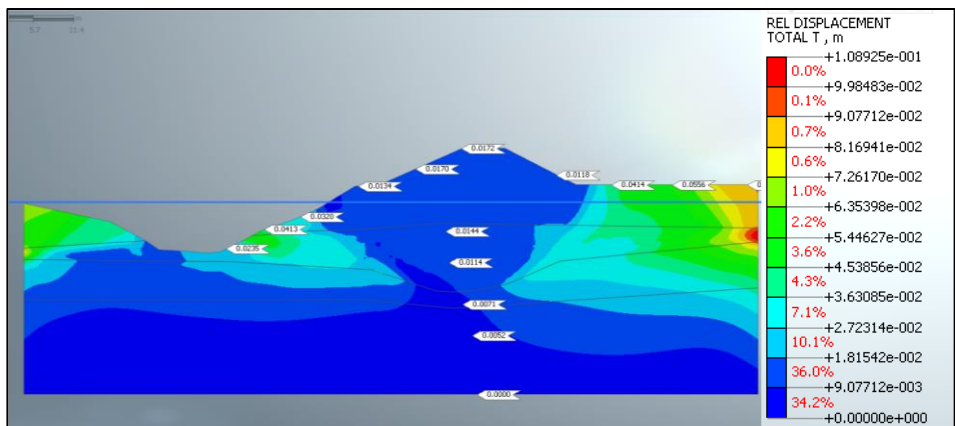


Fig 7.15 Control section 82 – case D – total vertical deformation



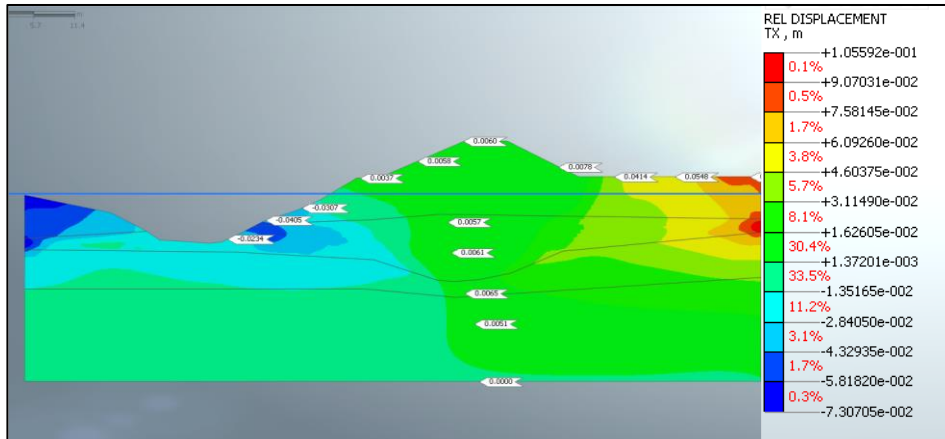


Fig 7.16 Control section 82 – case D – relative horizontal displacement

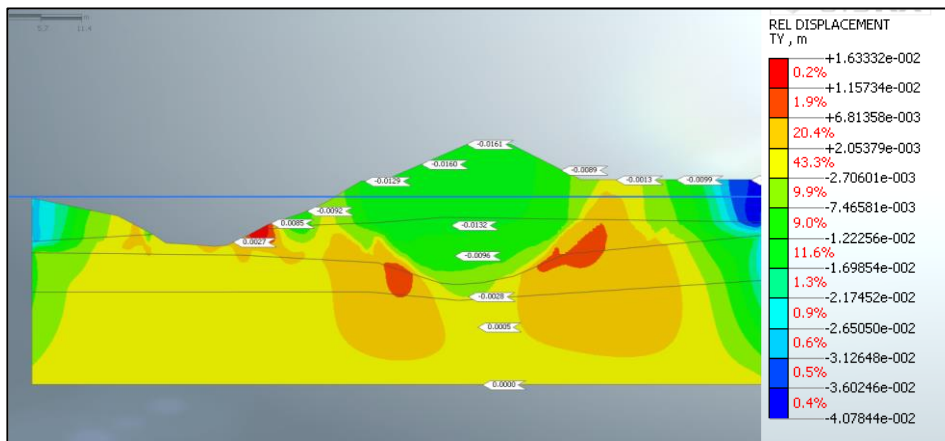
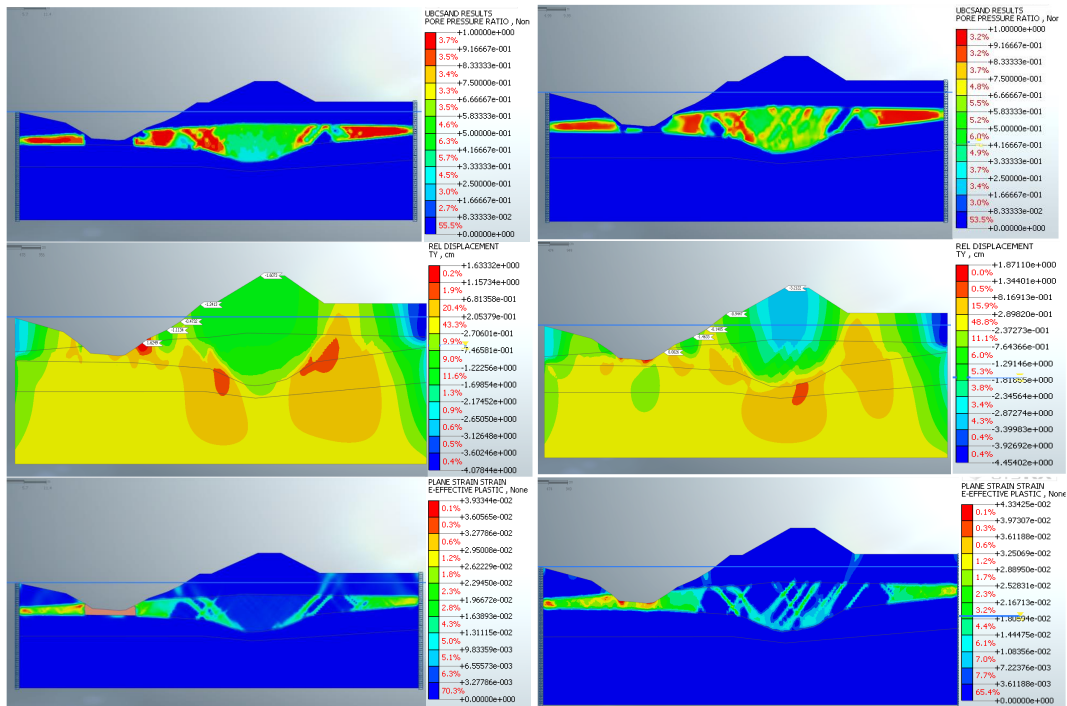


Fig 7.17 Control section 82 – case D – relative vertical displacement

The following figures show the direct comparison between the results of the analysis of the worst-case scenario with the parameters calibrated on the laboratory tests (right) and the same results obtained for the same case with the parameters calibrated on the site tests only (Fig.7.18).



**Fig 7.18 Control section 82 - scenario D: results with new parameters calibrated on laboratory tests (left); results with parameters calibrated on site tests only (right)**

## 7.5.4 Discussion

In previous analysis, four cases have been simulated concern in all cases the "state of fact" without the presence of works of defense and consolidation.

The cases investigated can be summarized here:

- Case A: use of approved geological report data. The value of  $K_0$  is equal to 0.46 and indicates the presence of geostatic forces in the normal-consolidated situation (the ratio between horizontal and vertical forces has been assumed to be 0.5). A design earthquake was applied which is an amplified earthquake of 2.3 times in the component x (horizontal) and 2.0 times in the component y (vertical).
- Case B: Use of data from the approved geological report. The value of  $K_0$  is set to 1 corresponding to an isotropic stress condition. It

applied a design earthquake that is a 2-fold amplified earthquake in the x component and 2.3-fold in the y component.

- Case C: increase in stiffness, corresponding to the elastic modulus (E) of 25%. The value of  $K_0$  is placed equal to 0.46. It was applied to the accelerogram of the real earthquake that occurred on May 29, 2012 with the epicenter of Medolla in the x and y components.
- Case D: increased stiffness corresponding to the elastic modulus (E) by 25%. The value of  $K_0$  is placed equal to 1 corresponding to an isotropic stress condition. It was applied to the accelerogram of the real earthquake that occurred on May 29, 2012 with the epicenter of Medolla in the x and y components.

For Cases A and B with regards to both Control sections, even with the design earthquake that presents amplification of the acceleration in the components x and y by a factor of 2.3 and 2 respectively, the phenomenon of liquefaction does not develop.

For Cases C and D, with variations of the order of 25-35% of some parameters and in particular of the stiffness expressed by the Young's Module (E), deformations and displacements of the detected increase, without ever reaching the collapse of significant portions of the bank itself.

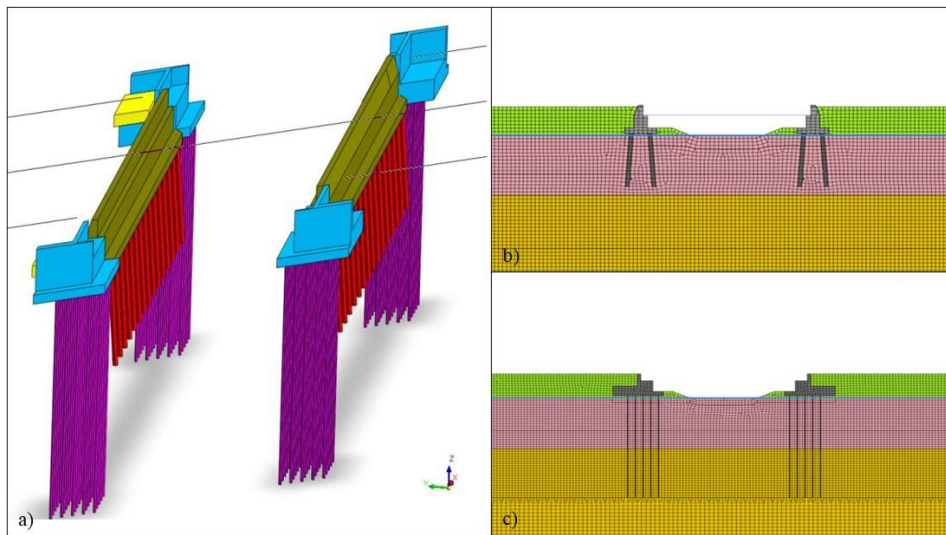
Case D results as the worst case, in which there are portions subject to liquefaction confirmed also by the presence in these areas of plastic deformations. The displacements remain below 10 cm.

It is important to mend that all the present analyses have been carried out on the embankment in the absence of consolidation works, works anyway planned to reach safety levels normally during and after floods (poles to the foot and on the low bank, cliffs to the foot and along the low bank) and that are also improving for the present analyses.

Starting from these assumptions, the most difficult scenario (Case D) made to run with the new parameters, based on the cyclic triaxial test has been simulated. The results of simulation shown less heavy subsidence and a lower value of  $R_u$  below the embankment than the previous simulation based on in-situ test. From what it infers, the previous results are more burdensome.

## 7.6 Case 2: the evaluation of the foundation system of the engineering work called Ponte Canale Ancona

The NTC'18 and the Safety Assessment Guidelines of existing bridges give particular importance to the phenomenon of liquefaction, excluding foundation checks in the absence of such a risk. It is therefore important to assess the site's susceptibility to liquefaction. The structure analyzed in this work (Fig.7.19), whose first installation dates back to the late 50s, consists of a scaffold in cao in simple support on the shoulders based on 400 diameter poles and length  $L=7.5$  m. In the 90s, following extensions for the third lane, a steel widening of the scaffold and the corresponding shoulders has been realized.



**Fig 7.19 a) Schematic representation of the structure under investigation; b) first plant calculation model; c) second plant calculation model**

Material properties were defined from the results of the geognostic tests and laboratory tests carried out. In particular, the following stratigraphic levels have been identified:

- Level 1: up to depths between 3 and 6 meters, consisting of silty sand, silt and sandy silt;
- Level 2: up to depths between 9.5 and 12.5 meters, consisting of medium coarse sand;
- Level 3: up to investigated depth, consisting of gravel sand and coarse sand.

The groundwater level was found at a depth of 4 meters from the ground floor.

With regard to levels 1 and 3, a perfect elastoplastic constitutive model has been assumed, Mohr-Coulomb. The definition of the mechanical parameters was made from the results of the SPT and CPTU tests performed on site. The mechanical parameters used are as follows:

	<b>Level 1</b>	<b>Level 3</b>
Density (kN/m <sup>3</sup> )	16	18
Poisson's coefficient	0.3	0.3
Elastic modulus (kPa)	9700	35300
$K_0$ parameter	0.53	0.49
Coesion (kPa)	4	2
Friction angle (°)	28	33.5
Dilatancy angle (°)	2	2

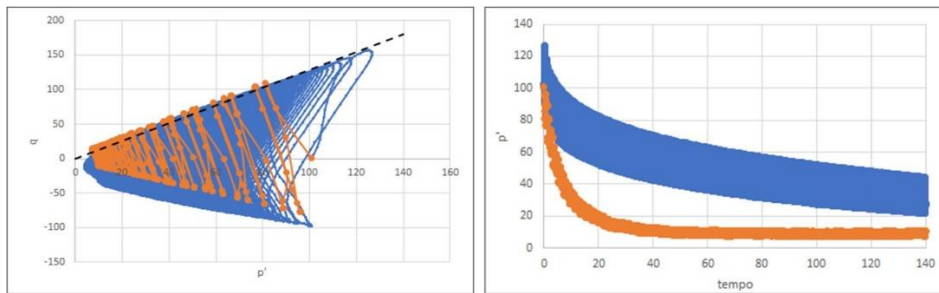
**Table 7-4 Mechanical parameters for non-liquefiable layers**

On the other hand, as regards level 2, which is considered to be susceptible to liquefaction, it was modelled with the constitutive model UBCSAND.

### **7.6.1 Calibration of the parameters of the UBC SAND constitutive model.**

In order to model the dynamic behaviour of the soil as closely as possible, cyclic laboratory tests were carried out on remoulded samples (given the nature of the soil on site). The calibration of the parameters of the UBCSAND constitutive model was carried out by researching the best-fitting between the results of the numerical simulation of the triaxial cyclic tests, and the results obtained in the laboratory. The parameters influencing the simulation, namely the relative density and stiffness of the soil, elastic and plastic, have been changed to bring the experimental curve closer to the numerical one. Due care should be taken in view of the numerous uncertainties regarding the removal of the soil core on site and the subsequent reconstruction of the test specimen in the laboratory. In particular, the numerical simulation of the laboratory tests was done in

deformation control, considering the dilatancy of the null soil. This calibration, which leads more quickly to a reduction of effective stresses, is, as already mentioned, precautionary for the purposes of calculations. Fig.7.20 shows the comparison between the experimental and numerical curves in the stress-path (deviatoric stress versus effective pressure) and effective pressure versus time.



**Fig 7.20 Calibration of the input parameters of the UBCSAND constituent model: comparison between experimental curve and numerical curve**

The parameters resulting from the calibration, for the constitutive model adopted, are shown in Fig.7.21:

Parameters	Description	Value	
$P_{ref}$	Reference pressure	100	kPa
Elastic			
$K_G^e$	Elastic shear modulus number	450	
$n_e$	Elastic shear modulus exponent	0.35	
Plastic			
$\phi_p$	Peak friction angle	28	
$\phi_{cv}$	Constant volume friction angle	28	
$c$	Cohesion	1	kPa
$K_G^p$	Plastic shear modulus number	920	
$n_p$	Plastic shear modulus exponent	0.35	
$R_f$	Failure ratio	0.74	
$F_{post}$	Post liquefaction calibration factor	0.9	
$F_{dens}$	Soil densification calibration factor	0.5	

**Fig 7.21 UBCSAND parameters derived from cyclic triaxial test chosen**

## 7.6.2 Numerical modelling

Numerical analysis has been conducted in order to assess susceptibility to liquefaction and plastic deformation of the structure.

An approach through the execution of 3D analysis was initially undertaken, but following costly computational times and several problems (localized in the most stressed finite elements) of a numerical nature, it was later abandoned in favor of simple 2D numerical analysis.

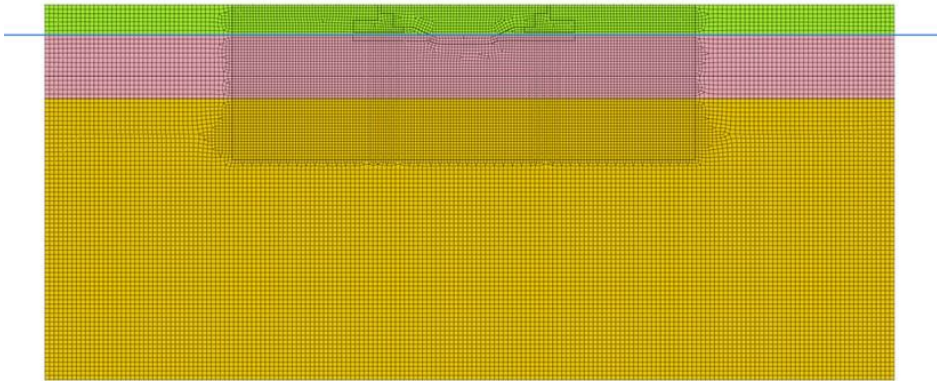
In particular, numerical stress-time history analyses were performed, in which the initial phases of geostatic stress initialization and plant construction were modelled, while in the last phase the seismic input was applied (spectrum compatible) resulting from the time history of the normalized acceleration  $g$  applied to the kinematic constraints at the basis of the calculation model. Subsequently, by a simple stress analysis, the excess of pore pressure established in the potentially liquefiable layer during the acceleration time series were initialized, in order to allow the drainage of such overpressures and thus assess the residual subsidence of the soil.

The dynamic numerical analyses were carried out using the "step" methodology, providing the calculation code with the acceleration normalized over time. The time series analysed have been derived from the Italian national database according to the spectrum-compatibility expected in the site of interest.

The type of analysis performed involves a succession between "static" (stress) and "dynamic" (Non-linear time History) calculation phases. In particular:

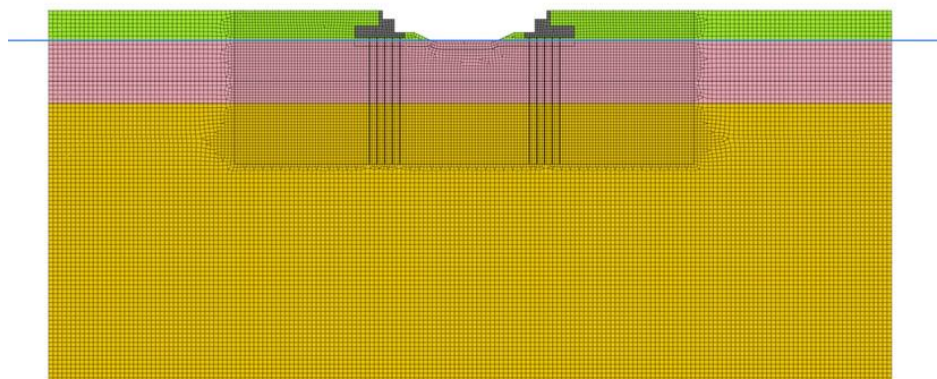
- Phase 1 (stress): initialization of geostatic stress by the  $K_0$  procedure: the original stress state of the area of interest is reproduced (Fig.7.22);





**Fig 7.22 Initialization of geostatic stress**

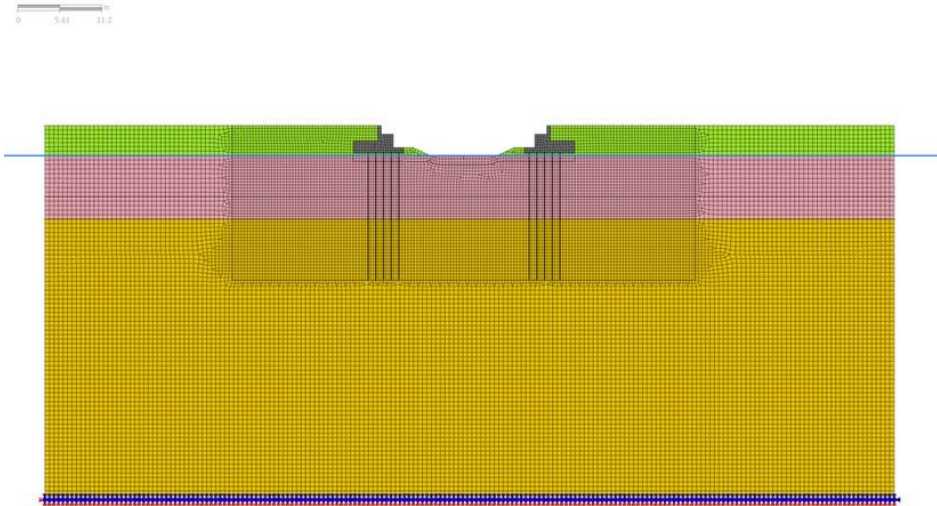
- Phase 2 (stress): construction of the plant (first plant/ expansion): the change of ownership of the mesh set that constitutes the shoulder of the bridge (and of the drilled poles in the case of the first plant) and activated the 1D elements (micropiles in the case of enlargement). At the same time, the mesh set that identifies the filling of the channel is deactivated (Fig.7.23). At the end of this phase all displacements are reset (clear displacement).



**Fig 7.23 System installation in the model**

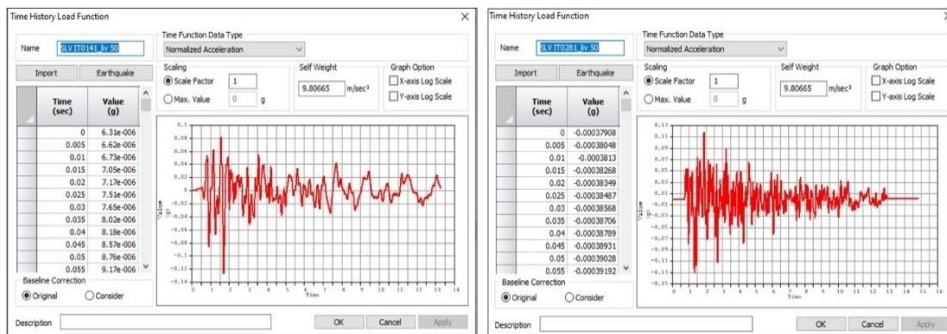


- Phase 3 (Nonlinear time history): Dynamic input: The computational accelerogram is applied to the kinematic constraint of the nodes at the base of the computational domain (Fig.7.24).

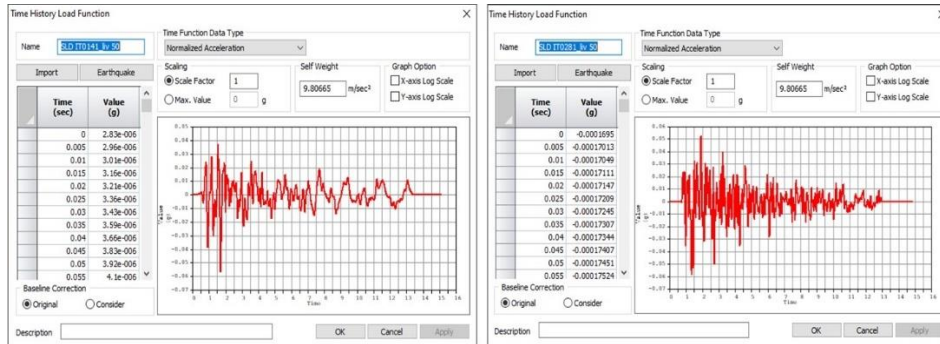


**Fig 7.24 Dynamic input applied at the base of the computational domain**

According to the standard, 7 accelerograms for SLV analysis and 3 accelerograms for SLD analysis were analysed (Fig.7.25-7.26).

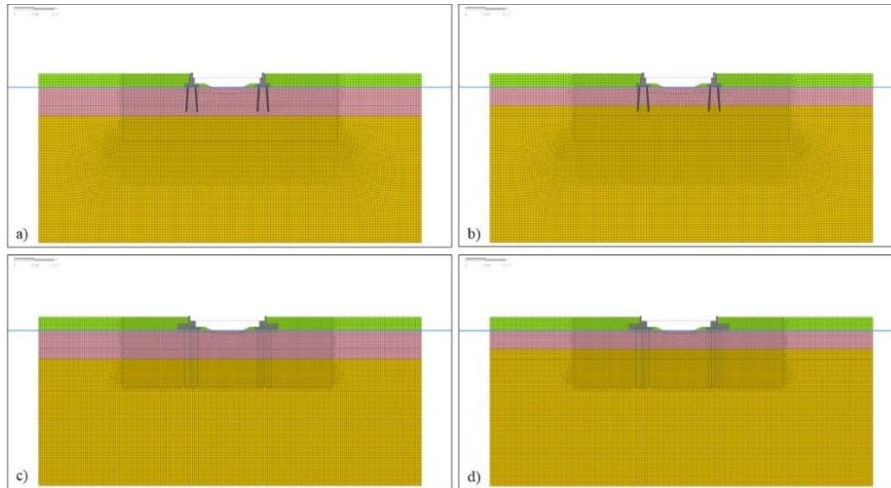


**Fig 7.25 Examples of SLD accelerograms**



**Fig 7.26 Example of SLD accelerograms**

The shoulders of the first and second system were analyzed with two different calculation models at the same stratigraphy. They, together with the ground, have been modeled by triangular and quadrangular 2D finite elements of linear order considering their real geometry. The foundation drilled poles (concerning the first plant) were also modeled using 2D finite elements, while the foundation micropiles (concerning the second plant) were modeled using beam 1D elements. In both cases, the stiffness of the structural elements has been reduced in order to take into account their geometric arrangement in plan (spacing). Due to the on-site stratigraphic uncertainty, two distinct models were analyzed (Fig.7.27): in model a) the potential liquefying layer depth reaches 12.5 meters, therefore the first drill poles are completely "floating" inside them; in model b) the depth of the potentially liquefiable layer reaches 9.5 meters, therefore the drilled poles of first planting are fixtures in the deepest layer consisting of coarse sand.

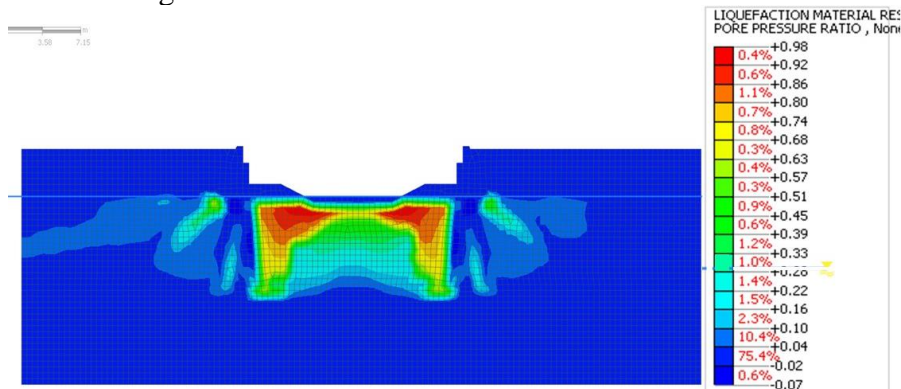


**Fig 7.27 Stratigraphic model: a) and c) model of liquefiable layer with floating piles; b) and d) model of liquefiable layer with poles fixed in the lower layer**

### 7.6.3 Results

At the time of earthquake, the assessment of subsidence in the state of damage (SLD) for three accelerogram has been conducted on original and new structure taking into account both model (a) (depth of the potentially liquefiable layer reaching 12.5 meters) and model (b) (depth of the potentially liquefiable layer reaching 9.5 meters). Results are presented in the following figures:

➤ Original structure



**Fig 7.28 Original structure: model (a) SLD: pore pressure ratio (ratio of neutral overpressures to effective pressures)**

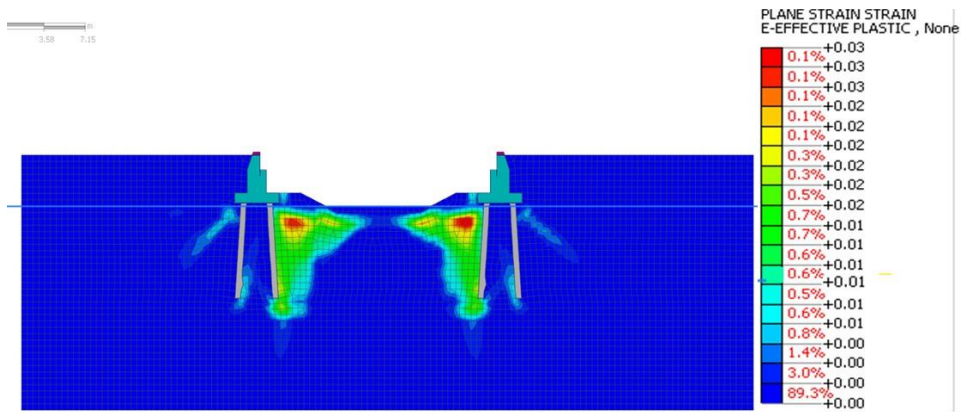


Fig 7.29 Original structure: model (a) SLD: plastic deformations

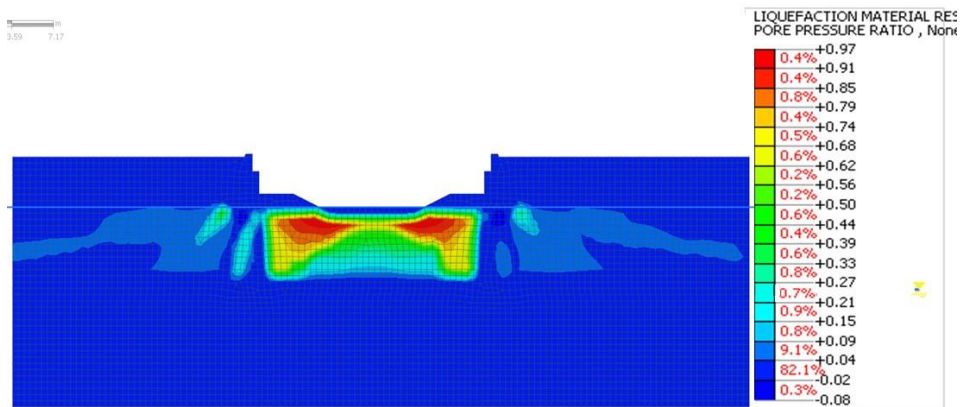


Fig 7.30 Original structure: model (b) SLD: pore pressure ratio (ratio of neutral overpressures to effective pressures)

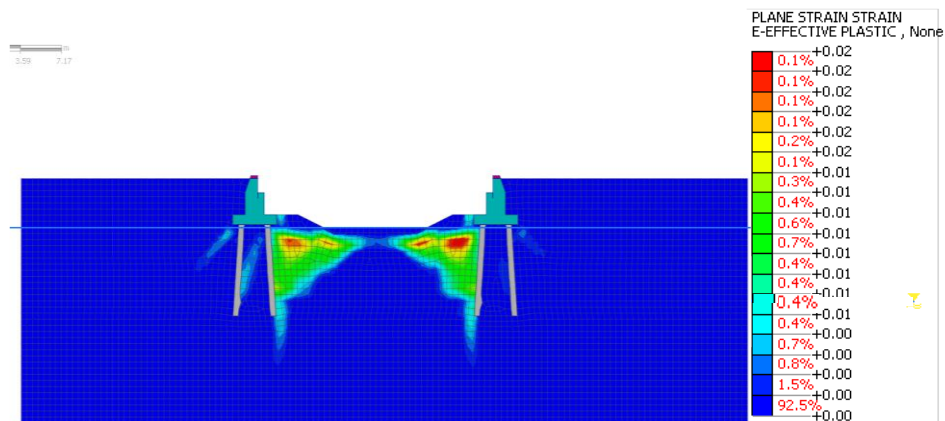


Fig 7.31 Original structure: model (b) SLD: plastic deformations



➤ New structure

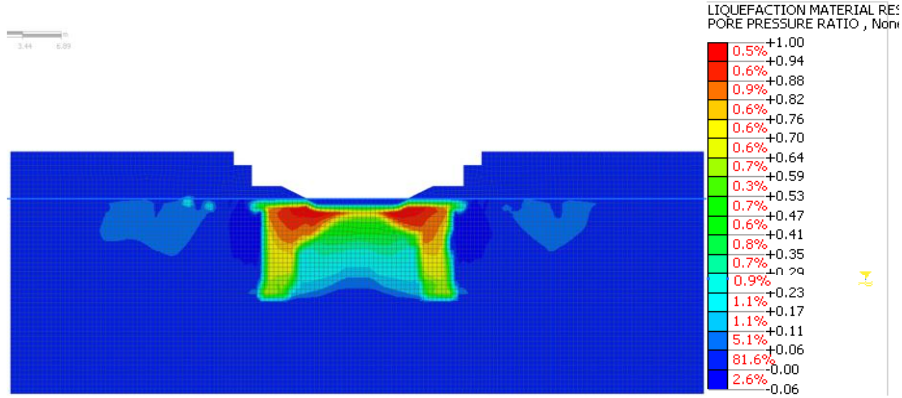


Fig 7.32 New structure: model (a) SLD: pore pressure ratio (ratio of neutral overpressures to effective pressures)

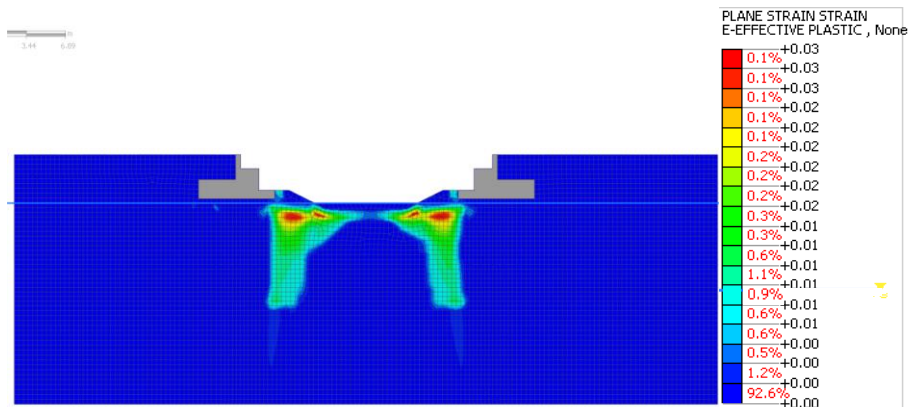


Fig 7.33 New structure: model (a) SLD: plastic deformations

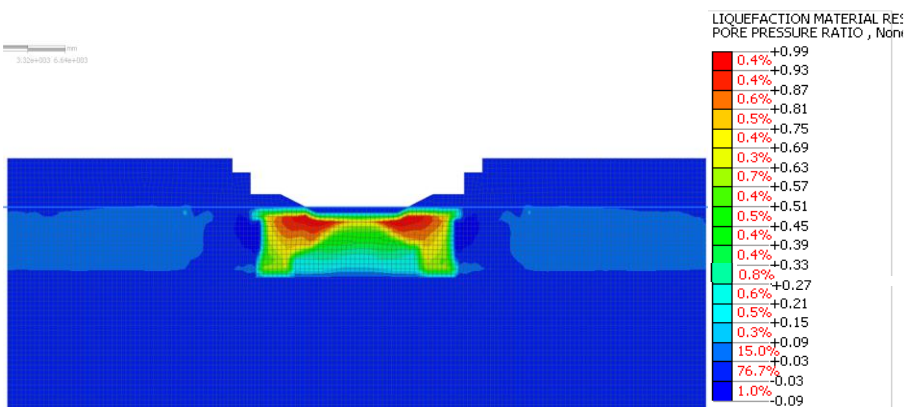
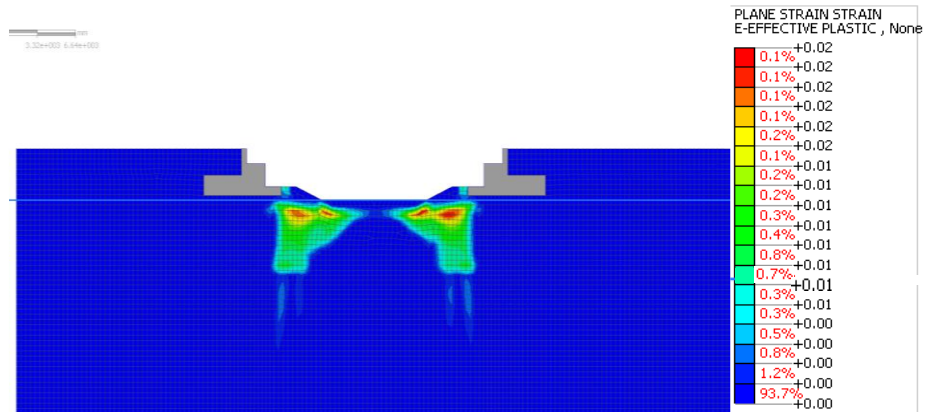
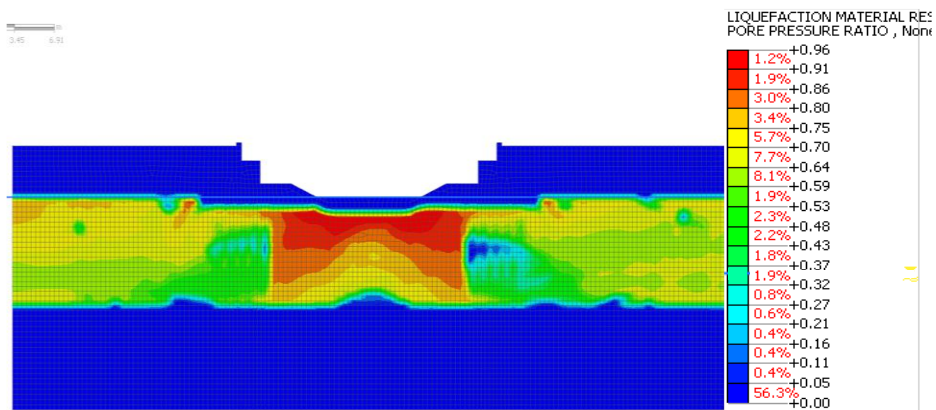


Fig 7.34 model (b) SLD: pore pressure ratio (ratio of neutral overpressures to effective pressures)



**Fig 7.35 New structure model (b) SLD: plastic deformations**

Also, the verification of actions in micropiles for the new structure, the Lifetime Limit State (SLV) was analysed for the considered accelerograms. Results are presented in the following figures.



**Fig 7.36 New structure model a) SLV pore pressure ratio (ratio of neutral overpressures to effective pressures)**

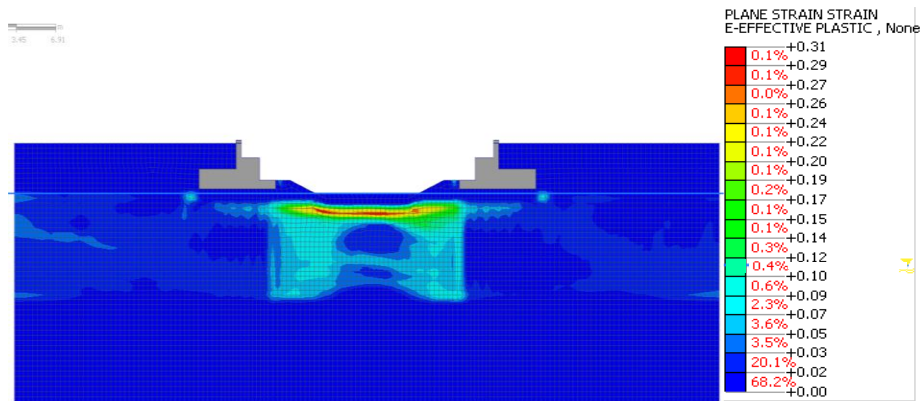


Fig 7.37 New structure model a) SLV: plastic deformation

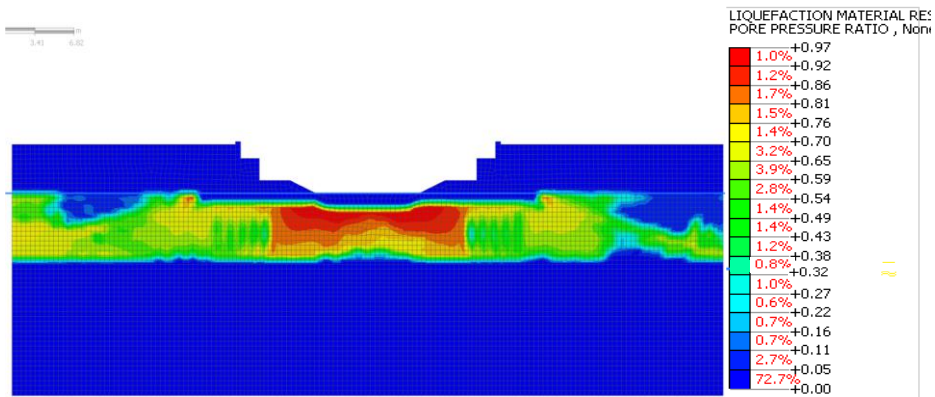


Fig 7.38 New structure model b) SLV pore pressure ratio (ratio of neutral overpressures to effective pressures)

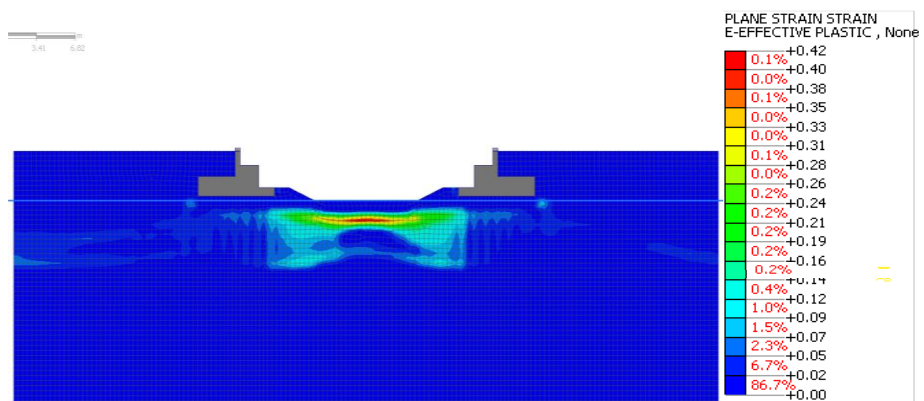


Fig 7.39 New structure model b) SLV: plastic deformation

The evaluation of residual "post-earthquake" subsidence was carried out by taking into consideration the worst results obtained in the SLO analysis. Results are shown in the following figures:

➤ Original structure

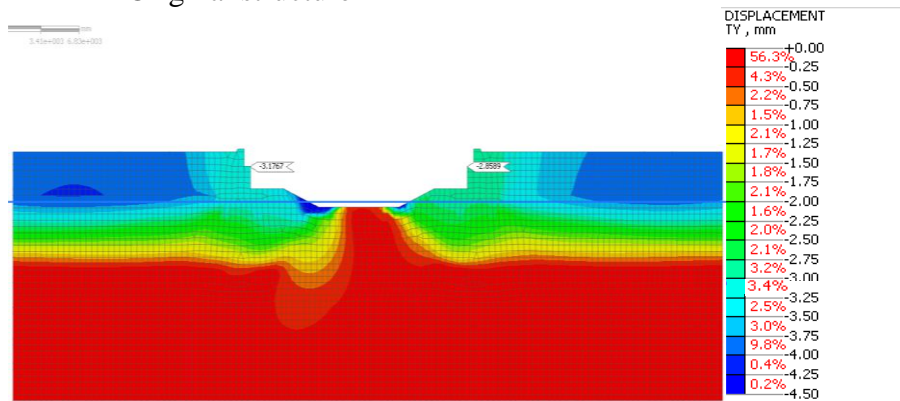


Fig 7.40 Original structure: model a) subsidence post-earthquake

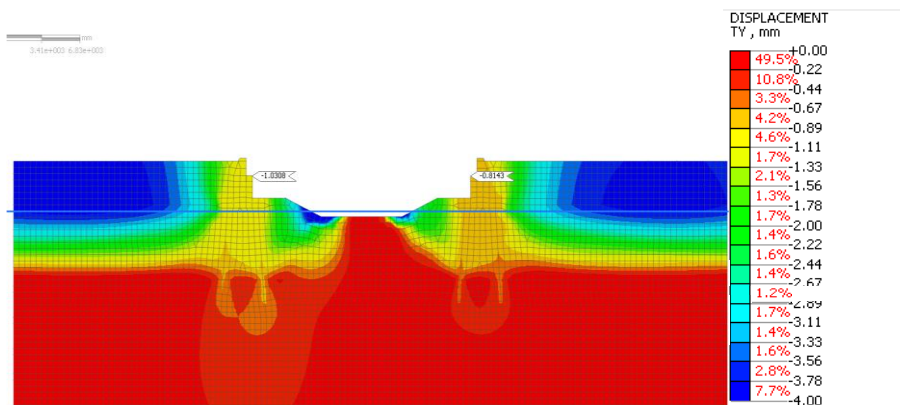


Fig 7.41 Original structure: model b) subsidence post-earthquake

The time history of the settlement of the two points marked with probes in the Fig.7.41 are reported in Fig.7.42. It's possible to see that the prediction of the settlement is of 10 mm.



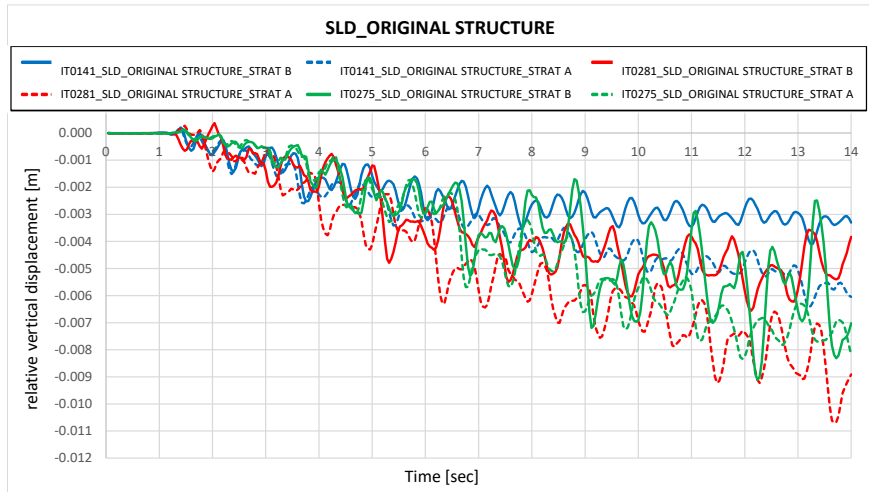


Fig 7.42 shows the trends in the settlement of the support nodes on the abutments of the bridge during the accelerogram. As regards the first system, it is possible to observe that the vertical settlements are within 10 mm.

➤ New structure

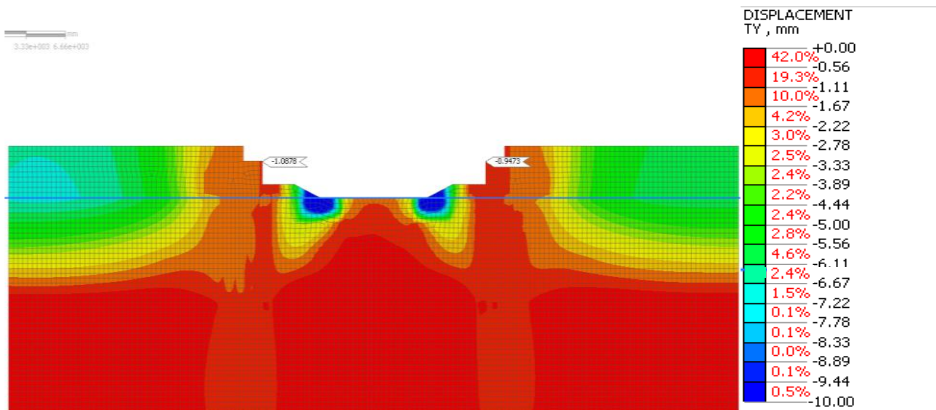
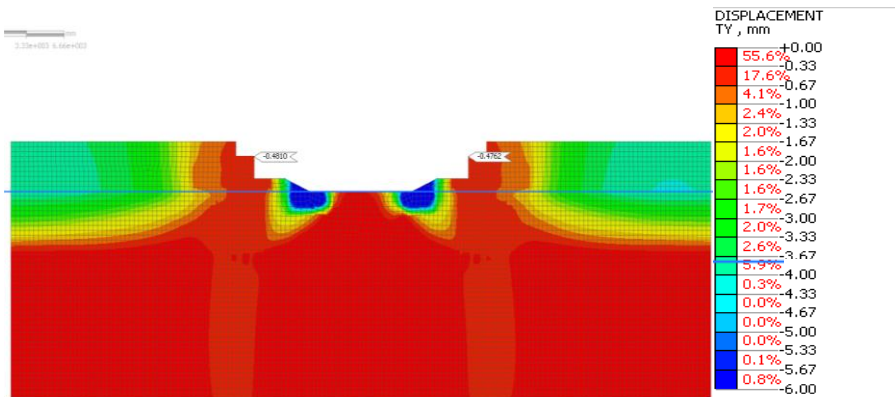
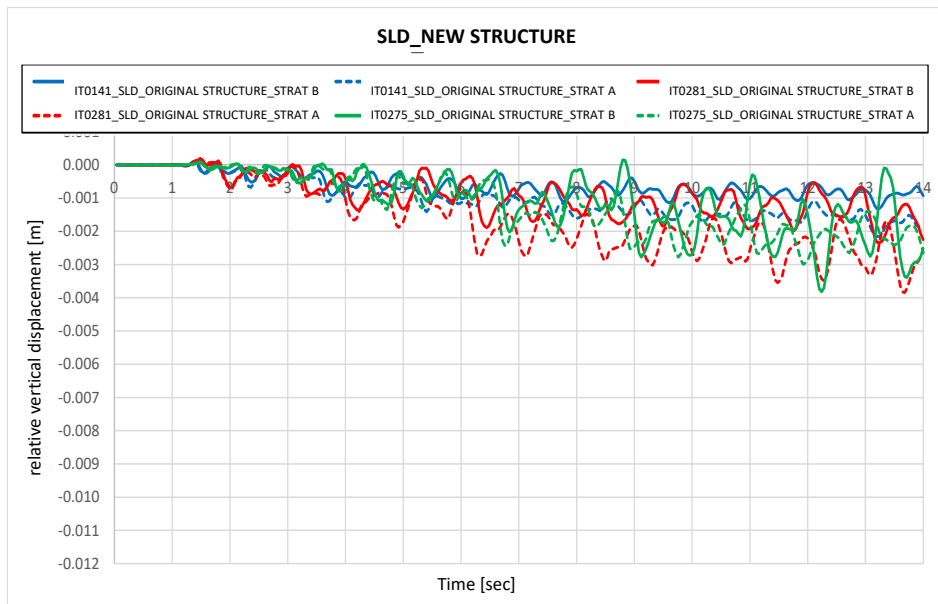


Fig 7.43 New structure model a) subsidence post-earthquake



**Fig 7.44 New structure model b) subsidence post-earthquake**

The time history of the settlement of the two points marked with probes in the Fig.7.44 are reported in Fig. 7.45. It's possible to see that the prediction of the settlement is of 4 mm.



**Fig 7.45 the trends in the settlement of the support nodes on the abutments of the bridge during the accelerogram. As regards the expansion, it is possible to observe that the vertical settlements are within 4 mm.**

#### 7.6.4 Discussion

The evaluation of foundational system of the structure called Ponte Canale Ancona has been conducted in accordance with NTC18 requirements. Since the structure is located in an area susceptible to liquefaction, so it is important to assess the earthquake-induced effects in terms of subsidence and foundation resisting capacity.

The study has been refined by 2D dynamic models of the work-ground complex to better investigate the site hazard. Mohr-Coulomb and UBCSAND constitutive model has been selected to calibrate the model respectively for non-liquefiable layers and liquefiable layer.

Dynamic analysis and post-earthquake analysis have been conducted, considering NTC18 requires assessment for SLD (Damage limit state) and SLV (Lifetime limit state) respectively for foundation and micropiles of the new structure.

From results of analysis, nullification of the effective pressure in the soil (pore pressure ratio tending to unity) tends to occur superficially for a limited thickness in the central part of the channel. In particular, liquefaction seems to localize mainly at the foot of the bridge abutments, near the top of the foundation piles. The plastic deformations associated with the dynamic action tend to arrange themselves with a wedge-shaped geometry reminiscent of the formation of a passive rupture mechanism toward the center of the channel. Two-dimensional modelling, with 1D elements (piles) modelled as continuous in the out-of-plane direction (despite scaling their stiffness to take into account their spacing), probably tends to amplify the formation of such plasticity distribution. In the present case, the stresses induced by the seismic action are not such as to trigger a failure mechanism. Evaluations post-earthquake reveal minor subsidence for both structures.

Design of this analysis has considered piles as continuous element in the model and this could affect the results. It means that due to the geometry of the model, it's not possible to understand if liquefaction will propagate among the piles. In this design piles are structured as sheet piling, resulting in no critical condition if liquefaction occurs.

For this case study the design, based on these results, will consist in insertion of new metallic diafram wall ("palancolata") to avoid that liquefaction move behind the foundation.

## Chapter 8

# 8 On-going developments for soil testing in static and dynamic conditions

### 8.1 Introduction

On the base of the experience in laboratory testing done for the two case studies, some improvements for soil testing both in static and dynamic conditions are carried out in collaboration with Matest company.

Matest is the world leading manufacturer of material testing equipment for the construction industry. Thanks to its strong capital, the company is a forerunner in technological innovation and in continuous expansion.

With an increasingly wide and comprehensive range of products, Matest offers advanced solutions for on-site and laboratory tests on concrete, cement, mortar, bitumen, asphalt, soil, aggregates, rocks, and steel, representing the ideal partner for anyone working in building and civil engineering industries.

Since taking our first steps into the world of concrete testing right up to the most recent and complex solutions for dynamic pavement testing, Matest continues to invest strongly into the research and development of highly-advanced technology for a sector in continuous evolution.

Matest's strength lies in a thorough control of the whole manufacturing process, from design to installation, according to strict quality criteria.

Due to great interesting in research and development of new products and technologies, this PhD project proved to be particularly successful for company.

In the role of product manager, I focused mainly on improvement of existing triaxial system and development of new technologies to complete the product range involved in triaxial tests, from static to cyclic ones.

## 8.2 Automatic static triaxial equipment

The automatic static triaxial equipment Matest made has been developed in these three years from software point of view, most of all.

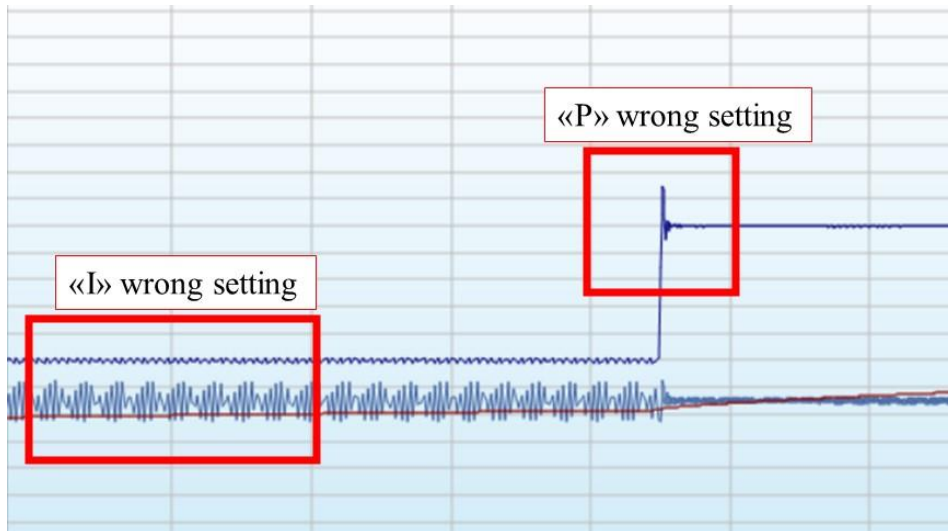
The TriaxLab (Fig.8.1) system is specially designed to minimize manual operator intervention and automatically perform static triaxial tests that generally take a long time. The system is fully electromechanical and it's controlled and managed through software, based on the feedback of control unit at which all the sensors are connected. Pressure and volume applied to the sample (cell and back pressure up to 3500 kPa) are generated by Pressurematic (PVC), which are automatic electromechanical devices for applying and regulating water pressures and volume via stepper motors, controlled directly by the software.



**Fig 8.1 TRIAXLAB equipment installed at Bicocca university for research and development of the system**

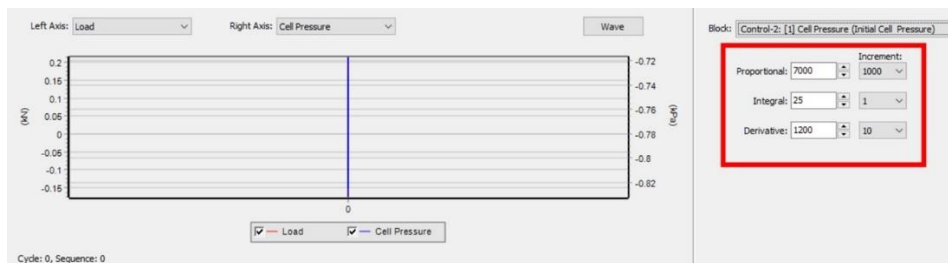
The hardware elements are controlled and monitored under a closed-loop integrated system with the CDAS (control unit) and TestLab Software. It means that PID (Proportional-Integral-Derivative) parameters manage the machine control. A PID controller continuously calculates an error value as the difference between a desired setpoint and a measured process variable and applies a correction based on proportional, integral, and derivative terms.

Due to the logic of the machine, accurate PID setting is very important in order to apply load to the sample without disturbing it but maintaining the target imposed. It could happen that wrong PID setting will produce peak in imposing target as in Fig.8.2. In general, P value will be set since it is inversely proportional to the stiffness of the sample (P increases as stiffness reduces).



**Fig 8.2 PID wrong setting explained in figure: P and I wrong setting**

A good feature of the software is to change PID in real time (Fig.8.3), allowing to reach the correct signal of sensor.



**Fig 8.3 PID window in Testlab software**

With this regard, it has been a goal to find the right PID in order to accommodate different type soil without User changes on machine answer in terms of feedback.

Triaxlab manages test through software Testlab. This software is structure is pre-programmed “Method files” to run the test according to the standard. Method files are totally customizable by the customer who has a full access to real-time data and graph. Method files are referred to a single test phase, so for a simple static triaxial test at least three of them are considered to be used (Saturation, Consolidation, Shear). Even if used for different purpose, Method file present the same design, but differ in

loading structure and managing of the control axes, along with all the calculation needed to perform automatically a test according to a standard. A full debug of the system has been conducted in this period for the automatic static triaxial equipment, improving the machine response in terms of calculations to allow the customer to obtain a report reducing manual elaboration and in terms of axis control (how the machine approaches to imposed target during the test, for load and for pressure, since in both cases we have electromechanical step-motor control).

Starting from a basic automatic system, on-sample transducer to measure radial deformation of the sample has been developed. On sample transducers are very useful in a triaxial system to measure the deformation with high accuracy, directly on specimen. Generally, an external displacement transducer is used, but this could affect measurement because stiffness of the load frame is not considered, for example. To measure radial deformation an accurate LVDT is used, connected to a chain encompassing the specimen along its circumference (Fig.8.4).



**Fig 8.4 On sample radial transducer, prototype developed in 2021**

Prototype shown in Fig.8.4 has been developed in 2021, but it resulted very heavy, expensive and presented difficult to assemble. In a second moment, the chain has been improved, trying to make it lighter, it means to reduce as possible the disturbing effect on the sample during the application. A series of materials has been analysed considering different parameter:

- Deformation (using a rigid sample)
- Water absorption
- Weight

- Practice application
- Price

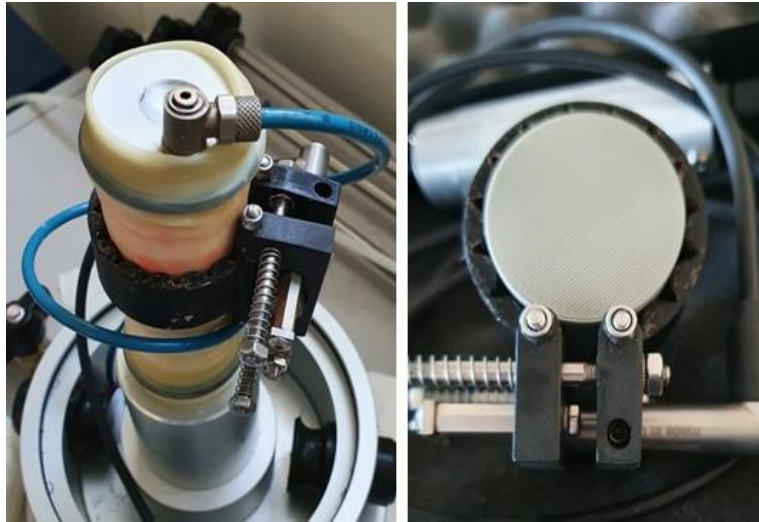
A 3D printer has been used to model the chain, with different material in order to test it directly on the sample and find the best one (Fig.8.5).



**Fig 8.5 Development of new on sample support: a) Radial chain made of different material; b) Rigid sample used to test different chain along with support for transducer; c) 3D printer used to prepare the chain and support**

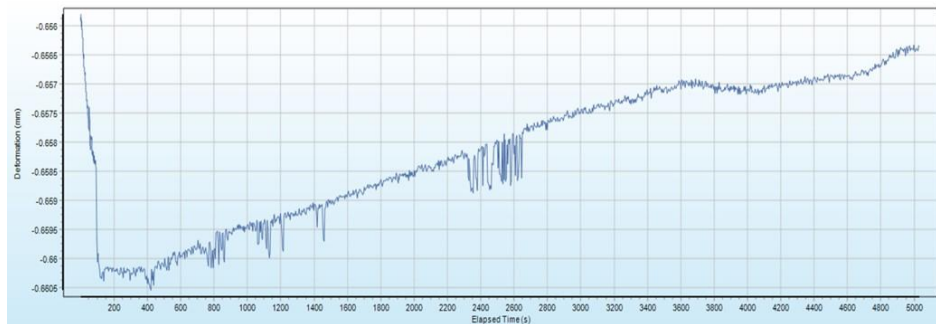
A test campaign was conducted on different chain to find the best model in order to solve previous problem. The final model is shown in Fig.8.6 which is light in weight, economic, easy to produce and elastic enough to make assembly simple.





**Fig 8.6 On-sample transducer with the latest model chain made of TPU85**

A new method file has been developed in order to include this new function. The test allows to maintain constant the area of the sample, which tends to change in consolidation phase when consolidation effective stress is applied to the sample: axial load is adjusted automatically by machine due to on-sample transducer feedback, the test will finish when the LVDT transducer reaches its initial value, it means no deformation on the sample diameter (Fig.8.7).

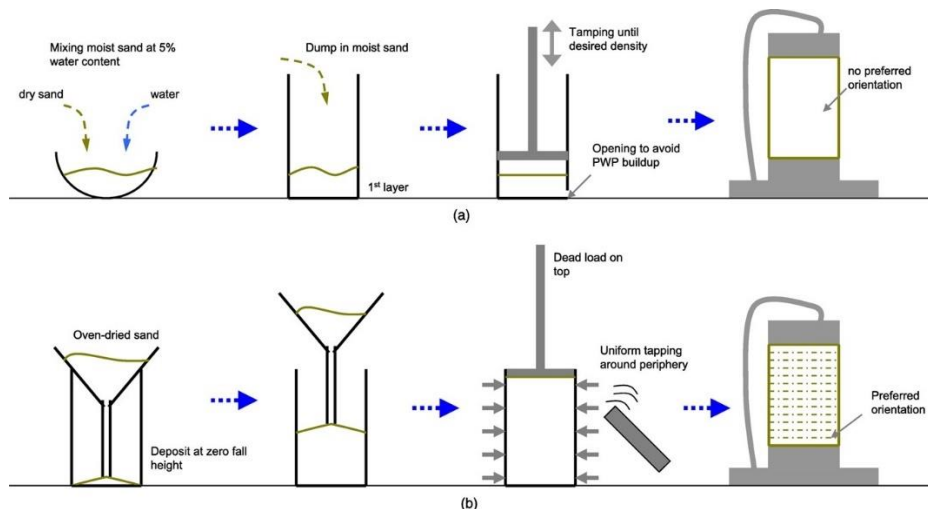


**Fig 8.7 Example of test performed with on sample transducer: test stops when sample recover the original diameter value**

### 8.3 Sample preparation and equipment requirements for cyclic tests

Sample preparation and machine calibrations are considered as pivotal requirements to perform cyclic triaxial test properly.

The techniques to reconstitute the sample have also made some controversy. Most of the studies have used two techniques to reproduce the samples including wet tamping and dry deposition (Fig.8.8). The wet tamping method is the most usually used method in triaxial testing, but the homogeneity in the sample produced by this method and its effect on the liquefaction of dense soil is not clear. Unlike the loose samples, the dense samples at the saturated state could be liquefied after a large number of cycles, and the heterogeneity of the soil in each sample can cause a big difference in the number of cycles causing liquefaction between tests although they have the same initial global void ratio (Khai 2020), even if sample with a high void ratio, generally, tends to liquefy faster.



**Fig 8.8 Schematic illustration of (a) Wet tamping and (b) Dry deposition methods for sample preparation (Sze 2014)**

Another difficulty is the method to make the sample with a high saturation degree. Arab et al. (2016) used CO<sub>2</sub> and de-aired water to circulate the sample until reaching the required saturation degree. The saturation phase results as fundamental to obtain representative results, it means to obtain Skempton' parameter B value >0.95 to reach the liquefaction faster.

Another important requirement is linked with machine setting before start the test. Cyclic triaxial apparatus is equipped with internal load cell that needs to be properly calibrated before and after connecting the piston and the top cap through the suction cup. This operation is essential to obtain representative results, mainly because ASTM standard considers test load-controlled and it reflects the importance of no overloading of the sample before start the test in machine setting, otherwise, the deviator stress shown by the software during the test is not the real value. The phases to follow for a right machine calibration can be listed as follow:

- Zeroed the load cell before mounting the triaxial cell
- Place the load cell on the suction cup above the top cap without loading
- Apply the vacuum to connect the piston and the top cap
- Load cell will read value different from zero, generally because the vacuum will stretch the sample (it's important to place the load cell as close as possible to the suction cup, it means reduce the space that potentially might stretch the sample); move the vertical axis manually or through software to return the load cell value to zero
- In addition, it is suggested to check the pore pressure transducer calibration by checking the zero value; also, in this case it could be needed to zeroed it.

Another parameter in cyclic triaxial test setting is the frequency, considered in a range from 0.1 to 2 Hz according to the standard ASTM D5311. This parameter is generally linked with the machine performance. In literature, value from 0.1 to 1Hz are suggested.

In order to evidence the importance of requirements explained in this paragraph, two tests performed on standard Hostun sand are shown in Fig.8.9. In detail, tests were performed with sample of 50mm diameter and 70mm diameter, to investigate the importance also in the choice of sample dimension (size) results to obtain a representative behaviour of the soil as close as possible.

- On the left: Dry deposition method to prepare sample of 50 mm diameter with initial void ratio 0.74.  
Skempton value= 0.92  
Deviator stress with amplitude of 50 kPa corresponding to CSR = 0.25

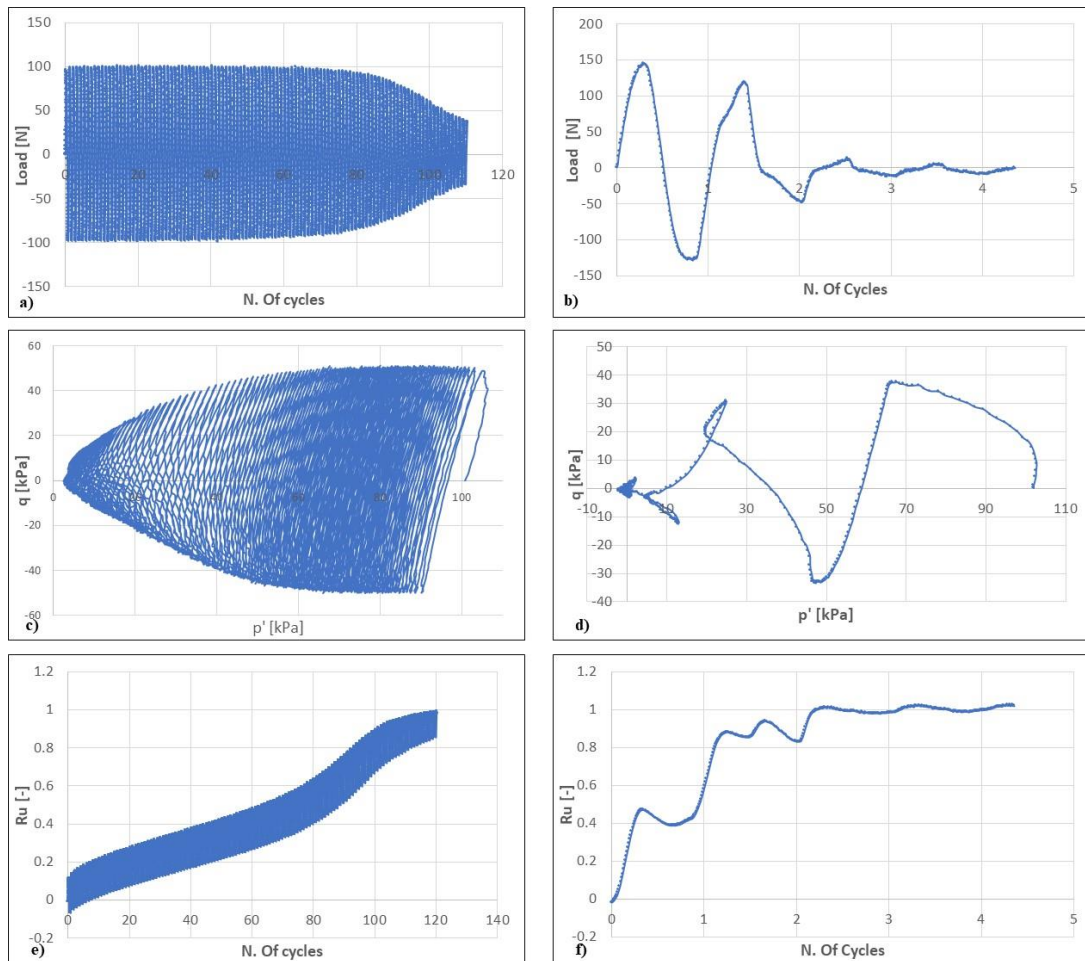
Stress frequency: 0.5 Hz

- On the right: Wet tamping method to prepare sample of 70 mm diameter with initial void ratio 0.83.

Skempton value= 0.97

Deviator stress with amplitude of 40 kPa corresponding to CSR = 0.2

Stress frequency: 0.1 Hz



**Fig 8.9** Load versus number of cycles; a) dry deposition, b) wet tamping; Stress pat: c) dry deposition, d) wet tamping; ru versus number of cycles: e) dry deposition f) wet tamping

Tests shown in the Fig.8.9 confirm mainly that sample prepared with wet tamping method, high void ratio and high saturation Skempton value reaches liquefaction in few cycles, considering an apparatus properly calibrated, as suggested.

#### 8.4 Cyclic automatic triaxial equipment

The Cyclic Triaxlab (Fig.8.10) automatic system is an update of the static model; as in the previous equipment, this machine is controlled and managed through software, based on the feedback of control unit at which all the sensors are connected. Pressure and volume applied to the sample (cell and back pressure up to 3500 kPa) are generated by Pressurematic (PVC), but in this case the system is not fully electromechanical, since the actuator is pneumatic.



Fig 8.10 Cyclic triaxlab automated system setup

Machine is able to perform cyclic triaxial test in accordance with ASTM D5311 for liquefaction assessment and ASTM D3999 for Damping and Elastic modulus evaluation.

To allow extension during cyclic loading, the top cap needs to be connected to the vertical axis loading. A suction cup system has been designed in order to avoid any disconnection of the sample during the test, it is shown in image below: the central hole and the shape of the upper part at which the suction cup is connected, allow to maintain the natural shape of the cup and this is very helpful as results from our tests (Fig.8.11).

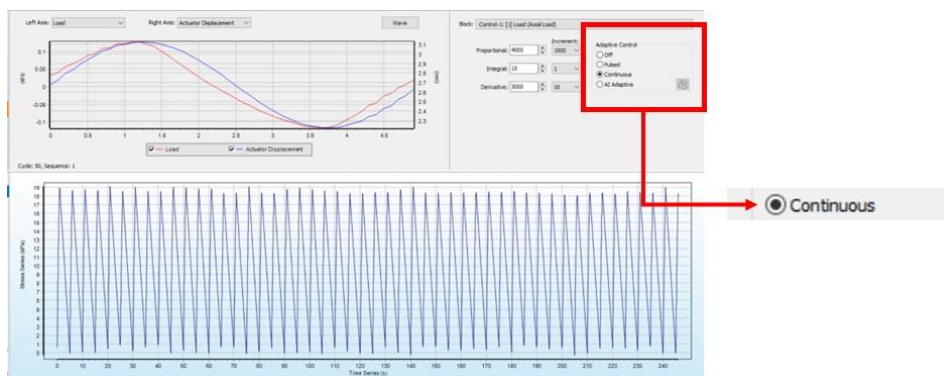


**Fig 8.11 Vacuum system with suction cup to allow extension of the sample during the test**

Another important aspect under investigation was the cell pressure behaviour during the cyclic loading. As known, due to the nature of the test, a quick response by pressure system is mandatory to keep it constant as only the load (or deformation) has a sinusoidal tendency. To make this more efficient, a pipe with bigger internal diameter has been installed in cell pressure line, in order to accommodate volume fluctuation during cyclic loading easier. PVC, in addition, controls not only the pressure but also the volume, so it is another advantage to understand the system response during the test and if needed change the PID parameters. In other word, it's possible to check the volume of water that goes inside and outside the triaxial cell and this allows to make some consideration on the quality of the test and also on the sample (if properly saturated).

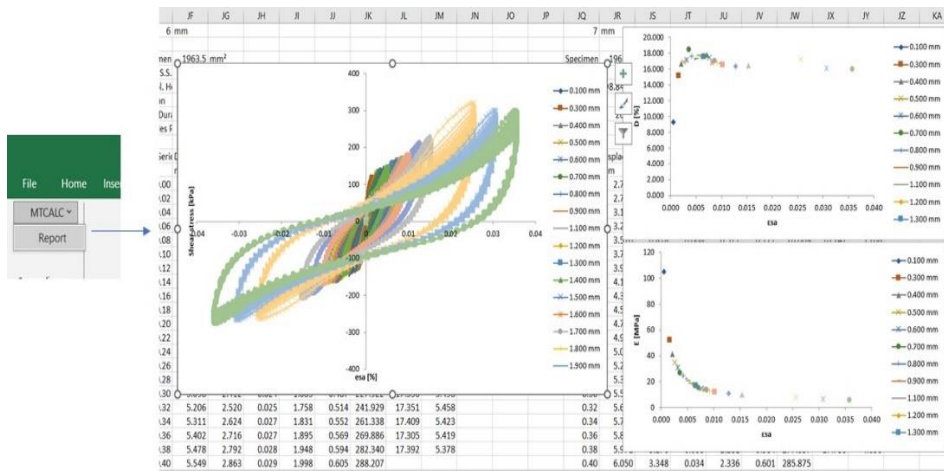


Test is managed by software Testlab, which perform each phase automatically; saturation and consolidation work with the same Method File implemented for static model, and the parametrization is the same. For the cyclic phase, new Method files have been implemented: for each standard, it's possible to manage the test in load-control and displacement-control. PID parametrization in this test is very important to keep the imposed cyclic input. Generally, in load-controlled test for liquefaction assessment (compliant with ASTM D5311), as the liquefaction begins, machine is not able to keep the imposed load at the beginning. If PID control could change during the test, it would be possible to “reach” target condition and record results in terms of deformation. A new function to satisfy this requirement has been introduced, the “Continuous” (Fig.8.12).



**Fig 8.12 Continuous function to adjust PID parameters in order to maintain the target constant during the cyclic loading**

Software, as previously explained, perform the cyclic loading phase automatically, with all the needed calculations. At the end of the test, it's possible to export the results in excel format (the report is customizable). There was no post-processing elaboration of multiple tests, needed in case of Damping and Elastic modulus evaluation. An Excel add-in has been developed that allows easy processing of Hysteresis cycle graph for each strain or stress level, and the main curve of Damping and Elastic modulus: collecting in a single folder all the single tests and importing this folder in Excel through the add-in (Fig.8.13) all the elaborations will be done automatically.



**Fig 8.13 Post processing for dynamic triaxial test – Construction of the main curve through Excel add-in**

The procedure has been approved and it's available for the customers.

## 8.5 Discussion

This Phd project has represented a good opportunity to collect more knowledge about dynamic equipment for soil testing, most of all for the triaxial. The possibility to work with different technologies has allowed to improve existing system in terms of hardware and software and to develop new products. Having gained greater awareness in triaxial, static and dynamic, testing procedures has enabled a focus on details that allow for refinement of equipment in order to supply a product to market that is complete and functional from the customer's perspective.

Due to this project, different aspects of testing procedure and testing equipment emerged, so in future, we expect new development in dynamic field, such as the replacing of the pneumatic actuator of cyclic triaxial equipment to become fully electromechanical system, it means no compressor needed and more accurate data.



## Conclusion

The main objective of the present work has been to develop an approach for liquefaction assessment of soil subjected to cyclic load, combining simplified and advanced experimental test along with numerical models. With this in mind, this project has improved the knowledge base for laboratory equipment in dynamic testing, enriching the company's know-how in terms of machine implementation and improvement of existing machines.

Liquefaction is a complex phenomenon which could lead to several damages in building and infrastructure. Starting from this assumption, two real cases of study have been analyzed, following the same procedure which involve in itself different techniques and technologies. Even if geotechnical structures under investigation are different (in detail, embankments and foundation), this work has confirmed the importance of deeper studies of liquefiable site, starting from simplified analysis based on in-situ test, then advanced analysis based on laboratory test and finally numerical simulation for prediction of the phenomenon.

For each case of study, the work has been divided in three main parts: Simplified procedure, Advanced procedure, Theoretical and numerical analysis.

The results obtained in each part are detailed in the following:

- *Simplified procedure*: this procedure, developed by Seed and Idriss in 1971, based on in situ tests, is generally consider the starting point in liquefaction susceptibility analysis, for the possibility to evaluate the site's Factor of Safety, defined by the ratio of the resistance available to liquefaction (CRR) and the stress induced by the design earthquake (CSR). SPT along with CPTu tests, present some advantages and disadvantages for different reason, but they are most widely used. In detail, CPT almost always provides better results than SPT because of better accuracy also for continuous profiling, data reliability, cost-effectiveness, and the details in the soil profile it returns. The definition of Factor of Safety helps in following analysis focusing attention in critical layers, in which results are less than unit.

- *Advanced procedure*: the material collected in site investigation campaign, properly analyzed according to NTC18 (Technical standard for construction) requirements, is tested in laboratory not only for evaluation of liquefaction susceptibility previously confirmed by on site analysis, but also to obtain representative curves, to be used for further analysis in numerical modelling. Cyclic triaxial test are generally the most widely used equipment for liquefaction evaluation, in stress or strain control mode (along with cyclic simple shear test). CSR, which is the seismic demand of the area, represents the ratio of deviatoric stress on effective radial stress in triaxial; calculation of CSR allows in testing sample under real seismic condition.
- *Numerical analysis*: the last part of the work provides simulation about predicted behavior of the soil under seismic condition based on real earthquake or design earthquake compliant with standard requirements (NTC18). Prediction elaborated in this work can be classified as class A because the event is not yet occurred, but they are very important for securing structures in case of liquefaction event. Numerical modelling takes on greater importance when constitutive models calibrated on actual laboratory tests are used; with this regard, UBCSAND model has been used for calibration of liquefiable layers, since this is a specific constitutive model for liquefaction analysis.

The novelty of knowledge of this work is focused on the proposal of a complete methodological approach to cope with liquefaction phenomena interacting with geotechnical structures. This work reinforces the possibility of using the combination of in-situ testing, laboratory testing, constitutive modeling and numerical analysis to make predictions, not only about susceptibility but also about the actual effects of liquefaction on structure. Through the analysis of these two cases study, it emerges that this procedure can be a real tool for choosing what to design in securing the area.

Future developments include an improvement in the laboratory testing procedure (starting with in-situ sampling) even on remanufactured materials, allowing as much standardization as possible in deciding which materials and with which parameters to test them in the laboratory under dynamic conditions. UBCSAND is currently among the best constitutive

models on the market, but a further development is to use different models and then different simulations in order to get the same results, however. 2D analyses have been shown in this work, so a further development is to provide for the use of 3D programs in order to refine the results which will be even more accurate and consequently the design choices.

From Matest point of view, further developments of the present work consist of improve existing laboratory equipment, taking into account the knowledge acquired in dynamic testing field.

## Bibliography

Andrews, D. C., & Martin, G. R. (2000, January). Criteria for liquefaction of silty soils. In Proc., 12th World Conf. on Earthquake Engineering (pp. 1-8). Upper Hutt, New Zealand: NZ Soc. for EQ Engrg.

Andrus, R. D., & Stokoe II, K. H. (2000). Liquefaction resistance of soils from shear-wave velocity. *Journal of geotechnical and geoenvironmental engineering*, 126(11), 1015-1025.

Arab, A., Belkhatir, M., & Sadek, M. (2016). Saturation effect on behaviour of sandy soil under monotonic and cyclic loading: A laboratory investigation. *Geotechnical and Geological Engineering*, 34, 347-358.

ASTM D3999 (2011) Standard Test Methods for the Determination of the Modulus and Damping Properties of Soils Using the Cyclic Triaxial Apparatus

ASTM D5311 (2011)- Standard Test Method for Load Controlled Cyclic Triaxial Strength of Soil

ASTM D8296 (2019)- Standard Test Method for Consolidated Undrained Cyclic Direct Simple Shear Test under Constant Volume with Load Control or Displacement Control

Beaty, M., & Byrne, P. M. (1998, August). An effective stress model for predicting liquefaction behaviour of sand. In *Geotechnical Earthquake Engineering and Soil Dynamics III* (pp. 766-777). ASCE.

Benahmed, N. (2001). Comportement mécanique d'un sable sous cisaillement monotone et cyclique: application aux phénomènes de liquéfaction et mobilité cyclique (Doctoral dissertation, Marne-la-vallée, ENPC).

Bishop, A. W. (1973). The stability of tips and spoil heaps. *Quarterly Journal of Engineering Geology and Hydrogeology*, 6(3-4), 335-376.

Bjerrum, L., & Landva, A. (1966). Direct simple-shear tests on a Norwegian quick clay. *Geotechnique*, 16(1), 1-20.

Boulanger, R. W., & Idriss, I. M. (2004). Evaluating the potential for liquefaction or cyclic failure of silts and clays (p. 131). Davis, California: Center for Geotechnical Modeling.

Boulanger, R. W., & Idriss, I. M. (2006). Liquefaction susceptibility criteria for silts and clays. *Journal of geotechnical and geoenvironmental engineering*, 132(11), 1413-1426.

Boulanger, R. W., & Idriss, I. M. (2016). CPT-based liquefaction triggering procedure. *Journal of Geotechnical and Geoenvironmental Engineering*, 142(2), 04015065.

Bray, J. D., & Sancio, R. B. (2006). Assessment of the liquefaction susceptibility of fine-grained soils. *Journal of geotechnical and geoenvironmental engineering*, 132(9), 1165-1177.

Byrne, P. M., Park, S. S., Beaty, M., Sharp, M., Gonzalez, L., & Abdoun, T. (2004). Numerical modeling of liquefaction and comparison with centrifuge tests. *Canadian Geotechnical Journal*, 41(2), 193-211.

Casagrande, A. (1936). Characteristics of cohesionless soils affecting the stability of slopes and earth fills. *J. Boston Society of Civil Engineers*, 23(1), 13-32.

Casagrande, A. (1965). Role of the calculated risk in earthwork and foundation engineering. *Journal of the Soil Mechanics and Foundations Division*, 91(4), 1-40.

Cetin, K. O., Seed, R. B., Der Kiureghian, A., Tokimatsu, K., Harder Jr, L. F., Kayen, R. E., & Moss, R. E. (2004). Standard penetration test-based probabilistic and deterministic assessment of seismic soil liquefaction potential. *Journal of geotechnical and geoenvironmental engineering*, 130(12), 1314-1340.

Cetin, K. O., Seed, R. B., Kayen, R. E., Moss, R. E., Bilge, H. T., Ilgac, M., & Chowdhury, K. (2018). The use of the SPT-based seismic soil

liquefaction triggering evaluation methodology in engineering hazard assessments. *MethodsX*, 5, 1556-1575.

Chang, W. J., & Hong, M. L. (2008). Effects of clay content on liquefaction characteristics of gap-graded clayey sands. *Soils and foundations*, 48(1), 101-114.

Chattaraj, R., & Sengupta, A. (2016). Liquefaction potential and strain dependent dynamic properties of Kasai River sand. *Soil Dynamics and Earthquake Engineering*, 90, 467-475.

Chen, C. J., & Juang, C. H. (2000). Calibration of SPT-and CPT-based liquefaction evaluation methods. In *Innovations and applications in geotechnical site characterization* (pp. 49-64).

Committee on Soil Dynamics of the Geotechnical Engineering Division. (1978). Definition of terms related to liquefaction. *Journal of the Geotechnical engineering division*, 104(9), 1197-1200.

CONSORZIO BONIFICA MUZZA BASSA LODIGIANA-RIPRISTINO DELLA FUNZIONALITA' E DELLA SICUREZZA DEL CANALE GENERALE DI BONIFICA ANCONA MEDIANTE RICOSTRUZIONE DELLA SICUREZZA STATICA DELLE RIVE E DELLE ALZAIE E LA DIFESA DAI FENOMENI DI EROSIONE E SCALZAMENTO AL PIEDE CON LA RICOSTRUZIONE DEL CORRETTO PROFILO DI SPONDA E POSA DI PIETRAMME TIPO REZZATO (2016)

Dang, Q. H. (2019). Comportement des sols sous liquéfaction artificielle, amélioration des sols à risques liquefiable (Doctoral dissertation, Paris Est).

Dobry, R., Ladd, R. S., Yokel, F. Y., Chung, R. M., & Powell, D. (1982). Prediction of pore water pressure buildup and liquefaction of sands during earthquakes by the cyclic strain method (Vol. 138, p. 150). Gaithersburg, MD: National Bureau of Standards.

Dobry, R., Abdoun, T., Stokoe, K. H., Moss, R. E. S., Hatton, M., & El Ganainy, H. (2015). Liquefaction potential of recent fills versus natural

sands located in high-seismicity regions using shear-wave velocity. *Journal of Geotechnical and Geoenvironmental Engineering*, 141(3), 04014112.

Dyvik, R., Berre, T., Lacasse, S., & Raadim, B. (1987). Comparison of truly undrained and constant volume direct simple shear tests. *Geotechnique*, 37(1), 3-10.

Fear, C. E., & Robertson, P. K. (1995). Estimating the undrained strength of sand: a theoretical framework. *Canadian Geotechnical Journal*, 32(5), 859-870.

Finn, W. L., Bransby, P. L., & Pickering, D. J. (1970). Effect of strain history on liquefaction of sand. *Journal of the Soil Mechanics and Foundations Division*, 96(6), 1917-1934.

Grozic, J. L., Robertson, P. K., & Morgenstern, N. R. (2000). Cyclic liquefaction of loose gassy sand. *Canadian Geotechnical Journal*, 37(4), 843-856.

Hayati, H., & Andrus, R. D. (2009). Updated liquefaction resistance correction factors for aged sands. *Journal of geotechnical and geoenvironmental engineering*, 135(11), 1683-1692.

Hatanaka, M., & Masuda, T. (2008). Experimental study on the relationship between degree of saturation and P-wave velocity in sandy soils. In *Geotechnical Engineering for Disaster Mitigation and Rehabilitation: Proceedings of the 2nd International Conference GEDMAR08, Nanjing, China 30 May–2 June, 2008* (pp. 346-351). Springer Berlin Heidelberg.

Hausler, E. A. (2002). Influence of ground improvement on settlement and liquefaction: A study based on field case history evidence and dynamic geotechnical centrifuge tests. University of California, Berkeley.

Hazirbaba, K., & Rathje, E. M. (2009). Pore pressure generation of silty sands due to induced cyclic shear strains. *Journal of geotechnical and geoenvironmental engineering*, 135(12), 1892-1905.

Heidari, T., & Andrus, R. D. (2012). Liquefaction potential assessment of Pleistocene beach sands near Charleston, South Carolina. *Journal of geotechnical and geoenvironmental engineering*, 138(10), 1196-1208.

Higo, Y., Lee, C. W., Doi, T., Kinugawa, T., Kimura, M., Kimoto, S., & Oka, F. (2015). Study of dynamic stability of unsaturated embankments with different water contents by centrifugal model tests. *Soils and Foundations*, 55(1), 112-126.

Hyodo, M., Yamamoto, Y., & Sugiyama, M. (1994). Undrained cyclic shear behaviour of normally consolidated clay subjected to initial static shear stress. *Soils and Foundations*, 34(4), 1-11.

Idriss, I. M., & Boulanger, R. W. (2003). Estimating  $K_{\alpha}$  for use in evaluating cyclic resistance of sloping ground. In 8th US–Japan Workshop on Earthquake Resistant Design of Lifeline Facilities and Countermeasures against Liquefaction, Report MCEER-03-0003, MCEER (SUNY Buffalo, NY, 2003a),(June 2003) (pp. 449-68).

Idriss, I. M., & Boulanger, R. W. (2006). Semi-empirical procedures for evaluating liquefaction potential during earthquakes. *Soil dynamics and earthquake engineering*, 26(2-4), 115-130.

Idriss, I. M., & Boulanger, R. W. (2008). Soil liquefaction during earthquakes. Earthquake Engineering Research Institute.

Ishihara, K., Troncoso, J., Kawase, Y., & Takahashi, Y. (1980). Cyclic strength characteristics of tailings materials. *Soils and Foundations*, 20(4), 127-142.

Ishihara, K. (1985). STABILITY OF NATURAL DEPOSITS DURING EARTHQUAKES. PROCEEDINGS OF THE ELEVENTH INTERNATIONAL CONFERENCE ON SOIL MECHANICS AND FOUNDATION ENGINEERING, SAN FRANCISCO, 12-16 AUGUST 1985. Publication of: Balkema (AA).

Ishihara, K. (1993). Liquefaction and flow failure during earthquakes. *Geotechnique*, 43(3), 351-451.

Ishihara, K. (1996). Soil behaviour in earthquake geotechnics.



Ishihara, K., Ueno, K., Yamada, S., Yasuda, S., & Yoneoka, T. (2015). Breach of a tailings dam in the 2011 earthquake in Japan. *Soil Dynamics and Earthquake Engineering*, 68, 3-22.

Jafarzadeh, F., & Sadeghi, H. (2012). Experimental study on dynamic properties of sand with emphasis on the degree of saturation. *Soil Dynamics and Earthquake Engineering*, 32(1), 26-41.

Jefferies, M., & Been, K. (2015). *Soil liquefaction: a critical state approach*. CRC press.

Kayen, R. E., Mitchell, J. K., Seed, R. B., Lodge, A., Nishio, S. Y., & Coutinho, R. (1992, May). Evaluation of SPT-, CPT-, and shear wave-based methods for liquefaction potential assessment using Loma Prieta data. In *Proceedings of the 4th Japan-US Workshop on Earthquake Resistant Design of Lifeline Facilities and Countermeasures for Soil Liquefaction*, Hamada, M. and O'Rourke, TD, eds.

Kayen, R., Moss, R. E. S., Thompson, E. M., Seed, R. B., Cetin, K. O., Kiureghian, A. D., ... & Tokimatsu, K. (2013). Shear-wave velocity-based probabilistic and deterministic assessment of seismic soil liquefaction potential. *Journal of Geotechnical and Geoenvironmental Engineering*, 139(3), 407-419.

Khai Hoan Tran (2020) Study of the liquefaction of geo-materials taking into account the unsaturation. *Civil Engineering*. Normandie Université, 2020. English

Kim, I. H., Yang, J. D., Lee, D. G., Chung, H. Y., & Cho, B. C. (2009). Evaluation of centrifugation technique and effect of epinephrine on fat cell viability in autologous fat injection. *Aesthetic Surgery Journal*, 29(1), 35-39.

Koppejan, A. W., Van Wamelen, B. M., & Weinberg, L. J. H. (1948). *Coastal flow slides in the Dutch province of Zeeland*.

Kramer, S.L. (1996) *Geotechnical Earthquake Engineering*. Prentice-Hall, New Jersey.

Lee, K. L., & Seed, H. B. (1967). Drained strength characteristics of sands. *Journal of the Soil Mechanics and Foundations Division*, 93(6), 117-141.

Liao, S. S., & Whitman, R. V. (1986). Overburden correction factors for SPT in sand. *Journal of geotechnical engineering*, 112(3), 373-377.

Liu, L., & Dobry, R. (1997). Seismic response of shallow foundation on liquefiable sand. *Journal of geotechnical and geoenvironmental engineering*, 123(6), 557-567.

Locati, M., R. Camassi, A. Rovida, E. Ercolani, F. Bernardini, V. Castelli, C.H. Caracciolo, A. Tertulliani, A. Rossi, R. Azzaro, S. D'Amico, S. Conte and E. Rocchetti (2016). DBMI15, the 2015 version of the Italian Macroseismic Database, Istituto Nazionale di Geofisica e Vulcanologia

Lombardi, D., Bhattacharya, S., Hyodo, M., & Kaneko, T. (2014). Undrained behaviour of two silica sands and practical implications for modelling SSI in liquefiable soils. *Soil Dynamics and Earthquake Engineering*, 66, 293-304.

López, C. L., Garzón, L. X., & Campagnoli, S. X. (2021). Geotechnical centrifuge applications in the teaching of applied soil mechanics. *Revista Educación en Ingeniería*, 16(32), 10-15.

Marcuson WF (1978) Definition of terms related to liquefaction. *J Geotech Eng Div ASCE* 104(9):1197–1200.

Matasovic, N., & Vucetic, M. (1992). A pore pressure model for cyclic straining of clay. *Soils and Foundations*, 32(3), 156-173.

Miao, F., Wu, Y., Li, L., Tang, H., & Li, Y. (2018). Centrifuge model test on the retrogressive landslide subjected to reservoir water level fluctuation. *Engineering geology*, 245, 169-179.

Mogami, T., and Kubo, K. (1953). "The behavior of soil during vibration. ", *Proceedings, 3rd International Conference on Soil Mechanics and Foundation Engineering, Zurich, Vol. 1, pp. 152-155.*

Mohkam, M. (1983). Contribution à l'étude expérimentale et théorique du comportement des sables sous chargements cycliques. These DI, Université scientifique et médicale de Grenoble.

Monkul, M. M., Gültekin, C., Gülver, M., Akın, Ö., & Eseller-Bayat, E. (2015). Estimation of liquefaction potential from dry and saturated sandy soils under drained constant volume cyclic simple shear loading. *Soil Dynamics and Earthquake Engineering*, 75, 27-36.

Montoya, B. M., DeJong, J. T., & Boulanger, R. W. (2014). Dynamic response of liquefiable sand improved by microbial-induced calcite precipitation. In *Bio-and Chemo-Mechanical Processes in Geotechnical Engineering: Géotechnique Symposium in Print 2013* (pp. 125-135). ICE Publishing.

Morales Peñuela, W. F. (2013). River dyke failure modeling under transient water conditions (Doctoral dissertation, ETH Zurich).

Moss, R. E., Seed, R. B., Kayen, R. E., Stewart, J. P., Der Kiureghian, A., & Cetin, K. O. (2006). CPT-based probabilistic and deterministic assessment of in situ seismic soil liquefaction potential. *Journal of Geotechnical and Geoenvironmental Engineering*, 132(8), 1032-1051.

Nakazawa, H., Ishihara, K., Tsukamoto, Y., & Kamata, T. (2004). Case studies on evaluation of liquefaction resistance of imperfectly saturated soil deposits. In *Cyclic behaviour of soils and liquefaction phenomena* (pp. 295-304).

National Research Council's Committee on Earthquake Engineering, 1985, United State of American.

NTC 2018 – Nuove norme sismiche per il calcolo strutturale

Okamura, M., & Soga, Y. (2006). Effects of pore fluid compressibility on liquefaction resistance of partially saturated sand. *Soils and Foundations*, 46(5), 695-700.

Ozaydin, K., & Erguvanh, A. (1980). The generation of pore pressures in clayey soils during earthquakes. In *Proc., 7th World Conf. on*

Earthquake Engineering (Vol. 3, pp. 326-330). Tokyo: The International Association for Earthquake Engineering (IAEE).

Pipatpongsa, T., Aroonwattanaskul, K., & Fang, K. (2021). On the progression of slope failures using inverse velocity of surface movements in an undercut slope model. *Understanding and Reducing Landslide Disaster Risk: Volume 4 Testing, Modeling and Risk Assessment 5th*, 293-301.

Porcino, D., & Diano, V. (2016). Laboratory study on pore pressure generation and liquefaction of low-plasticity silty sandy soils during the 2012 earthquake in Italy. *Journal of Geotechnical and Geoenvironmental Engineering*, 142(10), 04016048.

Poulos, S. J. (1981). The steady state of deformation. *Journal of the Geotechnical Engineering Division*, 107(5), 553-562. Terzaghi, K., Peck, R. B., & Mesri, G. (1996). *Soil mechanics in engineering practice*. John Wiley & sons.

Rahimi, S., Wood, C. M., Wotherspoon, L. M., & Green, R. A. (2020). Efficacy of aging correction for liquefaction assessment of case histories recorded during the 2010 Darfield and 2011 Christchurch Earthquakes in New Zealand. *Journal of Geotechnical and Geoenvironmental Engineering*, 146(8), 04020059.

Robertson, P. K., & Campanella, R. G. (1985). Liquefaction potential of sands using the CPT. *Journal of geotechnical engineering*, 111(3), 384-403.

Robertson, P.K. 1994. Suggested terminology for liquefaction. In *Proceedings of the 47th Canadian Geotechnical Conference*, Halifax, N.S. CGS. Sept. pp. 277–286

Robertson, P. K., & Wride, C. E. (1998). Evaluating cyclic liquefaction potential using the cone penetration test. *Canadian geotechnical journal*, 35(3), 442-459.

Robertson, P. K. (2004, September). Evaluating soil liquefaction and post-earthquake deformations using the CPT. In Proc. 2nd Int. Conf. on Site Characterization ISC (Vol. 2, pp. 233-249).

Robertson, P. K. (2009). Performance based earthquake design using the CPT. Proc. IS-Tokyo, 3-20.

Roscoe, K. H., Schofield, A., & Wroth, A. P. (1958). On the yielding of soils. *Geotechnique*, 8(1), 22-53.

Seed, H. B., & Lee, K. L. (1966). Liquefaction of saturated sands during cyclic loading. *Journal of the Soil Mechanics and Foundations Division*, 92(6), 105-134.

Seed, H. B., & Idriss, I. M. (1971). Simplified procedure for evaluating soil liquefaction potential. *Journal of the Soil Mechanics and Foundations division*, 97(9), 1249-1273.

Seed, H. B., Martin, P. P., & Lysmer, J. (1975). The generation and dissipation of pore pressures during soil liquefaction. Report No. EERC, 75-26.

Seed, H. B., Arango, I., & Chan, C. K. (1976). Evaluation of soil liquefaction potential for level ground during earthquakes. A summary report.

Seed, H. B., Mori, K., & Chan, C. K. (1977). Influence of seismic history on liquefaction of sands. *Journal of the Geotechnical Engineering Division*, 103(4), 257-270.

Seed, H. B. (1979). Soil liquefaction and cyclic mobility evaluation for level ground during earthquakes. *Journal of the geotechnical engineering division*, 105(2), 201-255.

Seed, H. B. (1982). Ground motions and soil liquefaction during earthquakes. *Earthquake engineering research insitutue*.

Seed, H. B., Idriss, I. M., & Arango, I. (1983). Evaluation of liquefaction potential using field performance data. *Journal of geotechnical engineering*, 109(3), 458-482.

Seed, H., Tokimatsu, K., Harder, L. F., & Chung, R. M. (1985). Influence of SPT procedures in soil liquefaction resistance evaluations. *Journal of geotechnical engineering*, 111(12), 1425-1445.

Seed, H. B., & De Alba, P. (1986). Use of SPT and CPT tests for evaluating the liquefaction resistance of sands. In *Use of in situ tests in geotechnical engineering* (pp. 281-302). ASCE.

Seid-Karbasi, M., & Byrne, P. M. (2006). Effects of partial saturation on liquefiable ground response. In *GeoCongress 2006: Geotechnical Engineering in the Information Technology Age* (pp. 1-6).

Sherif, M. A., Ishibashi, I., & Tsuchiya, C. (1978). Pore-pressure prediction during earthquake loadings. *Soils and Foundations*, 18(4), 19-30.

Sherif, M. A., Tsuchiya, C., & Ishibashi, I. (1977). Saturation effects on initial soil liquefaction. *Journal of the Geotechnical Engineering Division*, 103(8), 914-917.

Shibata, T., & Teparaksa, W. (1988). Evaluation of liquefaction potentials of soils using cone penetration tests. *Soils and Foundations*, 28(2), 49-60.

Skempton, A. W. (1986). Standard penetration test procedures and the effects in sands of overburden pressure, relative density, particle size, ageing and overconsolidation. *Geotechnique*, 36(3), 425-447.

Sonmez, H. (2003). Modification of the liquefaction potential index and liquefaction susceptibility mapping for a liquefaction-prone area (Inegol, Turkey). *Environmental Geology*, 44, 862-871.

Stark, T. D., & Olson, S. M. (1995). Liquefaction resistance using CPT and field case histories. *Journal of geotechnical engineering*, 121(12), 856-869.

Suzuki, Y., Tokimatsu, K., Taya, Y., & Kubota, Y. (1995). Correlation between CPT data and dynamic properties of in situ frozen samples.

Sze, H. Y., & Yang, J. (2014). Failure modes of sand in undrained cyclic loading: impact of sample preparation. *Journal of geotechnical and geoenvironmental engineering*, 140(1), 152-169.

Tamari, Y., Hyodo, J., Ichii, K., Nakama, T., & Hosoo, A. (2018). Analysis of liquefaction during 2011 east Japan earthquake—Part 1: Seismic Ground Behavior in Tokyo Port at the 2011 Off Pacific Coast of Tohoku earthquake—An effective stress dynamic analysis focusing on the impact of the aftershock. *Developments in Earthquake Geotechnics*, 201-217.

Terzaghi, K., Peck, R. B., & Mesri, G. (1996). *Soil mechanics in engineering practice*. John Wiley & sons.

Tokimatsu, K., & Yoshimi, Y. (1983). Empirical correlation of soil liquefaction based on SPT N-value and fines content. *Soils and Foundations*, 23(4), 56-74.

Tonkin & Taylor (2013) *Liquefaction Vulnerability Study for the Earthquake Commission*, February 2013 Ref 52020.0200 v1.0

Toprak, S., & Holzer, T. L. (2003). Liquefaction potential index: field assessment. *Journal of Geotechnical and Geoenvironmental Engineering*, 129(4), 315-322.

Towhata, I., & Towhata, I. (2008). Mitigation of liquefaction-induced damage. *Geotechnical Earthquake Engineering*, 588-642.

Towhata, I., Taguchi, Y., Hayashida, T., Goto, S., Shintaku, Y., Hamada, Y., & Aoyama, S. (2017). Liquefaction perspective of soil ageing. *Géotechnique*, 67(6), 467-478.

Tsuchida, H. (1970). Prediction and countermeasure against the liquefaction in sand deposits. In *Abstract of the seminar in the Port and Harbor Research Institute* (pp. 31-333).

Tsukamoto, Y., Ishihara, K., Nakazawa, H., Kamada, K., & Huang, Y. (2002). Resistance of partly saturated sand to liquefaction with reference to longitudinal and shear wave velocities. *Soils and foundations*, 42(6), 93-104.

Tsukamoto, Y., & Ishihara, K. (2022). *Advances in soil liquefaction engineering*. Berlin, Germany: Springer.

Vaid, Y. P., & Chern, J. C. (1985, October). Cyclic and monotonic undrained response of saturated sands. In *Advances in the art of testing soils under cyclic conditions* (pp. 120-147). ASCE.

Vaid, Y. P., & Finn, W. L. (1979). Static shear and liquefaction potential. *Journal of the Geotechnical Engineering Division*, 105(10), 1233-1246.

Varnes, D. J. (1984). *Landslide hazard zonation: a review of principles and practice* (No. 3).

Vernay, M., Morvan, M., & Breul, P. (2020). Experimental study on the influence of saturation degree on unstable behavior within granular material. *European Journal of Environmental and Civil Engineering*, 24(11), 1821-1839.

Yasuda, S., Harada, K., Ishikawa, K., & Kanemaru, Y. (2012). Characteristics of liquefaction in Tokyo Bay area by the 2011 Great East Japan earthquake. *Soils and Foundations*, 52(5), 793-810.

Yin, M., Rui, Y., & Xue, Y. (2019). Centrifuge study on the runout distance of submarine debris flows. *Marine Georesources & Geotechnology*, 37(3), 301-311.

Yoshimi, Y., & Oh-oka, H. (1975). Influence of degree of shear stress reversal on the liquefaction potential of saturated sand. *Soils and foundations*, 15(3), 27-40.

Yoshimi, Y., Tanaka, K., & Tokimatsu, K. (1989). Liquefaction resistance of a partially saturated sand. *Soils and foundations*, 29(3), 157-162.

Youd, T. L., & Bennett, M. J. (1983). Liquefaction sites, imperial valley, California. *Journal of Geotechnical Engineering*, 109(3), 440-457.

Youd, T. L., & Idriss, I. M. (2001). *Liquefaction resistance of soils: summary report from the 1996 NCEER and 1998 NCEER/NSF workshops*



on evaluation of liquefaction resistance of soils. *Journal of geotechnical and geoenvironmental engineering*, 127(4), 297-313.

Youd, T. L., Idriss, I. M., Andrus, R. D., Arango, I., Castro, G., Christian, J. T., ... & Stokoe, K. H. (2003). Closure to “Liquefaction Resistance of Soils: Summary Report from the 1996 NCEER and 1998 NCEER/NSF Workshops on Evaluation of Liquefaction Resistance of Soils” by TL Youd, IM Idriss, Ronald D. Andrus, Ignacio Arango, Gonzalo Castro, John T. Christian, Richardo Dobry, WD Liam Finn, Leslie F. Harder Jr., Mary Ellen Hynes, Kenji Ishihara, Joseph P. Koester, Sam SC Liao, William F. Marcuson III, Geoffrey R. Martin, James K. Mitchell, Yoshiharu Moriwaki, Maurice S. Power, Peter K. Robertson, Raymond B. Seed .... *Journal of Geotechnical and Geoenvironmental Engineering*, 129(3), 284-286.

Wang, W. (1979). Some findings in soil liquefaction Earthquake Engineering. Department Water Conservancy and Hydroelectric Power Scientific Research Institute, Beijing.

Zhang, G., Robertson, P. K., & Brachman, R. W. (2002). Estimating liquefaction-induced ground settlements from CPT for level ground. *Canadian Geotechnical Journal*, 39(5), 1168-1180.